UNIVERSIDAD DE CANTABRIA

PROGRAMA DE DOCTORADO EN INGENIERÍA QUÍMICA,
DE LA ENERGÍA Y DE PROCESOS

# New strategies in the generation of photocatalytic hydrogen

Nuevas estrategias en la generación de hidrógeno por fotocatálisis

Realizada por:

**Juan Corredor Ortega**

Dirigida por:

**Prof. Dra. Inmaculada Ortiz Uribe**

**Prof. Dra. María José Rivero Martínez**

**Escuela de Doctorado de la Universidad de Cantabria**

**Santander 2021**

UNIVERSIDAD DE CANTABRIA

PROGRAMA DE DOCTORADO EN INGENIERÍA QUÍMICA, DE LA ENERGÍA Y DE PROCESOS

# New strategies in the generation of photocatalytic hydrogen

Nuevas estrategias en la generación de hidrógeno por fotocatálisis

Realizada por:

**Juan Corredor Ortega**

Dirigida por:

**Prof. Dra. Inmaculada Ortiz Uribe**

**Prof. Dra. María José Rivero Martínez**

**Escuela de Doctorado de la Universidad de Cantabria**

**Santander 2021**

*Programa de Doctorado en Ingeniería Química, de la Energía de y Procesos (BOE núm. 16 de 19 de enero de 2015. RUCT: 5601000)*

The research described in this thesis has been conducted at the Advanced Separation Processes (ASP) group of the Department of Chemical and Biomolecular Engineering of the University of Cantabria.

This research has been financially supported by the Spanish Ministry of Economy and Competitiveness, Spanish State Research Agency and and the European Regional Development Fund through the projects: CTM2015-69845-R "New developments in photocatalysis for environmental applications" (MINECO/FEDER, UE), CTQ2015-66078-R "Modeling of advanced separation applications" (MINECO/FEDER, UE), "HYLANTIC" EAPA_204/2016 and RTI2018-099407-B-I00 "Challenges in the implementation of photocatalysis for environmental applications" (MICIU/AEI/FEDER, UE).

The author has been the recipient of a predoctoral fellowship (FPI BES-2016-079201) granted by the Spanish Ministry of Education.

This PhD thesis has been performed as a compendium of interrelated scientific publications. The scientific articles that enable this dissertation modality are published in international journals indexed in the Journal Citation Reports (JCR):

- J. Corredor, M. J. Rivero, C. M. Rangel, F. Gloaguen, I. Ortiz. "Comprehensive review and future perspectives on the photocatalytic hydrogen production". *Journal of Chemical Technology & Biotechnology*, 94, pp.3049–3063, 2019.
  DOI: 10.1002/jctb.6123.
  Q2, IF (2019): 2.750. Chemical Engineering (59/143).


- J. Corredor, M. J. Rivero and I. Ortiz. "New insights in the performance and reuse of rGO/$TiO_2$ composites for the photocatalytic hydrogen production". *International Journal of Hydrogen Energy*, 2020 (In Press).
  DOI: 10.1016/j.ijhydene.2020.01.181.
  Q2, IF (2019): 4.939. Energy & Fuels (30/112).

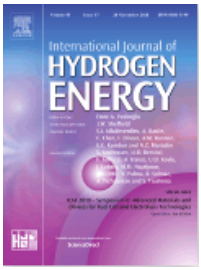


- J. Corredor, E. Perez-Peña M. J. Rivero and I. Ortiz. "Performance of rGO/$TiO_2$ photocatalytic membranes for hydrogen production". *Membranes*, 10(9), 1–13, 2020.
  DOI: 10.3390/membranes10090218.
  Q2, IF (2019): 3.094. Chemical Engineering (52/143). **Selected for the cover of the issue.**

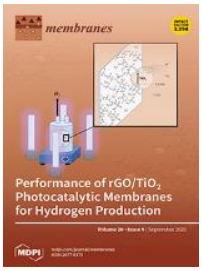

- J. Corredor, D. Harankahage, F. Gloaguen, M. J. Rivero, M. Zamkov and I. Ortiz. “Influence of QD photosensitizers in the photocatalytic production of hydrogen with biomimetic [FeFe]-hydrogenase. Comparative performance of CdSe and CdTe”. *Chemosphere*, 278, 130485, 2021.

  
  

  DOI: 10.1016/j.chemosphere.2021.130485.

  Q1, IF (2019): 5.778. Environmental Sciences (29/265).

# *Acknowledgments*

En primer lugar, quisiera agradecer a mis directoras de tesis, la profesora Inmaculada Ortiz y la doctora María José Rivero por ofrecerme la oportunidad de desarrollar esta tesis doctoral en el departamento de Ingenierías Química y Biomolecular, y por guiarme en la realización de la de la misma compartiendo todo su conocimiento.

También me gustaría extender estos agradecimientos al resto de compañeros del departamento por su ayuda en las labores de investigación y por todo lo que he aprendido de ellos. Por supuesto también agradecerles el buen ambiente de trabajo creado que me ha hecho estar tan a gusto durante estos años.

I thank to Mikhail Zamkov for welcoming me in the department of Physics and Astronomy of Bowling Green State University. His help and advice have hugely contributed to the last part of this thesis. I would also like to thank him and all the great people who work in his lab for their friendliness and help during my stay.

Finalmente, agradecer a mi familia y amigos por todo su apoyo.

# *Table of contents*

# *Abstract*

Nowadays the global earth surface temperature has increased by 1 ºC above pre-industrial levels due to the global warming caused by greenhouse gases emissions. The combustion of fossil fuels is the main contributor. In this context hydrogen is an excellent energy vector because its combustion only produces water. However, most of the hydrogen is currently produced by steam reforming from fossil fuels. This process is energy intensive, and it also involves the emission of greenhouse gases. The potential to produce hydrogen from alternative and green technologies has been widely investigated; among all, water electrolysis takes the leading role. Complementarily, hydrogen can be produced from photoreforming of gas or liquid wastes using sustainable technologies, such as photocatalysis. This is a way to harvest the sunlight energy and store it in form of solar fuels. In this doctoral thesis new strategies for the photocatalytic generation of hydrogen have been investigated.

First, a thorough review of the related literature about photocatalytic hydrogen production was carried out in chapter 3.1, providing an integrated overview of the different, heterogeneous, homogeneous and hybrid photocatalytic systems. The mechanisms of the different systems were described. The elementary units that take part in the photocatalytic process and their roles were categorized. Moreover, the influence of the experimental conditions on the process was analyzed and a critical comparison in terms of hydrogen generation rate was developed.

The use of $TiO_2$ as photocatalyst in heterogeneous systems has been widely studied. Although it is highly photoreactive, cost-effective, and chemically and thermally stable, the use of $TiO_2$ is limited by the high electron-hole

recombination rate and the activation restricted by visible light. Noble metals, such as platinum, have been coupled with $TiO_2$ fabricating photocatalysts with higher photoreactivity as they can reduce the charge recombination rate and increase activity under visible light. However, the scarcity and high cost of noble metals limit their large-scale application. In order to overcome this issue, research efforts have been focused on the use of noble metal-free materials. In this way, synthesis of composite photocatalysts with graphene oxide (GO) has been carried out in chapter 3.2. GO can be partially reduced to graphene which has large surface area and excellent electrical conductivity. These features can enhance the hydrogen production.

Another barrier for the implementation of this technology is the separation, recovery, and reuse of $TiO_2$ nanoparticles after the photoassissted process. Photocatalyst immobilization on polymeric membranes would avoid this recovery step. This work has evaluated in chapter 3.3 three immobilization techniques that are worth considering, such as spraying, dip-coating, and solvent-casting because they are cost-effective methods and the mild synthesis conditions do not provoke changes in the structure of the composite.

Although heterogeneous photocatalytic systems are closer to large-scale application, homogeneous systems offer the highest hydrogen production rates. In the last decade, the hydrogenase mimic molecules have shown great performance as catalyst in homogeneous systems. One of the main problems in these systems is the poor stability of the photosensitizers, especially the noble metal free photosensitizers. Hybrid systems may overcome this issue by combining semiconductors as photosensitizers and molecular catalysts. On this basis, hybrid systems composed of a biomimic

hydrogenase molecule as catalyst and CdSe or CdTe quantum dots (QDs) as photosensitizer have been studied in chapter 3.4.

# *Resumen*

Actualmente la temperatura de la superficie terrestre se ha incrementado en 1 ºC sobre los niveles de la época preindustrial debido al calentamiento global provocado por las emisiones de gases de efecto invernadero. El uso de combustibles fósiles es uno de los principales orígenes de estas emisiones. En este contexto, el hidrógeno es un excelente vector energético porque su combustión únicamente produce agua. Sin embargo, la mayor parte del hidrógeno actualmente se produce por reformado con vapor de combustibles fósiles. Este es un proceso con elevado consumo energético y también conlleva emisiones de gases de efecto invernadero. Se están desarrollando nuevas alternativas tecnológicas para la producción de hidrógeno, entre los que ahora mismo destaca la electrolisis. Además, el hidrógeno puede ser producido por el foto-reformado de gas o efluentes líquidos utilizando tecnologías sostenibles como la fotocatálisis, que permite aprovechar la energía de la luz solar y almacenarla en forma de combustibles. En la presente tesis doctoral se investigan nuevas estrategias para la generación de hidrógeno por fotocatálisis.

En primer lugar, se llevó a cabo en el capítulo 3.1 una exhaustiva revisión bibliográfica sobre la producción de hidrógeno por fotocatálisis, proporcionando una visión holística de los diferentes sistemas fotocatalíticos heterogéneos, homogéneos e híbridos. Se describieron los mecanismos de los diferentes sistemas, se categorizaron los diferentes componentes involucrados en el proceso y sus funciones y además, se analizó la influencia de las condiciones experimentales en el proceso y se desarrolló una comparación crítica basada en la velocidad de producción de hidrógeno.

El uso del fotocatalizador $TiO_2$ en sistemas heterogéneos fotocatalíticos ha sido ampliamente estudiado. A pesar de que el $TiO_2$ es altamente fotorreactivo, y química y térmicamente estable, su uso está limitado por la alta velocidad de recombinación electrón-hueco junto al hecho de que es activo fundamentalmente bajo radiación UV. Se han empleado elementos para dopar el $TiO_2$ y también se han desarrollado co-catalizadores con metales nobles como platino, dando lugar a materiales con alta fotorreactividad, ya que facilitan la reducción de la velocidad de recombinación de cargas y aumentan la actividad bajo luz visible. Sin embargo, la escasez y alto coste de los metales nobles limita su aplicación a gran escala. Para superar este problema, los esfuerzos de investigación se han centrado en el uso de materiales que no contengan metales nobles. En esta línea en el capítulo 3.2 se llevó a cabo la síntesis de fotocatalizadores con óxido de grafeno (GO). El GO puede ser parcialmente reducido a grafeno, que tiene una gran área superficial y una excelente conductividad eléctrica lo que puede contribuir a aumentar el rendimiento del fotocatalizador.

Otra barrera a la aplicación real de esta tecnología es la separación, recuperación y reutilización de las nanopartículas de $TiO_2$ después del proceso foto-asistido. La inmovilización del fotocatalizador en membranas poliméricas evitaría esta etapa de recuperación. En el capítulo 3.3, este trabajo evaluó varias técnicas, como el spraying, dip-coating y solvent-casting, porque son métodos más económicos y sus condiciones de síntesis suaves no provocan cambios en la estructura del fotocatalizador.

Aunque los sistemas fotocatalíticos heterogéneos están más cerca de la aplicación a gran escala, los sistemas homogéneos ofrecen las velocidades de producción de hidrógeno más altas. En la última década, las moléculas imitadoras de la hidrogenasa han demostrado un excepcional

funcionamiento como catalizadores. Uno de los problemas principales en estos sistemas es la baja estabilidad de los fotosensibilizadores, especialmente de los que no contienen metales nobles. Los sistemas híbridos podrían superar este problema combinando semiconductores como fotosensibilizadores y catalizadores moleculares. Basándose en esto, en el capítulo 3.4 se estudiaron sistemas híbridos formados por hidrogenasa biomimética como catalizador y puntos cuánticos de CdSe o CdTe como fotosensibilizadores.

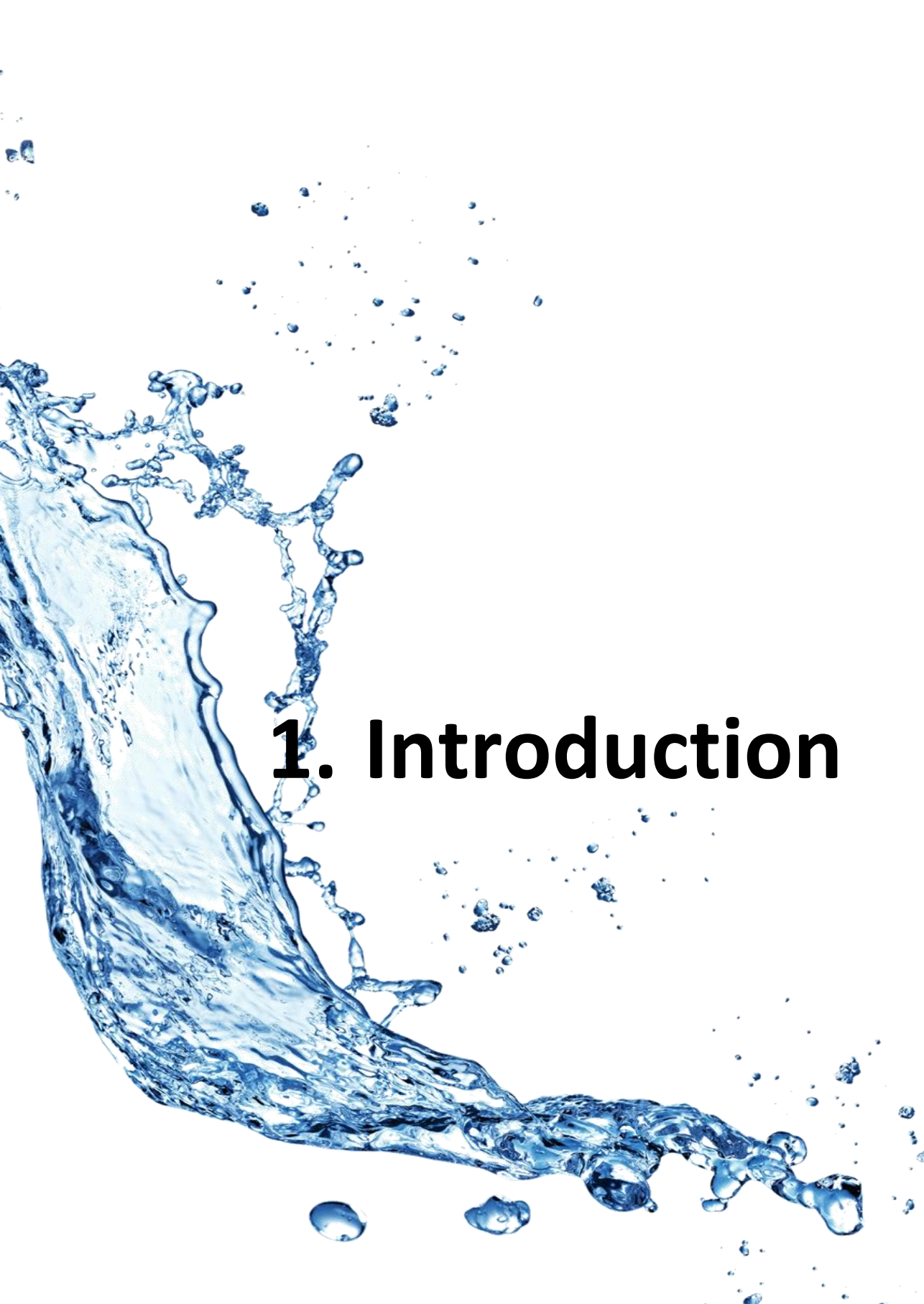

# 1. Introduction

## 1.1. Hydrogen as energy vector

Energy is one of the most crucial aspects in the socio-economic development of nations. Nowadays, it strongly depends on conventional fossil fuels. The combustion of fossil fuels is responsible for most of the greenhouse gases (GHG) emissions which contribute strongly to the global warming. The global surface temperature has progressively increased by 1 °C above pre-industrial levels [1,2]. This increase might seem small, but it means a significant increase in accumulated heat. This extra heat is driving regional and seasonal extreme temperatures, intensifying heavy rainfall, and changing habitat ranges for plants and animals, expanding some and shrinking others. Moreover, the reduction of the snow cover and sea ice have provoked an increase of the sea level of 3.5 mm per year. In order to avoid these catastrophic consequences, the Paris Agreement set out a global framework in 2015 to avoid dangerous climate change by limiting global warming to well below 2 °C above pre-industrial levels and pursuing efforts to limit it to 1.5°C [3]. As of November 2020, the Paris Agreement was signed by 194 countries representing almost 97% of the global GHG emissions.

According to the International Energy Agency (IEA), the energy-related $CO_2$ emissions were increased progressively every year, reaching 33 Gt in 2019 [4]. Although the advanced economies have reduced slightly their emissions since 2005, the global value has increased. According to the Paris Agreement, the involved countries have submitted their cut emissions pledges to the United Nations. The European Union currently aims to reduce greenhouse gas emissions by 40% by 2030 compared with 1990 levels.

In this global context, hydrogen comes out as a clean alternative energy vector because its direct combustion does not generate pollutants or greenhouse gases [5–7]. Its combustion produces only water as byproduct (equation 1.1).

$$H_2 + \frac{1}{2}O_2 \rightarrow H_2O \qquad (1.1)$$

Other advantages of hydrogen are: i) $H_2$ can be produced from hydrocarbon and, more significantly, from water and organic compounds; ii) it can be used as a chemical fuel and as a chemical feedstock in many industrial processes; iii) $H_2$, unlike electricity, can be stored in large quantities in a variety of forms depending on the final application; iv) there are different ways to transport hydrogen such as by pipeline, ship, or truck [8,9]. However, $H_2$ also has some disadvantages such as its energy density is less than that for gasoline, it can leak from containment vessels easier than other energy vectors, and its main drawback is the cost of production that nowadays is high compared to the cost of fossils fuels [10].

Different technologies have been developed for hydrogen production [9] that can be classified as grey hydrogen or green hydrogen production alternatives. Grey hydrogen is produced from fossil fuels while green hydrogen is produced from sustainable sources without $CO_2$ emissions [11,12]. Nowadays, 95% of $H_2$ is obtained by steam reforming of fossil fuels, mainly methane. This process produces hydrogen by the reaction of water vapor and methane in presence of a nickel catalyst. It operates at high temperatures and pressures, and thus is energy-intensive [13–15]. Autothermal reforming is a process for producing hydrogen by partially oxidizing a hydrocarbon feed, generating hydrogen and carbon monoxide. It is usually combined with steam reforming. Coal gasification is a practical option for producing hydrogen due to the worldwide reserves and

commercially available technologies. However, the carbon emissions and the cost of hydrogen production by this method are higher than by steam reforming [16]. Water electrolysis is one of the most promising $H_2$ production alternatives, especially, for storage of surplus electricity; a variety of commercial electrolyzers for large-scale applications is available on the market achieving hydrogen production rates up to 750 $Nm^3 \cdot h^{-1}$ [17–19]. Around 5% of hydrogen is produced using electrolysis of water [20]. However, the energy consumption associated with electrolysis must be significantly reduced before this process becomes competitive at large scale. Green hydrogen could be produced by electrolysis if the electricity is supplied from a renewable source such as photovoltaic cells. Thermolysis consist of the water dissociation above 2200 ºC producing $H_2$ and $O_2$. Biomass can be used as primary energy to extract hydrogen from steam by thermochemical biomass conversion. Dark fermentation is the conversion of biochemical energy stored in organic matter into hydrogen in the absence of light thanks to the activity of microorganisms. Biophotolysis consists of hydrogen production from water mediated by light-sensitive microorganisms under light irradiation. Table 1.1 collects the different hydrogen production methods. Some of them could produce green as well as grey hydrogen depending on the energy source they use [16].

Photocatalytic generation of $H_2$ from organic solutions or $H_2O$, although it is a minor source in terms of produced $H_2$ volume, it appears to be a complementary and renewable way for simultaneous $H_2$ generation and wastewater remediation [21–23].

**Table 1.1**. Classification of hydrogen production methods.

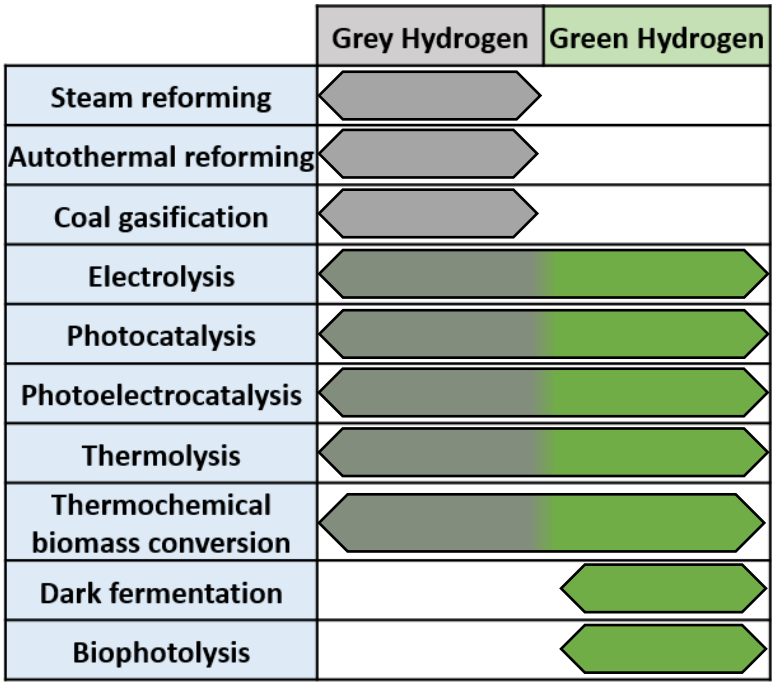


## 1.2. Photocatalytic hydrogen production

As early as in 1911, 76 years after Berzelius coined the word catalysis, the term photocatalysis appeared in several scientific communications [24]. In Germany, Eibner incorporated this concept in his studies about the effect of the illumination of ZnO on the bleaching of Prussian blue [25]. Contemporaneously, the term photocatalysis gained additional relevance when it appeared in the title of some articles dealing with the degradation of oxalic acid under irradiation in the presence of uranyl salts [26,27]. Nowadays, photocatalysis is defined as a catalytic reaction involving light absorption by a catalyst or by a substrate [28]. Photocatalysis, while varying in detail in terms of reactions and mechanisms, may be described

by four important steps: i) light absorption to generate electron-hole pairs; ii) excited charges separation; iii) transfer of electrons and holes to the surface of the photocatalysts or photosensitizer; and iv) utilization of charges on the surface for redox reactions.

Photocatalysis can be applied for a wide variety of purposes. The main fields of application are [29]:

- Purification and disinfection of water. Photocatalysis may be used for water disinfection by killing different water pathogens such as *Escherichia coli* or *Enterococcus faecalis* bacteria, and it can also degrade organic contaminants such as insecticides, antibiotics, or chlorinated organic compounds, cyanotoxins, and taste and odor compounds. It can also oxidize inorganic compounds such as chromium, uranium, or nitrates [30,31].
- Purification and disinfection of air. Photocatalysis has been used for removal of microbiological pathogens in air such as *Serratia marcescens* or *Streptococcus pneumoniae* bacteria, organic contaminants such as hydrocarbons, and inorganic compounds such as CO, $NO_x$ and $NH_3$ [32,33].
- Synthesis of chemicals. Photocatalysis can be used to synthetize different chemicals such us benzyl chloride or rose oxide through photocatalytic reactions such as oxidation, reduction and alkylations. Photocatalytic reactions in chemical synthesis are still limited in number, but some of the recent examples suggest that proper attention to this aspect may increase interest to this area [34,35].
- Photocatalytic hydrogen production. $H_2$ can be generated by photocatalysis [16,36].

The photocatalytic hydrogen can be produced from direct water splitting or using a sacrificial agent such as methanol, glycerol, or formic acid. The process is more efficient using sacrificial agents due to the higher effectiveness of the sacrificial agent as hole ($h^+$) scavenger and the suppression of the back reaction to produce $H_2O$ because $O_2$ is not evolved, thus, increasing $H_2$ yield [37]. The water-splitting reaction is a large uphill reaction with a Gibbs free energy change of $\Delta G = +237.1$ kJ·mol$^{-1}$ (Figure 1.1). The photocatalytic reaction using a sacrificial agent is still an uphill reaction, but less than the water-splitting one. For example, in the photocatalytic hydrogen production from methanol the Gibbs free energy change is +9.3 kJ·mol$^{-1}$ [38]. Moreover, some waste effluents containing easy to oxidize compounds, such as the glycerol waste generated in the biodiesel production, could be used for $H_2$ generation reporting an additional advantage to the photocatalytic remediation of these effluents [39,40].

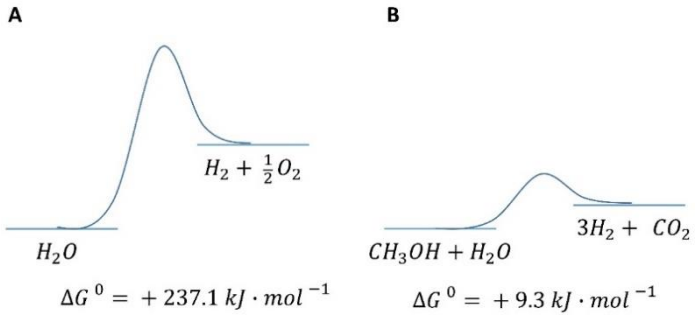


**Figure 1.1.** $H_2$ production reaction (a) from $H_2O$ (water splitting) and (b) from methanol.

Three different photocatalytic hydrogen production systems have been developed since in 1972 Honda and Fujishima carried out the water splitting for the first time in a photoelectrochemical cell using $TiO_2$ and Pt as electrodes: heterogeneous, homogeneous, and hybrid [41].

Heterogeneous systems use a semiconductor photocatalyst. Frequently, the photocatalyst is suspended in the solution and is irradiated by the light source. The reaction is carried out in aqueous media. $H_2O$ can act as a $H^+$ source. It has been found that low water/organic solvent ratios in the reaction media disfavor $H_2$ production [42,43]. The semiconductor acts as both catalyst for the generation of $H_2$ and photosensitizer or light harvester. The $H_2$ production mechanism by heterogeneous photocatalysis involves the following steps: (1) absorption of photons from a light source with sufficient energy to overcome the band gap of the semiconductor; this promotes the transfer of an electron from the valence band of the semiconductor to the conduction band, creating an electron–hole pair. (2) The electrons that reach the surface of the photocatalyst can reduce $H^+$. The holes can oxidize $H_2O$ or the sacrificial agent, depending on the band gap of the semiconductor. The electrons and holes which have not reacted recombine between themselves [44,45]. Figure 1.2A illustrates this mechanism.

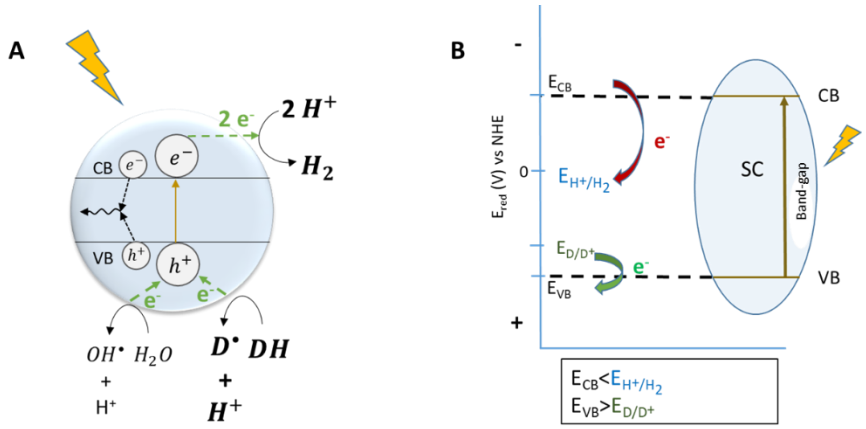


**Figure 1.2.** Heterogeneous photocatalytic $H_2$ production system: (A) reaction mechanism, (B) energy diagram. SC, photocatalyst semiconductor; D, electron donor/sacrificial agent.

In order to reduce protons to $H_2$, the photocatalyst conduction band potential ($E_{CB}$) has to be more negative than the proton reduction potential ($E_{H^+/H_2}$). In addition, to oxidize the sacrificial agent, the photocatalyst valence band potential ($E_{VB}$) has to be more positive than the sacrificial agent oxidation potential ($E_{D/D^+}$). Water can also be oxidized if the $E_{VB}$ is more positive than its oxidation potential. Figure 1.2B illustrates the energy diagrams of the different photocatalytic systems.

Regarding homogeneous systems, they are usually composed of a soluble molecular catalyst, a soluble molecular photosensitizer, and a sacrificial agent. Homogeneous and hybrid photocatalysis have been carried out in organic solvents as well as in aqueous media. The solvent selection depends on the nature of the photosensitizer and the catalysts. Homogenous photocatalytic hydrogen production mechanism (Figure 1.3A) consists of the following steps: (1) Absorption of photons from the light source by the photosensitizer to reach an excited state. (2) The excited state is quenched by electron transfer through a reductive or an oxidative reaction pathway. (2a) Reductive quenching of the excited photosensitizer involves an electron transfer from the electron donor to the excited photosensitizer, generating the photosensitizer reduced form. Then, an electron is transferred to the catalyst and the photosensitizer returns to its initial form. (2b) Oxidative quenching consists first of an electron transfer from the excited photosensitizer to the catalyst, generating the oxidized form of the photosensitizer that, secondly, oxidizes the sacrificial agent returning to its initial form [46]. (3) Finally, the catalyst reduces the protons to $H_2$. Because $H_2$ is formed upon the coupling of two electrons and protons, in at least two separate steps, several reaction pathways might occur, such as: two sequential electron transfers from the photosensitizer to the catalyst that then reacts with two protons, or the disproportionation

of two hydrid species (Cat-H) formed transiently by the reaction of one-electron reduced form of the catalyst with a proton [47].

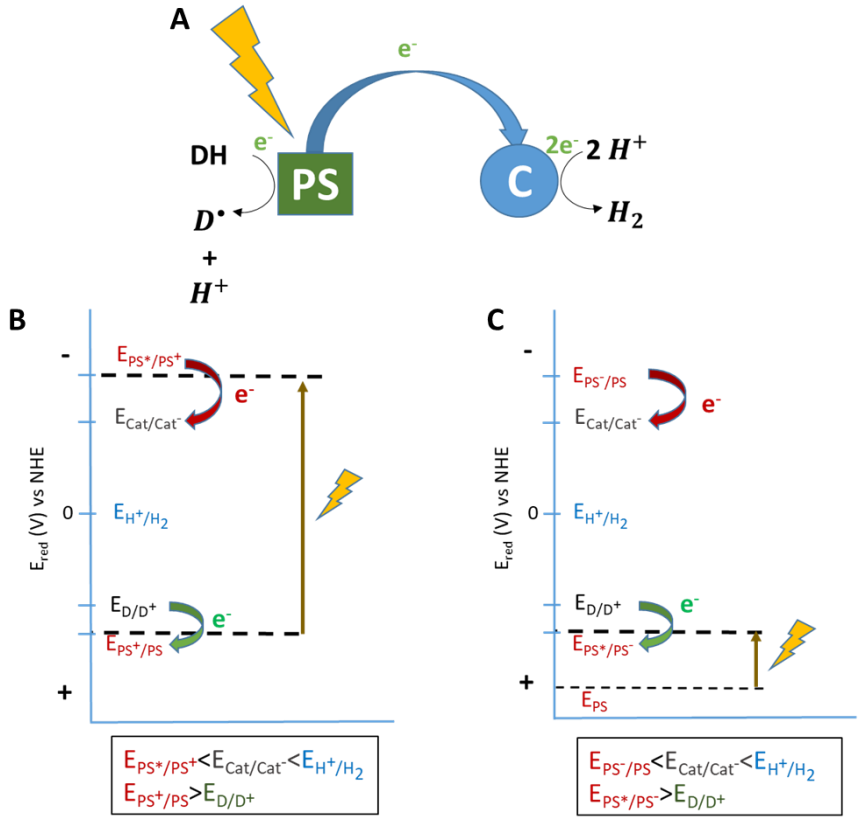


**Figure 1.3.** Homogeneous photocatalytic $H_2$ production system: (A) reaction mechanism, (B) energy diagram of oxidative quenching of excited photosensitizer, (C) energy diagram of reductive quenching of excited photosensitizer. PS, photosensitizer; Cat, catalyst. D, electron donor/sacrificial agent.

Regarding the thermodynamic of this process, the oxidation potential of the excited photosensitizer ($E_{PS^*/PS^+}$) in the oxidative quenching case (Figure 1.3B) and oxidation potential of the reduced photosensitizer ($E_{PS^-/PS}$) in the reductive quenching case (Figure 1.3C), must be more

negative than the reduction potential of the catalyst ($E_{Cat/Cat^-}$). Furthermore, the reduction potential of the oxidized photosensitizer ($E_{PS^+/PS}$) in the oxidative quenching case and the reduction potential of the excited photosensitizer ($E_{PS^*/PS^-}$) in the reductive case, must be more positive than the electron donor oxidation potential ($E_{D/D^+}$). The possibility of several proton reduction pathways contributes to the complexity of the determination of the redox potential at which the molecular catalyst is reduced.

The last photocatalytic mechanism is the hybrid system which consists of a soluble molecular catalyst, a semiconductor as photosensitizer, and a sacrificial agent. These configurations show high hydrogen production rates, broad visible light absorption, and long lifetimes. The steps of photocatalytic $H_2$ production mechanism in these systems (Figure 1.4A) are a combination between heterogeneous and homogeneous processes: (1) the semiconductor absorbs the photons from a light source with sufficient energy to promote the migration of an electron from the valence band to the conduction band, creating an electron–hole pair. (2) The electrons that reach the surface of the semiconductor photocatalyst are transferred to the homogeneous catalyst. (3) Finally, the catalyst reduces the protons to $H_2$.

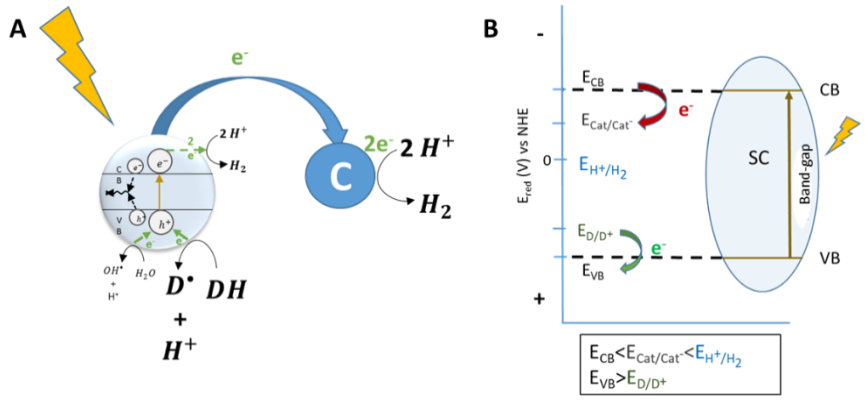


**Figure 1.4.** Hybrid photocatalytic $H_2$ production system: (A) reaction mechanism, (B) energy diagram. SC, photocatalyst semiconductor; Cat, catalyst; D, electron donor/sacrificial agent.

Regarding the thermodynamic of this process, $E_{CB}$ must be more negative than $E_{Cat/Cat^-}$ and $E_{VB}$ has to be more positive than the sacrificial agent oxidation potential ($E_{D/D^+}$). $E_{Cat/Cat^-}$ must be more negative than $E_{H^+/H2}$ (Figure 1.4B).

## 1.3. Strategies for improving the photocatalyst performance

In heterogeneous photocatalytic hydrogen production, the photocatalyst acts as both a light harvester and a catalyst. The function of a high performance heterogeneous photocatalyst is to: i) avoid fast electron–hole recombination; ii) allow fast diffusion of the electrons and holes to the surface of the semiconductor; iii) have band potentials suitable for the sacrificial agent oxidation and proton reduction; iv) be photoactive under visible light, which is related to the bandgap of the semiconductor; v) display good chemical stability; and vi) be cost-effective [48]. A wide variety of semiconductor photocatalysts has been investigated so far, such

as chalcogenides (ZnS, CdS, CdSe) [49,50], metal oxides ($TiO_2$, $Cu_2O$, $ZrO_2$) [15,51], carbonaceous materials (g-$C_3N_4$) [52–55], and solid solutions [$(Ga_{1-x}Zn_x)(N_{1-x}O_x)$, $(AgIn)_xZn_{2(1-x)}S_2$] [56–61]. However, $TiO_2$ is still the most widely used photocatalyst because of its good stability in a wide range of pH conditions, resistance to photo-corrosion, non-toxicity, and commercial availability. The small portion of the solar spectrum (c.4–8%) absorbed by $TiO_2$ and its relatively high charge recombination rate are its main drawbacks [62–65].

In order to design a stable and a high performance photocatalyst, a variety of strategies have been followed [36]. Figure 1.5 shows some of them.

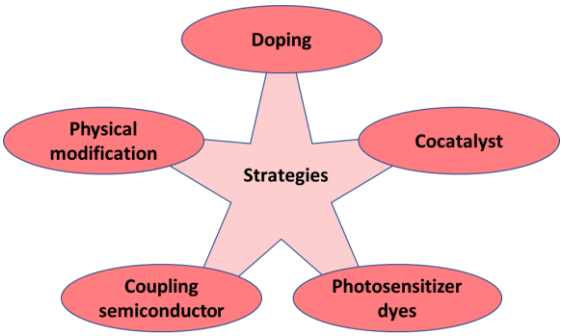


**Figure 1.5.** Strategies for improving the photocatalysts performance in heterogeneous photocatalytic hydrogen production.

The first strategy consists of doping the photocatalyst with different elements, by introducing or extracting atoms in/from its lattice structure. Iron (Fe), carbon (C), boron (B), and nitrogen (N) are common dopants that provide advantages such as narrowing the energy band gap and reducing the charge recombination rate [66–68]. The second strategy consists of coupling two semiconductors. The oxidation of the sacrificial agent or $H_2O$ and the reduction of hydrogen can be carried out on one of the semiconductors whereas the second one can contribute to (i) enhance

the separation and transport of the electron–hole pairs, (ii) sensitize the photocatalyst to visible light or, (iii) act as co-catalyst. If redox reactions occur one in each semiconductor, the structure is called a Z-scheme. It allows combination of a semiconductor with strong reduction power with another semiconductor with strong oxidation power. The third strategy consists of grafting an inorganic or organic dye such as Eosin Y to the semiconductor surface. These dyes can act as visible light photosensitizers [69,70]. Another strategy consists of the physical modification of the semiconductor 3D structure, optimizing its shape and size, and hence increasing the active surface to enhance the photocatalytic activity [71].

Coupling the photocatalyst with metals creating metal/semiconductor heterojunctions that form a Schottky barrier and avoid the fast charge recombination is another alternative. The metal also can act as co-catalyst reducing the overpotential for the surface electrochemical reactions. Moreover, the metal can improve the light absorption by surface plasmon resonance. The use of noble metals as co-catalysts has provided the highest $H_2$ production in heterogeneous photocatalytic hydrogen generation; however, their associated high cost, and scarcity limit their application [48]. Therefore, the use of noble metals should be substituted, and earth abundant compounds are good candidates.

Synthesis of composite photocatalysts with graphene oxide (GO) appears as an interesting alternative [72,73]. GO is a two-dimensional planar sheet composed by localized $sp^3$ defects within the $sp^2$ bonded carbon atoms structured in a honeycomb shaped network with oxygenated functional groups attached. GO can be partially reduced to graphene which has large surface area and excellent electrical conductivity. The properties of the reduced graphene oxide (rGO) can improve the photocatalytic performance of the $TiO_2$ by, i) reducing the electron-hole recombination

rate, due to the ability of rGO to carry charges from $TiO_2$ due to its fermi level being lower than the $TiO_2$ conduction band [74,75]; ii) improving the photocatalyst recovery due to the rGO morphology, and iii) narrowing the $TiO_2$ band-gap, this fact may be due to the creation of a hybrid orbital below the conduction band of $TiO_2$ with lower band-gap energy [76,77].

## 1.4. Photocatalyst immobilization

In heterogeneous photocatalysis, the photocatalyst is frequently used in suspension in order to reduce the mass transfer limitations of the process. The photocatalyst recovery from the treated solution can be carried out by coagulation and sedimentation processes, or by filtration [78]. Although photocatalyst recovery in heterogeneous systems is easier than in homogeneous or hybrid processes, the post-reaction separation step has been identified among the current engineering limitations of photocatalytic processes [79]. Another drawback associated with the use of suspended photocatalysts is the hazard associated with the manipulation of nanomaterials [80]. Therefore, techniques to immobilize the photocatalyst have been encouraged to facilitate catalyst reuse and to avoid the presence of nanomaterials in the treated waters and effluents. Photocatalyst immobilization has already been used in the removal of contaminants in wastewater and in air using different materials as support such as glass, zeolites, silica or polymers [81,82].

A wide variety of immobilization methods has been used in photocatalytic pollutant degradation, such as electrophoresis, chemical, and physical vapor deposition, sol-gel, thermal spraying, and solvent deposition [82]. A reliable technique for photocatalyst immobilization must provide a strong photocatalyst support, uniform coating, high degree of photocatalyst

irradiation, and preserve photocatalyst structure during preparation and immobilization [83]. The simplest techniques are worth considering, such as spraying, dip coating and solvent casting because they are economic methods and their soft operational synthesis conditions do not provoke changes in the structure of the composite.

Only few works can be found in literature about photocatalytic hydrogen generation with immobilized catalyst in a simple single chamber photoreactor using a membrane with the only function of photocatalyst support [84–87]. Some of these works have used glass substrates to support the photocatalyst; Cha et al. produced hydrogen with $TiO_2$/Pt nanotubes supported on a fluorine doped tin oxide (FTO) glass [84]. Ma et al. generated hydrogen with a $Er^{3+}$:$YAlO_3$Pt-$TiO_2$ composite on a glass substrate [85]. Della Foglia immobilized $TiO_2$/Pt on glass fibers for photo-steam reforming of low molecular weight alcohols [86]. Wu et al. obtained hydrogen using immobilized $TiO_2$/Pt and $TiO_2$/Pd on cellulose membranes [87].

Polymeric membranes have been used as photocatalyst support [88–90]. However, most of the polymer materials were damaged by UV irradiation. In order to overcome this problem, polytetrafluoroethylene (PTFE) has been used as photocatalyst support due to its photochemical resistance [91,92]. Sulfonated polytetrafluoroethylene (Nafion) is a polymer which is resistant to photochemical degradation and is a proton ($H^+$) conductor due to the sulfonic acid groups attached to the PTFE backbone [93–95]. Therefore, it could be a good candidate to act as photocatalyst support. Nafion has been used in the photocatalytic degradation of pollutants as a support membrane for the photocatalyst [88,89,96] as well as photocatalyst coating to improve the degradation of cationic molecules due to its anionic character [97,98]. Regarding photocatalytic hydrogen production, Nafion

has been used as a matrix to attach photocatalysts with visible light photosensitizers [99,100] and as a proton exchange membrane in H-type reactors. Nafion membranes should be investigated as photocatalyst support in hydrogen production. The simplest immobilization techniques such as spraying, dip coating and solvent casting are a reasonable starting point.

## 1.5. Hydrogenase mimic catalyst combined with quantum dots photosensitizers

Homogeneous catalysts can provide high hydrogen production rates. Among them, hydrogenases are promising catalysts with good hydrogen production performance [101,102]. Hydrogenases in nature are enzymes composed of metal complexes of Fe and/or Ni, synthesized from certain bacteria and algae which catalyze the reversible redox reaction of $H^+$ to $H_2$ [103–105]. Among hydrogenases, [Fe-Fe]$H_2$-ases have shown very high production activity of hydrogen, about 6000-9000 $H_2$ molecules per second per active site [103,106–108]. Therefore, they have been studied in the last decades and they have awakened the interest on the synthesis of biomimetic molecules [109–114].

[Fe-Fe]$H_2$-ases photocatalytic hydrogen production systems containing metal complexes, such a $[Ru(bpy)_3]^{2+}$ (bpy = 2,2'-bipyridine) or [Re(4,4´-dimethylbpy)$(CO)_3]^+$ [115–119] or organic dyes such a Eosin Y or Rose Bengal as photosensitizers have been extensively studied [111,120,121]. But the main drawbacks are the fast photocatalytic decay during the process, and their narrow wavelength absorption range. In order to overcome this problem, quantum dot (QD) semiconductors have been studied as photosensitizers in [Fe-Fe]$H_2$-ase hydrogen production systems

[122–130]. QDs are particles smaller than 10 nm of diameter whose band gap can be tuned by modifying their particle size [131–133]. The small particle size can contribute to enhance electron transfer rate and their tunable band gap can make them active under visible light. Jian et al. [129] compared, for the same aqueous system, the performance as photosensitizer of $Ru(bpy)_3^{2+}$ and CdSe QDs achieving a hydrogen production rate of 301 and 20840 mmol $H_2 \cdot g_{cat}^{-1} \cdot h^{-1}$, respectively, and duplicating the stability of the system.

The selection of the QD material is still a challenge. Cadmium chalcogenides, such as CdS, CdSe, and CdTe, are good candidates due to their response to visible light and the relative position of their energy bands which generally provides a high driving force to electron transfer favoring higher hydrogen production rates. Although CdS also has response to visible light, its band gap is higher than that of CdSe and CdTe, functioning in a narrower range of the visible spectrum. Therefore, CdSe and CdTe are commonly used. CdSe has been used as photosensitizer for hydrogen generation in combination with real hydrogenases, hydrogenase mimics and even with bacteria that produce hydrogenases [122,125,139–141,126,127,129,134–138]. CdTe has been also used with this purpose [123,142–146]. The different performance of both sensitizers has not been clarified so far in the existing works mainly due to the different experimental conditions.

## 1.6. Framework and objectives of the thesis

This work focuses on the advancement of photocatalytic hydrogen production systems, starting with the synthesis and characterization of high-performance materials. It is based on the wide experience of the

research group in the modification of photocatalysts for degradation of emerging pollutants and in the development of membranes for different applications. The scope of this thesis is the application of different strategies to increase the knowledge needed for process design and optimization of more technical and cost-effective systems for the photocatalytic hydrogen production from liquid wastes and residues.

The three main objectives of this thesis are:

- Improving the photocatalytic hydrogen production performance of $TiO_2$ combining it with noble metal free materials. rGO/$TiO_2$ composite was synthetized because GO nanosheets can improve the $TiO_2$ photoactivity due to its ability to trap electrons from the conduction band, reducing the electron-hole recombination rate of $TiO_2$.
- Evaluating different methods of photocatalyst immobilization on polymeric membranes to avoid the necessity of the separation and recovery of the photocatalyst from the treated solution after the process.
- In order to move towards achieving high hydrogen production rates under visible light irradiation, hybrid systems were studied using biomimic [Fe-Fe]$H_2$-ase as catalyst and chalcogenides QDs as photosensitizers. The performance of CdSe and CdTe as photosensitizers have been evaluated.

## 1.7. References

[1] The Intergovernmental Panel on Climate Change (IPCC), Global Warming of 1.5°C. An IPCC Special Report on the impacts of

global warming of 1.5°C above pre-industrial levels and related global greenhouse gas emission pathways, in the context of strengthening the global response to the threat of climate change, World Meteorological Organization, Geneva, Switzerland, 2018.

[2] National Centers for Environmental (NOAA), State of the Climate: Global Climate Report for Annual 2020, 2020.

[3] United Nations, Paris Agreement, Paris, 2015.

[4] International Energy Agency (IEA), Global $CO_2$ emissions in 2019, 2020. https://www.iea.org/articles/global-co2-emissions-in-2019 (accesed 09/04/2021)

[5] K. Hashimoto, Global Carbon Dioxide Recycling For Global Sustainable Development by Renewable Energy, Springer, Singapore, 2019.

[6] R. Guerrero-Lemus, J.M. Martínez-Duart, Renewable Energies and $CO_2$, Springer, London, 2013.

[7] K. Ota, S. Mitsushima, K. Matsuzawa, A. Ishihara, Assessing the environmental impact of hydrogen energy production, in: A. Basile, A. Iulianelli (Eds.), Advances in Hydrogen Production, Storage and Distribution, Woodhead Publishing, Cambridge, 2014, pp.: 32-42.

[8] P. Nikolaidis, A. Poullikkas, A comparative overview of hydrogen production processes, Renew. Sustain. Energy Rev. 67 (2017) 597–611.

[9] F. Dawood, M. Anda, G.M. Shafiullah, Hydrogen production for energy: An overview, Int. J. Hydrogen Energy. 45 (2020) 3847–3869.

[10] M.A. Rosen, S. Koohi-Fayegh, The prospects for hydrogen as an energy carrier: an overview of hydrogen energy and hydrogen energy systems, Energy, Ecol. Environ. 1 (2016) 10–29.

[11] I. Dincer, Green methods for hydrogen production, Int. J. Hydrogen Energy. 37 (2012) 1954–1971.

[12] Gobierno de España, Hoja de ruta del hidrógeno: una apuesta por el hidrógeno (Hoja de ruta España 2020) 2020. https://energia.gob.es/es-es/Novedades/Paginas/publicacion-hoja-de-ruta-del-hidrogeno-apuesta-hidrogeno-renovable.aspx (accesed 12/02/2021)

[13] J.D. Holladay, J. Hu, D.L. King, Y. Wang, An overview of hydrogen production technologies, Catal. Today. 139 (2009) 244–260.

[14] M. Cargnello, T. Montini, S.Y. Smolin, J.B. Priebe, J.J. Delgado-Jaén, V.V.T. Doan-Nguyen, I.S. McKay, J.A. Schwalbe, M.M. Pohl, T.R. Gordon, Y. Lu, J.B. Baxter, A. Brückner, P. Fornasiero, C.B. Murray, Engineering titania nanostructure to tune and improve its photocatalytic activity, Proc. Natl. Acad. Sci. U. S. A. 113 (2016) 3966–3971.

[15] C. García-Mendoza, S. Oros-Ruiz, S. Ramírez-Rave, G. Morales-Mendoza, R. López, R. Gómez, Synthesis of $Bi_2S_3$ nanorods supported on $ZrO_2$ semiconductor as an efficient photocatalyst for hydrogen production under UV and visible light, J. Chem. Technol. Biotechnol. 92 (2017) 1503–1510.

[16] C. Acar, I. Dincer, Comparative assessment of hydrogen production methods from renewable and non-renewable sources, Int. J.

Hydrogen Energy. 39 (2014) 1–12.

[17] S.M. Saba, M. Mu, M. Robinius, D. Stolten, The investment costs of electrolysis - A comparison of cost studies from the past 30 years, Int. J. Hydrogen Energy. 43 (2018) 1209–1223.

[18] A. Buttler, H. Spliethoff, Current status of water electrolysis for energy storage, grid balancing and sector coupling via power-to-gas and power-to-liquids: A review, Renew. Sustain. Energy Rev. 82 (2018) 2440–2454.

[19] O.A. Sosa, Diseño y caracterización de electrolizador alcalino para enriquecimiento de diésel, PhD thesis, Universidad de Quintana Roo, Chetumal, 2018.

[20] K. Scott, Introduction to Electrolysis, Electrolysers and Hydrogen Production, in: Electrochemical Methods for Hydrogen Production, RSC, 2019, pp. 1–27.

[21] A. V. Puga, Photocatalytic production of hydrogen from biomass-derived feedstocks, Coord. Chem. Rev. 315 (2016) 1–66.

[22] S.S. Mao, S. Shen, L. Guo, Nanomaterials for renewable hydrogen production, storage and utilization, Prog. Nat. Sci. Mater. Int. 22 (2012) 522–534.

[23] Y. Miseki, K. Sayama, Photocatalytic Water Splitting for Solar Hydrogen Production Using the Carbonate Effect and the Z-Scheme Reaction, Adv. Energy Mater. 1801294 (2018).

[24] J.M. Coronado, A Historical Introduction to Photocatalysis, in: J.M. Coronado, F. Fresno, M.D. Hernández-Alonso, R. Portela (Eds.), Desing of Advanced Photocatalytic Materials for Energy and Environmental Applications, Springer, London, 2013, pp.: 1-4

[25] A. Eibner, Action of light pigments I, Chem-Ztg. 35 (1911) 753–755.

[26] M. Landau, Le phénomène de la photocatalyse, Compt Rend. 156 (1913) 1894–1896.

[27] L. Bruner, J. Kozack, Information on the photocatalysis I the light reaction in uranium salt plus oxalic acid mixtures, Z Elktrochem Angew P. 17 (1911) 354–360.

[28] A. Salinaro, A. V Emeline, J. Zhao, H. Hidaka, V.K. Ryabchuk, N. Serpone, Terminology, relative photonic efficiencies and quantum yields in heterogeneous photocatalysis. Part II: Experimental determination of quantum yields, Pure & Appl. Chem. 71 (1999) 321–335.

[29] D.D. Dionysiou, G.L. Puma, J. Ye, J. Schneider, D. Bahnemann, Photocatalysis Applications, The Royal Society of Chemistry, London, 2016.

[30] R. Ratshiedana, A.T. Kuvarega, A.K. Mishra, Titanium dioxide and graphitic carbon nitride–based nanocomposites and nanofibres for the degradation of organic pollutants in water: a review, Environ. Sci. Pollut. Res. (2021) (In press).

[31] Y. Chen, X. Duan, X. Zhou, R. Wang, S. Wang, N. Ren, S.-H. Ho, Advanced oxidation processes for water disinfection: Features, mechanisms and prospects, Chem. Eng. J. 409 (2021) 128207.

[32] A.H. Mamaghani, F. Haghighat, C.S. Lee, Hydrothermal/solvothermal synthesis and treatment of $TiO_2$ for photocatalytic degradation of air pollutants: Preparation, characterization, properties, and performance, Chemosphere. 219

(2019) 804–825.

[33] S. Weon, F. He, W. Choi, Status and challenges in photocatalytic nanotechnology for cleaning air polluted with volatile organic compounds: Visible light utilization and catalyst deactivation, Environ. Sci. Nano. 6 (2019) 3185–3214.

[34] A. Mancuso, O. Sacco, D. Sannino, V. Venditto, V. Vaiano, One-step catalytic or photocatalytic oxidation of Benzene to phenol: Possible alternative routes for phenol synthesis, Catalysts. 10 (2020) 1424.

[35] H.K. Wu, F. Zhang, J.Y. Li, Z.R. Tang, Y.J. Xu, Photo-driven Fischer-Tropsch synthesis, J. Mater. Chem. A. 8 (2020) 24253–24266.

[36] J. Corredor, M.J. Rivero, C.M. Rangel, F. Gloaguen, I. Ortiz, Comprehensive review and future perspectives on the photocatalytic hydrogen production, J. Chem. Technol. Biotechnol. 94 (2019) 3049–3063.

[37] J. Schneider, D.W. Bahnemann, Undesired Role of Sacrificial Reagents in Photocatalysis, J. Phys. Chem. Lett. 4 (2013) 3479–3483.

[38] M. Yasuda, T. Matsumoto, T. Yamashita, Sacrificial hydrogen production over $TiO_2$-based photocatalysts: Polyols, carboxylic acids, and saccharides, Renew. Sustain. Energy Rev. 81 (2018) 1627–1635.

[39] E. Pulido Melián, C.R. López, D.E. Santiago, R. Quesada-Cabrera, J.A. Ortega Méndez, J.M. Doña-Rodríguez, O. González Díaz, Study of the photocatalytic activity of Pt-modified commercial

$TiO_2$ for hydrogen production in the presence of common organic sacrificial agents, Appl. Catal. A Gen. 518 (2016) 189–197.

[40] H. Yi, D. Huang, L. Qin, G. Zeng, C. Lai, M. Cheng, S. Ye, B. Song, X. Ren, X. Guo, Selective prepared carbon nanomaterials for advanced photocatalytic application in environmental pollutant treatment and hydrogen production, Appl. Catal. B Environ. 239 (2018) 408–424.

[41] A. Fujishima, K. Honda, Electrochemical photolysis of water at a semiconductor electrode, Nature. 238 (1972) 37–38.

[42] C.R. López, E.P. Melián, J.A. Ortega Méndez, D.E. Santiago, J.M. Doña Rodríguez, O. González Díaz, Comparative study of alcohols as sacrificial agents in $H_2$ production by heterogeneous photocatalysis using Pt/$TiO_2$ catalysts, J. Photochem. Photobiol. A Chem. 312 (2015) 45–54.

[43] P. Ribao, M. Alexandra Esteves, V.R. Fernandes, M.J. Rivero, C.M. Rangel, I. Ortiz, Challenges arising from the use of $TiO_2$/rGO/Pt photocatalysts to produce hydrogen from crude glycerol compared to synthetic glycerol, Int. J. Hydrogen Energy. 44 (2019) 28494–28506.

[44] M.R. Hoffmann, S.T. Martin, W. Choi, D.W. Bahnemann, Environmental Applications of Semiconductor Photocatalysis, Chem. Rev. 95 (1995) 69–96.

[45] J.M. Coronado, Photons, electrons and holes: fundamentals of Photocatalysis with semiconductors, in: J.M.. Coronado, F. Fresno, M. Hernández-Alonso, P. R (Eds.), Desing of Advanced Photocatalytic Materials for Energy and Environmental

Applications, Springer, London, 2013, pp.: 35–67.

[46] P. Atkins, J. de Paula, Physical Chemistry, 8th ed., W. H. Freeman and Company, New York, 2006.

[47] T. Stoll, C.E. Castillo, M. Kayanuma, M. Sandroni, C. Daniel, F. Odobel, J. Fortage, M.N. Collomb, Photo-induced redox catalysis for proton reduction to hydrogen with homogeneous molecular systems using rhodium-based catalysts, Coord. Chem. Rev. 304–305 (2015) 20-37.

[48] K.C. Christoforidis, P. Fornasiero, Photocatalytic Hydrogen production: A rift into the future energy supply, ChemCatChem. 9 (2017) 1523–1544.

[49] S. Oros-Ruiz, A. Hernández-Gordillo, C. García-Mendoza, A.A. Rodríguez-Rodríguez, R. Gómez, Comparative activity of CdS nanofibers superficially modified by Au, Cu, and Ni nanoparticles as co-catalysts for photocatalytic hydrogen production under visible light, J. Chem. Technol. Biotechnol. 91 (2016) 2205–2210.

[50] F. Mei, J. Zhang, K. Dai, G. Zhu, C. Liang, A Z-scheme $Bi_2MoO_6$/CdSe-diethylenetriamine heterojunction for enhancing photocatalytic hydrogen production activity under visible light, Dalt. Trans. 48 (2019) 1067–1074.

[51] D. Guerrero-Araque, P. Acevedo-Peña, D. Ramírez-Ortega, L. Lartundo-Rojas, R. Gómez, $SnO_2$–$TiO_2$ structures and the effect of CuO, CoO metal oxide on photocatalytic hydrogen production, J. Chem. Technol. Biotechnol. 92 (2017) 1531–1539.

[52] T. Montalvo-Herrera, D. Sánchez-Martínez, D.B. Hernandez-Uresti, E. Zarazua-Morin, Facile preparation of $KBiO_3$/g-$C_3N_4$

composites with microwave irradiation for photocatalytic hydrogen production, J. Chem. Technol. Biotechnol. 94 (2019) 3440-3446.

[53] S. Cao, J. Yu, g-$C_3N_4$-based photocatalysts for hydrogen generation, J. Phys. Chem. Lett. 5 (2014) 2101–2107.

[54] X. Wang, K. Maeda, A. Thomas, K. Takanabe, G. Xin, J.M. Carlsson, K. Domen, M. Antonietti, A metal-free polymeric photocatalyst for hydrogen production from water under visible light, Nat. Mater. 8 (2009) 76–80.

[55] N.F.F. Moreira, M.J. Sampaio, A.R. Ribeiro, C.G. Silva, J.L. Faria, A.M.T. Silva, Metal-free g-$C_3N_4$ photocatalysis of organic micropollutants in urban wastewater under visible light, Appl. Catal. B Environ. 248 (2019) 184–192.

[56] W.J. Chun, A. Ishikawa, H. Fujisawa, T. Takata, J.N. Kondo, M. Hara, M. Kawai, Y. Matsumoto, K. Domen, Conduction and valence band positions of $Ta_2O_5$, TaOn, and $Ta_3N_5$ by UPS and electrochemical methods, J. Phys. Chem. B. 107 (2003) 1798–1803.

[57] J. Hua, M. Wang, Y. Jiao, H. Li, Y. Yang, Strongly coupled CdX (X=S, Se and Te) quantum dots/$TiO_2$ nanocomposites for photocatalytic degradation of benzene under visible light irradiation, Optik (Stuttg). 171 (2018) 95–106.

[58] R. Bin Wei, Z.L. Huang, G.H. Gu, Z. Wang, L. Zeng, Y. Chen, Z.Q. Liu, Dual-cocatalysts decorated rimous CdS spheres advancing highly-efficient visible-light photocatalytic hydrogen production, Appl. Catal. B Environ. 231 (2018) 101–107.

[59] X.R. Cao, G.H. Tian, Y.J. Chen, J. Zhou, W. Zhou, C.G. Tian, H.G.

Fu, Hierarchical composites of $TiO_2$ nanowire arrays on reduced graphene oxide nanosheets with enhanced photocatalytic hydrogen evolution performance, J. Mater. Chem. A. 2 (2014) 4366–4374.

[60] J. Chen, Z. Hong, Y. Chen, B. Lin, B. Gao, One-step synthesis of sulfur-doped and nitrogen-deficient g-$C_3N_4$ photocatalyst for enhanced hydrogen evolution under visible light, Mater. Lett. 145 (2015) 129–132.

[61] K. Maeda, K. Teramura, D. Lu, T. Takata, N. Saito, Y. Inoue, K. Domen, Photocatalyst releasing hydrogen from water, Nature. 440 (2006) 295.

[62] C. Byrne, G. Subramanian, S.C. Pillai, Recent advances in photocatalysis for environmental applications, J. Environ. Chem. Eng. 6 (2018) 3531–3555.

[63] P. Ribao, M.J. Rivero, I. Ortiz, Enhanced photocatalytic activity using GO/$TiO_2$ catalyst for the removal of DCA solutions, Environ. Sci. Pollut. Res. 25 (2018) 34893–34902.

[64] S.Y. Mendiola-Alvarez, J.L. Guzmán-Mar, G. Turnes-Palomino, F. Maya-Alejandro, A. Hernández-Ramírez, L. Hinojosa-Reyes, UV and visible activation of Cr(III)-doped $TiO_2$ catalyst prepared by a microwave-assisted sol–gel method during MCPA degradation, Environ. Sci. Pollut. Res. 24 (2017) 12673–12682.

[65] P. Ribao, J. Corredor, M.J. Rivero, I. Ortiz, Role of reactive oxygen species on the activity of noble metal-doped $TiO_2$ photocatalysts, J. Hazard. Mater. 372 (2019) 45–51.

[66] N. Delegan, R. Daghrir, P. Drogui, M.A. El Khakani, Bandgap tailoring of in-situ nitrogen-doped $TiO_2$ sputtered films intended for

electrophotocatalytic applications under solar light, J. Appl. Phys. 116 (2014) 153510.

[67] Y. Liu, J. He, Y. Sun, J. Hu, C. Li, G. Xue, S. Ognier, A comparison of N-doped $TiO_2$ photocatalysts preparation methods and studies on their catalytic activity, J. Chem. Technol. Biotechnol. 88 (2013) 1815–1821.

[68] Y. Liu, G. Xu, H. Lv, Ag modified Fe-doping $TiO_2$ nanoparticles and nanowires with enhanced photocatalytic activities for hydrogen production and volatile organic pollutant degradation, J. Mater. Sci. Mater. Electron. 29 (2018) 10504–10516.

[69] Z. Jin, X. Zhang, G. Lu, S. Li, Improved quantum yield for photocatalytic hydrogen generation under visible light irradiation over eosin sensitized $TiO_2$-Investigation of different noble metal loading, J. Mol. Catal. A Chem. 259 (2006) 275–280.

[70] R. Daghrir, P. Drogui, D. Robert, Modified $TiO_2$ for environmental photocatalytic applications: A review, Ind. Eng. Chem. Res. 52 (2013) 3581–3599.

[71] S. Lee, S. Park, $TiO_2$ photocatalyst for water treatment applications, J. Ind. Eng. Chem. 19 (2013) 1761–1769.

[72] A. Tolosana-Moranchel, Application of photocatalytic processes for water treatment, PhD thesis, Universidad Autónoma de Madrid, Madrid, 2019.

[73] A. Tolosana-Moranchel, A. Manassero, M.L. Satuf, O.M. Alfano, J.A. Casas, A. Bahamonde, Influence of $TiO_2$-rGO optical properties on the photocatalytic activity and efficiency to photodegrade an emerging pollutant. Appl. Catal. B Environ. 2019,

246, 1–11.

[74] N.R. Khalid, A. Majid, M.B. Tahir, N.A. Niaz, S. Khalid, Carbonaceous-$TiO_2$ nanomaterials for photocatalytic degradation of pollutants: A review, Ceram. Int. 43 (2017) 14552–14571.

[75] M.J. Rivero, O. Iglesias, P. Ribao, I. Ortiz, Kinetic performance of $TiO_2$/Pt/reduced graphene oxide composites in the photocatalytic hydrogen production, Int. J. Hydrogen Energy. 44 (2019) 101–109.

[76] J. Jia, D. Li, J. Wan, X. Yu, Characterization and mechanism analysis of graphite/C-doped $TiO_2$ composite for enhanced photocatalytic performance, J. Ind. Eng. Chem. 33 (2016) 162–169.

[77] R. Leary, A. Westwood, Carbonaceous nanomaterials for the enhancement of $TiO_2$ photocatalysis, Carbon. 49 (2011) 741–772.

[78] O. Iglesias, M.J. Rivero, A.M. Urtiaga, I. Ortiz, Membrane-based photocatalytic systems for process intensification, Chem. Eng. J. 305 (2016) 136–148.

[79] K. Ghasemzadeh, A.A. Babaluo, A. Aghaeinejad-Meybodi, Membrane reactors for the decomposition of $H_2O$, $NO_x$ and $CO_2$ to produce hydrogen, in: A. Basile, L. Di Paola, F. L. Hai, V. Piemonte (Eds) Membrane Reactors for Energy Applications and Basic Chemical Production, Woodhead Publishing, 2015, pp.:209-247.

[80] H. Shi, R. Magaye, V. Castranova, J. Zhao, Titanium dioxide nanoparticles: A review of current toxicological data, Part. Fibre Toxicol. 10 (2013) 15.

[81] A.Y. Shan, T.I.M. Ghazi, S.A. Rashid, Immobilisation of titanium dioxide onto supporting materials in heterogeneous photocatalysis: A review, Appl. Catal. A Gen. 389 (2010) 1–8.

[82] D. Wood, S. Shaw, T. Cawte, E. Shanen, B. Van Heyst, An overview of photocatalyst immobilization methods for air pollution remediation, Chem. Eng. J. 391 (2020) 123490.

[83] C.S. Lugo-Vega, B. Serrano-Rosales, H. de Lasa, Immobilized particle coating for optimum photon and $TiO_2$ utilization in scaled air treatment photo reactors, Appl. Catal. B Environ. 198 (2016) 211–223.

[84] G. Cha, M. Altomare, N.N. Truong, N. Taccardi, K. Lee, P. Schmuki, Double-Side Co-Catalytic Activation of Anodic $TiO_2$ Nanotube Membranes with Sputter-Coated Pt for Photocatalytic $H_2$ Generation from Water/Methanol Mixtures, Chem. - An Asian J. 12 (2017) 314–323.

[85] C. Ma, Y. Li, H. Zhang, Y. Chen, C. Lu, J. Wang, Photocatalytic hydrogen evolution with simultaneous photocatalytic reforming of biomass by $Er_{3+}$: $YAlO_3$/Pt-$TiO_2$membranes under visible light driving, Chem. Eng. J. 273 (2015) 277–285.

[86] F. Della Foglia, G.L. Chiarello, M.V. Dozzi, P. Piseri, L.G. Bettini, S. Vinati, C. Ducati, P. Milani, E. Selli, Hydrogen production by photocatalytic membranes fabricated by supersonic cluster beam deposition on glass fiber filters, Int. J. Hydrogen Energy. 39 (2014) 13098–13104.

[87] M.C. Wu, A. Sápi, A. Avila, M. Szabó, J. Hiltunen, M. Huuhtanen, G. Tóth, Á. Kukovecz, Z. Kónya, R. Keiski, W.F. Su, H. Jantunen, K. Kordás, Enhanced Photocatalytic Activity of $TiO_2$ Nanofibers and Their Flexible Composite Films: Decomposition of Organic Dyes and Efficient $H_2$ Generation from Ethanol-Water Mixtures, Nano Res. 4 (2011) 360–369.

[88] S. Filice, D. D'Angelo, S. Libertino, I. Nicotera, V. Kosma, V. Privitera, S. Scalese, Graphene oxide and titania hybrid Nafion membranes for efficient removal of methyl orange dye from water, Carbon N. Y. 82 (2015) 489–499.

[89] D. D'Angelo, S. Filice, S. Libertino, V. Kosma, I. Nicotera, V. Privitera, S. Scalese, Photocatalytic properties of Nafion membranes containing graphene oxide/titania nanocomposites, in: 2014 IEEE 9th Nanotechnol. Mater. Devices Conf. NMDC 2014, IEEE, Aci Castello, Italy, 2014.

[90] M. Romay, N. Diban, M.J. Rivero, A. Urtiaga, I. Ortiz, Critical Issues and Guidelines to Improve the Performance of Photocatalytic Polymeric Membranes, Catalysts. 10 (2020) 570.

[91] D.E. Tsydenov, V.N. Parmon, A. V. Vorontsov, Toward the design of asymmetric photocatalytic membranes for hydrogen production: Preparation of $TiO_2$-based membranes and their properties, Int. J. Hydrogen Energy. 37 (2012) 11046–11060.

[92] D.E. Tsydenov, A. V. Vorontsov, Influence of Nafion loading on hydrogen production in a membrane photocatalytic system, J. Photochem. Photobiol. A Chem. 297 (2015) 8–13.

[93] W.Y. Wang, Y. Ku, Effect of solution pH on the adsorption and photocatalytic reaction behaviors of dyes using $TiO_2$ and Nafion-coated $TiO_2$, Colloids Surfaces A Physicochem. Eng. Asp. 302 (2007) 261-268.

[94] A. Kusoglu, A.Z. Weber, New Insights into Perfluorinated Sulfonic-Acid Ionomers, Chem. Rev. 117 (2017) 987–1104.

[95] F.C. Teixeira, A.I. de Sá, A.P.S. Teixeira, V.M. Ortiz-Martínez, A.

Ortiz, I. Ortiz, C.M. Rangel, New modified Nafion-bisphosphonic acid composite membranes for enhanced proton conductivity and PEMFC performance, Int. J. Hydrogen Energy. (2020) (In press).

[96] X. Ding, S. Zhou, L. Jiang, H. Yang, Preparation, photocatalytic activity and mechanism of nano-Titania/Nafion hybrid membrane, J. Sol-Gel Sci. Technol. 58 (2011) 345–354.

[97] M.S. Vohra, K. Tanaka, Enhanced photocatalytic activity of nafion-coated $TiO_2$, Environ. Sci. Technol. 35 (2001) 411–415.

[98] H. Park, W. Choi, Photocatalytic reactivities of nafion-coated $TiO_2$ for the degradation of charged organic compounds under UV or visible light, J. Phys. Chem. B. 109 (2005) 11667–11674.

[99] W. Choi, Photocatalytic hydrogen production using surface-modified titania nanoparticles, Sol. Hydrog. Nanotechnol. II, SPIE, San Diego, U.S.A., 2007.

[100] H. Park, Y. Park, E. Bae, W. Choi, Photoactive component-loaded Nafion film as a platform of hydrogen generation: Alternative utilization of a classical sensitizing system, J. Photochem. Photobiol. A Chem. 203 (2009) 112–118.

[101] M. Trincado, D. Banerjee, H. Grützmacher, Molecular catalysts for hydrogen production from alcohols, Energy Environ. Sci. 7 (2014) 2464–2503.

[102] S. Fukuzumi, Y.M. Lee, W. Nam, Thermal and photocatalytic production of hydrogen with earth-abundant metal complexes, Coord. Chem. Rev. 355 (2018) 54–73.

[103] R.X. Li, X.T. Ren, M.Y. Tang, M.X. Chen, G.B. Huang, C.H. Fang, T. Liu, Z.H. Feng, Y.B. Yin, Y.M. Guo, S.K. Mei, J. Yan,

Fabrication of covalently linked graphene-mediated [FeFe]-hydrogenases biomimetic photocatalytic hydrogen evolution system in aqueous solution, Appl. Catal. B Environ. 224 (2018) 772–782.

[104] F. Wang, W.G. Wang, H.Y. Wang, G. Si, C.H. Tung, L.Z. Wu, Artificial photosynthetic systems based on [FeFe]-hydrogenase mimics: The road to high efficiency for light-driven hydrogen evolution, ACS Catal. 2 (2012) 407–416.

[105] E.B. Hemming, B. Chan, P. Turner, L. Corcilius, J.R. Price, M.G. Gardiner, A.F. Masters, T. Maschmeyer, [$Fe(C_5Ar_5)(CO)_2Br$] complexes as hydrogenase mimics for the catalytic hydrogen evolution reaction, Appl. Catal. B Environ. 223 (2018) 234–241.

[106] F. Wittkamp, M. Senger, S.T. Stripp, U.P. Apfel, [FeFe]-Hydrogenases: Recent developments and future perspectives, Chem. Commun. 54 (2018) 5934–5942.

[107] S.T. Stripp, T. Happe, How algae produce hydrogen—news from the photosynthetic hydrogenase, Dalt. Trans. (2009) 9960–9969.

[108] W. Wang, X.W. Song, Z. Hong, B. Li, Y. Si, C. Ji, K. Su, Y. Tan, Z. Ju, Y. Huang, C.N. Chen, D. Yuan, Incorporation of iron hydrogenase active sites into a stable photosensitizing metal-organic framework for enhanced hydrogen production, Appl. Catal. B Environ. 258 (2019) 117979.

[109] J.F. Capon, F. Gloaguen, P. Schollhammer, J. Talarmin, Electrochemical proton reduction by thiolate-bridged hexacarbonyldiiron clusters, J. Electroanal. Chem. 566 (2004) 241–247.

[110] F. Quentel, G. Passard, F. Gloaguen, Electrochemical hydrogen production in aqueous micellar solution by a diiron benzenedithiolate complex relevant to [FeFe] hydrogenases, Energy Environ. Sci. 5 (2012) 7757–7761.

[111] C. Orain, F. Quentel, F. Gloaguen, Photocatalytic Hydrogen Production Using Models of the Iron-Iron Hydrogenase Active Site Dispersed in Micellar Solution, ChemSusChem. 7 (2014) 638–643.

[112] S. Roy, T.L. Groy, A.K. Jones, Biomimetic model for [FeFe]-hydrogenase: asymmetrically disubstituted diiron complex with a redox-active 2,2′-bipyridyl ligand, Dalt. Trans. 42 (2013) 3843–3853.

[113] T. Liu, M.Y. Darensbourg, A mixed-valent, Fe(II)Fe(I), diiron complex reproduces the unique rotated state of the [FeFe]hydrogenase active site, J. Am. Chem. Soc. 129 (2007) 7008–7009.

[114] M.E. Ahmed, S. Dey, M.Y. Darensbourg, A. Dey, Oxygen-Tolerant $H_2$ Production by [FeFe]-$H_2$ase Active Site Mimics Aided by Second Sphere Proton Shuttle, J. Am. Chem. Soc. 140 (2018) 12457–12468.

[115] Y. Na, M. Wang, J. Pan, P. Zhang, B. Åkermark, L. Sun, Visible light-driven electron transfer and hydrogen generation catalyzed by bioinspired [2Fe2S] complexes, Inorg. Chem. 47 (2008) 2805–2810.

[116] H.-Y. Wang, W.-G. Wang, G. Si, F. Wang, C.-H. Tung, L.-Z. Wu, Photocatalytic Hydrogen Evolution from Rhenium(I) Complexes to [FeFe] Hydrogenase Mimics in Aqueous SDS Micellar Systems: A

Biomimetic Pathway, Langmuir. 26 (2010) 9766–9771.

[117] D. Streich, Y. Astuti, M. Orlandi, L. Schwartz, R. Lomoth, L. Hammarström, S. Ott, High-turnover photochemical hydrogen production catalyzed by a model complex of the [FeFe]-hydrogenase active site, Chem. Eur. J. 16 (2010) 60–63.

[118] S. Pullen, H. Fei, A. Orthaber, S.M. Cohen, S. Ott, Enhanced photochemical hydrogen production by a molecular diiron catalyst incorporated into a metal-organic framework, J. Am. Chem. Soc. 135 (2013) 16997–17003.

[119] T. Yu, Y. Zeng, J. Chen, Y.Y. Li, G. Yang, Y.Y. Li, T. Yu, Y. Zeng, J. Chen, Y.Y. Li, G. Yang, Exceptional dendrimer-based mimics of diiron hydrogenase for the photochemical production of hydrogen, Angew. Chemie Int. Ed. 52 (2013) 5631–5635.

[120] C. Supplis, F. Gros, G. Dahi, J. Dauchet, M. Roudet, F. Gloaguen, J.F. Cornet, Spectral radiative analysis of bio-inspired $H_2$ production in a benchmark photoreactor: A first investigation using spatial photonic balance, Int. J. Hydrogen Energy. 43 (2018) 8221–8231.

[121] X. Li, M. Wang, L. Chen, X. Wang, J. Dong, L. Sun, Photocatalytic water reduction and study of the formation of Fe $^{I}Fe^{0}$ species in diiron catalyst sytems, ChemSusChem. 5 (2012) 913–919.

[122] F. Wang, W.J. Liang, J.X. Jian, C.B. Li, B. Chen, C.H. Tung, L.Z. Wu, Exceptional poly(acrylic acid)-based artificial [FeFe]-hydrogenases for photocatalytic $H_2$ production in water, Angew. Chemie Int. Ed. 52 (2013) 8134–8138.

[123] F. Wang, W.G. Wang, X.J. Wang, H.Y. Wang, C.H. Tung, L.Z.

Wu, A highly efficient photocatalytic system for hydrogen production by a robust hydrogenase mimic in an aqueous solution, Angew. Chemie Int. Ed. 50 (2011) 3193–3197.

[124] X.W. Song, H.M. Wen, C.B. Ma, M.Q. Hu, H. Chen, H.H. Cui, C.N. Chen, Photocatalytic hydrogen evolution by two comparable [FeFe]-hydrogenase mimics assembled to the surface of ZnS, Appl. Organomet. Chem. 28 (2014) 267–273.

[125] W.J. Liang, F. Wang, M. Wen, J.X. Jian, X.Z. Wang, B. Chen, C.H. Tung, L.Z. Wu, Branched polyethylenimine improves hydrogen photoproduction from a CdSe quantum dot/[FeFe]-hydrogenase mimic system in neutral aqueous solutions, Chem. Eur. J. 21 (2015) 3187–3192.

[126] S. Troppmann, B. König, Functionalized Vesicles with Co-Embedded CdSe Quantum Dots and [FeFe]-Hydrogenase Mimic for Light-Driven Hydrogen Production, ChemistrySelect. 1 (2016) 1405–1409.

[127] M. Wen, X.B. Li, J.X. Jian, X.Z. Wang, H.L. Wu, B. Chen, C.H. Tung, L.Z. Wu, Secondary coordination sphere accelerates hole transfer for enhanced hydrogen photogeneration from [FeFe]-hydrogenase mimic and CdSe QDs in water, Sci. Rep. 6 (2016) 29851.

[128] M. Wen, H.-L. Wu, J.-X. Jian, X.-Z. Wang, X.-B. Li, B. Chen, C.-H. Tung, L.-Z. Wu, Integrating CdSe Quantum Dots with a [FeFe]-Hydrogenase Mimic into a Photocathode for Hydrogen Evolution at a Low Bias Voltage, ChemPhotoChem. 1 (2017) 260–264.

[129] J.-X. Jian, C. Ye, X.-Z. Wang, M. Wen, Z.-J. Li, X.-B. Li, B. Chen,

C.-H. Tung, L.-Z. Wu, Comparison of $H_2$ photogeneration by [FeFe]-hydrogenase mimics with CdSe QDs and $Ru(bpy)_3$ $Cl_2$ in aqueous solution, Energy Environ. Sci. 9 (2016) 2083–2089.

[130] M. Wang, K. Han, S. Zhang, L. Sun, Integration of organometallic complexes with semiconductors and other nanomaterials for photocatalytic $H_2$ production, Coord. Chem. Rev. 287 (2015) 1–14.

[131] J. Yang, H. Miao, J. Jing, Y. Zhu, W. Choi, Photocatalytic activity enhancement of PDI supermolecular via π-π action and energy level adjusting with graphene quantum dots, Appl. Catal. B Environ. 281 (2021) 119547.

[132] L.K. Putri, B.J. Ng, W.J. Ong, H.W. Lee, W.S. Chang, A.R. Mohamed, S.P. Chai, Energy level tuning of CdSe colloidal quantum dots in ternary 0D-2D-2D CdSe QD/B-rGO/O-$gC_3N_4$ as photocatalysts for enhanced hydrogen generation, Appl. Catal. B Environ. 265 (2020) 118592.

[133] J. Cassidy, M. Zamkov, Nanoshell quantum dots: Quantum confinement beyond the exciton Bohr radius, J. Chem. Phys. 152 (2020) 110902.

[134] M.L.K. Sanchez, C.H. Wu, M.W.W. Adams, R. B. Dyer, Optimizing electron transfer from CdSe QDs to hydrogenase for photocatalytic $H_2$ production, Chem. Commun. 55 (2019) 5579–5582.

[135] M.L.K. Sanchez, C. Sommer, E. Reijerse, J.A. Birrell, W. Lubitz, R.B. Dyer, Investigating the Kinetic Competency of CrHydA1 [FeFe] Hydrogenase Intermediate States via Time-Resolved Infrared Spectroscopy, J. Am. Chem. Soc. 141 (2019) 16064–

16070.

[136] B. Chica, C.H. Wu, Y. Liu, M.W.W. Adams, T. Lian, R.B. Dyer, Balancing electron transfer rate and driving force for efficient photocatalytic hydrogen production in CdSe/CdS nanorod-[NiFe] hydrogenase assemblies, Energy Environ. Sci. 10 (2017) 2245–2255.

[137] C. Hamon, A. Ciaccafava, P. Infossi, R. Puppo, P. Even-Hernandez, E. Lojou, V. Marchi, Synthesis and enzymatic photo-activity of an $O_2$tolerant hydrogenase-CdSe@CdS quantum rod bioconjugate, Chem. Commun. 50 (2014) 4989–4992.

[138] X.B. Li, J.X. Jian, X.Z. Wang, Y. Wang, S.G. Xia, C.H. Tung, L.Z. Wu, Per-6-Thiol-Cyclodextrin Engineered [FeFe]-Hydrogenase Mimic/CdSe Quantum Dot Assembly for Photocatalytic Hydrogen Production, Sol. RRL. (2020) 2000474.

[139] Y. Ding, J.R. Bertram, C. Eckert, R.R. Bommareddy, R. Patel, A. Conradie, S. Bryan, P. Nagpal, Nanorg Microbial Factories: Light-Driven Renewable Biochemical Synthesis Using Quantum Dot-Bacteria Nanobiohybrids, J. Am. Chem. Soc. 141 (2019) 10272–10282.

[140] M. Shen, W. Jia, Y. You, Y. Hu, F. Li, S. Tian, J. Li, Y. Jin, D. Han, Luminescent properties of CdTe quantum dots synthesized using 3-mercaptopropionic acid reduction of tellurium dioxide directly, Nanoscale Res. Lett. 8 (2013) 1–6.

[141] C.B. Li, Z.J. Li, S. Yu, G.X. Wang, F. Wang, Q.Y. Meng, B. Chen, K. Feng, C.H. Tung, L.Z. Wu, Interface-directed assembly of a simple precursor of [FeFe]-$H_2$ase mimics on CdSe QDs for

photosynthetic hydrogen evolution in water, Energy Environ. Sci. 6 (2013) 2597–2602.

[142] A.M. Wroblewska-Wolna, A.J. Harvie, S.F. Rowe, K. Critchley, J.N. Butt, L.J.C. Jeuken, Quantum dot interactions with and toxicity to Shewanella oneidensis MR-1, Nanotechnology. 31 (2020) 134005.

[143] K.A. Brown, Q. Song, D.W. Mulder, P.W. King, Diameter dependent electron transfer kinetics in semiconductor-enzyme complexes, ACS Nano. 8 (2014) 10790–10798.

[144] B.L. Greene, C.A. Joseph, M.J. Maroney, R.B. Dyer, Direct evidence of active-site reduction and photodriven catalysis in sensitized hydrogenase assemblies, J. Am. Chem. Soc. 134 (2012) 11108–11111.

[145] K.A. Brown, S. Dayal, X. Ai, G. Rumbles, P.W. King, Controlled assembly of hydrogenase-CdTe nanocrystal hybrids for solar hydrogen production, J. Am. Chem. Soc. 132 (2010) 9672–9680.

[146] J.X. Jian, Q. Liu, Z.J. Li, F. Wang, X.B. Li, C.B. Li, B. Liu, Q.Y. Meng, B. Chen, K. Feng, C.H. Tung, L.Z. Wu, Chitosan confinement enhances hydrogen photogeneration from a mimic of the diiron subsite of [FeFe]-hydrogenase, Nat. Commun. 4 (2013) 2695.

# 2. Materials and methods

This chapter briefly discusses the materials, the experimental part of the present thesis, specifies the procedure used to synthesize the photocatalysts, explains the methodology followed during the photocatalytic experiments and describes the analytical methods. More detailed information can be found in the scientific publications gathered in Chapter 3 of the present thesis document.

## 2.1. Chemicals

The main chemical reagents used in this thesis are summarized in Table 2.1. All chemicals were reagent grade or higher. All solutions were prepared using ultrapure water (Milli-Q, Millipore) with a resistivity of 18.2 MΩ·cm.

**Table 2.1.** List of chemical reagents

| Reagent | Formula | Abbreviation | Characteristics | Supplier |
|---|---|---|---|---|
| Methanol | $CH_4O$ | - | 99.9% | Scharlau |
| Isopropanol | $C_3H_8O$ | - | 99.5% | Acros Organics |
| Titanium dioxide Aeroxide P25 | $TiO_2$ | - | Anatase/Rutile 80/20 w/w | Evonik |
| Graphene oxide | C:O | GO | 4 mg/mL | Graphenea |
| Argon | Ar | - | pure 3X | Praxair |
| Nafion solution D2020 | $C_9HF_{17}O_5S$ | PFSA | 20% Nafion 44% 1-propanol 34% water | Ion Power |
| Nafion solution D520 | $C_9HF_{17}O_5S$ | PFSA | 5% Nafion 48% 1-propanol 45% water | Ion Power |
| Nafion N115 | $C_9HF_{17}O_5S$ | PFSA | 250 $g \cdot m^{-2}$ | Ion Power |
| Oleic acid | $C_{18}H_{34}O_2$ | OA | 90% | Sigma Aldrich |
| 1-octadene | $C_{18}H_{36}$ | ODE | 90% | Sigma Aldrich |

**Table 2.1. (cont.)** List of chemical reagents

| Reagent | Formula | Abbreviation | Characteristics | Supplier |
|---|---|---|---|---|
| L-Ascorbic acid | $C_6H_8O_6$ | - | 98+% | Alfa Aesar |
| Trioctylphosphine oxide | $C_{24}H_{51}OP$ | TOPO | 99% | Sigma Aldrich |
| Cadmium oxide | CdO | - | 99.5% | Sigma Aldrich |
| Tellurium powder | Te | - | 99.8% | Sigma Aldrich |
| Tributylphosphine | $C_{12}H_{27}OP$ | TBP | 97% | Sigma Aldrich |
| N-octadecylphosphonic acid | $C_{18}H_{39}O_3P$ | ODPA | 99+% | PCI |
| Trioctylphosphine | $C_{24}H_{51}P$ | TOP | 97% | Strem Chemicals Inc. |
| Chloroform | $CHCl_3$ | - | 98.9+% | ChemPure Chemicals |
| Selenium powder | Se | - | 99.99% | Beantown Chemicals |
| 3-mercaptopropionic acid | $C_3H_6O_2S$ | MPA | 99+% | Acros Organics |
| Sodium dodecyl sulfate | $C_{12}H_{25}NaO_4S$ | SDS | 10% | Life Technologies |
| Diiron nonacarbonyl | $Fe_2(CO)_9$ | - | 98% | Sigma Aldrich |
| Benzene-1,2-dithiol | $C_6H_6S_2$ | - | 96% | Sigma Aldrich |
| Tetrahydrofuran | $C_4H_8O$ | THF | 99.5+% | Sigma Aldrich |
| Hexane | $C_6H_{14}$ | - | 98.5+% | Sigma Aldrich |

## 2.2. Synthesis of the photocatalysts, catalysts and quantum dots

### 2.2.1. Synthesis of rGO/$TiO_2$ photocatalysts

rGO/$TiO_2$ photocatalysts were synthetized following the hydrothermal method illustrated in Figure 2.1. Composites with different percentages of GO, 1, 2, 5, and 10%, were synthesized. $TiO_2$ was suspended in 150 mL of water and mixed with certain amount of GO dispersion under magnetic stirring. After 2 h of stirring the mixture was transferred to a Teflon-lined stainless-steel autoclave (HS Instrument) of 200 mL. In order to provoke the reduction of GO, the autoclave was kept at 120 ºC for 3 h. The resulting rGO/$TiO_2$ composite material was recovered by centrifugation in a

Centrifuge 5810 (Eppendorf) at 2000 rpm for 2 minutes and washed with ultrapure water 3 times. The composite was dried overnight at 50 ºC [1–3].

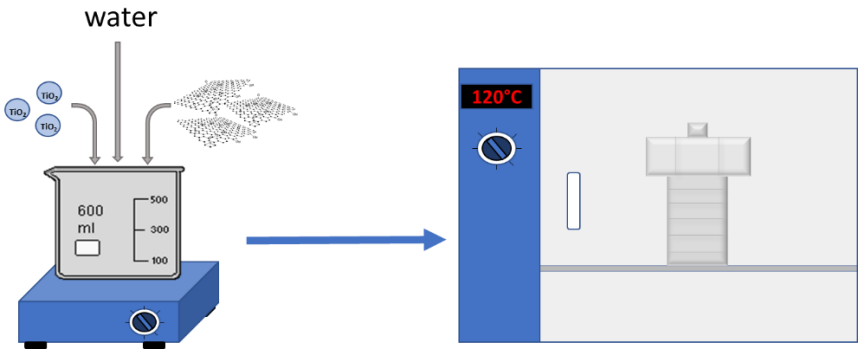


**Figure 2.1.** rGO/$TiO_2$ synthesis by the hydrothermal method

### 2.2.2. Synthesis of [FeFe]$H_2$-ase mimic

The [FeFe]$H_2$-ase mimic, [$Fe_2$ (μ-1,2-benzenedithiolate)$(CO)_6$] (Figure 2.2), was synthesized in the Unité Mixte de Recherche (UMR) 6521, Centre National de la Recherche Scientifique, Université de Bretagne Occidentale (France) by the method previously described in literature [4]. Briefly, a mixture of 0.275 mmol of $Fe_2(CO)_9$ and 0.302 mmol of benzene-1,2-dithiol was stirred in 10 mL of THF at reflux temperature for 70 min. The solution was filtered, and the filtrate was dried. The residue was redissolved in 2 mL of hexane and the product was purified by column of neutral alumina (activity I, 10 x 2 cm) with hexane as eluent.

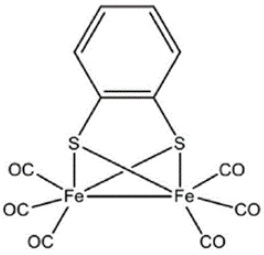


**Figure 2.2.** $Fe_2$ (μ-1,2-benzenedithiolate)$(CO)_6$ molecule

### 2.2.3. Synthesis of MPA-capped CdSe and CdTe QDs

CdSe and CdTe QDs were synthesized in the Department of Physics and the Center for Photochemical Sciences, Bowling Green State University (USA). They were synthesized with hydrophobic ligands followed by a ligand exchange process with 3-mercaptopropionic acid MPA which is hydrophilic. Figure 2.3 illustrates the synthesis process of both materials.

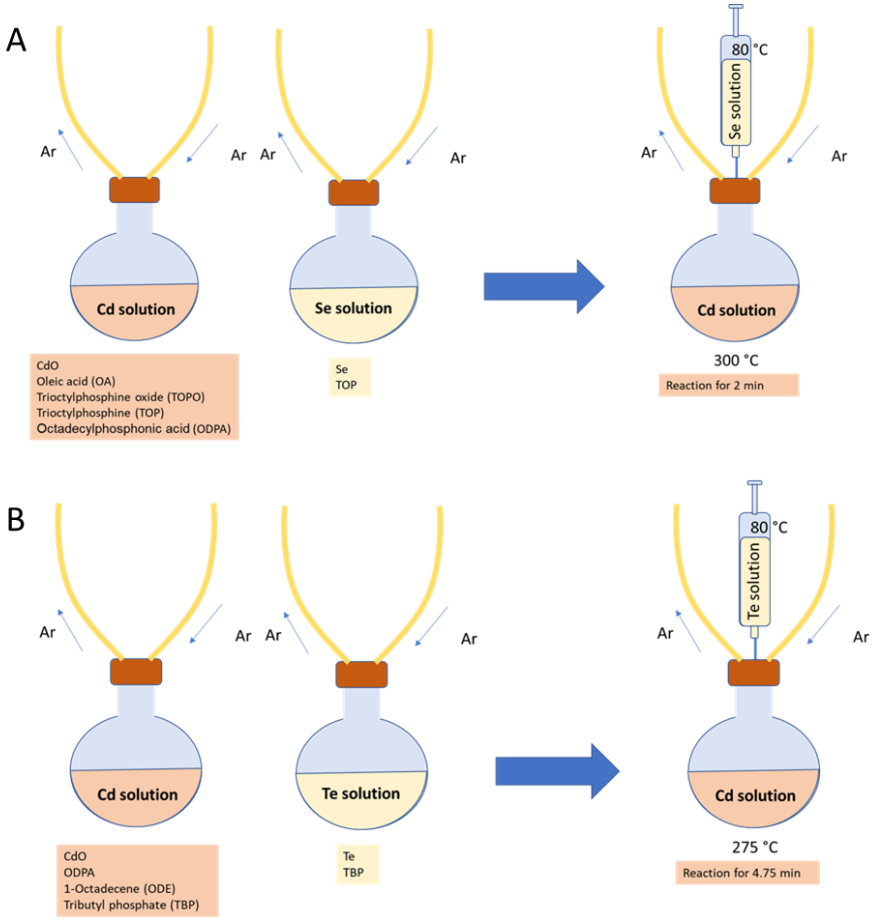


**Figure 2.3.** Synthesis of A) OA-CdSe and B) ODPA-CdTe

OA-capped CdSe QDs were synthesized from cadmium and selenium solutions. Cadmium solution was prepared dissolving 180 mg of CdO with 75 mg of n-octadecylphosphonic acid (ODPA), 9 g of trioctylphosphine oxide (TOPO), and 6 mL of oleic acid (OA) in a spherical flask at 300 ºC under Ar atmosphere. 5.4 mL of TOP were added when the solution turned clear. The selenium solution was prepared dissolving 180 mg of Se powder in 3 mL of trioctylphosphine (TOP) at 140 ºC under Ar atmosphere. The

selenium solution was cooled down to 80 ºC and it was injected into the cadmium solution. The reaction time was 2 min, and it was stopped cooling down the reaction mixture in a water bath. Every step was performed under magnetic stirring.

ODPA-capped CdTe QDs were synthesized from cadmium and tellurium solutions. The cadmium solution was prepared from 25.6 mg of CdO, 147.2 mg of ODPA and 8 mL of 1-octadene (ODE) at 300 ºC under Ar atmosphere. Tellurium solution was prepared from 51 mg of tellurium powder, 0.46 mL of tributylphosphine (TBP), and 4 mL of ODE at 80 ºC under Ar atmosphere. Tellurium solution was injected into cadmium solution and the reaction was stopped after 4.75 min by cooling down the reaction mixture in a water bath.

Both CdTe and CdSe suspensions were centrifuged for 4.5 min at 6500 rpm after adding ethanol:acetone solution, with a volume ratio 2:1, to cause precipitation of the crystals. The ratio between the crystals suspension and the ethanol-acetone mixture was 1:3 in volume. The precipitated crystals were resuspended in chloroform.

The ligand exchange process was carried out to allow the use of both QDs as photosensitizers in aqueous media. Briefly, 0.5 mL of MPA were dissolved in 10 mL of a basic pH 1:1 methanol:chloroform solution. 1.5 mL of crystals suspension were added and kept under stirring. The QDs were precipitated after centrifugation with acetone, suspended in water and re-precipitated in acetone. Finally, the QDs were suspended in deionized water [5].

## 2.3. Photocatalyst immobilization

2% rGO/$TiO_2$ photocatalyst was immobilized on polymeric membranes by three different methods: solvent-casting (SC), spraying (SP), dip-coating (DP). Figure 2.4 illustrates these methods. The theoretical percentage of composite for every membrane was 10% w/w.

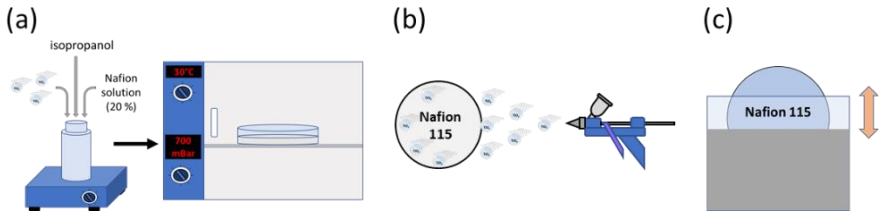


**Figure 2.4.** Photocatalytic immobilization methods: (a) solvent-casting, (b) spraying, and (c) dip-coating.

In SC method 42.2 mg of 2% rGO/$TiO_2$ were added to 1.8 g of Nafion solution D2020 and 0.5 mL of isopropanol. The mixture was stirred for 10 min and placed in an ultrasonication bath (Fisher scientific FB1505) with a frequency of 37 kHz for 30 min. The suspension was dried in a Petri dish set in a vacuum oven (PSelect) at 800 mbar and 30 ºC for 24 h. In order to facilitate the removal of the photocatalytic membrane from the Petri dish, a small volume of ultrapure water was added 2 h before removal.

SP method was employed to attach the 2% rGO/$TiO_2$ on the surface of Nafion N115 membrane. An ink composed of 0.3% photocatalyst, 2.7% of Nafion solution D520, and 97.0% of isopropanol as solvent was prepared and ultrasonicated for 45 min at 37 kHz before being sprayed on the membrane. The membrane was placed on a heating plate. The photocatalyst concentration on the membrane was 10% w/w. After spraying, the membrane was dried for 24 h under ambient conditions. The amount of coated photocatalyst was determined by the weight difference.

In the DP method Nafion N115 was immersed in a solution composed of 3.0% of photocatalyst, 25.7% of Nafion solution D520, and 71.3% of isopropanol. The solution was previously dispersed in an ultrasonication bath for 45 min. The membranes were immersed 6 consecutive times in the bath to reach the desired concentration of the composite. After each immersion the membrane was dried under ambient conditions for 10 min. After the last immersion, the photocatalytic membrane was dried under ambient conditions for 24 h.

## 2.4. Materials characterization

Thermogravimetric analyses (TGA) were performed in a DTG-60H Differential Thermal Gravimetric Analyzer (Shimadzu). The samples were heated from 25 ºC to 900 ºC in $N_2$ atmosphere with a flow of 50 mL·min$^{-1}$. The heating rate used in the measurements was 10 ºC·min$^{-1}$. The percentage of GO in the synthesized rGO/$TiO_2$ photocatalysts and the percentage of photocatalyst loaded in the photocatalytic membranes were confirmed by the thermogravimetric curves obtained by this technique.

Fourier Transform Infrared (FTIR) spectra of rGO/$TiO_2$, $TiO_2$ photocatalysts and photocatalytic membranes were recorded in a Spectrum Two spectrometer (PerkinElmer) equipped with an attenuated total reflection (ATR) accessory. This technique was used to confirm the presence of Ti-O bonds from $TiO_2$ at 500-800 cm$^{-1}$ in the rGO/$TiO_2$ as well as the C=O bonds at about 1720 cm$^{-1}$, and the C=C bonds at about 1620 cm$^{-1}$ from GO. FTIR spectroscopy also can provide a qualitative evidence of the GO reduction.

The infrared spectra of [$Fe_2$(μ-1,2-benzenedithiolate)$(CO)_6$] in hexane were recorded on a Nicolet Nexus FT-IR spectrometer (Thermo Fisher

Scientific). It was used to confirm the presence of the three corresponding bands to the CO groups between 2000 and 2100 $cm^{-1}$.

Proton nuclear magnetic resonance, $^{1}$HNMR, was performed to elucidate the composition and structure of the synthetized [$Fe_2$(μ-1,2-benzenedithiolate)$(CO)_6$]. $^{1}$HNMR spectra of [FeFe]$H_2$-ase mimic in deuterated acetone were recorded on an AC-300 FT-NMR spectrometer (Bruker) and were referenced against $SiMe_4$. The $^{1}$H-NMR together with the presence of the three CO bands in the FTIR, would confirm the successful synthesis of this compound.

Raman spectra of 2% rGO/$TiO_2$ photocatalysts were recorded by T64000 Raman Spectrometer (Horiba). The samples were excited with a 514.5 nm laser of Kr-Ar and an effective power of 5 mW on the sample. This technique was employed to analyze the $TiO_2$ and the rGO sheets in the composite. $TiO_2$ should present strong bands at around 140, 400, 515 and 635 $cm^{-1}$ which corresponded to $E_g$, $B_{1g}$, $A_{1g}$ and $E_g$ lattice vibrations of Ti and O atoms in the anatase unit cell. D and G bands at 1350 and 1600 $cm^{-1}$, respectively, could add information about the rGO. Raman spectra of 2% rGO/$TiO_2$ before and after being used were recorded.

Brunauer-Emmett-Teller nitrogen adsorption-desorption isotherms were determined to calculate the specific surface area of the photocatalysts. The measurements were collected in an ASAP 2000 equipment (Micromeritics). The BET method relates the gas adsorbed at a certain relative pressure to the volume adsorbed in a gas monolayer in the solid according to the equation 2.1 [6]:

$$\frac{P}{V(P_0 - P)} = \frac{1 + (c - 1)}{V_m \cdot c} \cdot \frac{P}{P_0} \qquad (2.1)$$

Where P is the equilibrium pressure, $P_0$ is the vapor saturation pressure, V is the volume of adsorbed gas at a relative pressure $P/P_0$, $V_m$ the volume adsorbed by the monolayer and c is the BET constant. $V_m$ is calculated from the data obtained in the adsorption-desorption equipment and it is used to calculate the specific surface area, $S_{BET}$ (2.2):

$$S_{BET} = \frac{V_m \cdot A_m \cdot N_A}{V_{mol}} \quad (2.2)$$

Where $V_{mol}$ is the molar volume of the gas under normal conditions, $A_m$ is the section occupied by the adsorbed molecules, and $N_A$ is the Avogadro's number.

Scanning Electron Microscopy (SEM) examination was carried out to the fresh and used photocatalytic membranes surfaces and to the fresh membranes cross-section in an EVO MA 15 microscope (Carl Zeiss). For the cross-section images, the membrane samples were frozen in liquid nitrogen and fractured. All the samples were gold sputtered to make the samples conductive. The membrane surface images would allow to confirm the distribution of the photocatalyst in the membrane surface. The cross-section images could reveal the thickness of the photocatalyst layer in SP and DP membranes and confirm the location of the photocatalyst in the membrane matrix in the SC membranes.

UV-Visible spectrophotometry was employed in the characterization of the CdSe and CdTe QDs. Their absorbance spectra allowed to calculate the diameter of the QDs from the first excitonic peak ($\lambda_{abs}$) by the Peng's correlations, Equations 2.3 and 2.4 [7]. The spectra of the QDs samples were recorded in a UV-Vis spectrophotometer Cary 60 (Agilent). This

technique was also used to measure the absorption spectra of [FeFe]$H_2$-ase mimic and ascorbic acid.

$$D_{CdSe} = (1.6122 \cdot 10^{-9})\lambda_{abs}{}^4 - (2.6575 \cdot 10^{-6}) \cdot \lambda_{abs}{}^3 + (1.6242 \cdot 10^{-3}) \cdot \lambda_{abs}{}^2 - 0.4277 \cdot \lambda_{abs} + 41.57 \quad (2.3)$$

$$D_{CdTe} = (9.8127 \cdot 10^{-7}) \cdot \lambda_{abs}{}^3 - (1.7147 \cdot 10^{-3}) \cdot \lambda_{abs}{}^2 + 1.0064 \cdot \lambda_{abs} - 194.84 \quad (2.4)$$

Time-resolved photoluminescence decay spectra and the photoluminescence spectra of CdSe and CdTe QDs were recorded out with 405 nm PDL 800-D pulsed laser (PicoQuant) as excitation source and an SR-303i-A spectrograph (Andor Technology) as emission detector. Time-resolved photoluminescence decay spectra were recorded to calculate the decay lifetime of the QDs. The photoluminescence spectra were also measured to obtain the photoluminescence emission peak of both materials. They were also used to calculate the electron transfer rate from the ascorbic acid to the QD, $k_{asc}$, and the electron transfer rate from the QD to the [FeFe]$H_2$-ase mimic, $k_{ET}$. In order to calculate them, emission quenching experiments were carried out measuring the emission intensity after adding different amounts of ascorbic acid (0-250 mM) or [FeFe]$H_2$-ase mimic (0-0.15 mM) to an aqueous QDs medium. Stern-Volmer plots were obtained using the Stern-Volmer equation (Equation 2.5) to the emission quenching results.

$$\frac{I_0}{I} = 1 + K_{sv} \cdot [Q] \quad (2.5)$$

Where $I_0$ is the fluorescence intensity without quencher, I is the fluorescence intensity for a certain concentration of quencher, $K_{sv}$ represents the Stern-Volmer constant, and Q is the quencher concentration.

## 2.5. Heterogeneous photocatalytic hydrogen production

Figure 2.5 depicts the experimental setup used for hydrogen generation with $TiO_2$ and rGO/$TiO_2$. A sealed 225 mL borosilicate photoreactor with 180 mL of 20% vol. methanol solution and 0.10 $g \cdot L^{-1}$ of photocatalyst was used for the comparison of the performance of the composite photocatalyst with different rGO/$TiO_2$ weight ratios. Long-term photocatalyst performance experiments and photocatalytic membrane experiments were carried out in a 330 mL borosilicate photoreactor using 240 mL of 20% vol. methanol solution as sacrificial agent and 0.18 $g \cdot L^{-1}$ of photocatalyst. The photocatalytic membranes were fixed between two PTFE rings and they were placed in the center of the reactor. Both photoreactors were irradiated with 4 Philips PL-S 9W lamps that operated within a wavelength range between 315 and 400 nm and a maximum emission at 365 nm (Figure 2.6). The irradiance on the reactor wall was 7.5 $W \cdot m^{-2}$, measured with a HD 2102.1 photoradiometer (Delta Ohm).

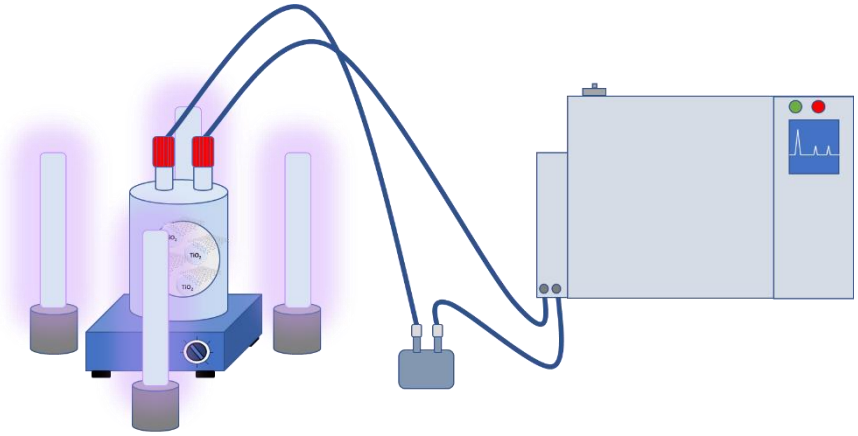

**Figure 2.5.** Heterogeneous photocatalytic hydrogen production experimental setup.

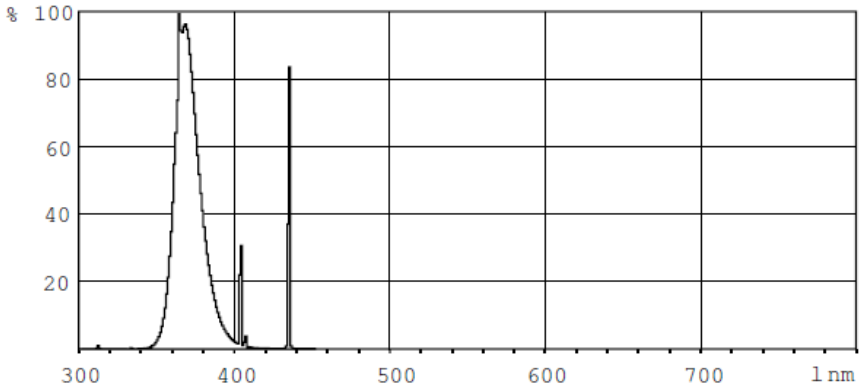


**Figure 2.6.** Lamp emission spectrum (retrieved from Phillips)

The photoreactor was connected to a Gas Chromatograph (GC) 2010 Plus (Shimadzu) equipped with a Shin Carbon ST 80/100 column using argon as carrier gas, and a thermal conductivity detector. Before collecting each sample, the gas phase in the reactor was homogenized by a micro diaphragm gas pump NMP 03 KP (KNF).

For photocatalytic hydrogen generation experiments, the reactor with 20% methanol solution and the photocatalyst, and the tubes of the sampling system were purged with Ar for 30 min. After purging, the system was illuminated to start the hydrogen production experiment. 500 µL samples were taken by the sampling system and they were injected directly in the GC. All the hydrogen production experiments were carried out at 20 ºC.

In order to quantify the photocatalyst leaching, the turbidity of the solution was measured with a Turbiquant 3000 IR spectrometer (Merck). The turbidity of the solution was calibrated as a function of the percentage of leached catalyst. Equation 2.6 relates these parameters:

$$Turbidity\ (NTU) = 13.24 \cdot leached\ cat.\ (\%) + 0.45 \qquad (2.6)$$

## 2.6. Hybrid photocatalytic hydrogen production

Figure 2.7 shows the experimental setup employed for the photocatalytic hydrogen production with the hybrid system. It consisted of a 4 mL of an aqueous media with ascorbic acid 200 mM, 0.1 mM of [FeFe]$H_2$-ase mimic, CdSe or CdTe QDs in a concentration between 0.001 mM and 0.1 mM, and SDS 10 mM to solubilize the [FeFe]$H_2$-ase mimic [8,9]. The reaction medium was contained in an 8 mL reactor with magnetic stirring. The reactor was illuminated by a 150 W halogen lamp OSL1 (Thorlabs) provided with a filter to allow only visible light to pass (400 nm < λ < 800 nm). Figure 2.8 shows the spectrum of the emitted radiation. The irradiance on the reactor wall was 31 $mW \cdot cm^{-2}$. It was measured with a Compact Power and Energy Meter Console PM100D (Thorlabs).

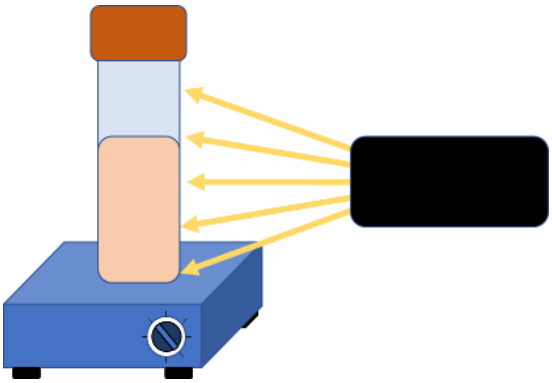

**Figure 2.7.** Hybrid photocatalytic hydrogen production experimental setup.

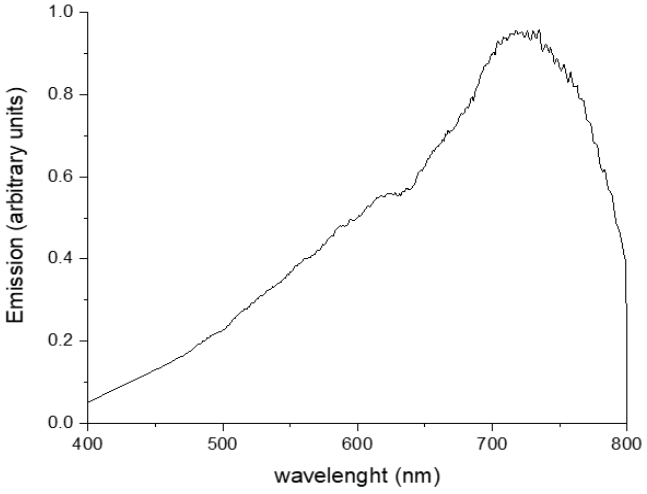


**Figure 2.8.** Spectrum of the emitted radiation.

The reaction medium in the photocatalytic hydrogen production experiments was prepared by dissolving the ascorbic acid in deionized water, followed by the addition of 100 µL of 4 mM [FeFe]$H_2$-ase mimic methanol solution.

Finally, the corresponding amount of CdSe or CdTe QDs was added. The reaction medium was sealed with a septum and it was ultrasonicated for 1 min. The reaction medium and the reactor were purged with Ar for 30 min. After purging, the reactor was illuminated and kept under magnetic stirring. 100 µL samples were taken with a syringe and they were analyzed in a GC 8A (Shimadzu) equipped with a thermal conductivity detector and a molecular sieve column 80/100 using Ar as carrier gas.

## 2.7. References

[1] P. Ribao, M.J. Rivero, I. Ortiz, Enhanced photocatalytic activity using GO/$TiO_2$ catalyst for the removal of DCA solutions, Environ. Sci. Pollut. Res. 25 (2018) 34893–34902.

[2] J. Corredor, M.J. Rivero, I. Ortiz, New insights in the performance and reuse of rGO/$TiO_2$ composites for the photocatalytic hydrogen production, Int. J. Hydrogen Energy (2020) (In press).

[3] A. Tolosana-Moranchel, A. Manassero, M.L. Satuf, O.M. Alfano, J.A. Casas, A. Bahamonde, Influence of $TiO_2$-rGO optical properties on the photocatalytic activity and efficiency to photodegrade an emerging pollutant, Appl. Catal. B Environ. 246 (2019) 1–11.

[4] J.A. Cabeza, M.A. Martínez-García, V. Riera, D. Ardura, S. García-Granda, Binuclear iron(I), ruthenium(I), and osmium(I) hexacarbonyl complexes containing a bridging benzene-1,2-dithiolate ligand. Synthesis, X-ray structures, protonation reactions, and EHMO calculations, Organometallics. 17 (1998) 1471–1477.

[5] C.M. Chang, K.L. Orchard, B.C.M. Martindale, E. Reisner, Ligand

removal from CdS quantum dots for enhanced photocatalytic H2 generation in pH neutral water, J. Mater. Chem. A. 4 (2016) 2856–2862.

[6] D. Dollimore, P. Spooner, A. Turner, The bet method of analysis of gas adsorption data and its relevance to the calculation of surface areas, Surf. Technol. 4 (1976) 121–160.

[7] W.W. Yu, L. Qu, W. Guo, X. Peng, Experimental determination of the extinction coefficient of CdTe, CdSe, and CdS nanocrystals, Chem. Mater. 15 (2003) 2854–2860.

[8] C. Orain, F. Quentel, F. Gloaguen, Photocatalytic Hydrogen Production Using Models of the Iron-Iron Hydrogenase Active Site Dispersed in Micellar Solution, ChemSusChem. 7 (2014) 638–643.

[9] C. Supplis, F. Gros, G. Dahi, J. Dauchet, M. Roudet, F. Gloaguen, J.F. Cornet, Spectral radiative analysis of bio-inspired $H_2$ production in a benchmark photoreactor: A first investigation using spatial photonic balance, Int. J. Hydrogen Energy. 43 (2018) 8221–8231.

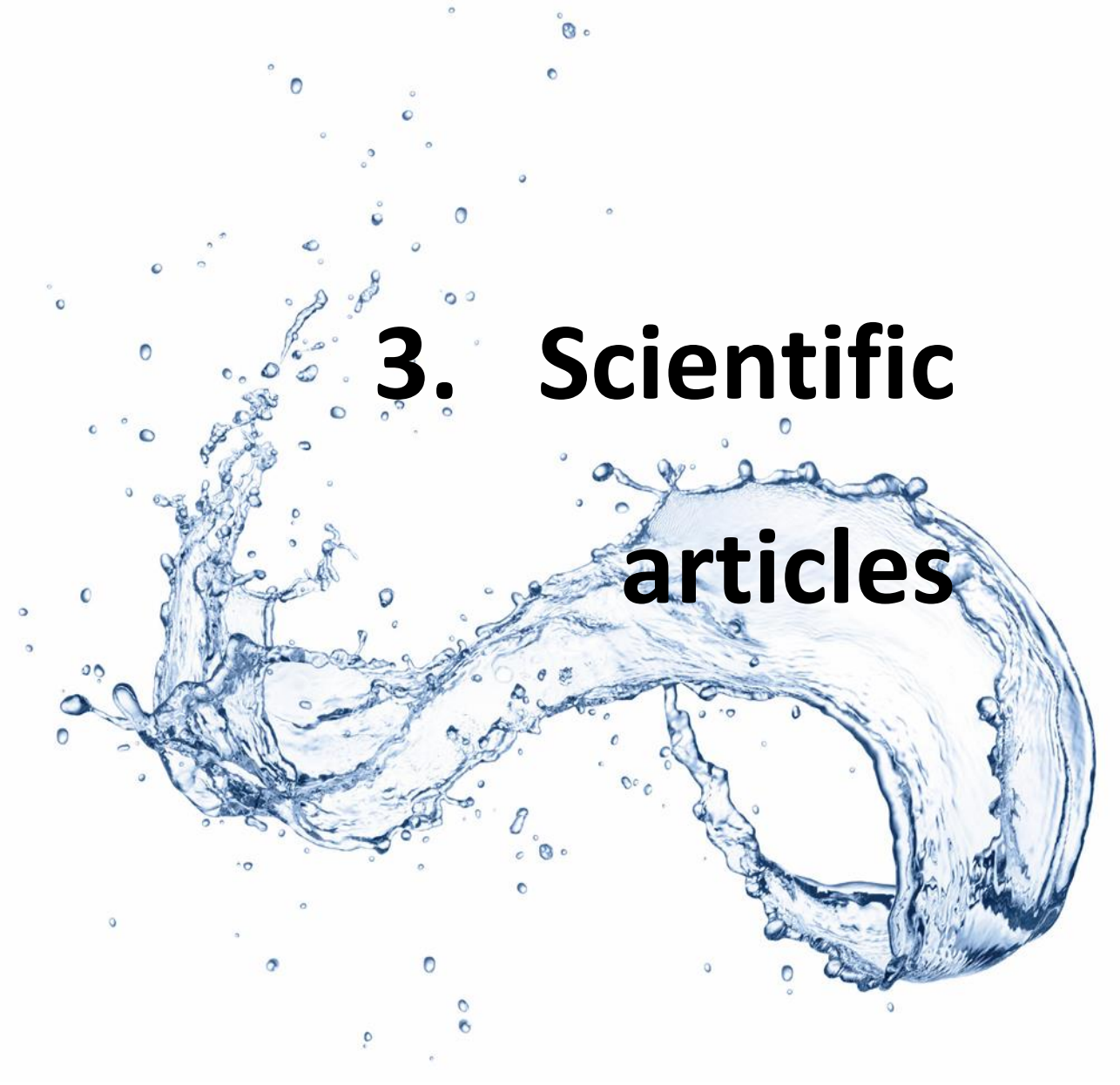

# 3. Scientific articles

Chapter 3 collects the scientific articles published on journals during the development of this thesis.

Chapter 3.1 is an integrated overview of the different photocatalytic hydrogen production systems: homogeneous, heterogeneous and hybrid. The units and mechanisms that take part in the photocatalytic process and their roles were analyzed. Moreover, a comparative analysis of the different systems was drawn.

In chapter 3.2, performance of the synthetized rGO/$TiO_2$ was compared to bare $TiO_2$ working with 20% volume methanol solution under UVA irradiation. This system was studied at long operations times. Argon purge was implemented to evaluate catalyst reuse.

Chapter 3.3 studies the performance of the rGO/$TiO_2$ supported on Nafion membranes to avoid the problem of the photocatalyst recovery. The photocatalytic membranes were synthetized by different methods: solvent-casting, spraying, and dip-coating. The hydrogen was produced from a 20% volume methanol solution under UVA irradiation. Leaching of the photocatalytic membranes was tested.

Chapter 3.4 moves towards the photocatalytic hydrogen production under visible light irradiation together with high production rates. A hybrid system was studied using biomimic [Fe-Fe]$H_2$-ase as catalyst and chalcogenides QDs as photosensitizers. The performance of CdSe and CdTe as photosensitizers was evaluated. The analysis of the results shed light on the mechanism of the photocatalytic hydrogen production and the role played by the QDs as photosensitizers.

## 3.1. Publication 1. Comprehensive review and future perspectives on the photocatalytic hydrogen production

Chapter 3.1 corresponds to the following paper:

J. Corredor, M. J. Rivero, C. M. Rangel, F. Gloaguen, I. Ortiz. "Comprehensive review and future perspectives on the photocatalytic hydrogen production". *Journal of Chemical Technology & Biotechnology*, 94, pp.3049–3063, 2019.
DOI: 10.1002/jctb.612

Received: 29 March 2019 Revised: 13 June 2019 Accepted article published: 19 June 2019 Published online in Wiley Online Library: 23 July 2019

(wileyonlinelibrary.com) DOI 10.1002/jctb.6123

# Comprehensive review and future perspectives on the photocatalytic hydrogen production

**Juan Corredor,[a] María J Rivero,[a] Carmen M Rangel,[b] Frederic Gloaguen[c] and Inmaculada Ortiz[a]***

## Abstract

**Hydrogen represents a renewable energy alternative that may positively contribute to get over the global energy crisis while at the same time reducing its environmental burden. Overcoming the challenge of reaching this potential could be helped by careful choice of hydrogen ($H_2$) sources. Photocatalytic generation of $H_2$, although a minor alternative, appears to be a very good option at the time that liquid wastes are being degraded; therefore, this approach has given rise to an increasing number of interesting studies. Here, we aim to provide an integrated overview of the different photocatalytic, heterogeneous, homogeneous and hybrid systems. First, we categorize the units and mechanisms that take part in the photocatalytic process, and secondly we analyze their role and draw comparative conclusions. Thus, we analyze the role of (i) the electron source to carry out proton reduction, (ii) the proton source, which can be free protons in the medium or a proton donor compound, (iii) the catalyst nature and concentration, and (iv) the photosensitizer nature and concentration. We also provide an analysis of the influence of the solvent, especially in homogenous systems as well as the influence of pH. We provide a comparison of the photocatalytic performance, highlighting the advantages and disadvantages, of different systems. Thus, this review is, on the one hand, an update on the state of the art of photocatalytic generation of $H_2$ from a full perspective that integrates homogeneous, heterogeneous and hybrid systems, and, on the other, a source of useful information for future research.**
**© 2019 Society of Chemical Industry**

**Keywords:** photocatalytic hydrogen production; homogeneous, heterogeneous and hybrid systems; comparative performance

## STATE OF THE ART OF PHOTOCATALYTIC GENERATION OF HYDROGEN

Increased emissions of greenhouse gases to the atmosphere due to fossil fuel combustion pose a serious threat to the environment. Hydrogen ($H_2$)-based energy comes out as a clean alternative because its direct combustion does not generate pollutants or greenhouse gases.[1–5] Nowadays, 95% of $H_2$ is obtained by steam reforming of fossil fuels, mainly methane. This process operates at high temperatures and pressures, and thus is energy-intensive.[6–8] Water ($H_2O$) electrolysis is one of the most promising $H_2$ production alternatives, especially, for storage of surplus electricity; a variety of commercial electrolysers for large-scale applications is available on the market.[9,10] However, the energy consumption associated with electrolysis must be significantly reduced before this process becomes competitive at large scales. Photocatalytic generation of $H_2$ from organic solutions or $H_2O$, although considered a minor source in terms of produced $H_2$ volume, appears to be a complementary and renewable way for simultaneous $H_2$ generation and wastewater remediation.[11–16]

In 1972, Fujishima and Honda reported the first heterogeneous photocatalytic $H_2$ production, HETPHP, by water splitting.[3,17] HETPHPs are assisted by a semiconductor that acts as catalyst and light harvester. Five years later, Lehn et al. (1977) published the first homogeneous photocatalytic $H_2$ production, HOMPHP, from triethanolamine (TEOA).[18] Typical HOMPHPs involve the use of an organometallic complex as catalyst and a second organic or organometalic compound as photosensitizer. More recently, hybrid photocatalytic $H_2$ production systems, HYBPHPs, have been developed making use of the system units of both HETPHPs and HOMPHPs, homogeneous catalysts and heterogeneous photosensitizer semiconductors.[19]

More recently, interesting reviews have addressed separately each of the three system categories[20–26] but there is no integrated and comparative analysis of the three systems. The present review provides such an integrated overview of the photocatalytic generation of $H_2$, and the influence of the photocatalytic units and process variables on $H_2$ production rate and stability. This comparison has been made in terms of $H_2$ production per unit time per gram of catalyst ($mol_{H2} \cdot g_{cat}^{-1} \cdot time^{-1}$) for HETPHPs, turnover Frequency (TOF) for HOMPHPs and HYBPHPs, and moles of $H_2$ per mole of catalyst, turnover number (TON), as defined in Eqns (1) and (2).

The stability of the photocatalytic system, and the process efficiency are determined through the 'Quantum Yield' (QY) and 'apparent Quantum Yield' (AQY) Eqns (3) and (4),[23–27] as indicators

* *Correspondence to: I Ortiz, Department of Chemical and Biomolecular Engineering, ETSIIT, University of Cantabria, Avda. de los Castros s/n, 39005, Santander, Spain. E-mail: inmaculada.ortiz@unican.es*

a *Department of Chemical and Biomolecular Engineering, ETSIIT, University of Cantabria, Santander, Spain*

b *Laboratório Nacional de Energia e Geologia, Lisbon, Portugal*

c *UMR 6521, CNRS, Université de Bretagne Occidentale, Brest, France*

that quantify the efficiency of the energy capture.

$$\mathrm{TOF} = \frac{mol_{H_2}}{mol_{cat.} \cdot time} \quad (1)$$

$$\mathrm{TON} = \frac{mol_{H_2}}{mol_{cat.}} \quad (2)$$

$$\mathrm{QY}\ (\%) = \frac{Number\ of\ reacted\ electrons}{Number\ of\ absorbed\ photons} \cdot 100 = \frac{2 \cdot Number\ of\ hydrogen\ molecules}{Number\ of\ absorbed\ photons} \cdot 100 \quad (3)$$

$$\mathrm{AQY}\ (\%) = \frac{Number\ of\ reacted\ electrons}{Number\ of\ incident\ photons} \cdot 100 = \frac{2 \cdot Number\ of\ hydrogen\ molecules}{Number\ of\ incident\ photons} \cdot 100 \quad (4)$$

In HETPHPs, the stability of the photocatalyst is an important parameter in process design and scale-up. A need for aging protocols that may predict photocatalyst lifetime is deemed crucial in the fostering of applications.

## INFLUENCE OF SYSTEM UNITS ON PHOTOCATALYTIC PERFORMANCE

As already stated, HETPHPs use a semiconductor photocatalyst and a sacrificial agent. The semiconductor acts as both a catalyst for the generation of $H_2$ and a photosensitizer or light harvester. The $H_2$ production mechanism by HETPHPs involves the following steps. (1) The absorption of photons from a light source with sufficient energy to overcome the band gap of the semiconductor photocatalyst promotes an electron from the valence band of the semiconductor to the conduction band, creating an electron–hole pair. (2) The electrons that reach the surface of the photocatalyst can reduce $H^+$. The holes can oxidize $H_2O$ or the sacrificial agent, depending on the band gap of the semiconductor. The electrons and holes which have not reacted recombine between themselves;[28,29] Fig. 1(a) illustrates this mechanism.

In order to reduce protons to $H_2$, the photocatalyst conduction band potential ($E_{CB}$) has to be more negative than the proton reduction potential ($E_{H^+/H2}$). In addition, in order to oxidize the sacrificial agent, the photocatalyst valence band potential ($E_{VB}$) has to be more positive than the sacrificial agent oxidation potential ($E_{D/D}{}^+$) [Fig. 2(a)]. Water also can be oxidized if the $E_{VB}$ is more positive than its oxidation potential.

Conventional HOMPHPs are composed of a soluble molecular catalyst, a soluble molecular photosensitizer and an electron donor. HOMPHPs consist of the following steps. (1) Absorption of photons from a light source by the photosensitizer to reach an excited state. (2) The excited state is quenched by electron transfer through a reductive or an oxidative reaction pathway (Fig. 3). It also can be quenched thermally by collision with other system compounds.[30] (2a) Reductive quenching of the excited photosensitizer involves an electron transfer from the electron donor to the excited photosensitizer, generating the reduced form of the photosensitizer. Then, an electron is transferred to the catalyst and the photosensitizer returns to its initial form. (2b) Oxidative quenching consists first of an electron transfer from the excited photosensitizer to the catalyst, generating the oxidized form of the photosensitizer that, secondly, oxidizes the sacrificial agent returning to its initial form. (3) Finally, the catalyst decreases the energetic barrier for the reduction of protons, which accelerates the rate of $H_2$ production. Because $H_2$ is formed upon the coupling of two electrons and protons, in at least two separate steps, several reaction pathways might occur, such as: two sequential electron transfers to the catalyst that then reacts with two protons, or the disproportionation of two hydrid species (Cat—H) formed transiently by reaction of the one-electron reduced form of the catalyst with a proton.[31] The overall mechanism is illustrated in Fig. 1(b).

The oxidation potential of the excited photosensitizer ($E_{PS^*/PS}{}^+$) in the oxidative quenching case [Fig. 2(b)] and oxidation potential of the reduced photosensitizer ($E_{PS}{}^-{}_{/PS}$) in the reductive quenching case [Fig. 2(c)], must be more negative than the reduction potential of the catalyst in its active form ($E_{Cat/Cat}{}^-$). Moreover, the reduction potential of the oxidized photosensitizer ($E_{PS}{}^+{}_{/PS}$) in the oxidative quenching case and reduction potential of the excited photosensitizer ($E_{PS}{}^*{}_{/PS}{}^-$) in the reductive case, have to be more positive than the electron donor oxidation potential ($E_{D/D}{}^+$). The possibility of several proton reduction pathways adds complexity to the determination of the redox potential at which the molecular catalysts are active.

HYBPHPs make use of a soluble molecular catalyst, a semiconductor as photosensitizer and a sacrificial agent. In this case, the first and second steps of photocatalytic $H_2$ production are the same as those in HETPHPs. As a third step, the catalyst accelerates the reduction of protons to $H_2$ via several reaction pathways as in homogeneous systems. Figure 1(c) illustrates this mechanism.

Thermodynamically, $E_{CB}$ has to be more negative than $E_{Cat/Cat}{}^-$ and $E_{VB}$ has to be more positive than the oxidation potential of the sacrificial agent ($E_{D/D}{}^+$)[Fig. 2(d)].

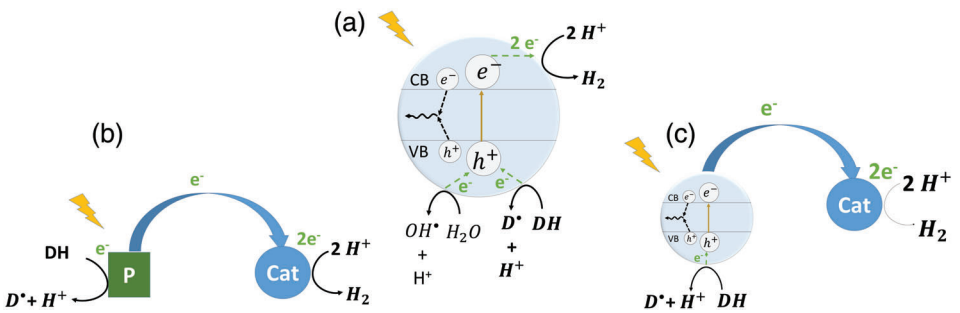


**Figure 1.** Photocatalytic $H_2$ production by: (a) heterogeneous system, (b) homogeneous system and (c) hybrid system. Cat, catalyst; PS, photosensitizer; D, electron donor/sacrificial agent.



 © 2019 Society of Chemical Industry 

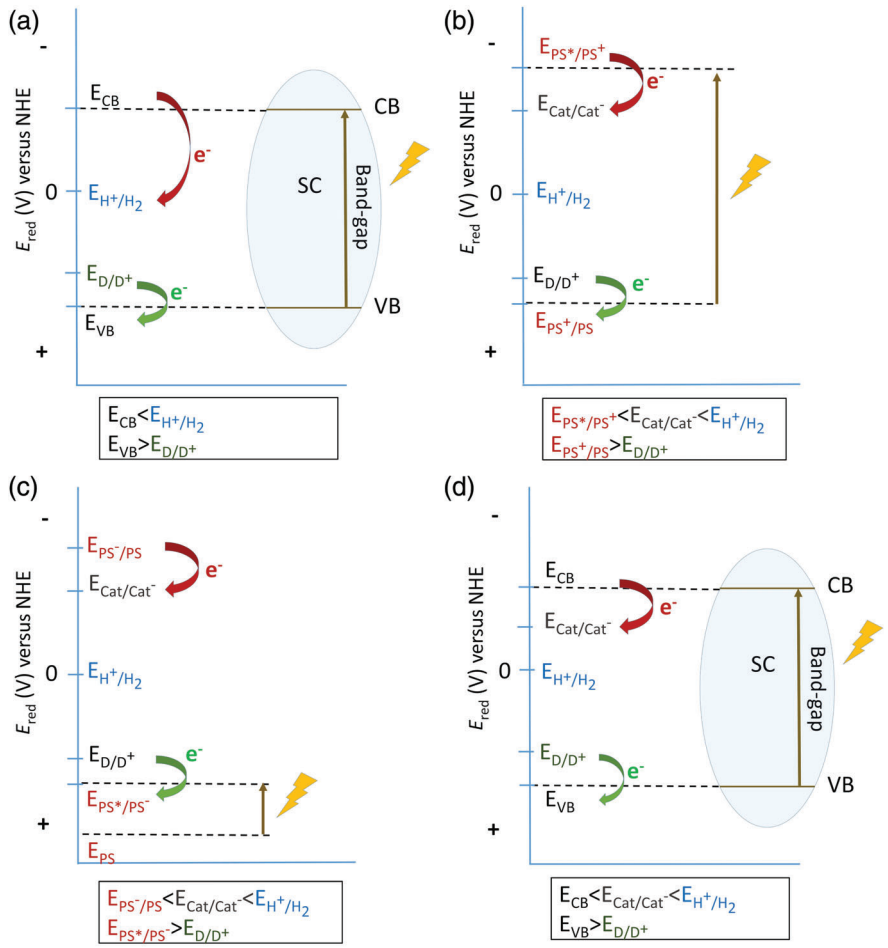


**Figure 2.** Potential schemes of the different photocatalytic $H_2$ production systems: (a) heterogenous system; (b) homogeneous system with oxidative quenching of excited photosensitizer; (c) homogeneous system with reductive quenching of excited photosensitizer; and (d) hybrid system. SC, semiconductor; D, electron donor; PS, photosensitizer. Cat, catalyst.

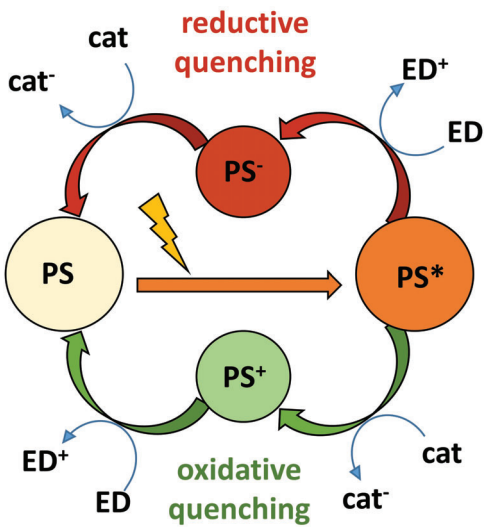


**Figure 3.** Scheme of reductive and oxidative quenching. PS, photosensitizer; ED, electron donor; cat, catalyst.

Therefore, adequate selection of the set of sacrificial agent, catalyst, photosensitizer and solvent is of paramount importance for the optimum performance of photocatalytic $H_2$ production.

### Sacrificial agent

The oxidation of $H_2O$, which provides electrons in the photocatalytic system, is an energy-intensive reaction. As a result, the use of sacrificial agents is common to most of the artificial photocatalytic systems for $H_2$ production. They act as electron donors to provide electrons for proton reduction and as hole scavengers preventing the electron–hole recombination and so increasing efficiency of the process.[32–34] HETPHPs use only one compound as sacrificial agent, whereas HOMPHPs and HYBPHPs can use either a compound as electron donor or a different one as proton donor, or the same compound for both functions, such as ascorbic acid or trimethylamine. Therefore, the term sacrificial agent is frequently used in heterogeneous systems, and electron donor and proton donor are most commonly used in homogeneous and hybrid systems.

Since the pioneering discovery of a photoelectrochemical water-splitting cell using a $Pt/TiO_2$ photoelectrode for $H_2$ production by Fujishima and Honda (1972), many works have researched water splitting to produce $H_2$.[17] However, water splitting is a less efficient process than using sacrificial donors to achieve high $H_2$ evolution rates. This can be attributed to a higher effectiveness of the sacrificial agent as hole ($h^+$) scavengers and the suppression of the back reaction to produce $H_2O$ because $O_2$ is not evolved, thus, increasing the $H_2$ yield.[35] The water-splitting reaction [Fig. 4(a)] is a large uphill reaction with a Gibbs free energy change



 © 2019 Society of Chemical Industry 

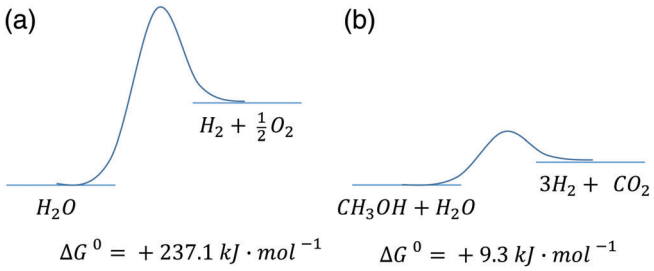


**Figure 4.** $H_2$ production reaction (a) from $H_2O$ (water splitting) and (b) from methanol.

of $\Delta G = +237.1$ kJ mol$^{-1}$. The photocatalytic reaction using a sacrificial agent is still an uphill reaction, but less so than the water-splitting one. For example, in the photocatalytic hydrogen production from methanol the Gibbs free energy change is +9.3 kJ mol$^{-1}$ [Fig. 4(b)].[36] Moreover, some waste effluents containing easy to oxidize compounds could be used for $H_2$ generation reporting an additional advantage to the photocatalytic remediation of these effluents.[2,22]

Sacrificial agents used in HETPHPs can be of inorganic or organic nature. The most common inorganic sacrificial agent is the $Na_2S/Na_2SO_3$ mixture, mainly used in the presence of metal sulfide photocatalysts such as CdS, $CuInS_2$-$AgInS_2$ and CdSe.[37,38] A wide variety of organic sacrificial agents has been used in literature such as alcohols (methanol and ethanol), acids (e.g. formic acid, acetic acid, dichloroacetic acid), aldehydes (formaldehyde and acetaldehyde), biomass derivatives[39] and other organic compounds as TEOA, azo dyes and ethylenediaminetetraacetic acid (EDTA). Alcohols are the organic compounds most widely used as sacrificial agents in photocatalytic $H_2$ production processes, especially with $TiO_2$-based photocatalysts. Among them, those with more OH groups and more $\alpha$-H show the best $H_2$ production rates. Therefore, methanol and glycerol are the most suitable alcohols for $H_2$ production.[2,40–43] Glycerol has received much attention as sacrificial agent because it provides a $H_2$ production rate of 70 mmol g$^{-1}$ h$^{-1}$.[36,44,45]

In order to select the most suitable sacrificial agent for HETPHPs, the redox potentials of all of the system units have to be considered (Fig. 3). However, there are other factors that can exert influence on the process performance, such as the stability of the sacrificial agent during the process and its interaction with the photocatalyst.[46] Wang et al. (2017) studied the photocatalytic $H_2$ generation when working with g-$C_3N_4$, $Zn_{0.5}Cd_{0.5}S$ and $TiO_2$ as catalysts and different sacrificial agents. Among the sacrificial agents that were screened, TEOA, $Na_2S/Na_2SO_3$ and methanol provided the best results with g-$C_3N_4$, $Zn_{0.5}Cd_{0.5}S$ and $TiO_2$, respectively.[46] TEOA has a lower oxidation potential and a higher permittivity than the other investigated amines.[47,48] $Na_2S/Na_2SO_3$ gives the best results with sulfide photocatalysts because it decreases self-photocorrosion.[37,46]

Optimal pH conditions in HETPHPs depend mainly on the nature of the sacrificial agent and on its adsorption on the surface of the semiconductor.[49] The influence of pH is related to the Point of Zero Charge (PZC) of the semiconductor, which will be discussed in the next section.

Low pH values increase the concentration of protons in the medium and facilitate the protonation of the molecular catalyst. Dissociation of the sacrificial agent is needed to provide electrons to the photosensitizer. Therefore, the optimal pH for $H_2$ evolution in HOMPHPs and HYBPHPs is usually a value close to the p$K_a$ of the electron donor.[50–52]

In HOMPHPs and HYBPHPs, tertiary aliphatic amines are the most widely used electron donors. The performance of triethylamine (TEA) and TEOA is favoured by their irreversible oxidation at about 0.9 V *versus* NHE and the ability to provide two reductive electrons for each absorbed photon. TEA (p$K_a$ 10.7) and TEOA (p$K_a$ 7.9)[53] are used under basic conditions (pH > 8). EDTA is the tertiary amine that can act as electron donor at a lower pH, ranging between 5 and 7.[53,54] Under relatively acidic conditions, ascorbic acid is used widely as electron donor (p$K_a$s 4 and 11.3),[53] it has the ability to act also as proton donor, providing $H^+$ to be reduced to $H_2$.[52,55] Carboxylic acids, such as lactic acid (p$K_a$ 3.9) and oxalic acid (p$K_a$ 1.2 and 4.2),[56] also have been used in aqueous solutions over a wide pH range from slightly acid to slightly basic.[57–59] Therefore, working at a pH value close to the p$K_a$ of the electron donor enhances the $H_2$ production rate.

In summary, according to prevailing knowledge, selecting the most suitable sacrificial agent and concentration for any photocatalytic hydrogen production system is mostly empirical, depending on the system units and the reaction medium. However, the relative redox potentials of the system compounds and the pH of the reaction medium should be considered for a good performance in photocatalytic hydrogen generation.[45,60]

## Catalyst

The function of a high performance heterogeneous photocatalyst is to: (i) avoid fast electron–hole recombination; (ii) allow fast diffusion of the electrons and holes to the surface of the semiconductor; (iii) have band potentials suitable to those of the sacrificial agent oxidation and proton reduction; (iv) be photoactive under visible light, which is related to the band gap of the semiconductor; (v) to display good chemical stability; and (vi) to be cost-effective.[61]

A wide variety of semiconductor photocatalysts has been investigated so far, such as chalcogenides (ZnS, CdS, CdSe),[62,63] metal oxides ($TiO_2$, $Cu_2O$, $ZrO_2$),[8,16] carbonaceous materials (g-$C_3N_4$)[64–67] and solid solutions $[(Ga_{1-x}Zn_x)(N_{1-x}O_x)$, $(AgIn)_xZn_{2(1-x)}S_2]$.[37,68–73] However, $TiO_2$ is still the most widely used photocatalyst because of its good stability in a wide range of pH conditions, resistance to photo-corrosion, nontoxicity and commercial availability. The small portion of the solar spectrum (*c.*4–8%) absorbed by $TiO_2$ is its main drawback.[74–78]

Figure 5 shows some materials that have been used in photocatalytic $H_2$ production. It is remarkable that catalytic materials need a sacrificial agent because they are not able to oxidize $H_2O$ molecules due to their low valence band potential.

In order to design a stable and a high performance photocatalyst, a variety of strategies have been developed [Fig. 6(a)]. The first one consists of doping the photocatalyst with different elements, by introducing or extracting atoms in/from its lattice structure. Iron (Fe), carbon (C), boron (B) and nitrogen (N) are common dopants that provide advantages such as narrowing the energy gap and reducing the yield of charge recombination.[79–82] The second strategy consists of coupling the photocatalyst with metals creating semiconductor/metal heterojunctions that can form a Schottky barrier and avoid the fast charge recombination. The metal also can act as co-catalyst reducing the overpotential for the surface electrochemical reactions. Moreover, the metal can improve the light absorption by surface plasmon resonance. The use of noble metals as co-catalysts provides higher $H_2$ production rates than the semiconductor catalyst alone; however, their associated high cost, and scarce availability limit their application.[61]



 © 2019 Society of Chemical Industry 

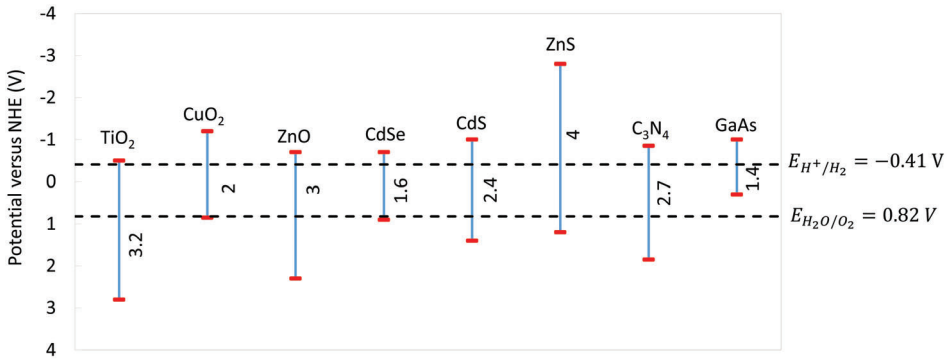


**Figure 5.** Band positions of some semiconductor photocatalysts and the redox potentials of water splitting at pH 7 in aqueous solution.

The third strategy consists of coupling two semiconductors. The oxidation of the sacrificial agent or $H_2O$ and the reduction of hydrogen can be carried out on one of the semiconductors, whereas the other one can contribute to (i) enhancing the separation and transport of the electron–hole pairs, (ii) sensitizing the photocatalyst to visible light or, (iii) acting as co-catalyst such as CdS/$TiO_2$ or $TiO_2$/PbS.[83–86] If redox reactions occur one in each semiconductor, the structure is called a Z-scheme. It allows combination of a semiconductor with strong reduction power with another semiconductor with strong oxidation power. As a result, the Z-scheme photocatalyst has strong redox potential and spatially separated active sites. Some Z-scheme catalysts make use of a charge carrier mediator such as $Fe^{2+}/Fe^{3+}$, $IO^{3-}/I^-$ or an electron conductor such as Au or Ag, that is used to facilitate charge carrier transfer between the semiconductors.[87]

Another advanced strategy consists of grafting an inorganic or organic dye such as eosin Y to the semiconductor surface. These dyes can act as visible light photosensitizers. They facilitate the initiation of the photochemical process by their own photoexcitation under visible light irradiation, followed by the transfer of electrons to the semiconductor.[88–90]

Yet another strategy consists of the physical modification of the semiconductor 3D structure, optimizing its shape and size, and hence increasing the active surface to enhance the photocatalytic activity. For example, $TiO_2$ has been synthesized in a wide range of morphologies such as spheres, rods, tubes, nanosheets, fibres or interconnected architectures.[91] Recently, quantum dots have been proposed as attractive materials with enhanced performance in the generation of $H_2$. Particles with diameters between 1 and 10 nm exhibit better charge transport and separation properties than conventional nanoparticles.[23]

Finally composite materials are gaining attention. The main candidate materials to allow the large-scale application of HETPHP are $TiO_2$, CdS and g-$C_3N_4$ based materials.

Photocatalyst modification strategies improve the $H_2$ production performance of the photocatalyst. However, the photocatalyst performance also can be improved by optimizing the operational conditions of the system. The most important parameter is the pH of the solution. The point of zero charge (PZC) of the semiconductor surface is an important parameter in HETPHPs in order to select the optimal pH conditions. At pHs higher than this value, the surface is deprotonated and becomes negatively charged, which attracts cations. Conversely, at pHs lower than the PZC, the photocatalyst surface becomes positively charged and attracts anions. In the case of commercial $TiO_2$ P25, pH at PZC is 6.4. Moreover, the superficial charge can influence the agglomeration of the semiconductor particles at pH close to PZC.[92–94]

In HOMPHPs and HYBPHPs, the first catalyst used was colloidal platinum (Pt), which produced hydrogen under visible light irradiation, using $[Ru(bpy)_3]^{2+}$ as chromophore, $[Rh(bpy)_3]^{3+}$ as electron mediator and TEOA as sacrificial agent.[95] An electron mediator was needed to transfer the electrons from the photosensitizer to the catalyst. Soon after, several studies demonstrated that $H_2$ production could be achieved by replacing Pt with a metal complex based on cobalt (Co) as catalyst and without electron mediator.[96–99] Since then, homogenous systems have used noble metal [Pt, palladium (Pd), rhodium (Rh)]-based catalysts or earth-abundant metals [Co, nickel (Ni), Fe, molybdenum (Mo)]. Although noble metal particles are generally more stable than organometallic catalysts,[19] their scarcity and high cost make them unsuitable for large-scale $H_2$ production.[100]

Earth abundant-based materials catalyzing $H_2$ production have been remarkably improved during the past ten years. Bio-inspired hydrogenase mimicking molecules have been developed trying to reproduce the active site of the hydrogenase enzyme, which is used by some microorganisms to catalyze the interconversion of protons and electrons into $H_2$. Hydrogenase active sites are based on Fe and/or Ni, which are earth-abundant first row transition metals.[24] Among them, [FeFe]-hydrogenase is effective at catalyzing the reduction of protons to $H_2$, achieving turnover frequencies (TOFs) greater than 6000 $s^{-1}$.[101] The use of bio-inspired [FeFe]-hydrogenase mimics in HOMPHPs allows reaching very high $H_2$ production yields; Jian et al. (2013) and Wang et al. (2013) reported a turnover number (TON) of 52 000 and 27 000 $mol_{H2}/mol_{cat.}$, respectively.[102,103]

The main challenges facing HOMPHPs and HYBPHPs are chemical stability over time, poor quantum yield of the process and the solubility of the system units in $H_2O$. Actually, it is unclear whether the lack of stability over time is due to the deactivation of the catalyst or the photosensitizer. In HOMPHPs, some authors have noticed that after a few hours the catalyst is decomposed,[104–106] whereas other authors have attributed the loss of activity to the decomposition of the photosensitizer.[51,107] Other works have shown that both system units are decomposed.[108,109] Therefore, there is no clear conclusion to be drawn on this issue. Concerning the quantum yield, these systems, which can reach high $H_2$ production rates, display, however, poor QY barely exceeding 1%. This is attributed to the weak efficiency of electron transfer between the photosensitizer in its excited state and the molecular catalyst.[107] Improving the aqueous solubility of the homogeneous catalyst is another important challenge, because $H_2O$ is the preferred proton source in practical systems.[19,110]

In order to overcome these challenges, various strategies have been developed [Fig. 6(b)]. One of them consists of anchoring



 © 2019 Society of Chemical Industry 

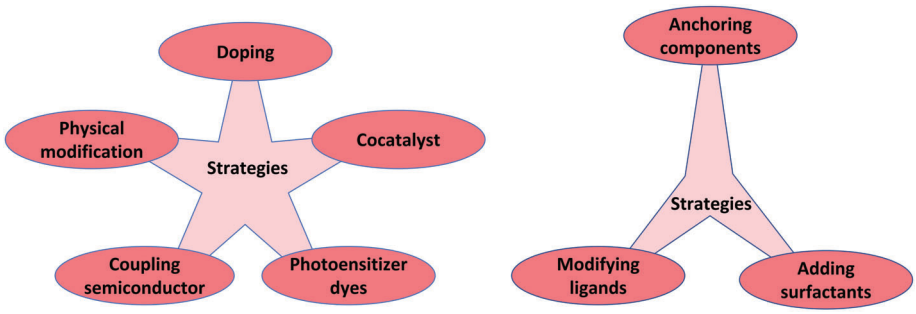


**Figure 6.** Strategies to enhance the photocatalyst performance: (a) heterogeneous systems; (b) homogeneous and hybrid systems.

together all the system units, which improves the electron transfer processes.[111,112] The use of surfactants, such as sodium dodecyl sulfate (SDS), helps to overcome the solubility problems. SDS forms micelles in $H_2O$, helping the dispersion of $H_2O$-insoluble transition-metal complexes used as proton reduction catalysts.[105,113] Modifying the catalyst coordination sphere by introducing hydrophilic ligands also can improve the catalyst solubility in $H_2O$.[19] These strategies improve the $H_2$ production performance of the catalyst. However, the catalyst performance also depends on the operational conditions of the system and has to be stable at the working pH.[104,114]

### Photosensitizer

The photosensitizer performance is essential for efficient light harvesting, generation and transfer of excited electrons, the most important factors that may limit the QY of the photocatalytic $H_2$ generation system.

The requirements for a high-performance photosensitizer are: (i) very broad light absorption range with high molar extinction coefficient in the visible light region; (ii) suitable redox potentials for electron transfer from the electron donor to the photosensitizer; (iii) long excited states lifetime; (iv) high photo-stability to allow for long-term $H_2$ production; and (v) good solubility in the reaction medium.[115,116]

In HETPHPs, the semiconductor generally acts as photosensitizer and catalyst simultaneously. However, some strategies such as the addition of an organic dye and a second semiconductor with narrow band gap, such as CdS, have been proposed to improve the photo-activity under visible light.[88,117,118]

In homogeneous configurations the catalyst and the photosensitizer are generally two separated units. However, there are several studies which have made use of photosensitizers chemically anchored to the catalysts forming the so-called supramolecular catalysts. Most of the photosensitizers used in HOMPHP have visible response. Metal-free organic dyes such as rose Bengal or Eosin Y,[119,120] and metal complexes such as $[Ru(bpy)_3]^{2+}$ or $[Ir(bpy)(ppy)_2]PF_6$[121,122] have been widely investigated during the last four decades. Although metal-free organic dyes are less expensive than metallic complexes, they typically suffer from short lifetimes due to photodegradation. More effective HOMPHPs have been prepared using noble metal complexes with ruthenium (Ru), iridium (Ir) or Pt as photosensitizers.[123–125] Among them, $[Ru(bpy)_3]^{2+}$ has been the most-studied metal complex. It has strong absorption in the range of visible light with $\lambda_{max}$ of 452 nm[126] and the lifetime of its excited specie is relatively long; however, $[Ru(bpy)_3]^{2+}$ suffers from poor photostability. Ir (III) complexes have higher stability and higher luminescence properties than $[Ru(bpy)_3]^{2+}$, and, in addition, their absorption wavelengths can be tunable. Therefore, Ir (III) complexes are the most effective photosensitizers due to their excellent excited-state properties.[115] Nevertheless, the scarcity of the noble metals limits their large-scale application. Consequently, noble metal-free complexes composed of earth-abundant compounds have been developed. Aluminium (Al) and copper (Cu) complexes[127–130] have been used, and zinc (Zn) porphyrins[131,132] have been synthesized leading to higher activities and longer lifetimes.

In order to increase the photosensitizer time stability, the use of semiconductors has been proposed. This turns the homogeneous system into a hybrid one. The most widely used are nanoparticles ($TiO_2$, ZnS, GaP),[133,134] carbonaceous semiconductors (g-$C_3N_4$),[135] and quantum dots (CdS, CdTe, CdSe).[50,136]

These configurations exhibit high catalytic activity, broad visible light absorption and long-term stability. The combination of molecular catalysts and quantum dots as photosensitizers, in a system with [FeFe]-hydrogenase mimics as catalyst, ascorbic acid as electron donor, methanol–$H_2O$ mixture as solvent and CdTe quantum dots as photosensitizer, has led to TON higher than 50 000 $mol_{H2}/mol_{cat.}$[102] Jian et al. (2016) compared the performance of CdSe quantum dots and $[Ru(bpy)_3]^{2+}$ as photosensitizer using [FeFe]-hydrogenase mimics as catalyst, ascorbic acid as electron donor and $H_2O$ as solvent. TON of >25 000 $mol_{H2}/mol_{cat.}$ was achieved with CdSe quantum dots, whereas TON of <200 $mol_{H2}/mol_{cat.}$ was achieved with $[Ru(bpy)_3]^{2+}$.[52] The use of semiconductor quantum dots as photosensitizers seems to be the best option because they usually have lifetimes longer than homogeneous photosensitizers. Among them, CdTe and CdSe offer the best $H_2$ production performance.

In general, the photosensitizer concentration has a remarkable influence on the $H_2$ production rate. The higher the photosensitizer concentration, the faster the $H_2$ production, although a compromise of an optimum value for a given photosensitizer concentration is usually searched for.[50,52,106]

The influence of pH on photosensitizer performance is less important than on the electron donor dissociation. However, it has to be accounted for regarding the photosensitizer stability.

### Solvent

In HETPHPs, the catalyst solubility is not an issue. Moreover, the system units can be easily recovered from the treated solution. Generally, the solvent is $H_2O$ that can act as proton donor in the $H_2$ production process. Water splitting also produces hydroxyl radicals that are able to carry out the indirect oxidation of the sacrificial agent. Some studies have shown that when the reaction mixture contains low $H_2O$ ratios, $H_2$ production is disfavoured.[2,45]

In HOMPHPs and HYBPHPs, the solvent selection depends on the nature of the molecular catalyst and the photosensitizer. Some



 © 2019 Society of Chemical Industry 

of them are soluble in organic solvents such as acetonitrile, acetone, dimethylformamide (DMF) and tetrahydrofuran (THF).[106,115] Encapsulating the catalyst inside micelles or cyclodextrins can help to overcome the solubility problem; this strategy has been used with low solubility [FeFe]-hydrogenase models.[51,110] The organic solvents can lead to weak dissociation of the sacrificial agent, which can decrease significantly the concentration of the species that react easily with the photosensitizer. Therefore, when mixtures of organic solvents and $H_2O$ are used, the optimum volume ratio to provide the best photocatalytic performance must be screened for.[137]

## COMPARATIVE PERFORMANCE OF THE DIFFERENT SYSTEMS

Making a thorough comparison of the results reported in the literature is a complex issue due to the difference in experimental conditions and setups. In this section, the different configurations and their suitability for large-scale applications will be discussed. Table 1 shows some data corresponding to systems with high photocatalytic $H_2$ production rates.

HETPHPs are usually evaluated using solution volumes of *c.* 0.1–2 L, whereas homogeneous and hybrid systems are tested in volumes of <10 mL, which is a ten- to 200-fold difference in volume that supports an advantageous scaling-up facility for heterogeneous systems.

The wavelength range of radiations used in heterogeneous systems depends on the semiconductor band gap. Sulfide photocatalysts are commonly irradiated by visible light because its band gap value is 2.4 eV.[138] $TiO_2$ photocatalysts need UV light because its band gap is 3 eV and 3.2 eV for rutile and anatase phases, respectively. However, $TiO_2$ modified by organic or inorganic dyes can produce $H_2$ under visible light irradiation. In homogeneous and hybrid systems, visible light is frequently used because most photosensitizers have good response in this wavelength range. Mercury-vapour lamps and xenon arc lamps, which emit both in the visible and UV regions are often used. Cutoff filters are then required to select the desired range. New developments in LEDs receive increasing attention, especially because they can emit in a narrow wavelength range and their low emission of heat.

It is remarkable that to achieve the highest $H_2$ production rates in HETPHPs, the sacrificial agent–catalyst pair is to be strongly connected. Therefore, $Na_2S$ and $Na_2SO_3$ are commonly used with sulfide photocatalysts to avoid photocorrosion. Glycerol provides the best results for $TiO_2$-based photocatalysts. However, the highest $H_2$ rate has been achieved by *Wang et al*. using lactic acid and CdS/$TiO_2$/Pt.[139] This work is an exception to the above-mentioned trend. In homogeneous and hybrid systems, ascorbic acid is the sacrificial agent involved in the systems achieving the highest $H_2$ production TON independently of the chosen catalyst.

Table 1 reports $H_2$ production rates per gram of catalyst in heterogeneous systems (mmol $H_2 \cdot g_{cat.}^{-1} \cdot h^{-1}$), and per mole of catalyst (TOF $h^{-1}$) in homogeneous and hybrid systems. In HETPHPs, bare $TiO_2$ produces a small volume of $H_2$ whereas $TiO_2$ with a co-catalyst enhances the photocatalyst performance and achieves high $H_2$ production rates. Chen et al. (2018) showed a 13-fold increase over the bare $TiO_2$, when attaching Au as a co-catalyst.[140] Coupling another semiconductor to $TiO_2$ also improved the $H_2$ production, as reported by Lakshmana Reddy et al. (2017) who coupled $TiO_2$ with $Bi_2O_3$ improving thus $H_2$ production ten-fold.[141] Moreover, both strategies can be implemented simultaneously. Wang et al. (2018) coupled $TiO_2$ with CdS and Pt as co-catalyst.[139] A 42-fold increase in $H_2$ production was achieved as compared to CdS/Pt. Nevertheless, the maximum value reported for $H_2$ production rate is <100 mmol $g^{-1}$ $h^{-1}$.

In HOMPHPs, anchoring the catalyst and photosensitizer with covalent bonds can improve the system performance. Gao et al. (2014) improved the hydrogen production rate more than five-fold with this strategy.[142] In order to increase the photosensitizer stability, dyes have been replaced by semiconductors, thus turning the homogeneous system into a hybrid one. Jian et al. (2016) reported an almost 70-fold increase in the initial rate and two-fold increase in the time stability with CdSe quantum dots as compared to the Ru-complex used as photosensitizer.[52] Therefore, hybrid systems are gaining attention.

In general, the highest $H_2$ production rates are achieved with HOMPHPs and HYBPHPs. This can be ascribed to the lack of mass transfer limitations. The kinetics of $H_2$ production in heterogeneous systems are almost linear during the evaluated reaction times when the sacrificial agent is in excess in the solution. Notwithstanding this, HOMPHPs and HYBPHPs exhibit stability issues, with the maximum rate being maintained only during the first few hours.

Time stability of the system is expressed as the period of time during which the system is producing $H_2$. Table 1 shows that HETPHP maintains its activity from 4 h to 25 h. Most studies on heterogeneous systems do not evaluate the performance of the catalyst for long periods if the photocatalyst does not show significant activity decrease during the first hours. One of the reasons of the wide use of $TiO_2$ as photocatalyst is its high stability. ZnO is another semiconductor metal oxide that has been highlighted for its high stability.[143,144] Sulfide photocatalysts have been studied widely due to their visible light response, especially CdS. This photocatalyst has poor stability due to the photocorrosion that oxidizes $S^{2-}$ by photogenerated valence band holes. This is accompanied by the release of $Cd^{2+}$ to the solution.[145] The photocorrosion phenomenon can be avoided by using a sacrificial agent that effectively takes photogenerated holes away from the valence band of CdS; the best results have been obtained with $Na_2S$ and $Na_2SO_3$,[146] for which stabilities of >100 h have been observed.[147] g-$C_3N_4$ has attracted special attention in the last decade due to its visible light response and its high stability.[64] Most homogenous and hybrid systems are studied as long as $H_2$ production carries on, but it frequently stops after few hours. This can be due to deactivation of the photosensitizer and/or the catalyst or both. Hybrid systems possess more time stability than homogenous systems because the semiconductor is more stable than the organic and metal-complex used as photosensitizer.

Suspended heterogeneous photocatalysts can be recovered from the solution through coagulation and sedimentation or membrane filtration.[148] Hybrid semiconductor photosensitizers also can be recovered from the solution. However, hybrid catalyst and homogeneous catalyst and photosensitizers are difficult and expensive to recover.[149] Table 2 collects the advantages and disadvantages of each system that can facilitate the adequate comparison and selection.

Up to now, real wastewaters have been treated solely by HETPHs, offering the double benefit of wastewater remediation and simultaneous $H_2$ production. Pretreated lignocellulosic biomass such as rice straw, silvergrass and ryegrass have been treated using $TiO_2$/Pt as photocatalyst.[150,151] Wastewater from biodiesel production[152] and other types of wastewater[153,154] also have been researched. Most of these studies include pre-treatment of wastewater and the use of $TiO_2$-based photocatalysts, although other photocatalysts



 © 2019 Society of Chemical Industry 

© 2019 Society of Chemical Industry









**Table 1.** Summary of high photocatalytic $H_2$ production rates in recent literature

| | Catalyst | Photosensitizer | Light source | Sacrificial agent | Maximum rate ($H_2$ mmol $g^{-1}$ $h^{-1}$) | TOF ($h^{-1}$) | Time stability | Solution Volume | Reference |
|---|---|---|---|---|---|---|---|---|---|
| Heterogeneous | CdS (45%)/$CoWO_4$ | - | Visible (Xe 300 W $\lambda > 420$ nm) | $Na_2S$ (0.35 mol $L^{-1}$) $Na_2SO_3$ (0.25 mol $L^{-1}$) | 15.9 | 3.7 | 15 h | 100 mL | 176 |
| | CdS/$TiO_2$(25%)/Pt (1%) | - | Visible Sun | $Na_2S$ (0.1 mol $L^{-1}$) $Na_2SO_3$ (0.02 mol $L^{-1}$) | 68.0 | 8.8 | 24 h | 50 mL | 177 |
| | CdS /$TiO_2$(nanosheets) (16.7%)/Pt(2%) | - | Visible (Xe 300 W $\lambda > 400$ nm) | Lactic acid (8.6%vol) | 128.3 | 17.3 | 15 h | 230 mL | 139 |
| | $Bi_2O_3$(0.4%)/$TiO_2$ | - | Visible Sun | Glycerol (5%) | 26.0 | 2.1 | 24 h | 50 mL | 141 |
| | $TiO_2$/rGO(3%)/Pt(3.8%) | - | UV–visible Hg lamp 450 W | Glycerol (20%) | 70.8 | 5.8 | 4 h | 300 mL | 45 |
| | $TiO_2$/Pd (1%) | - | UV (LEDs 365 nm 200 W) | Glycerol (10%) | 47.5 | 3.8 | 4 h | 20 mL | 178 |
| | g-$C_3N_4$(70%)-$TiO_2$(30%)/ rGO(1%) | - | Visible (Xe 250 W $\lambda$:300-800 nm) | Glycerol (5%) | 23.1 | 2.0 | 19 h | 50 mL | 179 |
| | $TiO_2$/Au (2%) | - | UV LEDs 100 W 365 nm) | Glycerol (10%) | 30.3 | 2.5 | 24 h | 20 mL | 140 |
| Homogeneous | Hydrogenase mimic | $[Ru(bpy)_3]^{2+}$ | Visible (LED 450 nm) | Ascorbic acid (0.2 mol $L^{-1}$) | 301.2 | 180.0 | 6 h | 10 mL | 52 |
| | Co-complex | $[Ru(bpy)_3]^{2+}$ | Visible (LED 469 nm) | Ascorbic acid (0.02 mol $L^{-1}$) | 319 737.7 | 156 000.0 | 15 h | 4 mL | 180 |
| | Hydrogenase mimic | $[Ir(ppy)_2(bpy)]^{+}$ | Visible (Xe) | TEA (0.6 () | 1197.5 | 7240.0 | 8 h | 10 mL | 181 |
| Hybrid | Hydrogenase mimic | CdSe QDs | Visible (LED 450 nm) | Ascorbic acid (0.2 mol $L^{-1}$) | 20 840.0 | 12 455 | 12 h | 10 mL | 52 |
| | Hydrogenase mimic | CdTe QDs | Visible (Hg lamo 500 W $\lambda > 400$ nm) | Ascorbic acid (0.0085 M) | 51.2 | 50.0 | 10 h | 10 mL | 50 |
| | Ni-complex | CdSe QDs | Visible LED 520 nm | Ascorbic acid (0.5 mol $L^{-1}$) | 7340.0 | 2280.0 | 130 h | 5 mL | 182 |
| | Hydrogenase mimic | CdTe QDs | Visible ($\lambda > 400$ nm) | Ascorbic acid (0.1 mol $L^{-1}$) | 8432.3 | 5040.0 | 60 h | 10 mL | 102 |

**Table 2.** Strengths and weaknesses of the different systems

| | Strengths | Weaknesses |
|---|---|---|
| Heterogeneous | • Easy recovery of the photocatalyst<br>• High time stability of the system | • Mass transfer limitations |
| Homogeneous | • High $H_2$ production rates | • Difficult recovery of the catalyst and photosensitizer<br>• Low time stability of the system |
| Hybrid | • High $H_2$ production rates<br>• Easy recovery of the photosensitizer<br>• Higher time stability as compared to homogeneous systems<br>• High photosensitizer stability | • Difficult recovery of the catalyst<br>• Low catalyst stability |

such as CdS also have been been reported. There are no reports of $H_2$ production from real wastewater using homogeneous and hybrid systems.

In summary, heterogeneous systems are closer to large-scale applications because they have already been assessed at pilot plant-scale when working with real effluents. They offer the most suitable alternative for the recovery of the photocatalyst after treatment. Moreover, heterogeneous systems could be used to treat residues of biodiesel production, where glycerol is the major byproduct[155]; this sacrificial agent has provided the best results in terms of $H_2$ production rate with $TiO_2$-based photocatalysts. Hybrid systems could represent a good alternative to processes where there is no need to remove the catalyst from the solution after treatment, because the high $H_2$ production rates and the reasonable time stability. Table 2 shows a summary of the strengths and weaknesses of each systems.

## MAIN CONCLUSIONS

This work provides an overview of photocatalytic $H_2$ production systems through the comparative performance of the three main configurations, HETPHP, HOMPHP and HYBPHP. The role of the process units is analyzed and discussed.

HETPHPs are the systems closest to large-scale application usually offering longer operation times due to the high semiconductor photocatalyst stability and ability to be recovered from the treated solution. Moreover, HETPHPs can be considered suitable to treat wastewater and to produce $H_2$ simultaneously. Pilot plant studies with real effluents are already available in literature. Photocatalysts modified by catalyst doping, use of co-catalyst, coupling to a semiconductor and physical modifications, generally provide higher yields and stabilities than single-component catalysts. Furthermore, photocatalysts without visible light response, such as $TiO_2$, can be sensitized by incorporation of different materials such as inorganic and organic dyes. Noble metals act as co-catalyst improving the photocatalyst performance and also can improve light absorption by surface plasmon resonance. However, their high cost and scarce availability limit their application. This problem has led to an increasing number of studies using photocatalysts based on earth-abundant materials. Suitable pairs of photocatalyst–sacrificial agent must be tuned, for significant $H_2$ production, based on their oxidation capability and tendency to adsorb on the catalyst surface.

The highest $H_2$ production rates under visible light irradiation have been achieved with HOMPHPs or HYBPHPs. However, homogeneous system stability is usually poor due to the decomposition of the catalyst, photosensitizer or both. Although noble metal catalysts and photosensitizers offer the best performance, efficient catalysts and photosensitizers of earth-abundant materials have to be developed. In this way, bio-inspired [FeFe]-hydrogenase mimics composed by an earth-abundant material appear as promising catalysts because they achieve very high hydrogen production rates. The difficulties in catalyst and photosensitizer recovery make this technology suitable to obtain hydrogen but the final effluent should be treated prior to discharge.

Hybrid systems can be regarded as the latest development that combine the catalyst used in HOMPHP with semiconductors of HETPHP as photosensitizers. Therefore, they would be a great alternative to overcome the low stability problem of homogeneous photosensitizers combined with the high performance of homogeneous catalysts. Semiconductor quantum dots seem to be very promising as photosensitizers due to the high $H_2$ production rate achieved, and the improvement in the time stability. Quantum dots of cadmium chalcogenides such as CdS, CdSe and CdTe seem to be proper candidates because of their visible light suitability. However, these materials are less stable than other semiconductors without visible light response, such as $TiO_2$.

## FUTURE PERSPECTIVES

Visible light-driven photocatalytic $H_2$ production is one of the main challenges hindering large-scale application of these processes. In HETPHP systems $TiO_2$, CdS and g-$C_3N_4$ based photocatalysts are the most promising materials. Therefore, further research should be done towards $TiO_2$ band-gap tuning. CdS-based materials offer appropriate band gap (CdS band gap = 2.4 eV) to absorb visible light, but they are toxic and generally unstable in aqueous environments.[37,70] These materials should be more deeply investigated to improve their stability. g-$C_3N_4$-based materials have received increasing attention since the first report in 2009 by Wang et al.[66] They are promising heterogeneous photocatalysts because they possess an appropriate band gap (g-$C_3N_4$ band gap = 2.7 eV),[64] slightly higher than CdS, and they show good stability. Therefore, modifications of these materials should be investigated to reduce the band gap and to improve their QY. The optimal modification to reduce their band gap could be through fabrication of Z-scheme g-$C_3N_4$ photocatalysts. This approximation appears to be more efficient than the doping and morphology design methods.[156]

Sluggish catalysis under real operating conditions is often limiting. Hydrogen production catalysts based on solid-state materials are usually stable but exhibit low selectivity and high sensitivity to poisoning. By contrast, as their chemical properties can be tailored through judicious choices of metal and ligands, molecular catalysts based on transition metal complexes enjoy good selectivity



 © 2019 Society of Chemical Industry 

and tolerance to varied experimental conditions.[157] Over the last decades, the design of molecular catalysts has been inspired by metalloenzymes,[158] which generally possess first row transition metals in their active sites. First row transition metals (e.g. Fe or Ni) are orders of magnitude more abundant in Earth's crust than heavier transition metals (e.g. Ru, Os, Pd or Pt) but they also form complexes that are chemically more reactive. In addition, detailed studies of the natural systems have revealed recurrent features that help tailor the reactivity of synthetic models. A typical example of this approach is the rational design by DuBois and coworkers of a Ni-based molecular catalyst that achieves a turnover frequency comparable to that of hydrogenase enzymes.[159] Unfortunately, most of the molecular catalysts for $H_2$ production are not soluble in $H_2O$, which is the most attractive solvent for sustainable conversion of sunlight to $H_2$. Practical use of molecular catalysts hence will be greatly facilitated if they are able to utilize $H_2O$ as proton source or at least tolerate the presence of $H_2O$.[51] The various strategies developed for immobilization of molecular catalysts on solid-state supports represent good solutions to this issue, while also helping the implementation and recycling of the catalytic system.[157] Anchoring to metal oxide semiconductor can be achieved by introducing carboxylate, phosphonate or silane groups in the ligands of the transition metal complexes. Choosing the appropriate molecular catalyst, solid-state support and anchoring strategy is hence of primary importance to obtain the desired performances under specific experimental conditions. Moreover, anchoring a molecular catalyst on a semiconductor or dye-sensitized semiconductor nanoparticles appears to be an attractive strategy to overcome diffusion-limited kinetics of electron transfer at the semiconductor/solution interface, thus, helping bridging the gap between fast light absorption/charge separation and slow catalysis. A representative example of this approach is the $H_2$ production by a cobalt-based molecular catalyst anchored on dye-sensitized nanoparticles of $TiO_2$.[160] Different examples also have been reported,[161,162] but avoiding the use of a sacrificial electron donor remains a key issue. In this context, few demonstrations that combine $H_2$ production with oxidation of organic compounds, including lignocelluloses, have been reported recently.[163,164] The gap between heterogeneous and homogeneous catalysis obviously blurs when molecular catalysts are immobilized on the surface of semiconductors. However, the chemical group used to link the two components can introduce fragility and efforts are currently placed on the incorporation of the molecular catalyst within the semiconducting material.[165]

Combining a $H_2$ evolution photocathode with a suitable anode or photoanode in a photoelectrochemical cell is another approach that allows the physical separation of the semiconductor/solution interfaces at which the complementary electrochemical reactions occur.[166] Quantum dots of cadmium chalcogenides such as CdS, CdSe and CdTe seem to be proper candidates for building the photocathode because of their visible light suitability. However, these materials are less stable than other semiconductors without visible light response, such as $TiO_2$. The use of molecular semiconductors as a promising alternative has been recently explored.[167,168] Therefore, an area of interest for future research consists on the development of high stable quantum dots semiconductors as well as other semiconductor materials with visible light response.

The photoreactor configuration plays an important role as well. There are critical reviews in which the design parameters and performance of the more common pilot and commercial-scale photoreactors are discussed. However, they are focused on wastewater treatment rather than $H_2$ production.[169–171] A limited number of works about photocatalytic $H_2$ production at pilot plant-scale have been reported.[172–175] All of them belong to the group of HETPHP systems. Some researchers have produced $H_2$ under solar irradiation using compound parabolic concentrator reactors (CPC), because they are considered as the best option to capture both direct and diffuse radiation. $TiO_2$- and CdS-based photocatalysts were used in these works. Solution volumes between 10 L and 25 L of different sacrificial agents such as methanol, glycerol and formic acid, and even municipal and industrial wastewaters were treated. Future research should take advantage of the accumulated knowledge in photoreactors for the treatment of $H_2O$ and the synthesis of fine chemicals and adapt them for their application to $H_2$ production. Future research should test further photocatalytic systems at pilot-plant scale such as g-$C_3N_4$-based materials with anchored molecular catalysts, which have not been proven yet. In addition, HOMPHP and HYBPHP systems should be tested in a pilot plant operating under solar irradiation.

In summary, cost-effective photocatalytic $H_2$ producing systems should focus on the use of noble metal-free, and visible light-sensitive system units in order to allow their practical deployment. Regarding the sacrificial agent, research in the pretreatment of waste effluents should be undertaken. Additionally, in order to allow a correct comparison among different photocatalytic $H_2$ production works, a standard procedure with modelling efforts and representative parameters regarding the quantification of the energy efficiency are needed.

## ACKNOWLEDGEMENTS

Financial support from projects 'HYLANTIC'-EAPA_204/2016 (Interreg Atlantic/FEDER UE), CTM2015-69845-R and CTQ2015-66078-R (MINECO/FEDER, UE) is gratefully acknowledged. Juan Corredor is grateful to a FPI contract grant (BES-2016-079201).

## REFERENCES

1 Alvarez LH and Cervantes FJ, (bio)nanotechnologies to enhance environmental quality and energy production. *J Chem Technol Biotechnol* **86**:1354–1363 (2011).
2 Pulido Melián E, López CR, Santiago DE, Quesada-Cabrera R, Ortega-Méndez JA, Doña-Rodríguez JM *et al.*, Study of the photocatalytic activity of Pt-modified commercial $TiO_2$ for hydrogen production in the presence of common organic sacrificial agents. *Appl Catal A* **518**:189–197 (2016).
3 Cha G, Altomare M, Truong NN, Taccardi N, Lee K and Schmuki P, Double-side co-catalytic activation of anodic $TiO_2$ nanotube membranes with sputter-coated Pt for Photocatalytic $H_2$ generation from water/methanol mixtures. *Chem Asian J* **12**:314–323 (2017).
4 Moon SY, Gwag H and Young J, Hydrogen generation on metal/mesoporous oxides: the effects of hierarchical structure, doping, and co-catalysts. *Energy Technol* **6**:459–469 (2018).
5 Karadag D, Köroğlu OE, Ozkaya B, Cakmakci M, Heaven S and Banks C, A review on fermentative hydrogen production from dairy industry wastewater. *J Chem Technol Biotechnol* **89**:1627–1636 (2014).
6 Holladay JD, Hu J, King DL and Wang Y, An overview of hydrogen production technologies. *Catal Today J* **139**:244–260 (2009).
7 Cargnello M, Montini T, Smolin SY, Priebe JB, Delgado-Jaén JJ, Doan-Nguyen VVT *et al.*, Engineering titania nanostructure to tune and improve its photocatalytic activity. *Proc Natl Acad Sci U S A* **113**:3966–3971 (2016).
8 García-Mendoza C, Oros-Ruiz S, Ramírez-Rave S, Morales-Mendoza G, López R and Gómez R, Synthesis of $Bi_2S_3$ nanorods supported on $ZrO_2$ semiconductor as an efficient photocatalyst for hydrogen production under UV and visible light. *J Chem Technol Biotechnol* **92**:1503–1510 (2017).

 © 2019 Society of Chemical Industry 

9 Saba SM, Mu M, Robinius M and Stolten D, The investment costs of electrolysis - a comparison of cost studies from the past 30 years. *Int J Hydrogen Energy* **43**:1209–1223 (2018).
10 Buttler A and Spliethoff H, Current status of water electrolysis for energy storage, grid balancing and sector coupling via power-to-gas and power-to-liquids: a review. *Renew Sustain Energy Rev* **82**:2440–2454 (2018).
11 Puga AV, Photocatalytic production of hydrogen from biomass-derived feedstocks. *Coord Chem Rev* **315**:1–66 (2016).
12 Mao SS, Shen S and Guo L, Nanomaterials for renewable hydrogen production, storage and utilization. *Prog Nat Sci Mater Int* **22**:522–534 (2012).
13 Miseki Y and Sayama K, Photocatalytic water splitting for Solar hydrogen production using the carbonate effect and the Z-scheme reaction. *Adv Energy Mater* **9**:1801294 (2018).
14 Xie H, Hou C, Wang H, Zhang Q and Li Y, S, N co-doped Graphene quantum dot/$TiO_2$ composites for efficient Photocatalytic hydrogen generation. *Nanoscale Res Lett* **12**:400 (2017).
15 Jitta RR, Gundeboina R, Veldurthi NK, Guje R and Muga V, Defect pyrochlore oxides: as photocatalyst materials for environmental and energy applications – a review. *J Chem Technol Biotechnol* **90**:1937–1948 (2015).
16 Guerrero-Araque D, Acevedo-Peña P, Ramírez-Ortega D, Lartundo-Rojas L and Gómez R, $SnO_2$–$TiO_2$ structures and the effect of CuO, CoO metal oxide on photocatalytic hydrogen production. *J Chem Technol Biotechnol* **92**:1531–1539 (2017).
17 Fujishima A and Honda K, Electrochemical photolysis of water at a semiconductor electrode. *Nature* **238**:37–38 (1972).
18 Lehn J-M and Sauvage J-P, Chemical storage of light energy-catalytic generation of hydrogen by visible-light or sunlight-irradiation of neutral aqueous-solutions. *Nouv J Chim* **1**:449–451 (1977).
19 Wang M, Han K, Zhang S and Sun L, Integration of organometallic complexes with semiconductors and other nanomaterials for photocatalytic $H_2$ production. *Coord Chem Rev* **287**:1–14 (2015).
20 Clarizia L, Russo D, Di Somma I, Andreozzi R and Marotta R, Hydrogen generation through solar photocatalytic processes: a review of the configuration and the properties of effective metal-based semiconductor nanomaterials. *Energies* **10**:1624 (2017).
21 Enferadi-Kerenkan A, Do T-O and Kaliaguine S, Heterogeneous catalysis by tungsten-based heteropoly compounds. *Cat Sci Technol* **8**:2257–2284 (2018).
22 Yi H, Huang D, Qin L, Zeng G, Lai C, Cheng M *et al.*, Selective prepared carbon nanomaterials for advanced photocatalytic application in environmental pollutant treatment and hydrogen production. *Appl Catal B* **239**:408–424 (2018).
23 Kandi D, Martha S and Parida KM, Quantum dots as enhancer in photocatalytic hydrogen evolution: a review. *Int J Hydrogen Energy* **42**:9467–9481 (2017).
24 Fukuzumi S, Lee YM and Nam W, Thermal and photocatalytic production of hydrogen with earth-abundant metal complexes. *Coord Chem Rev* **355**:54–73 (2018).
25 Utschig LM, Soltau SR and Tiede DM, Light-driven hydrogen production from photosystem I-catalyst hybrids. *Curr Opin Chem Biol* **25**:1–8 (2015).
26 Junge H, Rockstroh N, Fischer S, Brückner A, Ludwig R, Lochbrunner S *et al.*, Light to hydrogen: photocatalytic hydrogen generation from water with molecularly-defined iron complexes. *Inorganics* **5**:14 (2017).
27 Serpone N, Relative photonic efficiencies and quantum yields in heterogeneous photocatalysis. *J Photochem Photobiol A* **104**:1–12 (1997).
28 Hoffmann MR, Martin ST, Choi W and Bahnemann DW, Environmental applications of semiconductor Photocatalysis. *Chem Rev* **95**:69–96 (1995).
29 Coronado JM, Photons, electrons and holes: fundamentals of Photocatalysis with semiconductors, in *Design of Advanced Photocatalytic Materials for Energy and Environmental Applications*, ed. by Coronado JM, Fresno F, Hernández-Alonso MD and Portela R. Springer, London, pp. 35–67 (2013).
30 Atkins P and Paula d, The kinetics of complex reactions, in *Physical Chemistry*, ed. by Atkins P and de Paula J. WH Freeman and Co., New York, NY, pp. 830–868 (2006).
31 Stoll T, Castillo CE, Kayanuma M, Sandroni M, Daniel C, Odobel F *et al.*, Photo-induced redox catalysis for proton reduction to hydrogen with homogeneous molecular systems using rhodium-based catalysts. *Coord Chem Rev* **304–305**:20–37 (2015).
32 Pellegrino F, Sordello F, Minella M, Minero C and Maurino V, The role of surface texture on the photocatalytic $H_2$ production on $TiO_2$. *Catalysts* **9**:32 (2019).
33 Hernández-Gordillo A, Mendoza-Damián G and Gomez R, Blue-photodecomposition of hydrazine in aqueous solution for $H_2$ production by using CdS photocatalyst. *J Chem Technol Biotechnol* **91**:2179–2184 (2016).
34 García-Mendoza C, Oros-Ruiz S, Hernández-Gordillo A, López R, Jácome-Acatitla G, Calderón HA *et al.*, Suitable preparation of $Bi_2S_3$ nanorods–$TiO_2$ heterojunction semiconductors with improved photocatalytic hydrogen production from water/methanol decomposition. *J Chem Technol Biotechnol* **91**:2198–2204 (2016).
35 Schneider J and Bahnemann DW, Undesired role of sacrificial reagents in Photocatalysis. *J Phys Chem Lett* **4**:3479–3483 (2013).
36 Yasuda M, Matsumoto T and Yamashita T, Sacrificial hydrogen production over $TiO_2$-based photocatalysts: polyols, carboxylic acids, and saccharides. *Renew Sustain Energy Rev* **81**:1627–1635 (2018).
37 Li X, Low J and Yu J, Photocatalytic hydrogen generation, in *Photocatalysis Applications*, ed. by Dionysiou DD, Puma GL, Ye J, Schneider J and Bahnemann D. The Royal Society of Chemistry, Cambridge, pp. 255–302 (2016).
38 Yang M, Qian Y, Du J, Yuan S, Wang S, Zhu X *et al.*, Controlled synthesis of nanoplate, nanoprism and nanopyramid-shaped CdSe decorated on porous $TiO_2$ photocatalysts for visible-light-driven hydrogen evolution. *Ceram Int* **44**:12555–12563 (2018).
39 Shimura K and Yoshida H, Heterogeneous photocatalytic hydrogen production from water and biomass derivatives. *Energ Environ Sci* **4**:2467–2481 (2011).
40 Bahruji H, Bowker M, Davies PR, Al-Mazroai LS, Dickinson A, Greaves J *et al.*, Sustainable $H_2$ gas production by photocatalysis. *J Photochem Photobiol A* **216**:115–118 (2010).
41 Fu X, Wang X, Leung DYC, Gu Q, Chen S and Huang H, Photocatalytic reforming of C3-polyols for $H_2$ production. Part (I). Role of their OH groups. *Appl Catal B* **106**:681–688 (2011).
42 Castañeda C, Tzompantzi F, Rodríguez-Rodríguez A, Sánchez-Dominguez M and Gómez R, Improved photocatalytic hydrogen production from methanol/water solution using CuO supported on fluorinated $TiO_2$. *J Chem Technol Biotechnol* **93**:1113–1120 (2018).
43 Lv R, Wang X, Lv W, Xu Y, Ge Y, He H *et al.*, Facile synthesis of ZnO nanorods grown on graphene sheets and its enhanced photocatalytic efficiency. *J Chem Technol Biotechnol* **90**:550–558 (2015).
44 Estahbanati MRK, Feilizadeh M and Iliuta MC, Photocatalytic valorization of glycerol to hydrogen: optimization of operating parameters by artificial neural network. *Appl Catal B* **209**:483–492 (2017).
45 Ribao P, Alexandra Esteves M, Fernandes VR, Rivero MJ, Rangel CM and Ortiz I, Challenges arising from the use of $TiO_2$/rGO/Pt photocatalysts to produce hydrogen from crude glycerol compared to synthetic glycerol. *Int J Hydrogen Energy* (2018). https://doi.org/10.1016/j.ijhydene.2018.09.148.
46 Wang M, Shen S, Li L, Tang Z and Yang J, Effects of sacrificial reagents on photocatalytic hydrogen evolution over different photocatalysts. *J Mater Sci* **52**:5155–5164 (2017).
47 Zhang H, Guo L-H, Wang D, Zhao L and Wan B, Light-induced efficient molecular oxygen activation on a cu(II)- grafted $TiO_2$/graphene photocatalyst for phenol degradation. *ACS Appl Mater Interfaces* **7**:1816–1823 (2015).
48 Hong J, Wang Y, Wang Y, Zhang W and Xu R, Noble-metal-free NiS/$C_3N_4$ for efficient photocatalytic hydrogen evolution from water. *ChemSusChem* **6**:2263–2268 (2013).
49 Malinka EA and Kamalov GL, Influence of pH and surface complexes on the rate hydrogen evolution from photocatalytic systems Pt/$TiO_2$-electron donor. *J Photochem Photobiol A* **81**:193–197 (1994).
50 Wang F, Wang WG, Wang XJ, Wang HY, Tung CH and Wu LZ, A highly efficient photocatalytic system for hydrogen production by a robust hydrogenase mimic in an aqueous solution. *Angew Chem Int Ed* **50**:3193–3197 (2011).
51 Orain C, Quentel F and Gloaguen F, Photocatalytic hydrogen production using models of the iron-iron hydrogenase active site dispersed in micellar solution. *ChemSusChem* **7**:638–643 (2014).
52 Jian J-X, Ye C, Wang X-Z, Wen M, Li Z-J, Li X-B *et al.*, Comparison of $H_2$ photogeneration by [FeFe]-hydrogenase mimics with CdSe QDs and Ru(bpy)$_3$ $Cl_2$ in aqueous solution. *Energ Environ Sci* **9**:2083–2089 (2016).




 © 2019 Society of Chemical Industry 

53 Pellegrin Y and Odobel F, Sacrificial electron donor reagents for solar fuel production. *C R Chim* **20**:283–295 (2017).
54 Probst B, Rodenberg A, Guttentag M, Hamm P and Alberto R, A highly stable rhenium-cobalt system for photocatalytic $H_2$ production: unraveling the performance-limiting steps. *Inorg Chem* **49**:6453–6460 (2010).
55 Goy R, Bertini L, Rudolph T, Lin S, Schulz M, Zampella G *et al.*, Photocatalytic hydrogen evolution driven by [FeFe] hydrogenase models tethered to fluorene and silafluorene sensitizers. *Chem A Eur J* **23**:334–345 (2017).
56 Riemenschneider W and Tanifuji M, Oxalic acid, in *Ullmann's Encyclopedia of Industrial Chemistry*, ed. by Ullmann F and Elvers B. Wiley-VCH, Weinheim, p. 529 (2011).
57 Furlong DN, Wells D and Sasse WHF, Colloidal semiconductors in systems for the sacrificial photolysis of water. Hydrogen production with Pt/$TiO_2$ catalysts. *J Phys Chem* **89**:1922–1928 (1985).
58 Sun H and Hoffman MZ, Reductive quenching of the excited states of ruthenium(II) complexes containing 2,2′-bipyridine, 2,2′-bipyrazine, and 2,2′-bipyrimidine ligands. *J Phys Chem* **98**:11719–11726 (1994).
59 Neshvad G and Hoffman MZ, Reductive quenching of the luminescent excited state of tris(2,2′-bipyrazine)ruthenium(2+) ion in aqueous solution. *J Phys Chem* **93**:2445–2452 (1989).
60 Chen S, Li X, Zhou W, Zhang S and Fang Y, Carbon-coated cu-$TiO_2$ nanocomposite with enhanced photostability and photocatalytic activity. *Appl Surf Sci* **466**:254–261 (2019).
61 Christoforidis KC and Fornasiero P, Photocatalytic hydrogen production: a rift into the future energy supply. *ChemCatChem* **9**:1523–1544 (2017).
62 Oros-Ruiz S, Hernández-Gordillo A, García-Mendoza C, Rodríguez-Rodríguez AA and Gómez R, Comparative activity of CdS nanofibers superficially modified by au, cu, and Ni nanoparticles as co-catalysts for photocatalytic hydrogen production under visible light. *J Chem Technol Biotechnol* **91**:2205–2210 (2016).
63 Mei F, Zhang J, Dai K, Zhu G and Liang C, A Z-scheme $Bi_2MoO_6$/CdSe-diethylenetriamine heterojunction for enhancing photocatalytic hydrogen production activity under visible light. *Dalt Trans* **48**:1067–1074 (2019).
64 Cao S and Yu J, G-$C_3N_4$-based photocatalysts for hydrogen generation. *J Phys Chem Lett* **5**:2101–2107 (2014).
65 Montalvo-Herrera T, Sánchez-Martínez D, Hernandez-Uresti DB and Zarazua-Morin E, Facile preparation of $KBiO_3$/g-$C_3N_4$ composites with microwave irradiation for photocatalytic hydrogen production. *J Chem Technol Biotechnol* (2019). https://doi.org/10.1002/jctb.5921.
66 Wang X, Maeda K, Thomas A, Takanabe K, Xin G, Carlsson JM *et al.*, A metal-free polymeric photocatalyst for hydrogen production from water under visible light. *Nat Mater* **8**:76–80 (2009).
67 Moreira NFF, Sampaio MJ, Ribeiro AR, Silva CG, Faria JL and Silva AMT, Metal-free g-$C_3N_4$ photocatalysis of organic micropollutants in urban wastewater under visible light. *Appl Catal B* **248**:184–192 (2019).
68 Chun WJ, Ishikawa A, Fujisawa H, Takata T, Kondo JN, Hara M *et al.*, Conduction and valence band positions of $Ta_2O_5$, TaON, and $Ta_3N_5$ by UPS and electrochemical methods. *J Phys Chem B* **107**:1798–1803 (2003).
69 Hua J, Wang M, Jiao Y, Li H and Yang Y, Strongly coupled CdX (X=S, se and Te) quantum dots/$TiO_2$ nanocomposites for photocatalytic degradation of benzene under visible light irradiation. *Optik* **171**:95–106 (2018).
70 Wei RB, Huang ZL, Gu GH, Wang Z, Zeng L, Chen Y *et al.*, Dual-cocatalysts decorated rimous CdS spheres advancing highly-efficient visible-light photocatalytic hydrogen production. *Appl Catal B* **231**:101–107 (2018).
71 Cao XR, Tian GH, Chen YJ, Zhou J, Zhou W, Tian CG *et al.*, Hierarchical composites of $TiO_2$ nanowire arrays on reduced graphene oxide nanosheets with enhanced photocatalytic hydrogen evolution performance. *J Mater Chem A* **2**:4366–4374 (2014).
72 Chen J, Hong Z, Chen Y, Lin B and Gao B, One-step synthesis of sulfur-doped and nitrogen-deficient g-$C_3N_4$ photocatalyst for enhanced hydrogen evolution under visible light. *Mater Lett* **145**:129–132 (2015).
73 Maeda K, Teramura K, Lu D, Takata T, Saito N, Inoue Y *et al.*, Photocatalyst releasing hydrogen from water. *Nature* **440**:295 (2006).
74 Ribao P, Rivero MJ and Ortiz I, Enhanced photocatalytic activity using GO/$TiO_2$ catalyst for the removal of DCA solutions. *Environ Sci Pollut Res* **25**:34893–34902 (2018).
75 Byrne C, Subramanian G and Pillai SC, Recent advances in photocatalysis for environmental applications. *J Environ Chem Eng* **6**:3531–3555 (2018).
76 Mendiola-Alvarez SY, Guzmán-Mar JL, Turnes-Palomino G, Maya-Alejandro F, Hernández-Ramírez A and Hinojosa-Reyes L, UV and visible activation of Cr(III)-doped $TiO_2$ catalyst prepared by a microwave-assisted sol–gel method during MCPA degradation. *Environ Sci Pollut Res* **24**:12673–12682 (2017).
77 Ribao P, Corredor J, Rivero MJ and Ortiz I, Role of reactive oxygen species on the activity of noble metal-doped $TiO_2$ photocatalysts. *J Hazard Mater* **372**:45–51 (2018). https://doi.org/10.1016/j.jhazmat.2018.05.026.
78 Chan SHS, Wu TY, Juan JC and Teh CY, Recent developments of metal oxide semiconductors as photocatalysts in advanced oxidation processes (AOPs) for treatment of dye waste-water. *J Chem Technol Biotechnol* **86**:1130–1158 (2011).
79 Delegan N, Daghrir R, Drogui P and El Khakani MA, Bandgap tailoring of in-situ nitrogen-doped $TiO_2$ sputtered films intended for electrophotocatalytic applications under solar light. *J Appl Phys* **116**:153510 (2014).
80 Liu Y, Xu G and Lv H, Ag modified Fe-doping $TiO_2$ nanoparticles and nanowires with enhanced photocatalytic activities for hydrogen production and volatile organic pollutant degradation. *J Mater Sci Mater Electron* **29**:10504–10516 (2018).
81 Liu Y, He J, Sun Y, Hu J, Li C, Xue G *et al.*, A comparison of N-doped $TiO_2$ photocatalysts preparation methods and studies on their catalytic activity. *J Chem Technol Biotechnol* **88**:1815–1821 (2013).
82 Wen W, Lou Z, Chen Y, Chen D, Tian S and Xiong Y, Tuning the structural properties of $CeO_2$ by Pr and Fe codoping for enhanced visible-light catalytic activity. *J Chem Technol Biotechnol* **94**:1576–1584 (2019). https://doi.org/10.1002/jctb.5923.
83 Baker DR and Kamat PV, Photosensitization of $TiO_2$ nanostructures with CdS quantum dots: particulate versus tubular support architectures. *Adv Funct Mater* **19**:805–811 (2009).
84 Wang C, Thompson RL, Ohodnicki P, Baltrus J and Matranga C, Size-dependent photocatalytic reduction of $CO_2$ with PbS quantum dot sensitized $TiO_2$ heterostructured photocatalysts. *J Mater Chem* **21**:13452–13457 (2011).
85 Qu Y and Duan X, Progress, challenge and perspective of heterogeneous photocatalysts. *Chem Soc Rev* **42**:2568–2580 (2013).
86 Eskandari P, Farhadian M and SolaimanyNazar AR, Performance enhancement and optimization of photocatalytic cyanide degradation in aqueous solution using Zn (II) and Fe (III) oxides as nanostructure supported on activated carbon. *J Chem Technol Biotechnol* **92**:2360–2368 (2017).
87 Xu Q, Zhang L, Yu J, Wageh S, Al-Ghamdi AA and Jaroniec M, Direct Z-scheme photocatalysts: principles, synthesis, and applications. *Mater Today* **21**:1042–1063 (2018).
88 Jin Z, Zhang X, Lu G and Li S, Improved quantum yield for photocatalytic hydrogen generation under visible light irradiation over eosin sensitized $TiO_2$-investigation of different noble metal loading. *J Mol Catal A Chem* **259**:275–280 (2006).
89 Daghrir R, Drogui P and Robert D, Modified $TiO_2$ for environmental photocatalytic applications: a review. *Ind Eng Chem Res* **52**:3581–3599 (2013).
90 Abe R, Sayama K and Arakawa H, Dye-sensitized photocatalysts for efficient hydrogen production from aqueous I-solution under visible light irradiation. *J Photochem Photobiol A* **166**:115–122 (2004).
91 Lee S and Park S, $TiO_2$ photocatalyst for water treatment applications. *J Ind Eng Chem* **19**:1761–1769 (2013).
92 Kumar DP, Reddy NL, Srinivas B, Kumari VD and Shankar MV, Influence of reaction parameters for the enhanced photocatalytic hydrogen production using surface modified semiconductor Titania nanotubes. *Mater Today Proc* **4**:11653–11659 (2017).
93 Kosmulski M, Compilation of PZC and IEP of sparingly soluble metal oxides and hydroxides from literature. *Adv Colloid Interface Sci* **152**:14–25 (2009).
94 Lakshminarasimhan N, Kim W and Choi W, Effect of the agglomerated state on the photocatalytic hydrogen production with in situ agglomeration of colloidal $TiO_2$ nanoparticles. *J Phys Chem C* **112**:20451–20457 (2008).
95 Kirch M, Lehn J and Sauvage J, Hydrogen generation by visible light irradiation of aqueous solutions of metal complexes. An approach




 © 2019 Society of Chemical Industry 

to the photochemical conversion and storage of solar energy. *Helv Chim Acta* **62**:1345–1384 (1979).
96 Krishnan CV and Sutin N, Homogeneous catalysis of the photoreduction of water by visible light. Mediation by a tris(2, 2′-bipyridine)ruthenium(II)-cobalt (II) bipyridine system. *J Am Chem Soc* **103**:2141–2142 (1981).
97 DeLaive PJ, Sullivan BP, Meyer TJ and Whitten DG, Applications of light-induced electron-transfer reactions. Coupling of hydrogen generation with photoreduction of ruthenium(II) complexes by triethylamine. *J Am Chem Soc* **101**:4007–4008 (1979).
98 Kiwi J and Grätzel M, Hydrogen evolution from water by visible light, a homogeneous three component test system for redox catalysis. *Helv Chim Acta* **61**:2720–2721 (1978).
99 Brown GM, Brunschwig BS, Creutz C, Endicott JF and Sutin N, Homogeneous catalysis of the photoreduction of water by visible light. Mediation by a Tris(2, 2′-bipyridine)ruthenium(II)-cobalt(II) macrocycle system. *J Am Chem Soc* **101**:1298–1300 (1979).
100 Chen Y, Qin Z, Wang X, Guo X and Guo L, Noble-metal-free $Cu_2S$-modified photocatalysts for enhanced photocatalytic hydrogen production by forming nanoscale p-n junction structure. *RSC Adv* **5**:18159–18166 (2015).
101 Frey M, Hydrogenases: hydrogen-activating enzymes. *Chembiochem* **3**:153–160 (2002).
102 Jian JX, Liu Q, Li ZJ, Wang F, Li XB, Li CB *et al.*, Chitosan confinement enhances hydrogen photogeneration from a mimic of the diiron subsite of [FeFe]-hydrogenase. *Nat Commun* **4**:2695 (2013).
103 Wang F, Liang WJ, Jian JX, Li CB, Chen B, Tung CH *et al.*, Exceptional poly(acrylic acid)-based artificial [FeFe]-hydrogenases for photocatalytic $H_2$ production in water. *Angew Chem Int Ed* **52**:8134–8138 (2013).
104 Han Z, McNamara WR, Eum MS, Holland PL and Eisenberg R, A nickel thiolate catalyst for the long-lived photocatalytic production of hydrogen in a noble-metal-free system. *Angew Chem Int Ed* **51**:1667–1670 (2012).
105 Wang HY, Wang WG, Si G, Wang F, Tung CH and Wu LZ, Photocatalytic hydrogen evolution from rhenium(I) complexes to [FeFe] Hydrogenase mimics in aqueous SDS micellar systems: a biomimetic pathway. *Langmuir* **26**:9766–9771 (2010).
106 McLaughlin MP, McCormick TM, Eisenberg R and Holland PL, A stable molecular nickel catalyst for the homogeneous photogeneration of hydrogen in aqueous solution. *Chem Commun* **47**:7989–7991 (2011).
107 Khnayzer RS, Thoi VS, Nippe M, King AE, Jurss JW, El Roz KA *et al.*, Towards a comprehensive understanding of visible-light photogeneration of hydrogen from water using cobalt(II) polypyridyl catalysts. *Energ Environ Sci* **7**:1477–1488 (2014).
108 Li X, Wang M, Zheng D, Han K, Dong J and Sun L, Photocatalytic $H_2$ production in aqueous solution with host-guest inclusions formed by insertion of an FeFe-hydrogenase mimic and an organic dye into cyclodextrins. *Energ Environ Sci* **5**:8220–8224 (2012).
109 Li CB, Gong P, Yang Y and Wang HY, Cobalt(II)–Salen complexes for photocatalytic hydrogen production in noble metal-free molecular systems. *Catal Letts* **148**:3158–3164 (2018).
110 Berardi S, Drouet S, Francàs L, Gimbert-Suriñach C, Guttentag M, Richmond C *et al.*, Molecular artificial photosynthesis. *Chem Soc Rev* **43**:7501–7519 (2014).
111 Wang WG, Wang F, Wang HY, Si G, Tung CH and Wu LZ, Photocatalytic hydrogen evolution by [FeFe] hydrogenase mimics in homogeneous solution. *Chem Asian J* **5**:1796–1803 (2010).
112 Gao S, Zhang WY, Duan Q, Liang QC, Jiang DY, Zhao JX *et al.*, An artificial [FeFe]-hydrogenase mimic with organic chromophore-linked thiolate bridges for the photochemical production of hydrogen. *Chem Pap* **71**:617–625 (2017).
113 Quentel F, Passard G and Gloaguen F, A binuclear iron-thiolate catalyst for electrochemical hydrogen production in aqueous micellar solution. *Chem A Eur J* **18**:13473–13479 (2012).
114 Natali M, Elucidating the key role of pH on light-driven hydrogen evolution by a molecular cobalt catalyst. *ACS Catal* **7**:1330–1339 (2017).
115 Yuan YJ, Yu ZT, Chen DQ and Zou ZG, Metal-complex chromophores for solar hydrogen generation. *Chem Soc Rev* **46**:603–631 (2017).
116 Panda MK, Ladomenou K and Coutsolelos AG, Porphyrins in bio-inspired transformations: light-harvesting to solar cell. *Coord Chem Rev* **256**:2601–2627 (2012).
117 Chen W, Yu S, Zhong Y, Fan XB, Wu LZ and Zhou Y, Effect of electron transfer on the photocatalytic hydrogen evolution efficiency of faceted $TiO_2$/CdSe QDs under visible light. *New J Chem* **42**:4811–4817 (2018).
118 Xu J, Shi Y, Chen Y, Wang Q, Cheng J and Li P, Enhanced photocatalytic activity of $TiO_2$ in visible and infrared light through the synergistic effect of upconversion nanocrystals and quantum dots. *Mater Res Express* **6**:025055 (2019).
119 Lazarides T, McCormick T, Du PW, Luo GG, Lindley B and Eisenberg R, Making hyydrogen from water using a homogeneous system without noble metals. *J Am Chem Soc* **131**:9192–9194 (2009).
120 Zhang X, Jin Z, Li Y, Li S and Lu G, Efficient photocatalytic hydrogen evolution from water without an electron mediator over Pt-rose Bengal catalysts. *J Phys Chem C* **113**:2630–2635 (2009).
121 Gueret R, Poulard L, Oshinowo M, Chauvin J, Dahmane M, Dupeyre G *et al.*, Challenging the $[Ru(bpy)_3]^{2+}$ photosensitizer with a Triazatriangulenium robust organic dye for visible-light-driven hydrogen production in water. *ACS Catal* **8**:3792–3802 (2018).
122 Gärtner F, Sundararaju B, Surkus AE, Boddien A, Loges B, Junge H *et al.*, Light-driven hydrogen generation: efficient iron-based water reduction catalysts. *Angew Chem Int Ed* **48**:9962–9965 (2009).
123 Metza S and Bernhard S, Robust photocatalytic water reduction with cyclometalated Ir(III) 4-vinyl-2,2′-bipyridine complexes. *Chem Commun* **46**:7551–7553 (2010).
124 Martis M, Mori K, Kato K, Sanka G and Yamashita H, What are the active species in the Photoinduced H production with Terpyridyl Pt(II) complexes? An Investigation by in Situ XAFS. *ChemPhysChem* **14**:1122–1125 (2013).
125 Mori K, Watanabe K, Terai Y, Fujiwara Y and Yamashita H, Hybrid mesoporous-silica materials functionalized by Pt II complexes: correlation between the spatial distribution of the active center, photoluminescence emission, and photocatalytic activity. *Chem A Eur J* **18**:11371–11378 (2012).
126 Müller P and Brettel K, $[Ru(bpy)_3]^{2+}$ as a reference in transient absorption spectroscopy: differential absorption coefficients for formation of the long-lived $^3$MLCT excited state. *Photochem Photobiol Sci* **11**:632–636 (2012).
127 Mejía E, Luo SP, Karnahl M, Friedrich A, Tschierlei S, Surkus AE *et al.*, A noble-metal-free system for photocatalytic hydrogen production from water. *Chem A Eur J* **19**:15972–15978 (2013).
128 Luo SP, Mejía E, Friedrich A, Pazidis A, Junge H, Surkus AE *et al.*, Photocatalytic water reduction with copper-based photosensitizers: a noble-metal-free system. *Angew Chem Int Ed* **52**:419–423 (2013).
129 Natali M, Argazzi R, Chiorboli C, Iengo E and Scandola F, Photocatalytic hydrogen evolution with a self-assembling reductant-sensitizer-catalyst system. *Chem A Eur J* **19**:9261–9271 (2013).
130 Khnayzer RS, Mccusker CE, Olaiya BS and Castellano FN, Robust cuprous Phenanthroline sensitizer for solar hydrogen photocatalysis. *J Am Chem Soc* **135**:14068–14070 (2013).
131 Chou H, Reddy KSK, Wu H, Guo B, Lee H, Diau EW *et al.*, Influence of phenylethynylene of push–pull zinc porphyrins on the photovoltaic performance. *ACS Appl Mater Interfaces* **8**:3418–3427 (2016).
132 Lazarides T, Delor M, Sazanovich IV, TM MC, Georgakaki I, Charalambidis G *et al.*, Photocatalytic hydrogen production from a noble metal free system based on a water soluble porphyrin derivative and a cobaloxime catalyst. *Chem Commun* **50**:521–523 (2014).
133 Lakadamyali F, Reynal A, Kato M, Durrant JR and Reisner E, Electron transfer in dye-sensitised semiconductors modified with molecular cobalt catalysts: Photoreduction of aqueous protons. *Chem A Eur J* **18**:15464–15475 (2012).
134 Song XW, Wen HM, Ma CB, Hu MQ, Chen H, Cui HH *et al.*, Photocatalytic hydrogen evolution by two comparable [FeFe]-hydrogenase mimics assembled to the surface of ZnS. *Appl Organomet Chem* **28**:267–273 (2014).
135 Song XW, Wen HM, Ma CB, Cui HH, Chen H and Chen CN, Efficient photocatalytic hydrogen evolution with end-group-functionalized cobaloxime catalysts in combination with graphite-like $C_3N_4$. *RSC Adv* **4**:18853–18861 (2014).
136 Das A, Han Z, Haghighi MG and Eisenberg R, Photogeneration of hydrogen from water using CdSe nanocrystals demonstrating the importance of surface exchange. *Proc Natl Acad Sci U S A* **110**:16716–16723 (2013).
137 Na Y, Wang M, Pan J, Zhang P, Åkermark B and Sun L, Visible light-driven electron transfer and hydrogen generation catalyzed



 © 2019 Society of Chemical Industry 

by bioinspired [2Fe2S] complexes. *Inorg Chem* **47**:2805–2810 (2008).
138 Amano F, Nakata M, Yamamoto A and Tanaka T, Rutile titanium dioxide prepared by hydrogen reduction of Degussa P25 for highly efficient photocatalytic hydrogen evolution. *Cat Sci Technol* **6**:5693–5699 (2016).
139 Wang J, Wang Z, Qu P, Xu Q, Zheng J, Jia S *et al.*, A 2D/1D $TiO_2$ nanosheet/CdS nanorods heterostructure with enhanced photocatalytic water splitting performance for $H_2$ evolution. *Int J Hydrogen Energy* **43**:7388–7396 (2018).
140 Chen WT, Chan A, Sun-Waterhouse D, Llorca J, Idriss H and Waterhouse GIN, Performance comparison of Ni/$TiO_2$ and au/$TiO_2$ photocatalysts for $H_2$ production in different alcohol-water mixtures. *J Catal* **367**:27–42 (2018).
141 Reddy NL, Emin S, Valant M and Shankar MV, Nanostructured $Bi_2O_3$@$TiO_2$ photocatalyst for enhanced hydrogen production. *Int J Hydrogen Energy* **42**:6627–6636 (2017).
142 Gao S, Huang S, Duan Q, Hou J, Jiang D, Liang Q *et al.*, Iron-iron hydrogenase active subunit covalently linking to organic chromophore for light-driven hydrogen evolution. *Int J Hydrogen Energy* **39**:10434–10444 (2014).
143 Pardeshi SK and Patil AB, A simple route for photocatalytic degradation of phenol in aqueous zinc oxide suspension using solar energy. *Sol Energy* **82**:700–705 (2008).
144 Acar C, Dincer I and Naterer GF, Review of photocatalytic water-splitting methods for sustainable hydrogen production. *Int J Energy Res* **40**:1449–1473 (2016).
145 Colmenares JC, Luque R, Campelo JM, Colmenares F, Karpiński Z and Romero AA, Nanostructured photocatalysts and their applications in the photocatalytic transformation of lignocellulosic biomass: an overview. *Materials* **2**:2228–2258 (2009).
146 Yuan YJ, Chen D, Yu ZT and Zou ZG, Cadmium sulfide-based nanomaterials for photocatalytic hydrogen production. *J Mater Chem A* **6**:11606–11630 (2018).
147 Li K, Han M, Chen R, Li SL, Xie SL, Mao C *et al.*, Hexagonal@cubic CdS Core@Shell nanorod photocatalyst for highly active production of $H_2$ with unprecedented stability. *Adv Mater* **28**:8906–8911 (2016).
148 Iglesias O, Rivero MJ, Urtiaga AM and Ortiz I, Membrane-based photocatalytic systems for process intensification. *Chem Eng J* **305**:136–148 (2016).
149 Marras F, Kluwer AM, Siekierzycka JR, Vozza A, Brouwer AM and Reek JNH, Phosphorus Ligand Imaging with Two-Photon Fluorescence Spectroscopy: Towards Rational Catalyst Immobilization. *Angew Chem Int Ed* **49**:5480–5484 (2010).
150 Yasuda M, Misriyani TY, Kurogi R, Uehara S and Shiragami T, Fuelization of italian ryegrass and napier grass through a biological treatment and photocatalytic reforming. *J Sustainable Bioenergy Syst* **05**:1–9 (2015).
151 Yasuda M, Kurogi R, Tsumagari H, Shiragami T and Matsumoto T, New approach to fuelization of herbaceous lignocelluloses through simultaneous saccharification and fermentation followed by photocatalytic reforming. *Energies* **7**:4087–4097 (2014).
152 Pansa-Ngat P, Jedsukontorn T and Hunsom M, Optimal hydrogen production coupled with pollutant removal from biodiesel wastewater using a thermally treated $TiO_2$ photocatalyst (P25): influence of the operating conditions. *Nanomaterials* **8**:96 (2018).
153 Iervolino G, Vaiano V, Sannino D, Rizzo L, Galluzzi A, Polichetti M *et al.*, Hydrogen production from glucose degradation in water and wastewater treated by Ru-LaFeO3/$Fe_2O_3$ magnetic particles photocatalysis and heterogeneous photo-Fenton. *Int J Hydrogen Energy* **43**:2184–2196 (2018).
154 Souza EA and Silva LA, Energy recovery from tannery sludge wastewaters through photocatalytic hydrogen production. *J Environ Chem Eng* **4**:2114–2120 (2016).
155 Santibáñez C, Varnero MT and Bustamante M, Residual glycerol from biodiesel manufacturing, waste or potential source of bioenergy: a review. *Chil J Agric Res* **71**:469–475 (2011).
156 Naseri A, Samadi M, Pourjavadi A, Moshfegh AZ and Ramakrishna S, Graphitic carbon nitride (g-$C_3N_4$)-based photocatalysts for solar hydrogen generation: recent advances and future development directions. *J Mater Chem A* **5**:23406–23433 (2017).
157 Dalle K, Warnan J, Leung J, Reuillard B, Karmel I and Reisner E, Electro- and solar-driven fuel synthesis with first row transition metal complexes. *Chem Rev* **119**:2752–2875 (2019).
158 Gloaguen F and Rauchfuss T, Small molecule mimics of hydrogenases: hydrides and redox. *Chem Soc Rev* **38**:100–108 (2009).
159 Helm M, Stewart M, Bullock R, DuBois M and DuBois D, A synthetic nickel electrocatalyst with a turnover frequency above 100,000 $s^{-1}$ for $H_2$ production. *Science* **333**:863–866 (2011).
160 Lakadamyali F and Reisner E, Photocatalytic $H_2$ evolution from neutral water with a molecular cobalt catalyst on a dye-sensitised $TiO_2$ nanoparticle. *Chem Commun* **47**:1695–1697 (2011).
161 Han K, Wang M, Zhang S, Wu S, Yang Y and Sun L, Photochemical hydrogen production from water catalyzed by CdTe quantum dots/molecular cobalt catalyst hybrid systems. *Chem Commun* **51**:7008–7011 (2015).
162 Zhao W, Huang Y, Liu Y, Cao L, Zhang F, Guo Y *et al.*, A heterogeneous photocatalytic hydrogen evolution dyad: [(tpy-CHO)$_2$Ni]$Cl_2$ covalently anchored to CdS–amine inorganic–organic hybrid nanosheets. *Chem A Eur J* **22**:15049–15057 (2016).
163 Kasap H, Caputo C, Martindale B, Godin R, Lau V, Lotsch B *et al.*, Solar-driven reduction of aqueous protons coupled to selective alcohol oxidation with a carbon nitride–molecular Ni catalyst system. *J Am Chem Soc* **138**:9183–9192 (2016).
164 Kasap H, Achilleos D, Huang A and Reisner E, Photoreforming of lignocellulose into $H_2$ using Nanoengineered carbon nitride under benign conditions. *J Am Chem Soc* **140**:11604–11607 (2018).
165 Cui X, Li W, Ryabchuk P, Junge K and Beller M, Bridging homogeneous and heterogeneous catalysis by heterogeneous single-metal-site catalysts. *Nat Catal* **1**:385–397 (2018).
166 Yu Z, Li F and Sun L, Recent advances in dye-sensitized photoelectrochemical cells for solar hydrogen production based on molecular components. *Energ Environ Sci* **8**:760–775 (2015).
167 Lefebvre J-F, Schindler J, Traber P, Zhang Y, Kupfer S, Gräfe S *et al.*, An artificial photosynthetic system for photoaccumulation of two electrons on a fused dipyridophenazine (dppz)–pyridoquinolinone ligand. *Chem Sci* **9**:4152–4159 (2018).
168 Farnum B, Wee K-R and Meyer T, Self-assembled molecular p/n junctions for applications in dye-sensitized solar energy conversion. *Nat Chem* **8**:845–852 (2016).
169 Rodríguez SM, Gálvez JB, Rubio MIM, Ibáñez PF, Padilla DA, Pereira MC *et al.*, Engineering of solar photocatalytic collectors. *Sol Energy* **77**:513–524 (2004).
170 Braham RJ and Harris AT, Review of major design and scale-up considerations for solar photocatalytic reactors. *Ind Eng Chem Res* **48**:8890–8905 (2009).
171 Spasiano D, Marotta R, Malato S, Fernandez-Ibañez P, Di Somma I, Fernandez-Ibañez P *et al.*, Solar photocatalysis: materials, reactors, some commercial, and pre-industrialized applications. A comprehensive approach. *Appl Catal B* **170–171**:90–123 (2015).
172 Villa K, Domènech X, Malato S, Maldonado MI and Peral J, Heterogeneous photocatalytic hydrogen generation in a solar pilot plant. *Int J Hydrogen Energy* **38**:12718–12724 (2013).
173 Arzate Salgado SY, Ramírez Zamora RM, Zanella R, Peral J, Malato S and Maldonado MI, Photocatalytic hydrogen production in a solar pilot plant using a au/$TiO_2$ photo catalyst. *Int J Hydrogen Energy* **41**:11933–11940 (2016).
174 Jing D, Guo L, Zhao L, Zhang XX, Liu H, Li M *et al.*, Efficient solar hydrogen production by photocatalytic water splitting: from fundamental study to pilot demonstration. *Int J Hydrogen Energy* **35**:7087–7097 (2010).
175 Maldonado MI, López-Martín A, Colón G, Peral J, Martínez-Costa JI and Malato S, Solar pilot plant scale hydrogen generation by irradiation of Cu/$TiO_2$ composites in presence of sacrificial electron donors. *Appl Catal B* **229**:15–23 (2018).
176 Cui H, Li B, Zhang Y, Zheng X, Li X, Li Z *et al.*, Constructing Z-scheme based $CoWO_4$/CdS photocatalysts with enhanced dye degradation and $H_2$ generation performance. *Int J Hydrogen Energy* **43**:18242–18252 (2018).
177 El-Maghrabi HH, Barhoum A, Nada AA, Moustafa YM, Seliman SM, Youssef AM *et al.*, Synthesis of mesoporous core-shell CdS@$TiO_2$ (0D and 1D) photocatalysts for solar-driven hydrogen fuel production. *J Photochem Photobiol A* **351**:261–270 (2018).
178 Al-Azri ZHN, Chen WT, Chan A, Jovic V, Ina T, Idriss H *et al.*, The roles of metal co-catalysts and reaction media in photocatalytic hydrogen production: performance evaluation of M/$TiO_2$ photocatalysts (M = Pd, Pt, au) in different alcohol-water mixtures. *J Catal* **329**:355–367 (2015).

 © 2019 Society of Chemical Industry 

179 Hafeez HY, Lakhera SK, Bellamkonda S, Rao GR, Shankar MV, Bahnemann DW *et al.*, Construction of ternary hybrid layered reduced graphene oxide supported g-$C_3N_4$-$TiO_2$ nanocomposite and its photocatalytic hydrogen production activity. *Int J Hydrogen Energy* **43**:3892–3904 (2018).

180 Lei JM, Luo SP and Zhan SZ, A cobalt complex, a highly efficient catalyst for electro- and photochemical driven hydrogen generation in purely aqueous media. *Polyhedron* **154**:295–301 (2018).

181 Yu T, Zeng Y, Chen J, Li YY, Yang G and Li Y, Exceptional dendrimer-based mimics of diiron hydrogenase for the photochemical production of hydrogen. *Angew Chem Int Ed* **52**:5631–5635 (2013).

182 Das A, Han Z, Brennessel WW, Holland PL and Eisenberg R, Nickel complexes for robust light-driven and electrocatalytic hydrogen production from water. *ACS Catal* **5**:1397–1406 (2015).

 © 2019 Society of Chemical Industry 

## 3.2. Publication 2. New insights in the performance and reuse of rGO/$TiO_2$ composites for the photocatalytic hydrogen production

Chapter 3.2 corresponds to the following paper:

J. Corredor, M. J. Rivero and I. Ortiz. "New insights in the performance and reuse of rGO/$TiO_2$ composites for the photocatalytic hydrogen production". *International Journal of Hydrogen Energy.* 2020 (In Press). DOI: 10.1016/j.ijhydene.2020.01.181

Available online at www.sciencedirect.com

ScienceDirect

journal homepage: www.elsevier.com/locate/he

# New insights in the performance and reuse of rGO/$TiO_2$ composites for the photocatalytic hydrogen production

*Juan Corredor, Maria J. Rivero, Inmaculada Ortiz* *

*Department of Chemical and Biomolecular Engineering, ETSIIT, University of Cantabria, Avda. de Los Castros S/n, 39005, Santander, Spain*

## HIGHLIGHTS

- Evaluation of rGO/$TiO_2$ long term stability for photocatalytic hydrogen production.
- rGO/$TiO_2$ performance reduces progressively for photocatalytic hydrogen production.
- Initial hydrogen production rates for $TiO_2$ and rGO/$TiO_2$ catalysts are similar.
- Hydrogen accumulation inhibits its production.

## GRAPHICAL ABSTRACT

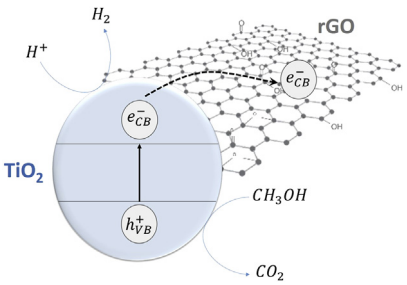


## ARTICLE INFO

*Article history:*
Received 8 November 2019
Received in revised form
21 January 2020
Accepted 24 January 2020
Available online xxx

*Keywords:*
rGO/$TiO_2$
Hydrogen production
Photocatalysis
Photocatalyst stability

## ABSTRACT

The viability of the photocatalytic hydrogen production is closely related to the performance and long term stability of the photocatalyst. In this work rGO/$TiO_2$ composites have been synthetized with graphene oxide (GO) ratios from 1% to 10% and experimentally assessed towards hydrogen generation from methanol solutions. The performance of the composite with 2% of rGO (2 GT) has been compared to bare $TiO_2$ working with 20% volume methanol solution. The hydrogen production initial rate showed similar values with both photocatalysts decreasing after about 24 h. Further analysis of the photocatalytic process at longer times showed the negative influence of hydrogen accumulation in the reaction system. Thus, an experimental procedure with argon purge was developed and the behavior of $TiO_2$ and 2 GT photocatalysts was compared. It is concluded that $TiO_2$ keeps its activity after 8 operation cycles while 2 GT performance reduces progressively. This can be attributed to the further reduction of GO and the increase of defects in its structure.

© 2020 Hydrogen Energy Publications LLC. Published by Elsevier Ltd. All rights reserved.

* *Corresponding author.*
E-mail address: inmaculada.ortiz@unican.es (I. Ortiz).

https://doi.org/10.1016/j.ijhydene.2020.01.181

0360-3199/© 2020 Hydrogen Energy Publications LLC. Published by Elsevier Ltd. All rights reserved.

Please cite this article as: Corredor J et al., New insights in the performance and reuse of rGO/$TiO_2$ composites for the photocatalytic hydrogen production, International Journal of Hydrogen Energy, https://doi.org/10.1016/j.ijhydene.2020.01.181

## Introduction

In the current global energy context of fossil fuel shortage and the need to mitigate climate change and the associated greenhouse gas emissions, the research and development of new and cleaner energy alternatives must be promoted. In this context, hydrogen appears as a promising clean energy vector [1–3]. Currently, about 95% of hydrogen is produced by steam reforming of natural gas under high temperatures and pressures. The remaining 5% is generated from electrolysis and from biofuels reforming. The recovery of hydrogen from the upgrading of organic wastes and from biomass, although a minor source, could contribute to increase hydrogen availability at the same time that environmental benefits are derived. Photocatalysis is among the alternatives to the recovery of hydrogen from organic liquid wastes with low-moderate energy consumption [4,5]. However, research efforts should be devoted to increase the process performance and stability.

Since the first work by Fujishima and Honda [6] on photoelectrochemical water-splitting cell for $H_2$ production (1972), the topic has attracted the attention of many researchers [7,8]. The low hydrogen yield associated to water splitting led to the use of sacrificial agents and photocatalysts aimed at increasing the process performance. In a recent review the state of the art and future prospectives on the photocatalytic hydrogen generation have been thoroughly analyzed. The photocatalytic hydrogen production systems are classified as heterogeneous, homogeneous and hybrid systems. Among them, heterogeneous systems are closer to large-scale application because they offer longer operation times and facilitate the photocatalyst recovery after treatment [7]. $TiO_2$ has been one of the most studied heterogeneous photocatalysts due to its suitable properties as chemical and thermal stability, high photoreactivity and low cost [9]. However, its wide band gap (3.2 eV) and the high recombination rate of the electron-hole pairs reduce its photocatalytic activity limiting its application. In order to improve the photocatalytic activity of $TiO_2$ different strategies have been developed [8]. One of them is doping the photocatalyst with different elements that will be incorporated in the $TiO_2$ lattice [10,11]. Attaching noble metals such as platinum to semiconductor photocatalysts leads to high hydrogen production rates because the Schottky barrier is formed in the metal/semiconductor interface and the recombination rate is reduced [12–14]. However, the scarcity and high price of noble metals limit its application. Currently, other strategies such as the use of earth-abundant metals as cocatalyst, and heterojunction structures, e.g., Z-scheme between two semiconductors, can effectively facilitate charge transfer and reduce the recombination of photogenerated electrons and holes, enhancing photocatalytic performance. Heterojunction catalysts composed of graphitic carbon nitride ($g\text{-}C_3N_4$) instead of $TiO_2$ have attracted increasing attention for hydrogen production under visible light [15–18] as well as the use of carbonaceous composite materials [19,20].

In this way, synthesis of composite photocatalysts incorporating graphene oxide (GO) appears as an interesting alternative. GO is a two-dimensional planar sheet composed by localized $sp^3$ defects within the $sp^2$ bonded carbon atoms structured in a honeycomb shaped network with binded oxygenated groups. It can be reduced to graphene which has excellent electrical conductivity and large surface area. These properties can improve the photocatalytic activity of the $TiO_2$ reducing the electron-hole recombination rate thanks to the ability of the graphene to carry charges due to its fermi level being lower than the $TiO_2$ conduction band [21–23].

In this work, rGO/$TiO_2$ composites have been synthesized for the photocatalytic hydrogen generation from methanol solutions. After analysis and optimization of the concentration of GO in the composite the performance and stability of the photocatalysts was studied for long operation times.

## Materials and methods

### Materials

HPLC grade methanol was provided by Scharlau and isopropanol 99.5% was supplied by Acros Organics. $TiO_2$ P25 was purchased to Evonik, and a dispersion of graphene oxide sheets in water solvent with 4 mg $mL^{-1}$ GO was supplied by Graphenea. Pure argon 3X was provided by Praxair.

### Photocatalyst preparation and characterization

rGO/$TiO_2$ composites with 1, 2, 5 and 10% of rGO weight were synthesized following the hydrothermal method described in previous works [22].

The materials characterization was carried out with different techniques. Fourier transform infrared spectra (FTIR) were recorded in a Spectrum Two spectrometer (PerkinElmer). Thermogravimetric analysis were performed in a Shimadzu DTG-60H Differential Thermal Gravimetric Analyzer by heating the samples in nitrogen atmosphere (50 mL $min^{-1}$) from 25 °C to 800 °C at 10 °C $min^{-1}$. Raman spectra were recorded by Horiba T64000 Raman Spectrometer with a 514.5 nm laser of Kr–Ar and an effective power of 5 mW on the sample. The specific surface area of the photocatalysts was measured by the Brunauer-Emmett-Teller (BET) method from nitrogen adsorption-desorption data in a Micromeritics ASAP 2000 equipment.

### Hydrogen production

The photocatalytic hydrogen production experiments aimed at comparing the performance of the composite catalysts with different rGO/$TiO_2$ weight ratios were carried out in a sealed 225 mL borosilicate photoreactor with 180 mL of 20% vol. methanol solution and 0.10 g $L^{-1}$ of photocatalyst. The photocatalyst long time performance experiments were carried out in a 330 mL borosilicate photoreactor using 240 mL of 20% vol. methanol solution as sacrificial agent and 0.18 g $L^{-1}$ of photocatalyst. The photoreactor was connected to a gas chromatograph Shimadzu 2010 Plus equipped with a thermal conductivity detector and a Shin Carbon ST 80/100 column using argon as carrier gas. 4 Philips PL-S 9W lamps, that operated within a wavelength range between 315 and 400 nm and a maximum emission at 365 nm, were used as light source. The irradiance was 7.5 W $m^{-2}$, measured with a Delta Ohm HD 2102.1 photoradiometer.

Please cite this article as: Corredor J et al., New insights in the performance and reuse of rGO/$TiO_2$ composites for the photocatalytic hydrogen production, International Journal of Hydrogen Energy, https://doi.org/10.1016/j.ijhydene.2020.01.181

Argon was bubbled through the suspension for 30 min in the dark to remove oxygen before the reaction. The temperature was 20 °C.

## Results

### *Photocatalysts characterization*

TGA curves of $TiO_2$ and rGO/$TiO_2$ photocatalysts are shown in Fig. 1. The GO thermogravimetric curve showed 3 different mass loss steps. The first step up to 100 °C corresponded to the adsorbed water in the material. From 150 to 300 °C, the mass loss was due to the removal of the oxygen-containing groups. Finally, the mass loss from 500 °C on was attributable to the destruction of the carbon skeleton of graphene oxide. Within these data the content of GO in the composites was determined as shown in Table 1.

FTIR spectra of $TiO_2$ and 2 GT before and after the photocatalytic experiments and FTIR spectrum of GO were obtained (Fig. 2). The 3400 $cm^{-1}$ band was assigned to the stretching vibration of the O–H groups of water. The bands at 1720 and 1619 $cm^{-1}$ in the GO spectrum were assigned to C=O stretching vibrations from carbonyl and carboxylic groups, and C=C stretching vibrations respectively. 1380, 1161 and 1037 $cm^{-1}$ bands were attributed to C–O stretching vibrations in GO. In 2 GT spectrum, bands of C=O groups did not appear, indicating a successful reduction of GO during the hydrothermal process. All composite materials presented intense bands at 500–800 $cm^{-1}$ that were attributed to the stretching vibrations of Ti–O–Ti [20].

The materials were also characterized after 96 h of experiment. For the recycled 2 GT, C=C band shifted to lower wavenumbers in comparison to the fresh photocatalysts [24]. This could be attributed to the modification of the photocatalyst structure during the photocatalytic process. In addition, the recycled photocatalysts showed intense bands at 1200 and 1150 $cm^{-1}$ that were assigned to C–F stretching vibrations from the polytetrafluoroethylene (PTFE) released from the magnetic stirring bar during the photocatalytic process [25].

**Table 1 – GO content in the composites determined thought TGA.**

| Catalyst code | 1 GT | 2 GT | 5 GT | 10 GT |
|---|---|---|---|---|
| Theoretical rGO (%) | 1 | 2 | 5 | 10 |
| Measured rGO (%) | 3.4 | 3.9 | 6.8 | 11.8 |

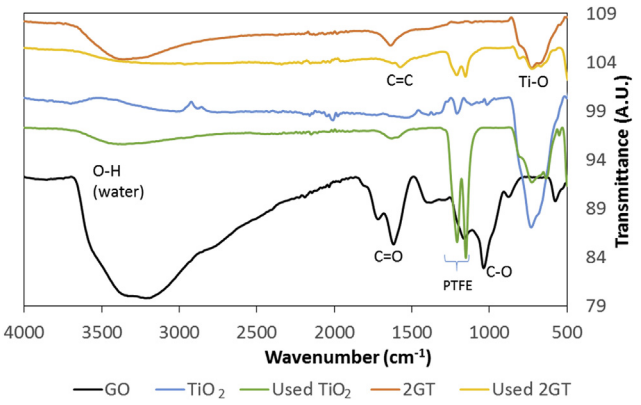


**Fig. 2 – Photocatalysts FTIR spectra before and after the photocatalytic process.**

Fig. 3 shows Raman spectra of GO and fresh and recycled photocatalysts. $TiO_2$ Raman spectrum showed strong bands at 140, 397, 515 and 635 $cm^{-1}$ which corresponded to $E_g$, $B_{1g}$, $A_{1g}$ and $E_g$ lattice vibrations of Ti and O atoms in the anatase unit cell [26]. No differences were found when comparing fresh and recycled photocatalysts suggesting that $TiO_2$ preserved its structure during the hydrothermal synthesis and after the photocatalytic hydrogen production process.

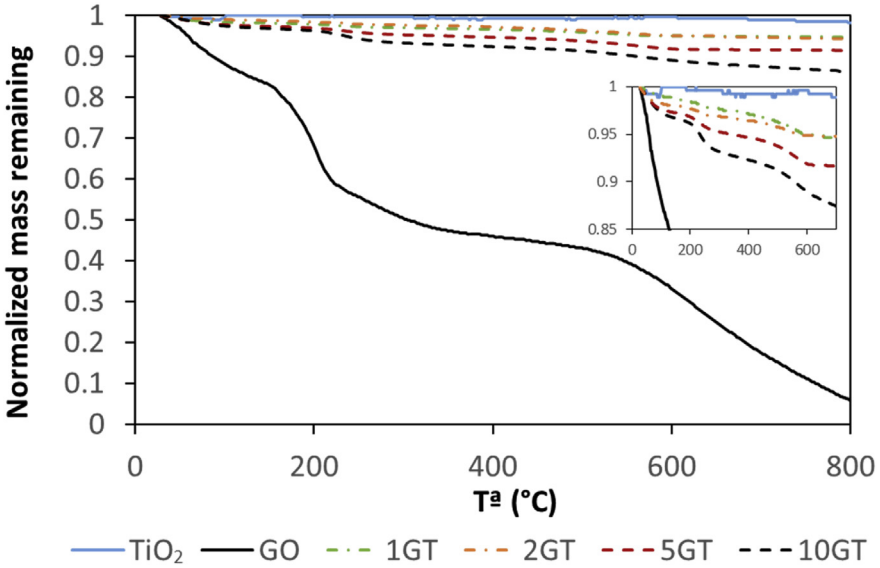


**Fig. 1 – TGA of the synthesized photocatalysts with different rGO/$TiO_2$ weight ratio.**

Please cite this article as: Corredor J et al., New insights in the performance and reuse of rGO/$TiO_2$ composites for the photocatalytic hydrogen production, International Journal of Hydrogen Energy, https://doi.org/10.1016/j.ijhydene.2020.01.181

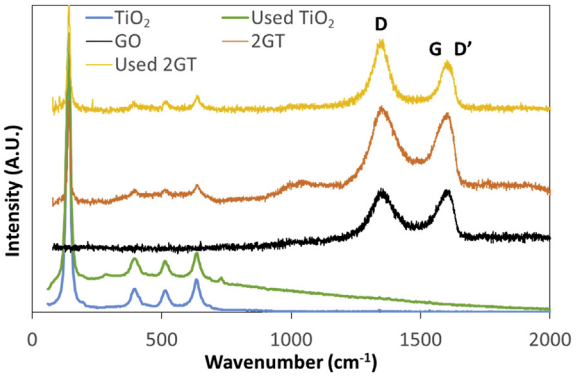


**Fig. 3 – Raman spectra of fresh and recycled photocatalysts, and GO.**

The band at 1353 $cm^{-1}$ corresponds to D bands of reduced graphene oxide. The bands G and D' were found from the deconvolution through a Lorenzian fitting of the band that appeared around 1600 $cm^{-1}$ (Table 2). These bands corresponding to reduced graphene oxide confirmed its presence in the composite. The recycled 2 GT, showed a noticeable blue shift (≈15 $cm^{-1}$) in the G band position. This fact could be attributed to changes in the rGO structure. The ratio $I_D/I_G$ increased in comparison to the fresh composite showing a higher number of defects in the rGO sheets which can be caused by a further reduction of the rGO sheets (Table 2). This fact was also observed by Sher Shah et al. in the degradation of Rhodamine B using rGO/$TiO_2$ photocatalyst [27]. In addition, after the photocatalytic process the composite colour became darker as it can be observed in Fig. 4, which suggests again that 2 GT suffered a reduction during the photocatalytic hydrogen production reaction. This reduction could be caused by the electron transfer from the $TiO_2$ conduction band to rGO.

BET specific surface areas of bare $TiO_2$ and the composites are shown in Table 3. An increase in the specific surface area was observed in the composites in comparison with bare $TiO_2$, due to the presence of the reduced graphene oxide sheets. Moreover, the specific surface area increases with GO content in the catalysts, which is in agreement with the literature [26,27]. However, photocatalytic hydrogen production not only depends on the surface area of the catalyst. Therefore, a straight relationship between both variables has not been proposed.

Considering the optical properties, band gap analyses for these catalysts have been previously reported in Ribao et al., 2018 [22]. A shift to less energy was observed in the composite band gap. Nevertheless, this behavior is not related to the results of this manuscript as they have been obtained working only with UV light.

**Table 2 – D, G and G′ bands position and $I_D/I_G$.**

| | D ($cm^{-1}$) | G ($cm^{-1}$) | D' ($cm^{-1}$) | $I_D/I_G$ |
|---|---|---|---|---|
| GO | 1355 | 1580 | 1610 | 1.63 |
| Fresh 2 GT | 1355 | 1580 | 1610 | 1.66 |
| Recycled 2 GT | 1350 | 1595 | 1618 | 1.86 |

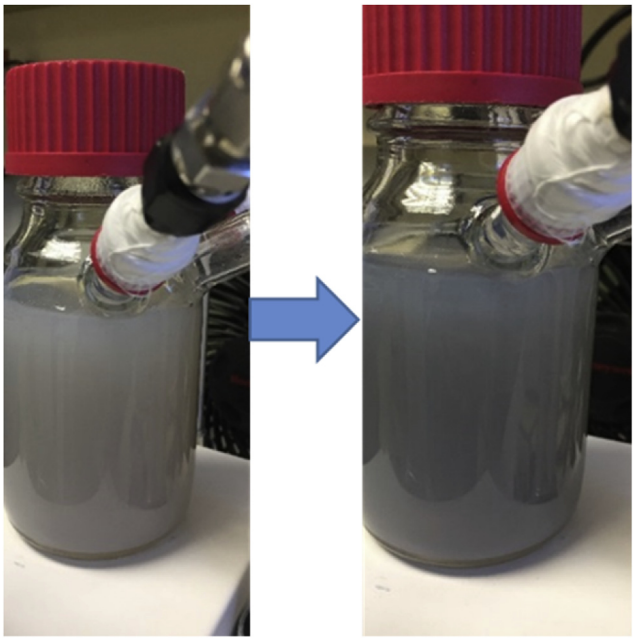

**Fig. 4 – 2 GT suspension before (left) and after (right) the photocatalytic hydrogen production.**

## *Photocatalyst performance*

### *Performance of the composite photocatalysts*

Two preliminary experiments, one with 20% vol. methanol solution in the absence of catalyst and the second one with photocatalyst in the absence of sacrificial agent, were carried out under UV irradiation to check the unlikely generation of hydrogen. In both cases no hydrogen production was detected.

As mentioned in the previous section after synthesis of the composites, they were tested for the photocatalytic hydrogen production (Fig. 5). The catalyst concentration was 0.1 g $L^{-1}$ and the experiments lasted for 5 h 2 GT and 1 GT showed similar hydrogen production with a maximum value of 40 μmol $g^{-1}_{catalyst}$. However, 5 GT and 10 GT performed lower hydrogen production. The presence of rGO can lower the charge carrier recombination rate in the photocatalyst because the photogenerated electrons on the conduction band can migrate from the $TiO_2$ to rGO improving the photocatalyst activity as consequence; but, on the contrary rGO sheets can reduce the number of available active sites in the photocatalyst decreasing its photoreactivity [28]. Therefore, 2 GT reached the best compromise between these effects.

### *Photocatalyst stability*

The comparative performance of $TiO_2$ and 2 GT was analyzed from the results achieved in experiments that lasted for 96 h (Fig. 6). The initial rate was very similar in both photocatalysts with a value of 1.6 μmol $H_2$ $g^{-1}_{catalyst}$ $h^{-1}$. After approximately 20 h in both experiments a progressive decrease of the hydrogen production rate was observed until the process stopped completely (plateau around 80 h). Thus, this loss of activity deserved further research as it will be detailed below.

Please cite this article as: Corredor J et al., New insights in the performance and reuse of rGO/$TiO_2$ composites for the photocatalytic hydrogen production, International Journal of Hydrogen Energy, https://doi.org/10.1016/j.ijhydene.2020.01.181

**Table 3 – Specific surface area of the photocatalysts.**

| Catalyst code | $TiO_2$ | 1 GT | 2 GT | 5 GT | 10 GT |
|---|---|---|---|---|---|
| Specific surface area ($m^2\ g^{-1}$) | 54.99 ± 0.29 | 57.70 ± 0.27 | 62.63 ± 0.15 | 77.79 ± 0.31 | 79.60 ± 0.31 |

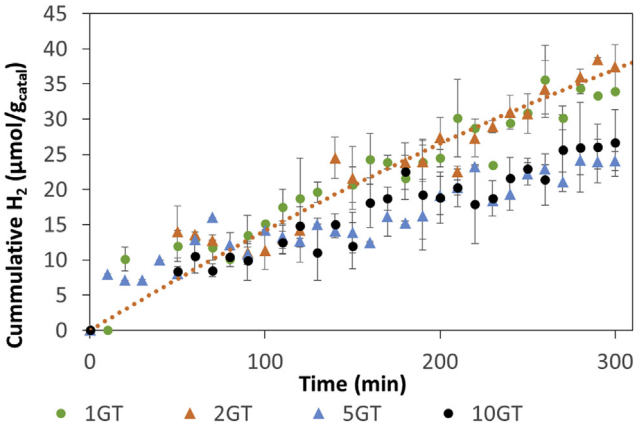


**Fig. 5 – Hydrogen production using photocatalysts with different rGO/$TiO_2$ weight ratios.**

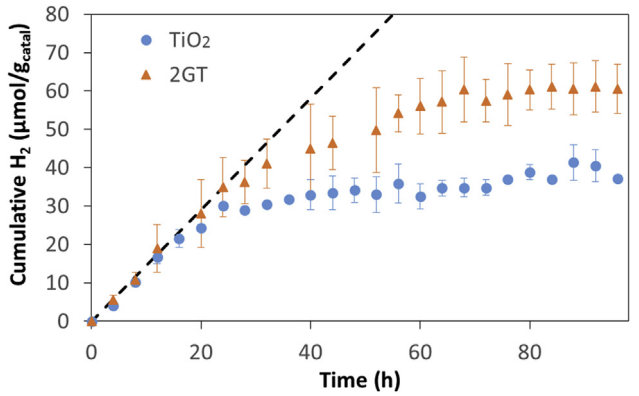


**Fig. 6 – Hydrogen production with photocatalyst in suspension.**

Next, a set of experiments with alternative periods of photocatalysis and argon purge were conducted with $TiO_2$ and 2 GT. The results achieved after 8 cycles are shown in Fig. 7. The first cycle of $TiO_2$ and 2 GT in Fig. 7 can be compared with the data corresponding to the first 12 h of both photocatalysts represented in Fig. 6. In both cases, the hydrogen production values are within the experimental error. The first 5 cycles were run for 12 h each; the rate of hydrogen generation was similar for both photocatalysts. While $TiO_2$ kept the rate almost constant, 2 GT suffered a slight decrease in the rate with the successive cycles, fact that was also observed after the 8th cycle performed under similar conditions. The rate decrease could be explained by the further reduction of GO in the composite with operation time and an increase in the number of defects that are detrimental for the photocatalytic activity. The 6th cycle (Fig. 7) showed a similar behavior in the hydrogen generation as in Fig. 6, that was attributed to the accumulation of hydrogen in the reaction vessel and the inhibitory effect of the reaction product as previously reported [29,30]. The difference between $H^+/H_2$ reduction potential and $TiO_2$ conduction band potential was diminished due to the accumulation of $H_2$ reducing the driving force until the hydrogen production stops. For long operation times (cycle 6th) it is remarkable that recycled 2 GT suffered a decrease in the production rate compared to the fresh catalyst that leads to less hydrogen production than for $TiO_2$.

Cycle 7 was performed by feeding hydrogen in order to check its inhibitory effect, and as expected no hydrogen was formed. After removal of the retained hydrogen with the argon purge the hydrogen generation rate was recovered as shown in cycle number 8.

The pH was measured after each cycle. Fig. 8 shows the change in this variable from the initial value of the methanol solution, 5.8. In the first cycle the sharpest decrease of pH took place, from 5.8 to 4.3 and in the second cycle from 4.3 to 4; in the successive cycles there was a slight decrease of pH that

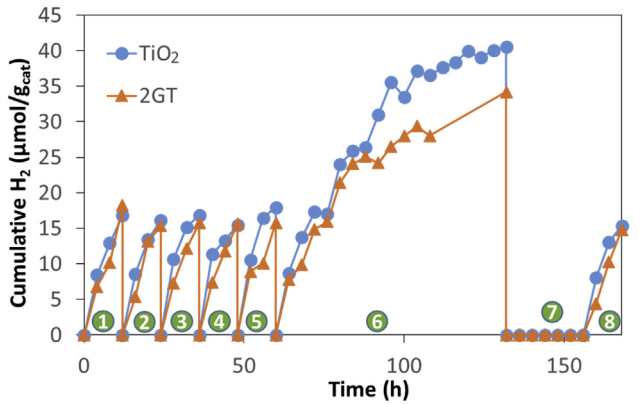


**Fig. 7 – $TiO_2$ and 2 GT photocatalytic hydrogen production during some cycles.**

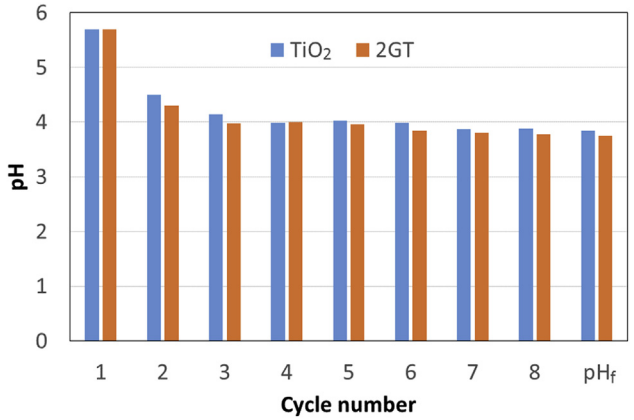


**Fig. 8 – Initial pH in each cycle and the final pH after the 8 cycles.**

Please cite this article as: Corredor J et al., New insights in the performance and reuse of rGO/$TiO_2$ composites for the photocatalytic hydrogen production, International Journal of Hydrogen Energy, https://doi.org/10.1016/j.ijhydene.2020.01.181

reached a value of 3.8 after the last cycle. This decrease of pH could be well attributed to the formation of formic acid produced as intermediate during the methanol decomposition as it can be observed in Eqs. (1)–(3) [31]. The pH was maintained around 3.8 because of the buffer capacity of the formic acid that smooths the pH change during the photocatalytic hydrogen production process and keeps it close to its $pK_a$ value of 3.8 [32].

The degradation mechanism of methanol is shown in Equations (1)–(3). This mechanism takes place by direct oxidation by the catalyst holes, which is the main oxidation pathway when the molar water/methanol ratio is lower than 300 [33].

$$CH_3OH \xrightarrow{rGO/TiO_2,vh} HCOH + H_2 \quad (1)$$

$$HCOH + H_2O \xrightarrow{rGO/TiO_2,vh} HCOOH + H_2 \quad (2)$$

$$HCOOH \xrightarrow{rGO/TiO_2,vh} CO_2 + H_2 \quad (3)$$

## Conclusions

Photocatalytic hydrogen production appears as a good opportunity when looking for sustainable energy resources at the same time that organic wastes are upgraded. The final deployment of the technology is strongly related to the availability of high performance and stability catalysts. Being $TiO_2$ the most widely used material, research efforts are focused on improving its main drawbacks, i.e., its wide band gap (3.2 eV) and the high recombination rate of the electron-hole pairs. The use of noble metals, although increasing the effectiveness, decrease the cost-effectiveness of the process, thus, a composite material made with $TiO_2$ and graphene oxide has been proposed. The presence of GO in the photocatalytic hydrogen generation was analyzed and best results were obtained with 2% of carbonaceous material.

The initial hydrogen production rates for fresh $TiO_2$ and 2 GT catalysts were similar with a value around 1.6 μmol $H_2$ $g_{catalyst}^{-1}$ $h^{-1}$. But, the accumulation of the generated hydrogen in the photocatalytic reactor slowed down the process kinetics until it was completely stopped after approximately 80 h. A protocol with argon purge in order to remove hydrogen from the reaction mixture has shown effective in recovering the hydrogen generation rate for long operation times.

$TiO_2$ and 2 GT were also evaluated in several operation cycles with argon purge after each cycle. While $TiO_2$ kept the initial hydrogen production rate almost constant, 2 GT suffered a slight decrease after the successive cycles compromising its performance. This could be attributed to the further 2 GT reduction after each cycle and the increase in the number of defects that are detrimental for the photocatalytic activity.

## .Acknowledgements

Financial support from projects CTM2015-69845-R (MINECO/FEDER, UE) and RTI2018-099407-B-I00 (MCIU/AEI/FEDER, UE) is gratefully acknowledged. Juan Corredor is grateful to a FPI contract grant (BES-2016-079201).

## REFERENCES

[1] Ruan ZH, Li YD, Yuan Y, Lin KF, Tan HP. Energy-absorption-based explanation of the photocatalytic activity enhancement mechanism of $TiO_2$ nanofibers. Int J Hydrogen Energy 2019;44:21569–76. https://doi.org/10.1016/j.ijhydene.2019.06.083.

[2] Sepahvand H, Sharifnia S. Photocatalytic overall water splitting by Z-scheme g-$C_3N_4$/$BiFeO_3$ heterojunction. Int J Hydrogen Energy 2019;44:23658–68. https://doi.org/10.1016/j.ijhydene.2019.07.078.

[3] Supplis C, Gros F, Dahi G, Dauchet J, Roudet M, Gloaguen F, et al. Spectral radiative analysis of bio-inspired $H_2$ production in a benchmark photoreactor: a first investigation using spatial photonic balance. Int J Hydrogen Energy 2018;43:8221–31. https://doi.org/10.1016/j.ijhydene.2018.03.097.

[4] Cargnello M, Montini T, Smolin SY, Priebe JB, Delgado-Jaén JJ, Doan-Nguyen VVT, et al. Engineering titania nanostructure to tune and improve its photocatalytic activity. Proc Natl Acad Sci U S A 2016;113:3966–71. https://doi.org/10.1073/pnas.1524806113.

[5] Holladay JD, Hu J, King DL, Wang Y. An overview of hydrogen production technologies. Catal Today J 2009;139:244–60. https://doi.org/10.1016/j.cattod.2008.08.039.

[6] Fujishima A, Honda K. Electrochemical photolysis of water at a semiconductor electrode. Nature 1972;238:37–8. https://doi.org/10.1038/238037a0.

[7] Corredor J, Rivero MJ, Rangel CM, Gloaguen F, Ortiz I. Comprehensive review and future perspectives on the photocatalytic hydrogen production. J Chem Technol Biotechnol 2019;94:3049–63. https://doi.org/10.1002/jctb.6123.

[8] Fajrina N, Tahir M. A critical review in strategies to improve photocatalytic water splitting towards hydrogen production. Int J Hydrogen Energy 2018;44:540–77. https://doi.org/10.1016/j.ijhydene.2018.10.200.

[9] Guan L, Chen X. Photoexcited charge transport and accumulation in anatase $TiO_2$. ACS Appl Energy Mater 2018;1:4313–20. https://doi.org/10.1021/acsaem.8b00944.

[10] Gao Q, Si F, Zhang S, Fang Y, Chen X, Yang S. Hydrogenated F-doped $TiO_2$ for photocatalytic hydrogen evolution and pollutant degradation. Int J Hydrogen Energy 2019;44:8011–9. https://doi.org/10.1016/j.ijhydene.2019.01.233.

[11] Lin J, Liu Y, Liu Y, Huang C, Liu W, Mi X, et al. $SnS_2$ nanosheets/H-$TiO_2$ nanotube Arrays as a type II heterojunctioned photoanode for photoelectrochemical water splitting. ChemSusChem 2019;12:961–7. https://doi.org/10.1002/cssc.201802691.

[12] Ribao P, Alexandra Esteves M, Fernandes VR, Rivero MJ, Rangel CM, Ortiz I. Challenges arising from the use of $TiO_2$/rGO/Pt photocatalysts to produce hydrogen from crude glycerol compared to synthetic glycerol. Int J Hydrogen Energy 2018;44:28494–506. https://doi.org/10.1016/j.ijhydene.2018.09.148.

[13] Lin X, Wang J. Green synthesis of well dispersed $TiO_2$/Pt nanoparticles photocatalysts and enhanced photocatalytic activity towards hydrogen. Int J Hydrogen Energy 2019;44:31853–9. https://doi.org/10.1016/j.ijhydene.2019.10.062.

[14] Hu H, Qian D, Lin P, Ding Z, Cui C. Oxygen vacancies mediated in-situ growth of noble-metal (Ag, Au, Pt) nanoparticles on 3D $TiO_2$ hierarchical spheres for efficient

Please cite this article as: Corredor J et al., New insights in the performance and reuse of rGO/$TiO_2$ composites for the photocatalytic hydrogen production, International Journal of Hydrogen Energy, https://doi.org/10.1016/j.ijhydene.2020.01.181

photocatalytic hydrogen evolution from water splitting. Int J Hydrogen Energy 2020;45:629–39. https://doi.org/10.1016/j.ijhydene.2019.10.231.
[15] Lu X, Xie J, Chen X, Li X. Engineering MPx (M = Fe, Co or Ni) interface electron transfer channels for boosting photocatalytic $H_2$ evolution over g-$C_3N_4$/$MoS_2$ layered heterojunctions. Appl Catal B Environ 2019;252:250–9. https://doi.org/10.1016/j.apcatb.2019.04.012.
[16] He K, Xie J, Liu Z, Li N, Chen X, Hu J, et al. Multi-functional $Ni_3C$ Cocatalyst/g-$C_3N_4$ nanoheterojunctions for robust photocatalytic $H_2$ evolution under visible light. J Mater Chem A 2018;6:13110–22. https://doi.org/10.1039/C8TA03048K.
[17] Ma X, Chen C, Hu J, Zheng M, Wang H, Dong S, et al. Evidence of direct Z-scheme g-$C_3N_4$/$WS_2$ nanocomposite under interfacial coupling: first-principles study. J Alloys Compd 2019;788:1–9. https://doi.org/10.1016/j.jallcom.2019.02.044.
[18] Lu X, Xie J, Liu SY, Adamski A, Chen X, Li X. Low-cost $Ni_3B$/$Ni(OH)_2$ as an ecofriendly hybrid cocatalyst for remarkably boosting photocatalytic H2 production over g-$C_3N_4$ nanosheets. ACS Sustainable Chem Eng 2018;6:13140–50. https://doi.org/10.1021/acssuschemeng.8b02653.
[19] Hafeez HY, Lakhera SK, Bellamkonda S, Rao GR, Shankar MV, Bahnemann DW, et al. Construction of ternary hybrid layered reduced graphene oxide supported g-$C_3N_4$-$TiO_2$ nanocomposite and its photocatalytic hydrogen production activity. Int J Hydrogen Energy 2018;43:3892–904. https://doi.org/10.1016/j.ijhydene.2017.09.048.
[20] Xie H, Hou C, Wang H, Zhang Q, Li YS. N Co-doped graphene quantum dot/$TiO_2$ composites for efficient photocatalytic hydrogen generation. Nanoscale Res Lett 2017;12:400. https://doi.org/10.1186/s11671-017-2101-1.
[21] Khalid NR, Majid A, Tahir MB, Niaz NA, Khalid S. Carbonaceous-$TiO_2$ nanomaterials for photocatalytic degradation of pollutants: a review. Ceram Int 2017;43:14552–71. https://doi.org/10.1016/j.ceramint.2017.08.143.
[22] Ribao P, Rivero MJ, Ortiz I. Enhanced photocatalytic activity using GO/$TiO_2$ catalyst for the removal of DCA solutions. Environ Sci Pollut Res 2018;25:34893–902. https://doi.org/10.1007/s11356-017-0901-6.
[23] Rivero MJ, Iglesias O, Ribao P, Ortiz I. Kinetic performance of $TiO_2$/Pt/reduced graphene oxide composites in the photocatalytic hydrogen production. Int J Hydrogen Energy 2019;44:101–9. https://doi.org/10.1016/j.ijhydene.2018.02.115.
[24] Ding YH, Zhang P, Zhuo Q, Ren HM, Yang ZM, Jiang Y. A green approach to the synthesis of reduced graphene oxide nanosheets under UV irradiation. Nanotechnology 2011;22:215601. https://doi.org/10.1088/0957-4484/22/21/215601.
[25] Wang R, Xu G, He Y. Structure and properties of polytetrafluoroethylene (PTFE) fibers. E-Polymers 2017;17:215–20. https://doi.org/10.1515/epoly-2016-0059.
[26] Šćepanović MJ, Grujić-Brojčin M, Dohčević-Mitrović ZD, Popović ZV. Characterization of anatase $TiO_2$ nanopowder by variable-temperature Raman spectroscopy. Sci Sinter 2009;41:67–73. https://doi.org/10.2298/SOS0901067S.
[27] Sher Shah MSA, Park AR, Zhang K, Park JH, Yoo PJ. Green synthesis of biphasic $TiO_2$-reduced graphene oxide nanocomposites with highly enhanced photocatalytic activity. ACS Appl Mater Interfaces 2012;4:3893–901. https://doi.org/10.1021/am301287m.
[28] Cao XR, Tian GH, Chen YJ, Zhou J, Zhou W, Tian CG, et al. Hierarchical composites of $TiO_2$ nanowire arrays on reduced graphene oxide nanosheets with enhanced photocatalytic hydrogen evolution performance. J Mater Chem 2014;2:4366–74. https://doi.org/10.1039/c3ta14272h.
[29] Kuang L, Zhang W. Enhanced hydrogen production by carbon-doped $TiO_2$ decorated with reduced graphene oxide (rGO) under visible light irradiation. RSC Adv 2016;6:2479–88. https://doi.org/10.1039/C5RA26096E.
[30] Choi W. Photocatalytic hydrogen production using surface-modified titania nanoparticles. Sol Hydrog Nanotechnol II 2007;6650:164–72. https://doi.org/10.1117/12.737292.
[31] Ahmed AY, Kandiel TA, Ivanova I, Bahnemann D. Photocatalytic and photoelectrochemical oxidation mechanisms of methanol on $TiO_2$ in aqueous solution. Appl Surf Sci 2014;319:44–9. https://doi.org/10.1016/j.apsusc.2014.07.134.
[32] Muckerman JT, Skone JH, Ning M, Wasada-Tsutsui Y. Toward the accurate calculation of pKa values in water and acetonitrile. Biochim Biophys Acta Bioenerg 2013;1827:882–91. https://doi.org/10.1016/j.bbabio.2013.03.011.
[33] Wang CY, Groenzin H, Shultz MJ. Direct observation of competitive adsorption between methanol and water on $TiO_2$: an in situ sum-frequency generation study. J Am Chem Soc 2004;126:8094–5. https://doi.org/10.1021/ja048165l.

Please cite this article as: Corredor J et al., New insights in the performance and reuse of rGO/$TiO_2$ composites for the photocatalytic hydrogen production, International Journal of Hydrogen Energy, https://doi.org/10.1016/j.ijhydene.2020.01.181

## 3.3. Publication 3. Performance of rGO/$TiO_2$ photocatalytic membranes for hydrogen production

Chapter 3.3 corresponds to the following paper:

J. Corredor, E. Perez-Peña M. J. Rivero and I. Ortiz. "Performance of rGO/$TiO_2$ photocatalytic membranes for hydrogen production". *Membranes*, 10(9), 1–13, 2020.
DOI: 10.3390/membranes10090218

membranes

MDPI

Article

# Performance of rGO/$TiO_2$ Photocatalytic Membranes for Hydrogen Production

**Juan Corredor, Eduardo Perez-Peña, Maria J. Rivero and Inmaculada Ortiz ***

Department of Chemical and Biomolecular Engineering, ETSIIT, University of Cantabria, Avda. de los Castros s/n, 39005 Santander, Spain; corredorj@unican.es (J.C.); eduardo.perezp@alumnos.unican.es (E.P.-P.); mariajose.rivero@unican.es (M.J.R.)

* Correspondence: ortizi@unican.es; Tel.: +34-942-201-585

Received: 11 August 2020; Accepted: 30 August 2020; Published: 1 September 2020


**Abstract:** Although there are promising environmental and energy characteristics for the photocatalytic production of hydrogen, two main drawbacks must be overcome before the large-scale deployment of the technology becomes a reality, (i) the low efficiency reported by state of the art photocatalysts and, (ii) the short life time and difficult recovery of the photocatalyst, issues that need research and development for new high performance catalysts. In this work 2% rGO/$TiO_2$ composite photocatalysts were supported over Nafion membranes and the performance of the photocatalytic membrane was tested for hydrogen production from a 20% vol. methanol solution. Immobilization of the composite on Nafion membranes followed three different simple methods which preserve the photocatalyst structure: solvent-casting (SC), spraying (SP), and dip-coating (DP). The photocatalyst was included in the matrix membrane using the SC method, while it was located on the membrane surface in the SP and DP membranes showing less mass transfer limitations. The performance of the synthesized photocatalytic membranes for hydrogen production under UVA light irradiation was compared. Leaching of the catalytic membranes was tested by measuring the turbidity of the solution. With respect to catalyst leaching, both the SC and SP membranes provided very good results, the leaching being lower with the SC membrane. The best results in terms of initial hydrogen production rate (HPR) were obtained with the SP and DP membrane. The SP was selected as the most suitable method for photocatalytic hydrogen production due to the high HPR and the negligible photocatalyst leaching. Moreover, the stability of this membrane was studied for longer operation times. This work helps to improve the knowledge on the application of photocatalytic membranes for hydrogen production and contributes in facilitating the large-scale application of this process.

**Keywords:** rGO/$TiO_2$; Nafion; hydrogen production; photocatalysis; photocatalytic membrane

## 1. Introduction

In the current global energy framework and according to the new commitments to reduce greenhouse gas emissions (GHG), the use of renewable hydrogen is an interesting option to facilitate energy transition [1–4]. Nowadays, 95% of hydrogen is produced by steam reforming from fossil fuels, mainly natural gas, which is energy intensive and still contributes to GHG emissions [5–7]. The rest of the hydrogen is mainly produced by electrolysis, that today is particularly energy and cost intensive [8–10]. Other processes, less extensive, make use of renewable energy sources in the generation of hydrogen, e.g., biological processes, electrolysis combined with solar panels and photocatalysis [11,12] thus driven by solar light. The latter being an interesting alternative in terms of energy as it takes advantage of the use of waste effluents as sacrificial agents that contribute further to the transition from a linear to a circular economy.

State of the art heterogeneous photocatalysts have been widely investigated such as, metal oxides ($TiO_2$, $Cu_2O$), carbonaceous materials (g-$C_3N_4$), and chalcogenides (CdS, ZnS) [13]. Among the studied photocatalysts, $TiO_2$ reports good properties such as chemical and thermal stability, high photo-reactivity, and low cost. However, its wide band gap (3.2 eV) restricts its applications to ultraviolet light, which represents only about 4–8% of the solar spectrum. An additional drawback is the high recombination rate of the electron-hole pairs, which reduces its photocatalytic activity [14,15]. Photocatalytic hydrogen production has been mainly studied using alcohols (such as methanol or ethanol) as sacrificial agents or performing only water splitting. Most of these studies used Pt coupled to the photocatalyst because of the higher hydrogen production achieved with this noble metal. This fact is due to the high value of the Pt work function (5.93 eV) which allows an efficient transfer of the photogenerated electrons from the photocatalyst to the noble metal [16]. However, Pt is a very scarce and high cost material [17,18]. Coupling $TiO_2$ with graphene oxide (GO) results in a low-cost alternative to improve the photocatalytic activity of $TiO_2$. GO is a two- dimensional planar sheet composed of $sp^2$ bonded carbon atoms structured in a hexagonal lattice network highly functionalized with oxygenated groups. It can be reduced to graphene, which can improve the photocatalytic activity of $TiO_2$ due to its ability to carry charges from the $TiO_2$ conduction band reducing the electron-hole recombination rate. Moreover, the band gap shift can contribute by taking advantage of the solar spectrum [19,20].

Regarding the photocatalytic reactor configuration, slurry type reactors have been widely used in order to reduce mass transfer limitations. However, two major drawbacks are associated with the use of suspended solid reactors: (i) the requirement of a separation and recovery step of the photocatalyst after the photocatalytic process which is especially difficult with nanomaterials due to their small size and, (ii) hazards associated with the manipulation of nanomaterials [21]. Therefore, techniques to immobilize the photocatalyst leading to immobilized photocatalytic membrane reactors (IPMR) have been encouraged to facilitate catalyst reuse and to avoid the presence of nanomaterials in the treated waters and effluents. When using a membrane, it can offer a role of support to the photocatalyst and it can also act as selective barrier for the compounds to be degraded. In IPMRs where the membrane exerts an immobilization and filtration function, dead-end or cross- flow configurations are possible [22,23]. In the case of hydrogen production, most of the works use an H-type reactor which consists of two compartments, the first one containing the photoanode, the second one containing a Pt cathode and a proton exchange membrane that divides both compartments to allow $H^+$ transport between both chambers. These reactors have the advantage of producing $H_2$ and $O_2$ separately. Most of the H-type reactors immobilize $TiO_2$-based photocatalysts on a Ti foil and use Nafion as proton exchange membrane [24–29]. A cross-flow type reactor was employed by Hattori et al. They used a $TiO_2$ nanotube array deposited on a Pd thin film to produce hydrogen from the reforming of low molecular weight alcohols. The generated hydrogen was purified through the Pd film [30]. With regard to hydrogen production with immobilized catalyst in a simple single chamber photoreactor using a membrane with the sole function of photocatalyst support only a few works can be found in the literature [31–34]. Some works have made use of glass substrates to support the photocatalyst; Cha et al. evaluated the effect of Pt location and amount in $TiO_2$ nanotubes supported on a fluorine doped tin oxide (FTO) glass, using a methanol solution as sacrificial agent [31]. Ma et al. synthesized $Er^{3+}$:$YAlO_3$Pt-$TiO_2$ composite on a glass substrate for hydrogen production from an aqueous solution of glucose [32]. Della Foglia immobilized Pt/$TiO_2$ on glass fibers for photo-steam reforming of low molecular weight alcohols [33]. Wu et al. obtained hydrogen from an ethanol solution using immobilized $TiO_2$/Pt and $TiO_2$/Pd on cellulose membranes [35].

Photocatalysts have also been immobilized on polymeric membranes [35–39]. However, most of the polymer materials were damaged by UV irradiation. Polytetrafluoroethylene (PTFE) has been used as photocatalyst support because of its photochemical resistance [38,39]. Sulfonated polytetrafluoroethylene (Nafion) is resistant to photochemical degradation and in addition is a proton ($H^+$) conductor due to the sulfonic acid groups attached to the PTFE backbone [40–42].

Nafion has been used as membrane support of the photocatalyst in the photocatalytic degradation of different pollutants [43–45]; it has been also employed as photocatalyst coating to improve the degradation of cationic molecules due to the anionic character of the sulfonic groups contained in Nafion membranes [46,47]. Regarding photocatalytic hydrogen production, Nafion has been used as a matrix to attach photocatalysts with visible light photosensitizers [34,48] as well as a proton exchange membrane in H-type reactors. Park et al. used ($Ru(bpy)_3^{2+}$) as photosensitizer, (methyl viologen) as electron mediator and Pt supported on a Nafion membrane for hydrogen production from ethylenediaminetetraacetic acid (EDTA) [34]. Choi bonded $Ru(bpy)_3^{2+}$ to $TiO_2$ within a Nafion layer to produce hydrogen from an EDTA solution [48].

A wide variety of immobilization methods have been used in photocatalytic pollutant degradation, such as electrophoresis, chemical and physical vapor deposition, sol-gel, thermal spraying, and solvent deposition [49]. A reliable technique for photocatalyst immobilization must provide a strong photocatalyst support, uniform coating, high degree of photocatalyst irradiation, and preserve photocatalyst structure during preparation and immobilization [50]. In this work, two solvent deposition methods (SP and DP) and SC were compared because these methods are simple and the soft operational conditions do not provoke changes in the composite structure [49]. SC was chosen because it prevents photocatalyst leaching as it is embedded in the polymeric membrane. However, mass transfer limitations are expected to be higher than in the other methods. Lower mass transfer limitations are expected in DP and SP methods due to the location of the photocatalyst on the membrane surface; although DP is a simpler method, the SP method allows a uniform coating.

Although there is interesting information already reported in the literature, several gaps need to be filled before the large scale application of photocatalytic hydrogen production, such as: (i) the comparison of the performance of slurry type and IPMR for similar catalysts and operating conditions, and (ii) increasing photocatalyst stability and life time for long operation times. This study advances the knowledge of IPMRs by experimentally assessing the performance of newly synthesized $rGO/TiO_2$ composite photocatalysts supported on Nafion polymeric membranes. Furthermore, several methods to immobilize the catalyst for photocatalytic hydrogen production in a one-chamber photoreactor were developed and the results compared in terms of hydrogen generation rate, membrane reuse capacity, and catalyst leaching.

## 2. Materials and Methods

### *2.1. Materials*

Methanol HPLC grade was purchased from Scharlau and isopropanol 99.5% was supplied by Acros Organics (Madrid, Spain). $TiO_2$ P25 was purchased from Evonik; a dispersion of graphene oxide sheets in water solvent and 4 mg $mL^{-1}$ GO was provided by Graphenea; while 20% Nafion in alcohol solution and Nafion membranes N115, with a thickness of 127 μm according to the supplier, were purchased from Ion Power. Pure argon 3X from Praxair (Camargo, Spain) was used to ensure an inert atmosphere in the reactor.

### *2.2. Photocatalyst Preparation and Characterization*

The photocatalytic membrane diameter was 4.4 cm. The membranes were loaded with 10% *w*/*w* of photocatalyst. The photocatalyst was immobilized on Nafion membranes by three different methods: SC, SP, and DP. 2% (*w*/*w*) of $rGO/TiO_2$ was hydrothermally synthesized as described in previous works [15,20]. Figure 1 illustrates the different immobilization methods.

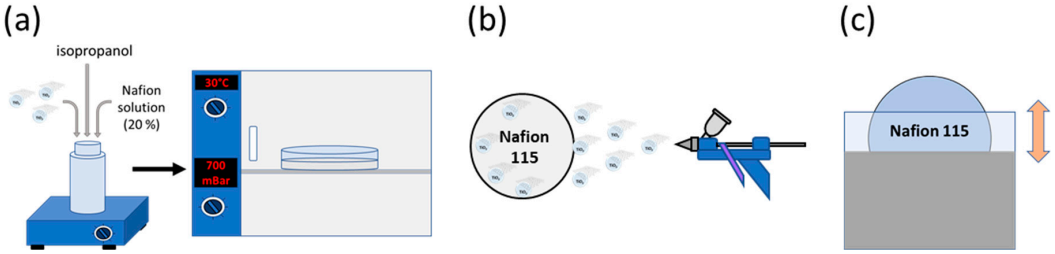


**Figure 1.** Photocatalytic immobilization methods: solvent-casting (SC) (**a**), spraying (SP) (**b**) and dip-coating (DP) (**c**).

In the SC method, 42.2 mg of photocatalyst were added to 1.81 g of Nafion solution and 0.5 mL of isopropanol. The mixture was stirred for 10 min and placed in an ultrasonication bath (Fisher scientific FB1505, Madrid, Spain) with a frequency of 37 kHz for 30 min. The resulting suspension was dried in a Petri dish set in a vacuum oven at 800 mbar and 30 °C over 24 h.

The SP method was applied to attach the composite catalyst to the Nafion N115 membrane. An ink composed of 0.3% photocatalyst, 2.7% of 5% Nafion solution, and 97.0% of isopropanol was prepared and ultrasonicated for 45 min at 37 kHz before being applied to the membrane. The membrane was placed on a heating plate at 60 °C while it was sprayed to achieve a photocatalyst concentration of 10% *w/w* on the membrane. After spraying, the membrane was dried for 24 h at ambient conditions.

The DP method was carried out by immersing the membrane for 10 min in a solution composed of 3.0% of photocatalyst, 25.7% of 5% Nafion solution, and 71.3% of isopropanol. The solution was dispersed using an ultrasonication bath for 45 min before it was applied. After each immersion, the membrane was dried at ambient conditions for 10 min. The membranes were immersed for 6 consecutive times to reach the desired concentration of photocatalyst. After the last immersion, the membrane was dried for 24 h at ambient conditions.

The detailed characterization of the rGO/$TiO_2$ composite material can be found in previous works [13,15]. Membrane characterization was carried out through different techniques. Fourier transform infrared (FTIR) spectra were recorded on a Spectrum Two spectrometer (Perkin Elmer, Madrid, Spain) equipped with an attenuated total reflection (ATR) accessory. Thermogravimetric analysis (TGA) was carried out in a Shimadzu DTG-60H Differential Thermal Gravimetric Analyzer (Barcelona, Spain) by heating the samples under nitrogen atmosphere (50 mL $min^{-1}$) from 25 °C to 900 °C at 10 °C $min^{-1}$. Scanning electron microscopy images were recorded with a SEM EVO MA 15, Carl Zeiss microscope (Madrid, Spain). For the cross-section images, the membrane samples were frozen in liquid nitrogen and fractured. All the samples were gold sputtered to make the samples conductive. The cross-section images of the photocatalytic membranes made it possible to measure the thickness of the different layers. The photocatalyst layer thickness averages values were calculated after measurement in 5 different layer locations.

### *2.3. Hydrogen Production*

The photocatalytic hydrogen production experiments were carried out in a 330 mL borosilicate photoreactor using 240 mL of 20% methanol solution as sacrificial agent. The photocatalytic membranes were fixed between two PTFE rings and they were placed in the center of the reactor. The photoreactor was coupled to a gas chromatograph Shimadzu 2010 Plus (Barcelona, Spain) equipped with a Shin Carbon ST 80/100 column using argon as carrier gas, and a thermal conductivity detector. Four Philips PL-S 9W lamps, with a wavelength range between 315 and 400 nm and a maximum emission at 365 nm, were used as light source. The irradiance, measured with a Delta Ohm HD 2102.1 photoradiometer (Padova, Spain), was 7.5 W $m^{-2}$.

The reaction media was bubbled with argon for 30 min in the dark to remove oxygen before the reaction was started. The operation temperature was 20 °C. The experiments were carried out twice to calculate the error bands.

In order to quantify the photocatalyst leaching, the turbidity of the solution was measured with a Turbiquant 3000 IR spectrometer (Merck, Madrid, Spain).

## 3. Results

### *3.1. Materials Characterization*

Figure 2a shows the TGA curves of different solid samples, i.e., $TiO_2$, pure GO and rGO/$TiO_2$. The GO thermogravimetric curve showed a weight loss up to 100 °C, that corresponded to the water contained in the material. The mass decrease from 150 to 300 °C was attributed to the loss of the oxygen-containing groups. The last mass loss step started around 500 °C and was assigned to the pyrolysis of the GO carbon skeleton [51]. For bare $TiO_2$, the initial mass loss was attributed to the adsorbed water in the material. Therefore, comparing the TG curves of the pure compounds and of the rGO/$TiO_2$ solid a composition of 3.9% GO in the composite was calculated.

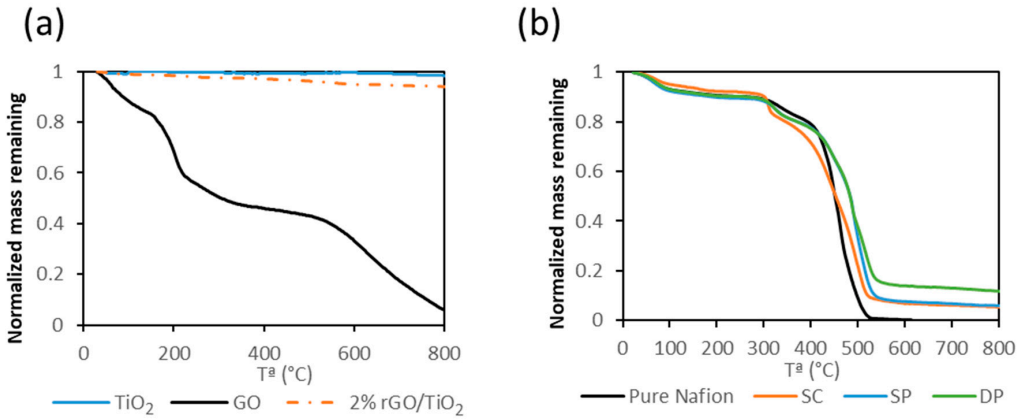


**Figure 2.** TGA of $TiO_2$, pure GO and rGO/$TiO_2$ (**a**). TGA of pure Nafion and photocatalytic membranes (**b**).

Figure 2b shows the TGA curves of the different membranes. Pure Nafion TGA curve showed three mass loss steps. The first one was attributed to the loss of absorbed water up to 100 °C. The second one, between 300 and 400 °C was related to the decomposition of the $–SO_3H$ groups. The last step was assigned to the degradation of the polymer backbone between 400 and 550 °C [52,53]. The thermal decomposition of the photocatalytic membranes was similar to that of pure Nafion. However, the decomposition temperature of the polymer backbone was shifted to higher temperatures due to the inorganic content. This fact could be due to the interaction between the Nafion backbone and inorganic particles. TGA results revealed that the content of photocatalyst was 8.8 ± 0.8%, 11.1 ± 3.0%, and 8.9 ± 7.0% in SC, SP, and DP membranes respectively. The variability of the photocatalyst concentration in the DP membrane was attributed to the heterogeneity of the particle concentration distribution on the membrane surface. This fact was due to the difficulty of obtaining a uniform photocatalyst layer on the membrane through this method.

Figure 3 shows FTIR spectra of pure Nafion and photocatalytic membranes. The pure Nafion curve showed the typical bands of this material. The bands at 1200 and 1140 $cm^{-1}$ were assigned to the stretching vibrations from $C–F_2$ and C–F, respectively. The 1056 and 975 $cm^{-1}$ bands were attributed to S–O stretching vibrations and C–O–C stretching vibrations, respectively. The bands at 627 and 512 $cm^{-1}$ were assigned to $C–F_2$ bending vibrations. Photocatalytic membrane spectra showed the typical bands of Nafion suggesting that the addition of photocatalyst does not affect the molecular structure of the Nafion membrane. This fact was also observed by Ding et al. [45]. However, the intensity of these bands was different for the different membranes. Pure Nafion showed the highest band intensity followed by the SC membrane in which most of the photocatalyst is contained inside the membrane matrix. SP and DP membranes showed less intensity in the FTIR spectra because the photocatalyst remains on the surface of the Nafion membranes. The slightly smaller thickness of the photocatalyst

layer (9.8 and 12.6 µm in DP and SP membranes, respectively) of DP membranes that was revealed in cross section SEM images (Figure 4) could explain the higher FTIR signal intensity in the DP compared to the SP membrane.

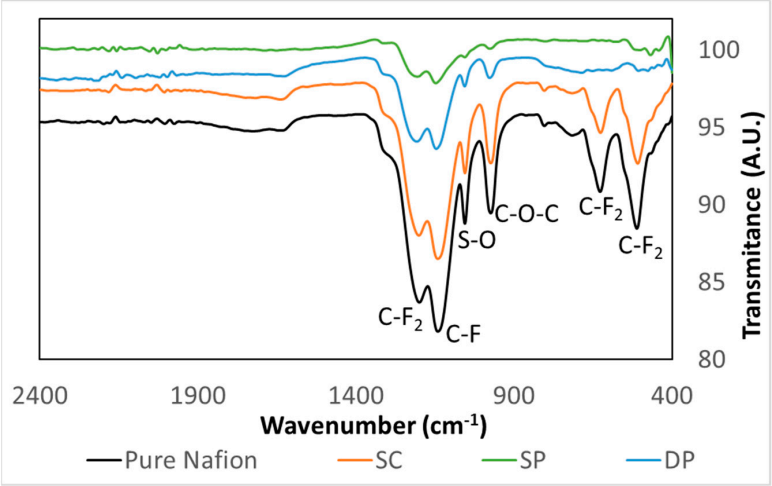


**Figure 3.** Pure Nafion and photocatalytic membrane FTIR spectra.

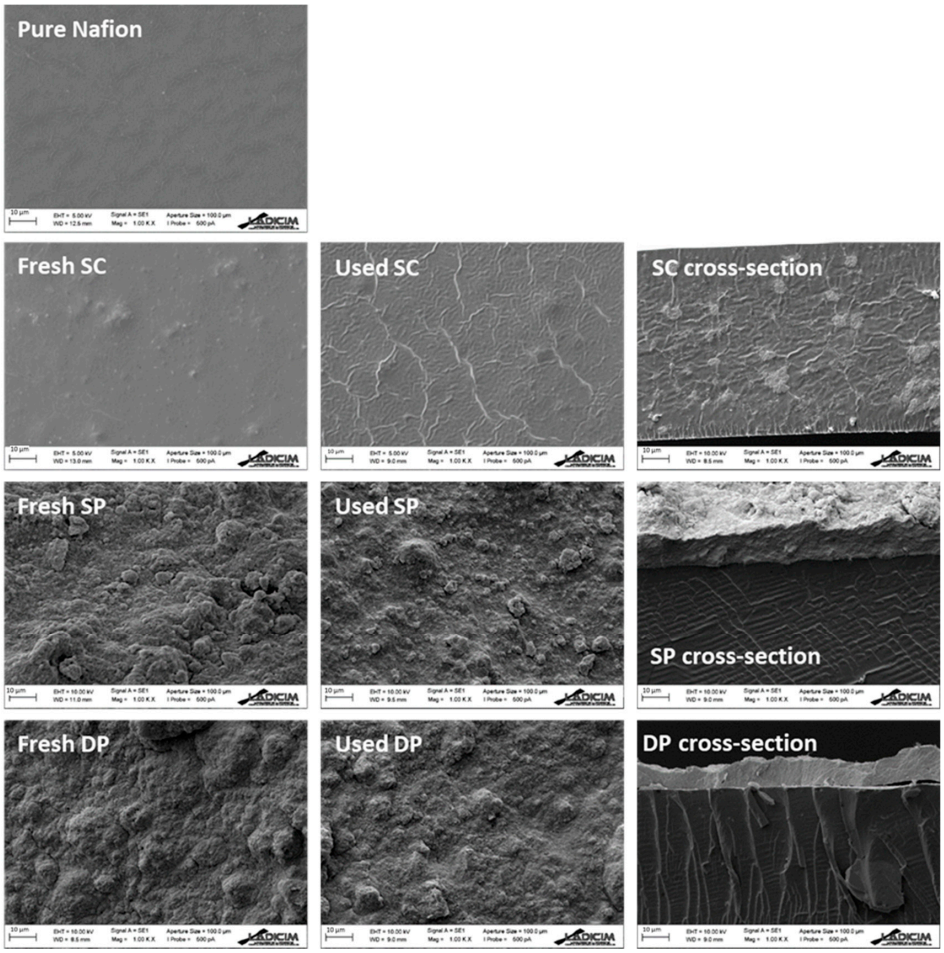


**Figure 4.** SEM images of pure Nafion, fresh membrane and used membrane surfaces, and fresh membrane cross-section. Scale bar = 10 µm.

Figure 4 shows the SEM surface images of the fresh and used membranes, and the cross section of the fresh membranes. The fresh SC SEM image revealed bulges in the membrane surface, which indicated the presence of photocatalyst inside the membrane matrix. Meanwhile, the micrographs of the fresh SP and DP membranes revealed that photocatalyst covered the whole Nafion surface.

The comparison between fresh and used SC membranes showed a ribbed surface in the used SC membrane indicating damage in the Nafion structure during the hydrogen production process. The rest of the used membranes did not show any appreciable change on the surface after the hydrogen production process.

The SC membrane cross-section revealed the presence of the photocatalyst in the whole membrane matrix, whereas in the SP and DP membrane cross-sections the expected photocatalyst layer deposition on the surface of the Nafion membrane was observed; photocatalyst layer thickness and membrane thickness were also determined (Table 1).

**Table 1.** Photocatalyst layer and membrane thickness.

| Thickness | Solvent-Casting | Spraying | Dip-Coating |
|---|---|---|---|
| Photocatalyst Layer (μm) | n.a. | 12.6 ± 2.6 | 9.8 ± 2.1 |
| Membrane Thickness (μm) | 72.0 ± 0.7 | 165.6 ± 1.6 | 162.5 ± 1.2 |

n.a.: not applicable.

### 3.2. Photocatalytic Membrane Performance

In order to confirm the higher photocatalytic activity of the composite photocatalyst compared with bare $TiO_2$ when they are immobilized on Nafion membranes, SP and $TiO_2$ immobilized catalysts were tested for photocatalytic hydrogen production (Figure 5). Although the initial rate of hydrogen production with both photocatalysts was similar (ca. 1.1 μmol $H_2$ $gcat^{-1}$ $h^{-1}$), the initial rate using $TiO_2$ decreased after 4 h and reached a total hydrogen production of 9 μmol $H_2$ $gcat^{-1}$ while the composite decreased its initial rate after 8 h with a total hydrogen production of 12 μmol $H_2$ $gcat^{-1}$. It was confirmed that 2% rGO/$TiO_2$ photocatalytic membranes performed better than $TiO_2$ membranes for hydrogen production.

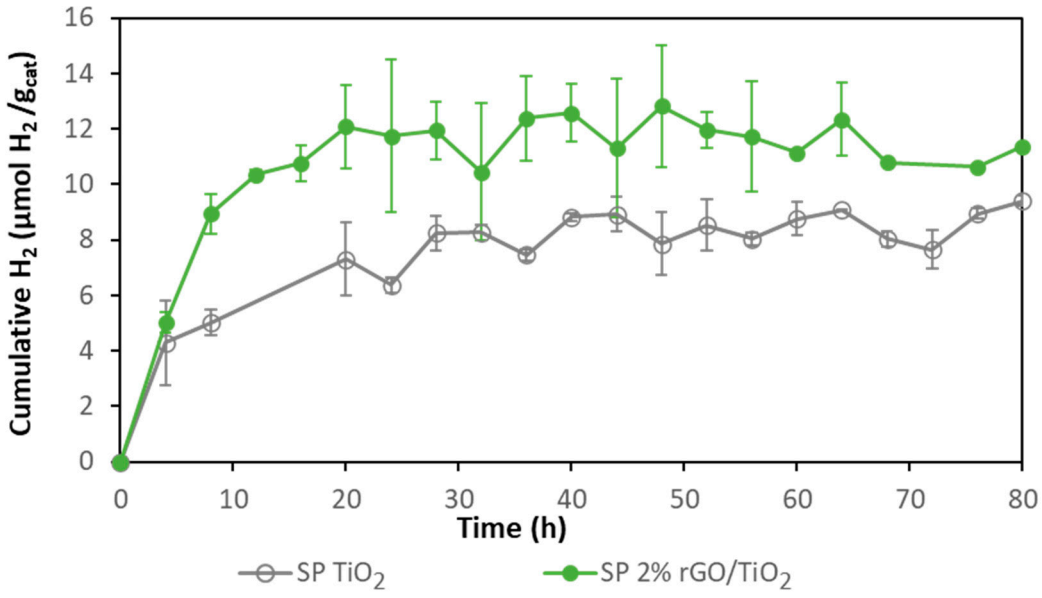


**Figure 5.** Comparison of hydrogen production with 2% rGO/$TiO_2$ SP and bare $TiO_2$ SP membranes.

Membranes obtained following the three different photocatalyst immobilization methods were tested for hydrogen production (Figure 6). Composite SP and DP membranes achieved HPRs of

1.11 ± 0.09 and 1.01 ± 0.10 μmol $H_2$ gcatalyst$^{-1}$ h$^{-1}$, respectively. With these membranes, hydrogen production was stopped after around 20 h. The composite SC membrane achieved an initial rate of 0.38 ± 0.03 μmol $H_2$ gcatalyst$^{-1}$ h$^{-1}$ during the first 8 h, but the hydrogen production continued to increase smoothly and stopped around 60 h of photoreaction. The higher initial activity of SP and DP membranes was attributed to the higher accessibility to the photocatalyst provided by these membranes, as the catalyst was mainly deposited on the membrane surface while SC membranes had most of the photocatalyst embedded in the membrane matrix, thus, exerting higher resistance to mass transport of the sacrificial agent.

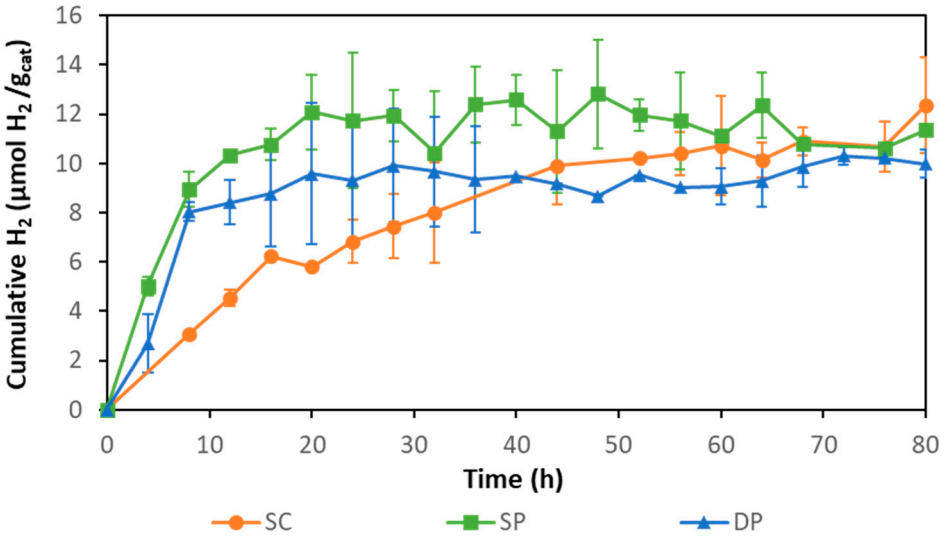


**Figure 6.** Hydrogen production with SC, SP, and DP photocatalytic membranes.

The three types of photocatalytic membranes reached a total hydrogen production ca. 11 μmol $H_2$ gcat$^{-1}$ after 80 h. Hydrogen production stopped most likely due to the inhibitory effect of accumulated hydrogen in the system as has been previously reported [48,54]. The accumulated hydrogen could reduce the difference between the $H^+$ reduction potential and the $TiO_2$ conduction band potential, diminishing the driving force for hydrogen production until it finally stops.

In our previous work, 2% rGO/$TiO_2$ composite suspensions were used for photocatalytic hydrogen production in the same experimental setup with the same equivalent photocatalyst concentration (0.18 g/L), achieving an initial HPR of 1.6 μmol $H_2$ gcatalyst$^{-1}$ h$^{-1}$ [55]. Comparing this value with the highest hydrogen production initial rate achieved by the immobilized photocatalyst (1.1 μmol $H_2$ gcatalyst$^{-1}$ h$^{-1}$), a reduction of 30% is deduced when the immobilized photocatalyst is used. Filice et al. observed different behavior in the degradation of methyl orange [43]. These authors reported that the photocatalyst immobilized on Nafion membranes achieved higher pollutant removal than in suspension. Vohra and Tanaka observed an improvement in the photocatalytic activity in Paraquat degradation by coating Nafion with $TiO_2$ [46]. In this work, the decrease in HPR when using the IMPR vs the slurry reactor is explained by the increase in the mass transfer resistance that the sacrificial agent must overcome before reaching the catalyst.

Next, the catalyst leaching from the membranes was evaluated; to this end the turbidity of the solution before and after the photocatalytic process was analyzed. A linear relationship was found between turbidity and the composite concentration in suspension in the range between 0 and 10% photocatalyst (*w*/*w*). Therefore, knowing the turbidity in the solution the amount of photocatalyst in suspension that was leached from the membrane was determined. Table 2 shows the solution turbidity and the resulting percentage of photocatalyst leached after 80 h of reaction. SC and SP showed the lowest percentage of photocatalyst leaching. DP showed the highest percentage of photocatalyst leaching with a more than ten-fold increase compared to the other methods. SC showed

an extremely low leaching percentage because the photocatalyst was embedded in the membrane matrix, thus showing higher stability. The high leaching percentage of DP membranes could be because the photocatalyst was weakly deposited on the membrane surface. Although SP photocatalyst was also deposited on the membrane surface, it resulted in a lower leaching percentage than DP, very similar to SC membranes. This fact could be attributed to a stronger photocatalyst attachment on the membrane surface by the SP method than by the DP method.

**Table 2.** Leaching percentage of the immobilized photocatalytic membranes.

| Parameter | SC | SP | DP |
|---|---|---|---|
| Turbidity (NTU) | 2.6 ± 0.9 | 7.5 ± 2.5 | 64.3 ± 12.9 |
| Photocatalyst Leaching (%) | 0.2 ± 0.1 | 0.4 ± 0.2 | 4.8 ± 1.0 |

The highest hydrogen production initial rate together with the low photocatalyst leaching provide preliminary information for decision making for the catalyst immobilization procedure; thus, the SP membrane turned out to be the best method to immobilize the composite on a Nafion membrane.

In order to evaluate the reuse of the SP membrane several cycles of hydrogen production were carried out. After each cycle, the system was purged with argon to prevent the inhibitory effect of the accumulated hydrogen (Figure 7). It was observed that at the end of the first cycle hydrogen production had stopped and after an argon purge, hydrogen production continued. This fact supports the inhibitory effect of the reaction product on the HPR, as was expected. The initial rate in the reuse cycles was 0.79 μmol $H_2$ gcatalyst$^{-1}$ h$^{-1}$ while with the fresh membrane it was 1.19 μmol $H_2$ gcatalyst$^{-1}$ h$^{-1}$. Therefore, the membrane photoactivity had been reduced by 33%. Ma et al. evaluated the re-use of $Er^{3+}$:$YAlO_3$Pt-$TiO_2$ on a glass substrate [32]. They carried out 5 cycles of 5 h. The loss of photocatalyst activity after 25 h was 80%, while in this work the loss of activity after 64 h of operation was quantified as 33%.

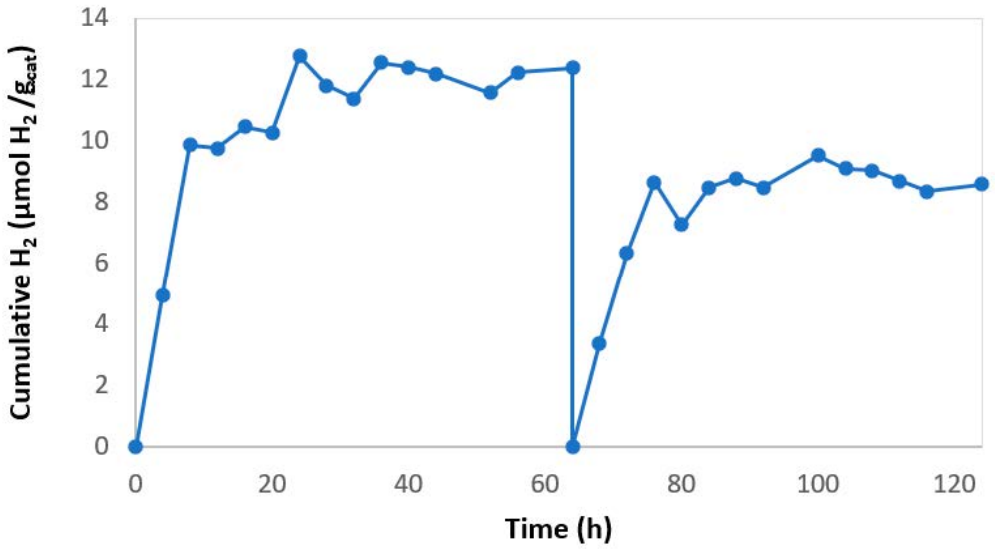


**Figure 7.** Hydrogen production with reused 2% rGO/$TiO_2$ SP membrane.

Darkening was observed in the used membranes in comparison with the pristine photocatalytic membranes (Figure 8). This darkening could be attributed to the further reduction of graphene. The reduction of graphene during photocatalytic experiments has been previously reported. Shah et al. observed darkening after reduction of graphene oxide [56]. In our previous study, darkening of $TiO_2$/rGO composites was observed after being used in photocatalytic hydrogen production in slurry photoreactors, the reduction of the composite being confirmed through Raman spectra [55]. A decrease in the photoactivity after the first hydrogen production cycle was also observed.

**Figure 8.** 2% rGO/$TiO_2$ membrane before (**left**) and after 96 h of use (**right**).

## 4. Conclusions

Although there are environmental and energy advantages of photocatalytic hydrogen production, its large-scale application is still far from adoption, mainly due to the low performance and short lifetime of the state of the art photocatalysts. This work takes a step toward by advancing the knowledge on the application of immobilized composite photocatalysts. Cost-effective rGO/$TiO_2$ composite was synthesized showing improved photocatalytic properties compared to bare $TiO_2$ membranes. In addition, the influence of different process variables such as the composite immobilization method, SC, SP, and DP, to attach the catalyst to Nafion membranes was analyzed. SP and DP achieved the highest initial HPRs, about 1 μmol $H_2$ $gcatalyst^{-1}$ $h^{-1}$. However, the SP method showed only 0.4% photocatalyst leaching after 80 h of operation, whereas DP leaching resulted in 4.8% at the same time. This fact could be due to a stronger photocatalyst attachment on the SP membrane surface than on the DP membrane surface. Therefore, SP seems to be the most effective method to immobilize the composite on Nafion membranes.

The higher initial hydrogen generation rate of SP and DP compared to SC membranes was attributed to the easier accessibility to the photocatalyst deposited on the membrane surface in the two former cases, confirmed by SEM analysis; this reduced the mass transfer limitations in the transport of methanol to reach the immobilized catalyst.

An SP composite reused membrane showed 33% decrease in the initial rate in comparison with a fresh membrane after 64 h of operation. This fact may be attributed to the further reduction of GO in the composite during the photocatalytic process.

**Author Contributions:** Conceptualization, J.C., M.J.R., and I.O.; methodology, J.C., M.J.R., and I.O.; formal analysis, J.C. and E.P.-P.; investigation, J.C. and E.P.-P.; writing—original draft preparation, J.C.; writing—review and editing J.C., M.J.R., and I.O.; supervision, M.J.R. and I.O.; project administration, M.J.R.; funding acquisition, M.J.R. and I.O. All authors have read and agreed to the published version of the manuscript.

**Funding:** This research was funded by MCIU/AEI/FEDER UE (RTI2018-099407-B-I00, RTI2018-093310-B-I00 and RTC2019-006820-5).

**Acknowledgments:** Juan Corredor is grateful to an FPI contract grant (BES-2016-079201). The authors also want to acknowledge the Electron Microscopy Service from the LADICIM of the University of Cantabria for their support in the SEM analysis.

**Conflicts of Interest:** The authors declare no conflict of interest.

## References

1. Figaj, R.; Vanoli, L. Hybrid and novel solar hydrogen systems. In *Solar Hydrogen Production*; Calise, F., D'Accadia, M.D., Santarelli, M., Lanzini, A., Ferrero, D., Eds.; Academic Press: Cambridge, MA, USA, 2019; pp. 487–510, ISBN 978-0-12-814853-2.
2. Petkov, I.; Gabrielli, P. Power-to-hydrogen as seasonal energy storage: An uncertainty analysis for optimal design of low-carbon multi-energy systems. *Appl. Energy* **2020**, *274*, 115197. [CrossRef]
3. Nolan, H.; Browne, M.P. Hydrogen energy currency: Beyond state-of-the-art transition metal oxides for oxygen electrocatalysis. *Curr. Opin. Electrochem.* **2020**, *21*, 55–61. [CrossRef]

4. Merino-Garcia, I.; Albo, J.; Solla-Gullón, J.; Montiel, V.; Irabien, A. Cu oxide/ZnO-based surfaces for a selective ethylene production from gas-phase $CO_2$ electroconversion. *J. $CO_2$ Util.* **2019**, *31*, 135–142. [CrossRef]
5. Ribao, P.; Alexandra Esteves, M.; Fernandes, V.R.; Rivero, M.J.; Rangel, C.M.; Ortiz, I. Challenges arising from the use of $TiO_2$/rGO/Pt photocatalysts to produce hydrogen from crude glycerol compared to synthetic glycerol. *Int. J. Hydrogen Energy* **2018**, *44*, 28494–28506. [CrossRef]
6. Holladay, J.D.; Hu, J.; King, D.L.; Wang, Y. An overview of hydrogen production technologies. *Catal. Today* **2009**, *139*, 244–260. [CrossRef]
7. Christoforidis, K.C.; Fornasiero, P. Photocatalytic Hydrogen production: A rift into the future energy supply. *ChemCatChem* **2017**, *9*, 1523–1544. [CrossRef]
8. Nikolaidis, P.; Poullikkas, A. A comparative overview of hydrogen production processes. *Renew. Sustain. Energy Rev.* **2017**, *67*, 597–611. [CrossRef]
9. Buttler, A.; Spliethoff, H. Current status of water electrolysis for energy storage, grid balancing and sector coupling via power-to-gas and power-to-liquids: A review. *Renew. Sustain. Energy Rev.* **2018**, *82*, 2440–2454. [CrossRef]
10. Partidário, P.; Aguiar, R.; Martins, P.; Rangel, C.M.; Cabrita, I. The hydrogen roadmap in the Portuguese energy system–Developing the P2G case. *Int. J. Hydrogen Energy* **2019**. [CrossRef]
11. Dincer, I. Green methods for hydrogen production. *Int. J. Hydrogen Energy* **2012**, *37*, 1954–1971. [CrossRef]
12. Acar, C.; Dincer, I.; Naterer, G.F. Review of photocatalytic water-splitting methods for sustainable hydrogen production. *Int. J. Energy Res.* **2016**, *40*, 1449–1473. [CrossRef]
13. Corredor, J.; Rivero, M.J.; Rangel, C.M.; Gloaguen, F.; Ortiz, I. Comprehensive review and future perspectives on the photocatalytic hydrogen production. *J. Chem. Technol. Biotechnol.* **2019**, *94*, 3049–3063. [CrossRef]
14. Fajrina, N.; Tahir, M. A critical review in strategies to improve photocatalytic water splitting towards hydrogen production. *Int. J. Hydrogen Energy* **2018**, *44*, 540–577. [CrossRef]
15. Ribao, P.; Rivero, M.J.; Ortiz, I. $TiO_2$ structures doped with noble metals and/or graphene oxide to improve the photocatalytic degradation of dichloroacetic acid. *Environ. Sci. Pollut. Res.* **2017**, *24*, 12628–12637. [CrossRef] [PubMed]
16. Beasley, C.; Kumaran Gnanamani, M.; Santillan-Jimenez, E.; Martinelli, M.; Shafer, W.D.; Hopps, S.D.; Wanninayake, N.; Kim, D.Y. Effect of Metal Work Function on Hydrogen Production from Photocatalytic Water Splitting with $MTiO_2$ Catalysts. *ChemistrySelect* **2020**, *5*, 1013–1019. [CrossRef]
17. Koe, W.S.; Lee, J.W.; Chong, W.C. An overview of photocatalytic degradation: Photocatalysts, mechanisms, and development of photocatalytic membrane. *Environ. Sci. Pollut. Res.* **2020**, *27*, 2522–2565. [CrossRef]
18. Che, Y.; Liu, Q.; Lu, B.; Zhai, J.; Wang, K.; Liu, Z. Plasmonic ternary hybrid photocatalyst based on polymeric g-$C_3N_4$ towards visible light hydrogen generation. *Sci. Rep.* **2020**, *10*, 721. [CrossRef]
19. Khalid, N.R.; Majid, A.; Tahir, M.B.; Niaz, N.A.; Khalid, S. Carbonaceous-$TiO_2$ nanomaterials for photocatalytic degradation of pollutants: A review. *Ceram. Int.* **2017**, *43*, 14552–14571. [CrossRef]
20. Ribao, P.; Rivero, M.J.; Ortiz, I. Enhanced photocatalytic activity using GO/$TiO_2$ catalyst for the removal of DCA solutions. *Environ. Sci. Pollut. Res.* **2018**, *25*, 34893–34902. [CrossRef]
21. Shi, H.; Magaye, R.; Castranova, V.; Zhao, J. Titanium dioxide nanoparticles: A review of current toxicological data. *Part. Fibre Toxicol.* **2013**, *10*, 15. [CrossRef]
22. Kumari, P.; Bahadur, N.; Dumée, L.F. Photo-catalytic membrane reactors for the remediation of persistent organic pollutants–A review. *Sep. Purif. Technol.* **2020**, *230*, 115878. [CrossRef]
23. Romay, M.; Diban, N.; Rivero, M.J.; Urtiaga, A.; Ortiz, I. Critical Issues and Guidelines to Improve the Performance of Photocatalytic Polymeric Membranes. *Catalysts* **2020**, *10*, 570. [CrossRef]
24. Kitano, M.; Tsujimaru, K.; Anpo, M. Decomposition of water in the separate evolution of hydrogen and oxygen using visible light-responsive $TiO_2$ thin film photocatalysts: Effect of the work function of the substrates on the yield of the reaction. *Appl. Catal. A Gen.* **2006**, *314*, 179–183. [CrossRef]
25. Tode, R.; Ebrahimi, A.; Fukumoto, S.; Iyatani, K.; Takeuchi, M.; Matsuoka, M.; Lee, C.H.; Jiang, C.S.; Anpo, M. Photocatalytic decomposition of water on double-layered visible light-responsive $TiO_2$ thin films prepared by a magnetron sputtering deposition method. *Catal. Lett.* **2010**, *135*, 10–15. [CrossRef]
26. Huang, C.W.; Liao, C.H.; Wu, J.C.S.; Liu, Y.C.; Chang, C.L.; Wu, C.H.; Anpo, M.; Matsuoka, M.; Takeuchi, M. Hydrogen generation from photocatalytic water splitting over $TiO_2$ thin film prepared by electron beam-induced deposition. *Int. J. Hydrogen Energy* **2010**, *35*, 12005–12010. [CrossRef]

27. Liao, C.-H.H.; Huang, C.-W.W.; Wu, J.C.S. Novel dual-layer photoelectrode prepared by RF magnetron sputtering for photocatalytic water splitting. *Int. J. Hydrogen Energy* **2012**, *37*, 11632–11639. [CrossRef]
28. Liao, Y.T.; Huang, C.W.; Liao, C.H.; Wu, J.C.S.; Wu, K.C.W. Synthesis of mesoporous titania thin films (MTTFs) with two different structures as photocatalysts for generating hydrogen from water splitting. *Appl. Energy* **2012**, *100*, 75–80. [CrossRef]
29. Selli, E.; Chiarello, G.L.; Quartarone, E.; Mustarelli, P.; Rossetti, I.; Forni, L. A photocatalytic water splitting device for separate hydrogen and oxygen evolution. *Chem. Commun.* **2007**, 5022–5024. [CrossRef]
30. Hattori, M.; Noda, K.; Matsushige, K. High-purity hydrogen generation by ultraviolet illumination with the membrane composed of titanium dioxide nanotube array and Pd layer. *Appl. Phys. Lett.* **2011**, *99*, 2–5. [CrossRef]
31. Cha, G.; Altomare, M.; Truong, N.N.; Taccardi, N.; Lee, K.; Schmuki, P. Double-Side Co-Catalytic Activation of Anodic $TiO_2$ Nanotube Membranes with Sputter-Coated Pt for Photocatalytic $H_2$ Generation from Water/Methanol Mixtures. *Chem.—Asian J.* **2017**, *12*, 314–323. [CrossRef]
32. Ma, C.; Li, Y.; Zhang, H.; Chen, Y.; Lu, C.; Wang, J. Photocatalytic hydrogen evolution with simultaneous photocatalytic reforming of biomass by $Er^{3+}$: $YAlO_3$/Pt-$TiO_2$ membranes under visible light driving. *Chem. Eng. J.* **2015**, *273*, 277–285. [CrossRef]
33. Della Foglia, F.; Chiarello, G.L.; Dozzi, M.V.; Piseri, P.; Bettini, L.G.; Vinati, S.; Ducati, C.; Milani, P.; Selli, E. Hydrogen production by photocatalytic membranes fabricated by supersonic cluster beam deposition on glass fiber filters. *Int. J. Hydrogen Energy* **2014**, *39*, 13098–13104. [CrossRef]
34. Park, H.; Park, Y.; Bae, E.; Choi, W. Photoactive component-loaded Nafion film as a platform of hydrogen generation: Alternative utilization of a classical sensitizing system. *J. Photochem. Photobiol. Chem.* **2009**, *203*, 112–118. [CrossRef]
35. Wu, M.C.; Sápi, A.; Avila, A.; Szabó, M.; Hiltunen, J.; Huuhtanen, M.; Tóth, G.; Kukovecz, Á.; Kónya, Z.; Keiski, R.; et al. Enhanced Photocatalytic Activity of $TiO_2$ Nanofibers and Their Flexible Composite Films: Decomposition of Organic Dyes and Efficient $H_2$ Generation from Ethanol-Water Mixtures. *Nano Res.* **2011**, *4*, 360–369. [CrossRef]
36. Bai, H.; Liu, Z.; Sun, D.D. Hierarchically multifunctional $TiO_2$ nano-thorn membrane for water purification. *Chem. Commun.* **2010**, *46*, 6542–6544. [CrossRef]
37. Nair, A.K.; Jagadeesh, J.B. $TiO_2$ nanosheet-graphene oxide based photocatalytic hierarchical membrane for water purification. *Surf. Coatings Technol.* **2017**, *320*, 259–262. [CrossRef]
38. Tsydenov, D.E.; Parmon, V.N.; Vorontsov, A.V. Toward the design of asymmetric photocatalytic membranes for hydrogen production: Preparation of $TiO_2$-based membranes and their properties. *Int. J. Hydrogen Energy* **2012**, *37*, 11046–11060. [CrossRef]
39. Tsydenov, D.E.; Vorontsov, A.V. Influence of Nafion loading on hydrogen production in a membrane photocatalytic system. *J. Photochem. Photobiol. Chem.* **2015**, *297*, 8–13. [CrossRef]
40. Wang, W.-Y.; Ku, Y. Effect of solution pH on the adsorption and photocatalytic reaction behaviors of dyes using $TiO_2$ and Nafion-coated $TiO_2$. *Aspects* **2007**, *302*, 261–268. [CrossRef]
41. Kusoglu, A.; Weber, A.Z. New Insights into Perfluorinated Sulfonic-Acid Ionomers. *Chem. Rev.* **2017**, *117*, 987–1104. [CrossRef]
42. Teixeira, F.C.; de Sá, A.I.; Teixeira, A.P.S.; Ortiz-Martínez, V.M.; Ortiz, A.; Ortiz, I.; Rangel, C.M. New modified Nafion-bisphosphonic acid composite membranes for enhanced proton conductivity and PEMFC performance. *Int. J. Hydrogen Energy* **2020**, 1–10. [CrossRef]
43. Filice, S.; D'Angelo, D.; Libertino, S.; Nicotera, I.; Kosma, V.; Privitera, V.; Scalese, S. Graphene oxide and titania hybrid Nafion membranes for efficient removal of methyl orange dye from water. *Carbon* **2015**, *82*, 489–499. [CrossRef]
44. D'Angelo, D.; Filice, S.; Libertino, S.; Kosma, V.; Nicotera, I.; Privitera, V.; Scalese, S. Photocatalytic properties of Nafion membranes containing graphene oxide/titania nanocomposites. In Proceedings of the 2014 IEEE 9th Nanotechnology Materials and Devices Conference, NMDC 2014, Aci Castello, Italy, 12–15 October 2014.
45. Ding, X.; Zhou, S.; Jiang, L.; Yang, H. Preparation, photocatalytic activity and mechanism of nano-Titania/Nafion hybrid membrane. *J. Sol-Gel Sci. Technol.* **2011**, *58*, 345–354. [CrossRef]
46. Vohra, M.S.; Tanaka, K. Enhanced photocatalytic activity of nafion-coated $TiO_2$. *Environ. Sci. Technol.* **2001**, *35*, 411–415. [CrossRef] [PubMed]

47. Park, H.; Choi, W. Photocatalytic reactivities of nafion-coated $TiO_2$ for the degradation of charged organic compounds under UV or visible light. *J. Phys. Chem. B* **2005**, *109*, 11667–11674. [CrossRef]
48. Choi, W. Photocatalytic hydrogen production using surface-modified titania nanoparticles. In Proceedings of the Solar Hydrogen and Nanotechnology II, SPIE, San Diego, CA, USA, 27–30 August 2007.
49. Wood, D.; Shaw, S.; Cawte, T.; Shanen, E.; Van Heyst, B. An overview of photocatalyst immobilization methods for air pollution remediation. *Chem. Eng. J.* **2020**, *391*, 123490. [CrossRef]
50. Lugo-Vega, C.S.; Serrano-Rosales, B.; de Lasa, H. Immobilized particle coating for optimum photon and $TiO_2$ utilization in scaled air treatment photo reactors. *Appl. Catal. B Environ.* **2016**, *198*, 211–223. [CrossRef]
51. Huang, N.M.; Chang, B.Y.S.; An'Amt, M.N.; Marlinda, A.R.; Norazriena, Y.; Muhamad, M.R.; Harrison, I.; Lim, H.N.; Chia, C.H. Facile hydrothermal preparation of titanium dioxide decorated reduced graphene oxide nanocomposite. *Int. J. Nanomed.* **2012**, *7*, 3379–3387. [CrossRef]
52. Devrim, Y.; Erkan, S.; Baç, N.; Eroglu, I. Improvement of PEMFC performance with Nafion/inorganic nanocomposite membrane electrode assembly prepared by ultrasonic coating technique. *Int. J. Hydrogen Energy* **2012**, *37*, 16748–16758. [CrossRef]
53. Zhang, F.; Zhang, Z.; Liu, Y.; Lu, H.; Leng, J. The quintuple-shape memory effect in electrospun nanofiber membranes. *Smart Mater. Struct.* **2013**, *22*, 085020. [CrossRef]
54. Kuang, L.; Zhang, W. Enhanced hydrogen production by carbon-doped $TiO_2$ decorated with reduced graphene oxide (rGO) under visible light irradiation. *RSC Adv.* **2016**, *6*, 2479–2488. [CrossRef]
55. Corredor, J.; Rivero, M.J.; Ortiz, I. New insights in the performance and reuse of rGO/$TiO_2$ composites for the photocatalytic hydrogen production. *Int. J. Hydrogen Energy* **2020**. [CrossRef]
56. Sher Shah, M.S.A.; Park, A.R.; Zhang, K.; Park, J.H.; Yoo, P.J. Green synthesis of biphasic $TiO_2$-reduced graphene oxide nanocomposites with highly enhanced photocatalytic activity. *ACS Appl. Mater. Interfaces* **2012**, *4*, 3893–3901. [CrossRef] [PubMed]


© 2020 by the authors. Licensee MDPI, Basel, Switzerland. This article is an open access article distributed under the terms and conditions of the Creative Commons Attribution (CC BY) license (http://creativecommons.org/licenses/by/4.0/).

## 3.4. Publication 3. Influence of QD photosensitizers in the photocatalytic production of hydrogen with biomimetic [FeFe]-hydrogenase. Comparative performance of CdSe and CdTe.

Chapter 3.4 corresponds to the following paper:

J. Corredor, D. Harankahage, F. Gloaguen, M. J. Rivero, M. Zamkov, I. Ortiz. “Influence of QD photosensitizers in the photocatalytic production of hydrogen with biomimetic [FeFe]-hydrogenase. Comparative performance of CdSe and CdTe”. *Chemosphere,* 278, 130485, 2021
DOI: 10.1016/j.chemosphere.2021.130485.

Chemosphere 278 (2021) 130485

Contents lists available at ScienceDirect

Chemosphere

journal homepage: www.elsevier.com/locate/chemosphere

# Influence of QD photosensitizers in the photocatalytic production of hydrogen with biomimetic [FeFe]-hydrogenase. Comparative performance of CdSe and CdTe

Juan Corredor [a], Dulanjan Harankahage [b], Frederic Gloaguen [c], Maria J. Rivero [a], Mikhail Zamkov [b], Inmaculada Ortiz [a, *]

[a] Department of Chemical and Biomolecular Engineering, ETSIIT, University of Cantabria, Avda. de Los Castros S/n, 39005, Santander, Spain
[b] Department of Physics and Center for Photochemical Sciences, Bowling Green State University, Bowling Green, OH, 43043, USA
[c] UMR 6521, CNRS, Université de Bretagne Occidentale, CS 93837, 29238, Brest, France

## HIGHLIGHTS

- Photocatalytic hydrogen production system with [Fe-Fe]$H_2$-ase mimic, and CdSe or CdTe QDs as photosensitizers.
- Comparison of CdSe and CdTe QDs performance as photosensitizers.
- CdSe showed the best performance for hydrogen production.
- Electron transfer rate from ascorbic acid to QDs and from QDs to catalysts has been investigated.
- Electron transfer rate from ascorbic acid to QDs was found as rate limiting step.

## GRAPHICAL ABSTRACT

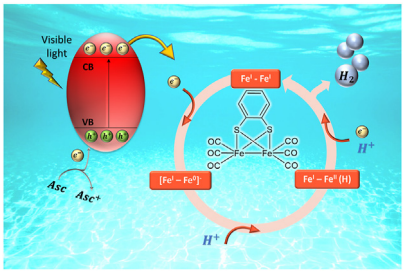


## ARTICLE INFO

*Article history:*
Received 27 January 2021
Received in revised form
20 March 2021
Accepted 2 April 2021
Available online 3 April 2021

Handling Editor: E. Brillas

*Keywords:*
Photocatalytic hydrogen production
Hydrogenase mimic
Quantum dot
CdSe
CdTe
Electron transfer
Hybrid systems

## ABSTRACT

Photocatalytic systems comprising a hydrogenase-type catalyst and CdX (X = S, Se, Te) chalcogenide quantum dot (QD) photosensitizers show extraordinary hydrogen production rates under visible light excitation. What remains unknown is the mechanism of energy conversion in these systems. Here, we have explored this question by comparing the performance of two QD sensitizers, CdSe and CdTe, in photocatalytic systems featuring aqueous suspensions of a [$Fe_2$ (μ-1,2-benzenedithiolate) $CO_6$] catalyst and an ascorbic acid sacrificial agent. Overall, the hydrogen production yield for CdSe-sensitized reactions QDs was found to be 13 times greater than that of CdTe counterparts. According to emission quenching experiments, an enhanced performance of CdSe sensitizers reflected a greater rate of electron transfer from the ascorbic acid ($k_{Asc}$). The observed difference in the QD-ascorbic acid charge transfer rates between the two QD materials was consistent with respective driving forces for these systems.
© 2021 Elsevier Ltd. All rights reserved.

* Corresponding author.
*E-mail address:* inmaculada.ortiz@unican.es (I. Ortiz).

https://doi.org/10.1016/j.chemosphere.2021.130485
0045-6535/© 2021 Elsevier Ltd. All rights reserved.

## 1. Introduction

In the current global context, greenhouse gas emissions due to the combustion of fossil fuels pose a threat to the global climate change (Hinojosa-Reyes et al., 2017; Fang et al., 2018; Seadira et al., 2018). Therefore, research efforts have been directed towards finding alternative and environmentally-friendly energy sources. In this context, hydrogen appears as a clean energy vector whose combustion only produces water (Chen et al., 2018; Munfarida et al., 2020; Oh et al., 2020). Nowadays, it is mainly produced by steam reforming from fossil fuels (Chu et al., 2017; Nikolaidis and Poullikkas, 2017; Corredor et al., 2020a). This process is energy intensive and plagued by the emission of greenhouse gases (Holladay et al., 2009; Ribao et al., 2019). As a result, the potential to produce hydrogen from alternative and greener technologies, where electrolysis takes the leading role, is becoming increasingly important. Complementarily, hydrogen can be released from residual gas or liquid effluents through the use of cost-effective technologies, such as photocatalysis (Yue et al., 2017; Nasir et al., 2019; Rivero et al., 2019). Photocatalysis is a way to harvest sunlight energy and store it in the form of solar fuels, just as nature has done through natural photosynthesis (Christoforidis and Fornasiero, 2017; El-Khouly et al., 2017; Zamkov, 2017; Giannoudis et al., 2020; Brillas et al., 2021).

As an alternative to noble metal catalysts, (Cho et al., 2021; Lai et al., 2021; Y. Yang et al., 2021), recent studies have explored heterogeneous photocatalytic systems comprising hydrogenases catalysts and semiconductor quantum dot (QD) photosensitizers. The hydrogen production rates for these materials approaching 2 mmol $H_2 \cdot g_{cat}^{-1} \cdot h^{-1}$ were below those of homogeneous catalysts but showed an impressive long-term stability (Putri et al., 2020; Elsayed et al., 2021; J. Yang et al., 2021).

Hydrogenase mimics is another promising noble metal-free catalyst that shows compelling hydrogen production performance (Trincado et al., 2014; Fukuzumi et al., 2018). Hydrogenases in nature are enzymes, which active sites are composed of Fe and/or Ni, synthesized by certain bacteria and algae; these enzymes catalyze the reversible redox reaction of $H^+$ to $H_2$ (Wang et al., 2012; Hemming et al., 2018; Li et al., 2018). Among hydrogenases, [Fe-Fe] $H_2$-ases have shown a very high production activity of hydrogen, about 6000–9000$H_2$ molecules per second per active site (Stripp and Happe, 2009; Li et al., 2018; Wittkamp et al., 2018; Wang et al., 2019). Therefore, they have been studied in the last decades and have awakened interest in the synthesis of biomimetic molecules (Capon et al., 2004; Liu and Darensbourg, 2007; Quentel et al., 2012; Roy et al., 2013; Orain et al., 2014; Ahmed et al., 2018).

[Fe-Fe]$H_2$-ases photocatalytic hydrogen production systems containing metal complexes, such as $[Ru(bpy)_3]^{2+}$ (bpy = 2,2′-bipyridine) or $[Re(4,4'\text{-dimethylbpy})(CO)_3]^+$ (Na et al., 2008; Streich et al., 2010; Wang et al., 2010; Pullen et al., 2013; Yu et al., 2013) or organic dyes such as Eosin Y or Rose Bengal as photosensitizers have been extensively studied (Li et al., 2012; Orain et al., 2014; Supplis et al., 2018). Orain et al. studied the photocatalytic hydrogen production in aqueous solutions with [Fe-Fe]$H_2$-ase mimics, and organic dyes as photosensitizers (Orain et al., 2014). Despite promising performance, their main drawback was the fast excitation decay and the spectrally-narrow absorption band of dye sensitizers. In order to overcome these issues, semiconductor QDs have been employed as photosensitizers (Wang et al., 2011, 2013; Song et al., 2014; Liang et al., 2015; M. Wang et al., 2015; Jian et al., 2016; Troppmann and König, 2016; Wen et al., 2016, 2017). Jian et al. compared the performance of $[Ru(bpy)_3]^{2+}$ and CdSe QDs as a photosensitizer for the same aqueous system achieving a hydrogen production rate of 301 and 20840 mmol $H_2 \cdot g_{cat}^{-1} \cdot h^{-1}$, respectively, duplicating the stability of the system. Hydrogen production was further enhanced by using a sacrificial agent that acted as an electron donor, such as ascorbic acid (Fig. 1) (Goy et al., 2017).

The selection of the QD material for sensitizing hydrogen production is still a challenge. Cadmium chalcogenides, CdS, CdSe and CdTe, are good candidates due to their visible-range absorbance and energetically favorable positions of band edges for driving the hydrogen production processes (Hernandez-Ramirez et al., 2015). Since CdS absorbs the smallest fraction of the solar energy, CdSe and CdTe QDs, exhibiting absorption in the visible and near-IR, are usually preferred. For instance, CdSe has been used as photosensitizer for hydrogen generation in combination with hydrogenases, hydrogenase mimics, and even with bacteria that produce

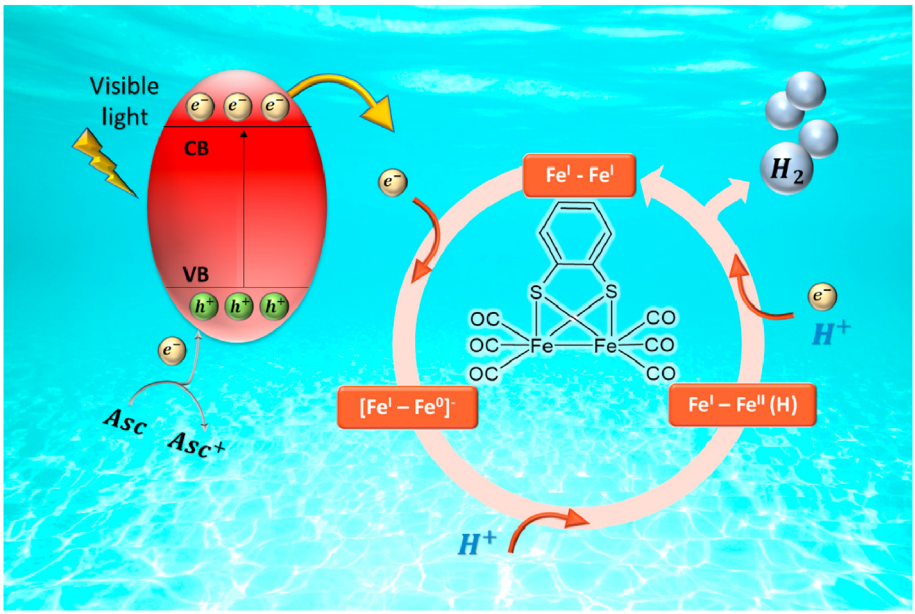


**Fig. 1.** Hydrogen production by a [FeFe]$H_2$-ase mimic from ascorbic acid aqueous solution with QDs as photosensitizer.

hydrogenases (Li et al., 2013, 2020; Wang et al., 2013; Shen et al., 2013; Hamon et al., 2014; Liang et al., 2015; Jian et al., 2016; Troppmann and König, 2016; Wen et al., 2016; Chica et al., 2017; Ding et al., 2019; Sanchez et al., 2019a, 2019b). CdTe has been also used for this purpose (Brown et al., 2010, 2014; Wang et al., 2011; Greene et al., 2012; Jian et al., 2013; Wroblewska-Wolna et al., 2020). Overall, the two QD sensitizers appeared to perform differently in the presence of the same sacrificial agent and catalyst components (Acharya et al., 2011; Brown et al., 2012), which makes this pair of QDs a promising model system for interrogating energy conversion processes in sacrificial hydrogen production reactions.

The present study offers a comprehensive analysis of the hydrogen production performance for CdSe and CdTe QD photosensitizers under visible light irradiation. The photocatalytic systems in present experiments featured a biomimetic hydrogenase catalyst and ascorbic acid as a sacrificial agent. By drawing a comparison between the two sensitizer QDs, we were able to infer that the primary rate-limiting step in these systems is an electron transfer between the sacrificial agent and semiconductor QDs. This conclusion was supported by cyclic voltammetry measurements showing a larger difference between the oxidation potential of ascorbic acid and the valence band of CdSe, as compared to CdTe.

## 2. Materials and methods

### 2.1. Materials

Oleic acid (OA) 90%, 1-octadene (ODE) 90%, trioctylphosphine oxide (TOPO), cadmium oxide (CdO) 99.5%, tellurium powder 99.8% and tributylphosphine 97% (TBP) were purchased from Sigma Aldrich. Chloroform and acetone were purchased from ChemPure Chemicals. L-Ascorbic acid 98+% and methanol were provided by Alfa Aesar. N-octadecylphosphonic acid (ODPA) was supplied by PCI. Trioctylphosphine (TOP) was purchased from Strem Chemicals Inc. Selenium powder 99.99% was supplied by Beantown Chemicals. 3-mercaptopropionic acid (MPA) was acquired from Acros Organics. Sodium dodecyl sulfate (SDS) 10% was provided by LifeTechnologies.

### 2.2. Hydrogenase synthesis

[$Fe_2$(μ-1,2-benzenedithiolate)$(CO)_6$], the [Fe-Fe]$H_2$-ase mimic, was synthesized as previously described in the literature (Cabeza et al., 1998).

### 2.3. Synthesis of CdSe and CdTe quantum dots

OA-capped CdSe QDs were synthesized according to a procedure adapted from the literature (Mongin et al., 2018). Briefly, OA-capped CdSe QDs were synthesized from cadmium and selenium solutions. To prepare cadmium solution, 180 mg of CdO were combined with 75 mg of ODPA, 9 g of TOPO and 6 mL of OA in a flask at 300 °C under Ar atmosphere. When the solution turned clear, 5.4 mL of TOP were added. Selenium solutions were prepared with 180 mg of Se powder and 3 mL of TOP at 140 °C under Ar atmosphere. After, the solution was cooled down to 80 °C and it was injected into the cadmium solution. The reaction time was 2 min. Every step was performed under magnetic stirring.

To synthetize ODPA-capped CdTe QDs, the cadmium solution was prepared with 25.6 mg of CdO, 147.2 mg of ODPA and 8 mL of ODE at 300 °C under Ar atmosphere. Tellurium solution was prepared from 51 mg of tellurium powder, 4 mL of ODE, and 0.46 mL of TBP at 80 °C under Ar atmosphere. Tellurium solution was injected into the cadmium solution and the reaction was carried out for 4.75 min.

Both CdTe and CdSe suspensions were centrifuged for 4.5 min at 6500 rpm after adding ethanol:acetone solution, with a volume ratio 2:1, to cause precipitation of the crystals. The ratio between the crystals suspension and the ethanol-acetone mixture was 1:3 in volume. The precipitated crystals were re-suspended in chloroform.

The ligand exchange process was carried out according to a procedure adapted from the literature (Chang et al., 2016). Briefly, 0.5 mL of MPA were dissolved in 10 mL of a 1:1 methanol:chloroform solution at basic pH. 1.5 mL of crystals suspension were added under constant stirring. QDs precipitated after centrifugation in acetone. They were suspended in water and re-precipitated in acetone. Finally, the QDs were suspended and stored in water.

### 2.4. Materials characterization

$^1$H NMR spectra of [$Fe_2$(μ-1,2-benzenedithiolate)$(CO)_6$] in deuterated acetone were recorded on a Bruker AC-300 FT-NMR spectrometer and were referenced against $SiMe_4$. The infrared spectra of [$Fe_2$(μ-1,2-benzenedithiolate)$(CO)_6$] in hexane were recorded on a Nicolet Nexus FT-IR spectrometer.

The materials absorbance spectra were recorded in a UV−Vis spectrophotometer Cary 60 (Agilent). Photoluminescence spectra and excitation decay lifetime ($\tau_0$) of CdSe and CdTe QDs were obtained, exciting them with 405 nm PicoQuant PDL 800-D pulsed laser and measuring their emission with an AndornewtonEM SR-303i-A spectrograph.

### 2.5. Hydrogen production

Hydrogen production experiments were carried out in an 8 mL reactor under magnetic stirring. The reaction medium consisted of 4 mL of aqueous suspension with ascorbic acid 200 mM (the amount of the sacrificial agent was used to assure excess of ascorbic acid concentration during the experiments while avoiding the influence of its concentration changes due to its consumption during the process), 0.1 mM of [Fe-Fe]$H_2$-ase mimic, QDs in a concentration between 0.001 mM and 0.1 mM, and 10 mM SDS sodium dodecyl sulfate (SDS) to solubilize the [Fe-Fe]$H_2$-ase mimic (Orain et al., 2014; Supplis et al., 2018). The light source consisted of a 150 W halogen lamp, provided with a filter which allowed only visible light to pass (400 nm < λ < 800 nm). The irradiance on the reactor wall was 31 mW cm$^{-2}$. It was measured with a Compact Power and Energy Meter Console PM100D from Thorlabs. The concentration of hydrogen was measured with a Shimadzu 8A gas chromatograph, equipped with a thermal conductivity detector and a molecular sieve column 80/100 using argon as a carrier gas. Hydrogen production experiments were performed at pH 4.5, which is close to the ascorbic acid p$K_a$ (4.2) (Tu et al., 2017); it has been reported that working close to the sacrificial agent p$K_a$ enhances hydrogen production (Corredor et al., 2019).

## 3. Results

The [Fe-Fe]$H_2$-ase mimic [$Fe_2$(μ-1,2-benzenedithiolate)$(CO)_6$] was characterized by FTIR and $^1$H NMR spectroscopy. Three bands were displayed in the infrared spectra in the $\nu_{CO}$ region: 2006, 2045 and 2079 cm$^{-1}$. $^1$H NMR (300 MHz, $(CD_3)_2CO$): δ 7.24 (m, 2H), 7.46 (m, 2H). These data are in good agreement with those reported by Cabeza et al. (1998). The [Fe-Fe]$H_2$-ase mimic absorbance spectra (Fig. SM-1) showed an absorption peak at 330 nm and absorption at wavelengths lower than 300 nm. Therefore, the catalyst did not absorb radiation during hydrogen production experiments, which were carried out using visible light excitation (400–800 nm).

The influence of the QD diameter on the effectiveness of hydrogen production with hydrogenase enzymes has been investigated previously (Brown et al., 2014). In this work, we only focus on single sizes of CdTe and CdSe QDs (2.95 and 2.68 nm, respectively, see Fig. SM-2. Yu et al., 2003), which were chosen to enable similar extinction values for the two sensitizers in the visible range. In this size range, the rate of electron transfer to a catalysis was not expected to be influenced by the particle size (Brown et al., 2014).

The UV–Vis absorbance and the emission spectra of the synthesized CdSe and CdTe QDs before and after the ligand exchange process are shown in Fig. SM-3. Peng's correlations were used to calculate the QD diameter from the spectral position of the QD absorption edge (Yu et al., 2003). The QDs diameter was controlled via the reaction time. A slight blue-shift was observed in the absorbance peak of both materials when the hydrophobic ligands were exchanged with MPA.

Fig. SM-4 shows the time-resolved luminescence decay curves of excited CdSe-OA, CdSe-MPA, CdTe-ODPA and CdTe-MPA. The fluorescence intensity decay lifetime ($\tau_0$) was calculated by fitting the data to a three-phase exponential decay function (Gong et al., 2013). The $\tau_0$ values for CdSe-OA, CdSe-MPA, CdTe-ODPA and CdTe-MPA were determined to be 38.4, 2.6, 14.7 and 9.6 ns, respectively. The value of $\tau_0$ decreases upon the ligand exchange with MPA for both materials. This decrease was previously explained by the photoinduced hole transfer from a nanocrystal to MPA, which exhibits a more negative energy relative to the semiconductor valence band (Ben-Shahar et al., 2015; P. Wang et al., 2015).

### 3.1. Influence of photosensitizer concentration on hydrogen production

Control tests were carried out in the absence of catalyst, in absence of photosensitizers and with all components in the dark, successfully confirming the lack of hydrogen production. In the next step, the influence of the CdSe QD concentration on hydrogen production was investigated in the 0.001 mM–0.1 mM range. The pH of the reaction medium was the natural pH of the ascorbic acid (pKa 4.2) (Tu et al., 2017), as the optimal pH for these systems has a value close to the $pK_a$ of the sacrificial agent. In addition, Gloaguen and coworkers reported that a pH between 3 and 6 favored the protonation of the electrochemically reduced [Fe-Fe]$H_2$-ase mimic leading to higher hydrogen production (Quentel et al., 2012). The selected concentration of ascorbic acid was 200 mM following previous reports (Jian et al., 2016). Fig. 2 shows that the highest amount of hydrogen was produced using [CdSe] = 0.01 mM, giving a turnover number (TON) of 18.3 mol of $H_2$ produced per mol of [$Fe_2$(μ-1,2-benzenedithiolate)$(CO)_6$] during 3 h. The corresponding turnover number frequency (TOF), measured in mol of produced $H_2$ per mol of catalyst per unit of time, was 6.5 $h^{-1}$. Under the conditions of this study, the generated hydrogen increased with the QD concentration up to a maximum value obtained at a concentration of CdSe 0.01M, and after that it decreased as the concentration of the QD increased.

Further insights into the influence of the CdSe QD concentration on hydrogen generation are provided in Fig. SM-5, which shows the number of excited CdSe particles per second versus the total number of CdSe nanoparticles in the medium. The procedure for estimating the number of excited QDs is given in SM, together with the absorption spectra of QD media (Fig. SM-6) and the excitation spectrum (Fig. SM-7). The dashed line in Fig. SM-5 shows an ideal case in which the average number of excited nanoparticles approaches that of the nanoparticles in the medium. These conditions are observed when the concentration of the photosensitizer is less than 0.01 mM. However, only about 75% and 20% of the total particles were excited for QD concentrations of 0.025 and 0.1 mM, respectively. Therefore, the decrease in hydrogen production for concentrations of CdSe greater than 0.01 mM was attributed to the inefficient activation of the photosensitizer particles. This is clarified by equation S6, which shows that the irradiation of the light source strongly influences the optimal concentration of the photosensitizer because the number of excited particles depends on the number of accessible photons.

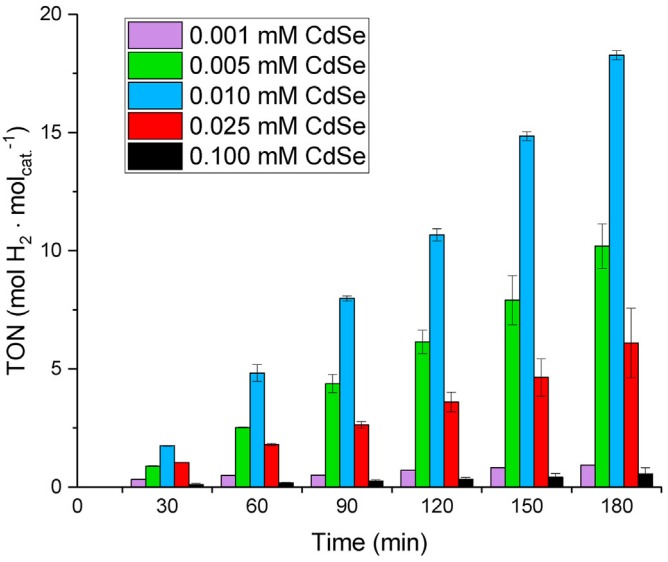


**Fig. 2.** Hydrogen production for different CdSe-MPA concentrations. [Ascorbic acid]: 200 mM, [$Fe_2$(μ-1,2-benzenedithiolate)$(CO)_6$]: 0.1 mM, pH: 4.5.

### 3.2. Comparative performance of the photosensitizers CdSe and CdTe

In order to compare the performance of photosensitizers MPA-CdSe and MPA-CdTe, experiments were carried out with a concentration 0.01 mM of each photosensitizer. Fig. 3 shows the data of

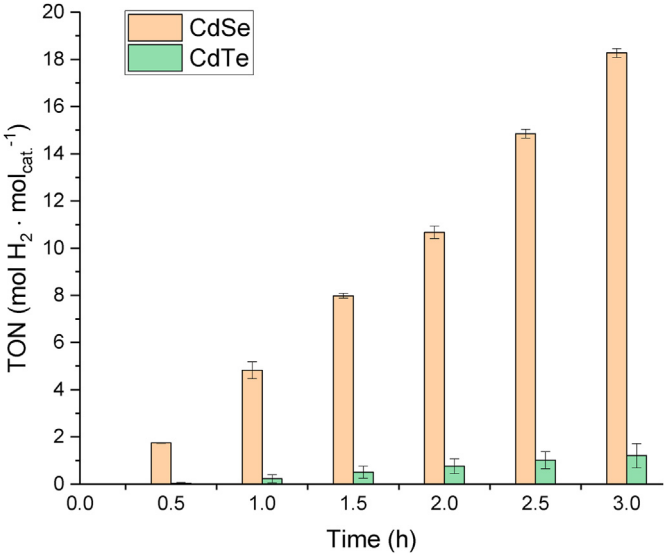


**Fig. 3.** Hydrogen production with CdSe and CdTe as photosensitizers. [Photosensitizer]: 0.01 mM [Ascorbic acid]: 200 mM and [$Fe_2$(μ-1,2-benzenedithiolate)$(CO)_6$]: 0.1 mM, pH 4.5.

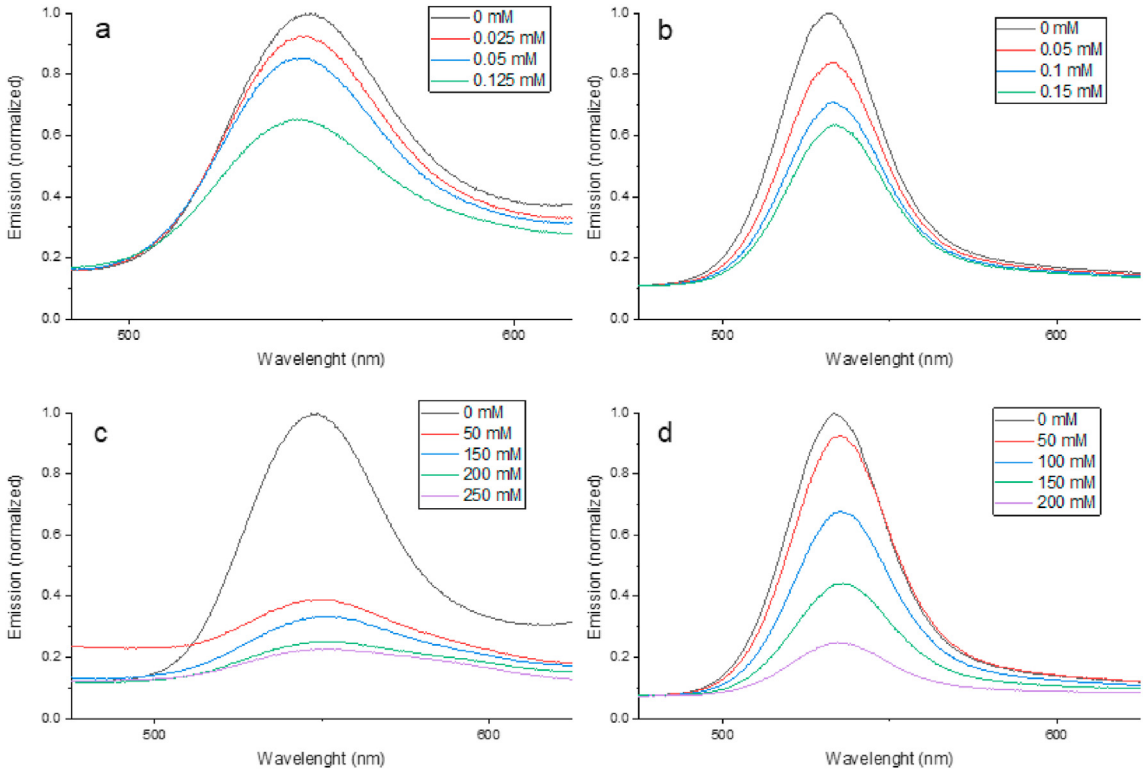


**Fig. 4.** Emission spectra at different concentrations of (a) catalyst in CdSe-MPA medium; (b) catalyst in CdTe-MPA medium; (c) ascorbic acid in CdSe-MPA medium; (d) ascorbic acid in CdTe-MPA medium.

hydrogen production expressed as TON with CdSe and CdTe during 3 h. Under similar experimental conditions, a TOF of 6.5 $h^{-1}$ was observed with CdSe, which is 13-fold higher than with CdTe (TOF = 0.5 $h^{-1}$). Table S1 collects the values of the total hydrogen production and the production rate. The reported TOF values for aqueous systems with ascorbic acid as sacrificial agent, MPA-capped CdSe or CdTe QDs as photosensitizers and natural or biomimetic [Fe-Fe]$H_2$-ase as catalyst, are included in Table SM-2. Although TOF values reached in this work are smaller than other values reported in literature, it is worth noting that reported data have been obtained by working with different concentrations of catalyst and different light irradiation, making it difficult to extract precise conclusions. However, it is interesting to note that the system proposed in this work exhibited higher stability than other systems exhibiting greater TOF.

Emission quenching spectra with progressive addition of catalyst and ascorbic acid to CdSe-MPA and CdTe-MPA media are shown in Fig. 4. According to Fig. 4a and b, addition of a catalyst causes a decrease in the fluorescence intensity, which is consistent with the transfer of photoexcited electrons from CdSe/CdTe to the catalyst. The comparison of the UV–Vis spectrum of [$Fe_2$(μ-1,2-benzenedithiolate)$(CO)_6$] (Fig. SM-1), which shows an absorption peak around 340 nm, with the emission spectra of CdSe and CdTe showing maxima around 545 and 540 nm, respectively (Fig. SM-3), leads to the conclusion that the catalyst does not absorb the fluorescence emitted by the photosensitizer. Thus, the loss of fluorescence intensity is due to the transfer of electrons from the conduction band of the photosensitizer to the catalyst. Consequently, the quenching constant ($k_q$), calculated using the Stern-Volmer equation (Fig. SM-9) (Stern and Volmer, 1919), is equal to the rate constant of electron transfer from the photosensitizer to the catalyst ($k_{ET}$), $k_q = k_{ET}$, with values of $1.55 \cdot 10^{12}$ and $4.02 \cdot 10^{11}$ $M^{-1}$ $s^{-1}$ for CdSe and CdTe, respectively. Similarly, quenching of fluorescence was also observed with increasing concentration of the ascorbic acid (scavenger) in medium (see Fig. 4c and d). Since there is no overlap between the ascorbic acid

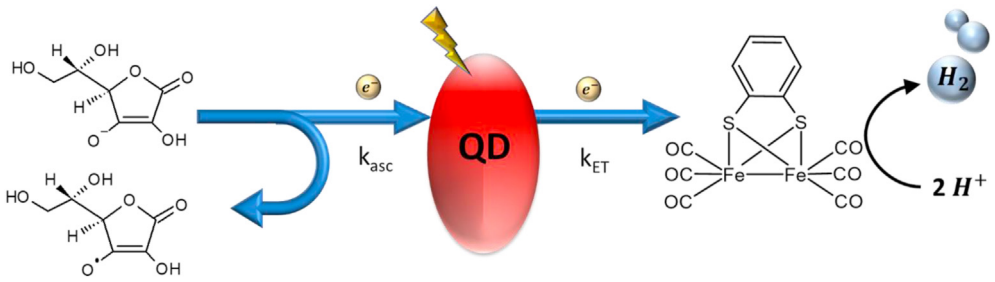


**Fig. 5.** Mechanism of photocatalytic hydrogen production.

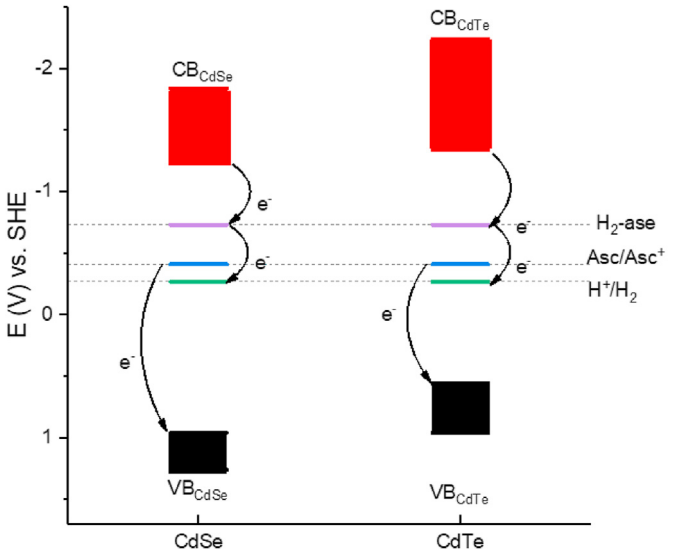


**Fig. 6.** Energy levels at pH 4.5 of CdSe, CdTe, [FeFe]$H_2$-ase mimic and ascorbic acid.

absorption (Fig. SM-8) and the photosensitizer emission (Fig. SM-3), it was concluded that the quenching effect is due to the transfer of electrons from ascorbic acid to the photosensitizer valence band. In this case, the rate constant of electron transfer from ascorbic acid to the photosensitizer ($k_{asc}$), was found to be $5.42 \cdot 10^9$ and $4.31 \cdot 10^8$ $M^{-1}$ $s^{-1}$ for CdSe and CdTe, respectively.

A difference of 2-3 orders of magnitude was observed between $k_{ET}$ and $k_{asc}$ in both materials. This difference agrees with previous reports (Jian et al., 2016; Wen et al., 2016). Fig. 5 depicts the proposed mechanism where the acceptance of the electrons from the ascorbic acid by the photogenerated holes in the QD's valence band is the rate-limiting step as $k_{asc}$ is two orders of magnitude smaller than $k_{ET}$. Furthermore, CdSe sensitizer showed a greater $k_{asc}$ which was nearly 13 times higher than for CdTe. This fact is consistent with the 13 times greater hydrogen production rate obtained with CdSe than with CdTe. Therefore, it was concluded that the electron transfer from the ascorbic acid to the QD was the primary rate-limiting step in hydrogen production reactions.

Fig. 6 represents the energy diagram of both systems at pH 4.5. The reduction potential of the [Fe-Fe]$H_2$-ase mimic was determined by cyclic voltammetry as $E_{1/2} \sim -0.68$ V at pH 4.5 (Quentel et al.,

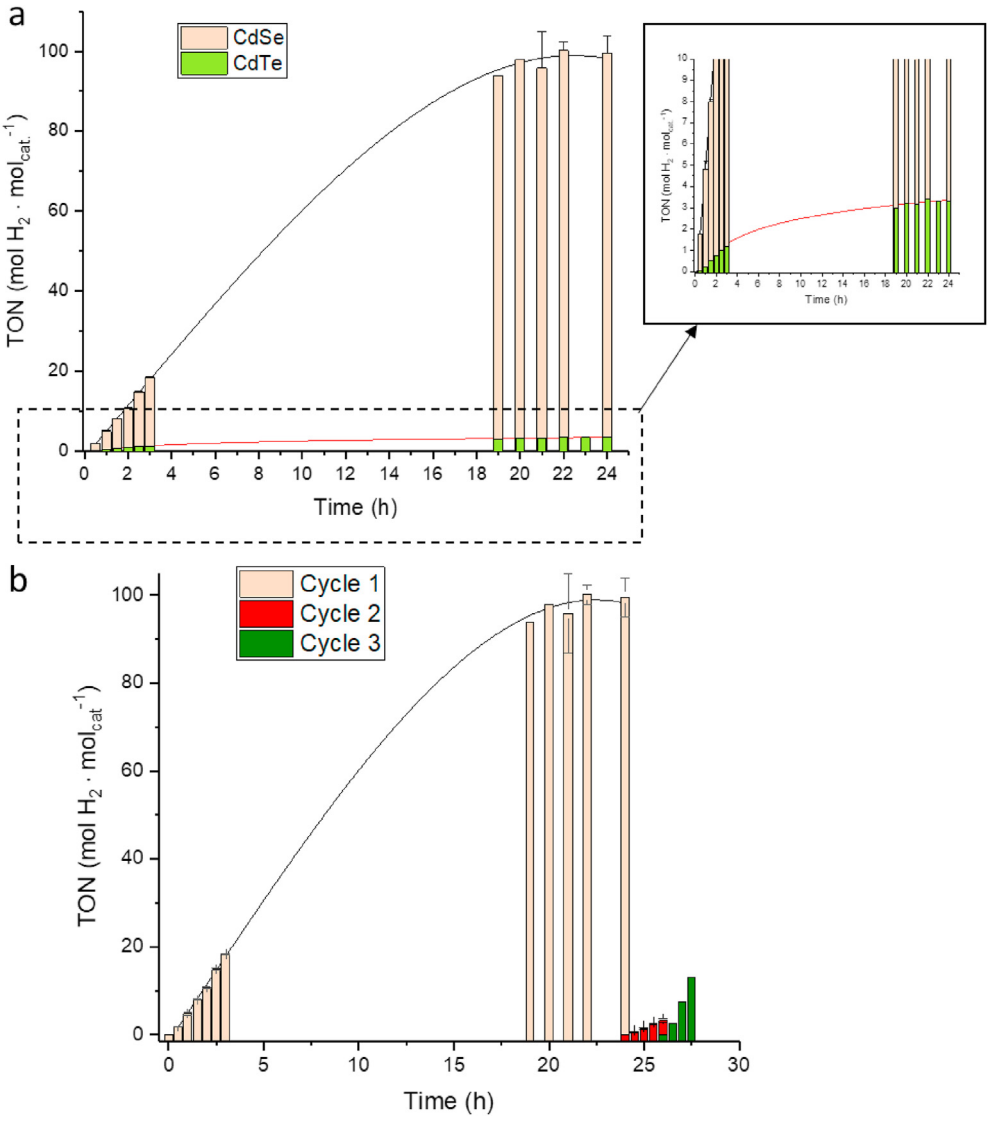


**Fig. 7.** Hydrogen production with (a) CdSe and CdTe for longer operation times, and (b) catalyst reuse with CdSe.

2012) and for ascorbic acid the corresponding value was −0.41 V (Tu et al., 2017). Although it is energetically favorable for the ascorbic acid to produce hydrogen directly, it was confirmed experimentally that this redox reaction did not occur. For both semiconductors, Fig. 6 illustrates the conduction and valence band edge energies for CdSe and CdTe QDs adjusted for present particle diameters considering the variability range found in literature. (Jasieniak et al., 2011). Notably, the energy difference between the oxidation potential of ascorbic acid and the valence band of the QD is greater for CdSe than for CdTe, which is consistent with the higher value of $k_{Asc}$ of CdSe with respect to CdTe. This causes a comparatively greater driving force for the photoinduced electron transfer from sacrificial agent to the CdSe.

Overall, the above experiments demonstrate that the rate-limiting step for the hydrogen production in the QD-([FeFe]$H_2$-ase mimic)-(ascorbic acid) system is the electron transfer from the ascorbic acid (sacrificial agent) to the valence band of the photosensitizer characterized by the kinetic constant $k_{Asc}$.

In an effort to assess the stability of the investigated catalytic system, several selected experiments were carried out for the duration of 24 h. According to Fig. 7a, CdSe reached a TON value of 100 while CdTe achieved a TON value of 3.5 after 24 h. The initial TOF with CdSe was 6.5 $h^{-1}$ decreasing to 1.8 $h^{-1}$ after 18 h while the initial TOF with CdTe was 0.5 $h^{-1}$ decreasing to 0.1 $h^{-1}$ after 18 h. Therefore, hydrogen production rate decreased about 75% for both materials in this period of time. Fig. 7b shows hydrogen production with CdSe operating in different cycles. Cycle 1 shows hydrogen production with a fresh catalyst. Hydrogen production rate decreased to 1.8 $h^{-1}$after 18 h of reaction. Before starting cycle 2, a purge with argon was carried out in the photoreactor to eliminate any possible inhibitory effect of the product, as has been previously reported (Corredor et al., 2020b). After this purge, the TOF was 1.7 $h^{-1}$, similar to the value at the end of cycle 1. Therefore, the decrease in hydrogen production was not attributed to the hydrogen inhibitory effect. Next, catalyst deactivation was examined by addition of $7.5 \cdot 10^{-3}$ mM of fresh catalyst at the beginning of cycle 3; hydrogen production recovered similar values to the initial experimental conditions. Therefore, the decline and stop of hydrogen production is attributed to the loss of catalyst activity.

## 4. Conclusions

In this work, we compare the photocatalytic performance of two QD photosensitizers, CdSe and CdTe, in hydrogen production systems composed of a hydrogenase mimic catalyst and ascorbic acid as sacrificial agent. CdSe QDs showed an overall better performance. For these materials, the highest hydrogen production rate was observed using 0.01 mM nanoparticle concentration, 200 mM of ascorbic acid, and 0.1 mM of [Fe-Fe]$H_2$-ase mimic (excitation intensity = 31 mW $cm^{-2}$ of 400 nm < λ < 800 nm).

Quenching experiments revealed that the rate of electron transfer from photosensitizer to the catalyst, $k_{ET}$, is of 2-3 orders of magnitude higher than that of sacrificial agent→ photosensitizer transfer process, $k_{Asc}$. In particular, we found that $k_{asc}$ for CdSe was 13 times greater than that of CdTe. The ratio of hydrogen production rates for the two materials, CdSe and CdTe, exhibited roughly the same value (13:1), suggesting that the acceptance of the electrons from the ascorbic acid by the photogenerated holes in the QD's valence band was the rate limiting step. A relatively greater value of $k_{asc}$ for CdSe was attributed to the larger difference between the oxidation potential of ascorbic acid and the valence band energy of CdSe in comparison with CdTe. This conclusion suggests that photosensitizers that enable faster sacrificial regenerations may hold the key to improving the hydrogen production rate. Another important area to be addressed by the future research is the long-term stability of hydrogenase mimic catalysts, which lost 25% of catalytic activity after 18 h in present measurements.

## Author contributions

Conceptualization: Juan Corredor, Maria J. Rivero, Inmaculada Ortiz, Frederic Gloaguen and Mikhail Zamkov. Methodology: Juan Corredor, Maria J. Rivero, Inmaculada Ortiz, Dulanjan Harankahage and Mikhail Zamkov. Validation: Juan Corredor, Dulanjan Harankahage and Mikhail Zamkov. Investigation: Juan Corredor, Dulanjan Harankahage and Mikhail Zamkov. Writing—original draft preparation: Juan Corredor. Writing— review and editing: Juan Corredor, Maria J. Rivero, Inmaculada Ortiz, Frederic Gloaguen and Mikhail Zamkov. Supervision: Maria J. Rivero, Inmaculada Ortiz and Mikhail Zamkov. Resources: Maria J. Rivero, Inmaculada Ortiz, Frederic Gloaguen and Mikhail Zamkov. Project administration: Maria J. Rivero, Inmaculada Ortiz and Mikhail Zamkov. Funding acquisition: Maria J. Rivero, Inmaculada Ortiz and Mikhail Zamkov.

## Declaration of competing interest

The authors declare that they have no known competing financial interests or personal relationships that could have appeared to influence the work reported in this paper.

## Acknowledgements

Financial support from projects RTI2018-099407-B-I00, RTI2018-093310-B-I00, RTC2019-006820-5 (MCIU/AEI/FEDER, UE) and 'HYLANTIC'-EAPA_204/2016 (Interreg Atlantic/FEDER UE) is gratefully acknowledged. Juan Corredor is grateful to FPI contract grant (BES-2016-079201). MZ and DH were supported by the Award DE-SC0016872 (MZ) funded by the U.S. Department of Energy, Office of Science.

## Appendix A. Supplementary data

Supplementary data to this article can be found online at https://doi.org/10.1016/j.chemosphere.2021.130485.

## References

Acharya, K.P., Khnayzer, R.S., O'Connor, T., Diederich, G., Kirsanova, M., Klinkova, A., Roth, D., Kinder, E., Imboden, M., Zamkov, M., 2011. The role of hole localization in sacrificial hydrogen production by semiconductor-metal heterostructured nanocrystals. Nano Lett. 11, 2919–2926. https://doi.org/10.1021/nl201388c.

Ahmed, M.E., Dey, S., Darensbourg, M.Y., Dey, A., 2018. Oxygen-Tolerant $H_2$ production by [FeFe]-$H_2$ase active site mimics aided by second sphere proton shuttle. J. Am. Chem. Soc. 140, 12457–12468. https://doi.org/10.1021/jacs.8b05983.

Ben-Shahar, Y., Scotognella, F., Waiskopf, N., Kriegel, I., Dal Conte, S., Cerullo, G., Banin, U., 2015. Effect of surface coating on the photocatalytic function of hybrid CdS-Au nanorods. Small 11, 462–471. https://doi.org/10.1002/smll.201402262.

Brillas, E., Serrà, A., Garcia-Segura, S., 2021. Biomimicry designs for photoelectrochemical systems: strategies to improve light delivery efficiency. Curr. Opin. Electrochem. 26, 100660. https://doi.org/10.1016/j.coelec.2020.100660.

Brown, K.A., Dayal, S., Ai, X., Rumbles, G., King, P.W., 2010. Controlled assembly of hydrogenase-CdTe nanocrystal hybrids for solar hydrogen production. J. Am. Chem. Soc. 132, 9672–9680. https://doi.org/10.1021/ja101031r.

Brown, K.A., Song, Q., Mulder, D.W., King, P.W., 2014. Diameter dependent electron transfer kinetics in semiconductor-enzyme complexes. ACS Nano 8, 10790–10798. https://doi.org/10.1021/nn504561v.

Brown, K.A., Wilker, M.B., Boehm, M., Dukovic, G., King, P.W., 2012. Characterization of photochemical processes for $H_2$ production by CdS nanorod-[FeFe] hydrogenase complexes. J. Am. Chem. Soc. 134, 5627–5636. https://doi.org/10.1021/ja2116348.

Cabeza, J.A., Martínez-García, M.A., Riera, V., Ardura, D., García-Granda, S., 1998. Binuclear iron(I), ruthenium(I), and osmium(I) hexacarbonyl complexes containing a bridging benzene-1,2-dithiolate ligand. Synthesis, X-ray structures, protonation reactions, and EHMO calculations. Organometallics 17, 1471–1477. https://doi.org/10.1021/om970922j.

Capon, J.F., Gloaguen, F., Schollhammer, P., Talarmin, J., 2004. Electrochemical

proton reduction by thiolate-bridged hexacarbonyldiiron clusters. J. Electroanal. Chem. 566, 241–247. https://doi.org/10.1016/j.jelechem.2003.11.032.
Chang, C.M., Orchard, K.L., Martindale, B.C.M., Reisner, E., 2016. Ligand removal from CdS quantum dots for enhanced photocatalytic $H_2$ generation in pH neutral water. J. Mater. Chem. A 4, 2856–2862. https://doi.org/10.1039/c5ta04136h.
Chen, Y., Xiao, K., Shen, N., Zeng, R.J., Zhou, Y., 2018. Hydrogen production from a thermophilic alkaline waste activated sludge fermenter: effects of solid retention time (SRT). Chemosphere 206, 101–106. https://doi.org/10.1016/j.chemosphere.2018.04.170.
Chica, B., Wu, C.H., Liu, Y., Adams, M.W.W., Lian, T., Dyer, R.B., 2017. Balancing electron transfer rate and driving force for efficient photocatalytic hydrogen production in CdSe/CdS nanorod-[NiFe] hydrogenase assemblies. Energy Environ. Sci. 10, 2245–2255. https://doi.org/10.1039/c7ee01738c.
Cho, H., Joo, H., Kim, H., Kim, J.E., Kang, K.S., Yoon, J., 2021. Improved photoelectrochemical properties of $TiO_2$ nanotubes doped with Er and effects on hydrogen production from water splitting. Chemosphere 267, 129289. https://doi.org/10.1016/j.chemosphere.2020.129289.
Christoforidis, K.C., Fornasiero, P., 2017. Photocatalytic Hydrogen production: a rift into the future energy supply. ChemCatChem 9, 1523–1544. https://doi.org/10.1002/cctc.201601659.
Chu, K.H., Ye, L., Wang, W., Wu, D., Chan, D.K.L., Zeng, C., Yip, H.Y., Yu, J.C., Wong, P.K., 2017. Enhanced photocatalytic hydrogen production from aqueous sulfide/sulfite solution by $ZnO_{0.6}S_{0.4}$ with simultaneous dye degradation under visible-light irradiation. Chemosphere 183, 219–228. https://doi.org/10.1016/j.chemosphere.2017.05.112.
Corredor, J., Perez-Peña, E., Rivero, M.J., Ortiz, I., 2020a. Performance of rGO/$TiO_2$ photocatalytic membranes for hydrogen production. Membranes 10, 1–13. https://doi.org/10.3390/membranes10090218.
Corredor, J., Rivero, M.J., Ortiz, I., 2020b. New insights in the performance and reuse of rGO/$TiO_2$ composites for the photocatalytic hydrogen production. Int. J. Hydrogen Energy. https://doi.org/10.1016/j.ijhydene.2020.01.181 (in press).
Corredor, J., Rivero, M.J., Rangel, C.M., Gloaguen, F., Ortiz, I., 2019. Comprehensive review and future perspectives on the photocatalytic hydrogen production. J. Chem. Technol. Biotechnol. 94, 3049–3063. https://doi.org/10.1002/jctb.6123.
Ding, Y., Bertram, J.R., Eckert, C., Bommareddy, R.R., Patel, R., Conradie, A., Bryan, S., Nagpal, P., 2019. Nanorg microbial factories: light-driven renewable biochemical synthesis using quantum dot-bacteria nanobiohybrids. J. Am. Chem. Soc. 141, 10272–10282. https://doi.org/10.1021/jacs.9b02549.
El-Khouly, M.E., El-Mohsnawy, E., Fukuzumi, S., 2017. Solar energy conversion: from natural to artificial photosynthesis. J. Photochem. Photobiol. C Photochem. Rev. 31, 36–83. https://doi.org/10.1016/j.jphotochemrev.2017.02.001.
Elsayed, M.H., Jayakumar, J., Abdellah, M., Mansoure, T.H., Zheng, K., Elewa, A.M., Chang, C.L., Ting, L.Y., Lin, W.C., Yu, H., Wang, W.H., Chung, C.-C., Chou, H.-H., 2021. Visible-light-driven hydrogen evolution using nitrogen-doped carbon quantum dot-implanted polymer dots as metal-free photocatalysts. Appl. Catal. B Environ. 283, 119659. https://doi.org/10.1016/j.apcatb.2020.119659.
Fang, X., Cui, L., Pu, T., Song, J., Zhang, X., 2018. Core-shell CdS@MnS nanorods as highly efficient photocatalysts for visible light driven hydrogen evolution. Appl. Surf. Sci. 457, 863–869. https://doi.org/10.1016/j.apsusc.2018.07.012.
Fukuzumi, S., Lee, Y.M., Nam, W., 2018. Thermal and photocatalytic production of hydrogen with earth-abundant metal complexes. Coord. Chem. Rev. 355, 54–73. https://doi.org/10.1016/j.ccr.2017.07.014.
Giannoudis, E., Benazzi, E., Karlsson, J., Copley, G., Panagiotakis, S., Landrou, G., Angaridis, P., Nikolaou, V., Matthaiaki, C., Charalambidis, G., Gibson, E.A., Coutsolelos, A.G., 2020. Photosensitizers for $H_2$ evolution based on charged or neutral Zn and Sn porphyrins. Inorg. Chem. 59, 1611–1621. https://doi.org/10.1021/acs.inorgchem.9b01838.
Gong, K., Zeng, Y., Kelley, D.F., 2013. Extinction coefficients, oscillator strengths, and radiative lifetimes of CdSe, CdTe, and CdTe/CdSe nanocrystals. J. Phys. Chem. C 117, 20268–20279. https://doi.org/10.1021/jp4065449.
Goy, R., Bertini, L., Rudolph, T., Lin, S., Schulz, M., Zampella, G., Dietzek, B., Schacher, F.H., De Gioia, L., Sakai, K., Weigand, W., 2017. Photocatalytic hydrogen evolution driven by [FeFe] hydrogenase models tethered to fluorene and silafluorene sensitizers. Chem. Eur J. 23, 334–345. https://doi.org/10.1002/chem.201603140.
Greene, B.L., Joseph, C.A., Maroney, M.J., Dyer, R.B., 2012. Direct evidence of active-site reduction and photodriven catalysis in sensitized hydrogenase assemblies. J. Am. Chem. Soc. 134, 11108–11111. https://doi.org/10.1021/ja3042367.
Hamon, C., Ciaccafava, A., Infossi, P., Puppo, R., Even-Hernandez, P., Lojou, E., Marchi, V., 2014. Synthesis and enzymatic photo-activity of an $O_2$tolerant hydrogenase-CdSe@CdS quantum rod bioconjugate. Chem. Commun. 50, 4989–4992. https://doi.org/10.1039/c3cc49368g.
Hemming, E.B., Chan, B., Turner, P., Corcilius, L., Price, J.R., Gardiner, M.G., Masters, A.F., Maschmeyer, T., 2018. [$Fe(C_5Ar_5)(CO)_2Br$] complexes as hydrogenase mimics for the catalytic hydrogen evolution reaction. Appl. Catal. B Environ. 223, 234–241. https://doi.org/10.1016/j.apcatb.2017.04.053.
Hernandez-Ramirez, A., Medina-Ramirez, I., 2015. Semiconducting materials. In: Hernandez-Ramirez, A., Medina-Ramirez, I. (Eds.), Photocatalytic Semiconductors. Springer, pp. 1–40. https://doi.org/10.1007/978-3-319-10999-2_1.
Hinojosa-Reyes, M., Camposeco-Solís, R., Zanella, R., Rodríguez González, V., 2017. Hydrogen production by tailoring the brookite and $Cu_2O$ ratio of sol-gel Cu-$TiO_2$ photocatalysts. Chemosphere 184, 992–1002. https://doi.org/10.1016/j.chemosphere.2017.06.066.
Holladay, J.D., Hu, J., King, D.L., Wang, Y., 2009. An overview of hydrogen production technologies. Catal. Today 139, 244–260. https://doi.org/10.1016/j.cattod.2008.08.039.
Jasieniak, J., Califano, M., Watkins, S.E., 2011. Size-dependent valence and conduction band-edge energies of semiconductor nanocrystals. ACS Nano 5, 5888–5902. https://doi.org/10.1021/nn201681s.
Jian, J.X., Liu, Q., Li, Z.J., Wang, F., Li, X.B., Li, C.B., Liu, B., Meng, Q.Y., Chen, B., Feng, K., Tung, C.H., Wu, L.Z., 2013. Chitosan confinement enhances hydrogen photogeneration from a mimic of the diiron subsite of [FeFe]-hydrogenase. Nat. Commun. 4, 2695. https://doi.org/10.1038/ncomms3695.
Jian, J.X., Ye, C., Wang, X.-Z., Wen, M., Li, Z.-J., Li, X.-B., Chen, B., Tung, C.-H., Wu, L.-Z., 2016. Comparison of $H_2$ photogeneration by [FeFe]-hydrogenase mimics with CdSe QDs and $Ru(bpy)_3Cl_2$ in aqueous solution. Energy Environ. Sci. 9, 2083–2089. https://doi.org/10.1039/C6EE00629A.
Lai, G.J., Lyu, L.M., Huang, Y.S., Lee, G.C., Lu, M.P., Perng, T.P., Lu, M.Y., Chen, L.J., 2021. Few-layer $WS_2$–$MoS_2$ in-plane heterostructures for efficient photocatalytic hydrogen evolution. Nanomater. Energy 81, 105608. https://doi.org/10.1016/j.nanoen.2020.105608.
Li, C.B., Li, Z.J., Yu, S., Wang, G.X., Wang, F., Meng, Q.Y., Chen, B., Feng, K., Tung, C.H., Wu, L.Z., 2013. Interface-directed assembly of a simple precursor of [FeFe]-H2ase mimics on CdSe QDs for photosynthetic hydrogen evolution in water. Energy Environ. Sci. 6, 2597–2602. https://doi.org/10.1039/c3ee40992a.
Li, R.X., Ren, X.T., Tang, M.Y., Chen, M.X., Huang, G.B., Fang, C.H., Liu, T., Feng, Z.H., Yin, Y.B., Guo, Y.M., Mei, S.K., Yan, J., 2018. Fabrication of covalently linked graphene-mediated [FeFe]-hydrogenases biomimetic photocatalytic hydrogen evolution system in aqueous solution. Appl. Catal. B Environ. 224, 772–782. https://doi.org/10.1016/j.apcatb.2017.09.062.
Li, X., Wang, M., Chen, L., Wang, X., Dong, J., Sun, L., 2012. Photocatalytic water reduction and study of the formation of $Fe^IFe^0$ species in diiron catalyst sytems. ChemSusChem 5, 913–919. https://doi.org/10.1002/cssc.201100490.
Li, X.B., Jian, J.X., Wang, X.Z., Wang, Y., Xia, S.G., Tung, C.H., Wu, L.Z., 2020. Per-6-Thiol-Cyclodextrin engineered [FeFe]-Hydrogenase mimic/CdSe quantum dot assembly for photocatalytic hydrogen production. Sol. RRL. https://doi.org/10.1002/solr.202000474 (in press).
Liang, W.J., Wang, F., Wen, M., Jian, J.X., Wang, X.Z., Chen, B., Tung, C.H., Wu, L.Z., 2015. Branched polyethylenimine improves hydrogen photoproduction from a CdSe quantum dot/[FeFe]-hydrogenase mimic system in neutral aqueous solutions. Chem. Eur J. 21, 3187–3192. https://doi.org/10.1002/chem.201406361.
Liu, T., Darensbourg, M.Y., 2007. A mixed-valent, Fe(II)Fe(I), diiron complex reproduces the unique rotated state of the [FeFe]hydrogenase active site. J. Am. Chem. Soc. 129, 7008–7009. https://doi.org/10.1021/ja071851a.
Mongin, C., Moroz, P., Zamkov, M., Castellano, F.N., 2018. Thermally activated delayed photoluminescence from pyrenyl-functionalized CdSe quantum dots. Nat. Chem. 10, 225–230. https://doi.org/10.1038/nchem.2906.
Munfarida, S., Widayat Satriadi, H., Cahyono, B., Hadiyanto Philia, J., Prameswari, J., 2020. Geothermal industry waste-derived catalyst for enhanced biohydrogen production. Chemosphere 258, 127274. https://doi.org/10.1016/j.chemosphere.2020.127274.
Na, Y., Wang, M., Pan, J., Zhang, P., Åkermark, B., Sun, L., 2008. Visible light-driven electron transfer and hydrogen generation catalyzed by bioinspired [2Fe2S] complexes. Inorg. Chem. 47, 2805–2810. https://doi.org/10.1021/ic702010w.
Nasir, M.S., Yang, G., Ayub, I., Wang, S., Wang, L., Wang, X., Yan, W., Peng, S., Ramakarishna, S., 2019. Recent development in graphitic carbon nitride based photocatalysis for hydrogen generation. Appl. Catal. B Environ. 257, 117855. https://doi.org/10.1016/j.apcatb.2019.117855.
Nikolaidis, P., Poullikkas, A., 2017. A comparative overview of hydrogen production processes. Renew. Sustain. Energy Rev. 67, 597–611. https://doi.org/10.1016/j.rser.2016.09.044.
Oh, W.C., Nguyen, D.C.T., Areerob, Y., 2020. Novel cadmium oxide-graphene nanocomposite grown on mesoporous silica for simultaneous photocatalytic $H_2$-evolution. Chemosphere 239, 124825. https://doi.org/10.1016/j.chemosphere.2019.124825.
Orain, C., Quentel, F., Gloaguen, F., 2014. Photocatalytic hydrogen production using models of the iron-iron hydrogenase active site dispersed in micellar solution. ChemSusChem 7, 638–643. https://doi.org/10.1002/cssc.201300631.
Pullen, S., Fei, H., Orthaber, A., Cohen, S.M., Ott, S., 2013. Enhanced photochemical hydrogen production by a molecular diiron catalyst incorporated into a metal-organic framework. J. Am. Chem. Soc. 135, 16997–17003. https://doi.org/10.1021/ja407176p.
Putri, L.K., Ng, B.J., Ong, W.J., Lee, H.W., Chang, W.S., Mohamed, A.R., Chai, S.P., 2020. Energy level tuning of CdSe colloidal quantum dots in ternary 0D-2D-2D CdSe QD/B-rGO/O-$gC_3N_4$ as photocatalysts for enhanced hydrogen generation. Appl. Catal. B Environ. 265, 118592. https://doi.org/10.1016/j.apcatb.2020.118592.
Quentel, F., Passard, G., Gloaguen, F., 2012. Electrochemical hydrogen production in aqueous micellar solution by a diiron benzenedithiolate complex relevant to [FeFe] hydrogenases. Energy Environ. Sci. 5, 7757–7761. https://doi.org/10.1039/c2ee21531d.
Ribao, P., Alexandra Esteves, M., Fernandes, V.R., Rivero, M.J., Rangel, C.M., Ortiz, I., 2019. Challenges arising from the use of $TiO_2$/rGO/Pt photocatalysts to produce hydrogen from crude glycerol compared to synthetic glycerol. Int. J. Hydrogen Energy 44, 28494–28506. https://doi.org/10.1016/j.ijhydene.2018.09.148.
Rivero, M.J., Iglesias, O., Ribao, P., Ortiz, I., 2019. Kinetic performance of $TiO_2$/Pt/reduced graphene oxide composites in the photocatalytic hydrogen production. Int. J. Hydrogen Energy 44, 101–109. https://doi.org/10.1016/j.ijhydene.2018.02.115.
Roy, S., Groy, T.L., Jones, A.K., 2013. Biomimetic model for [FeFe]-hydrogenase: asymmetrically disubstituted diiron complex with a redox-active 2,2′-

bipyridyl ligand. Dalton Trans. 42, 3843–3853. https://doi.org/10.1039/c2dt32457a.
Sanchez, M.L.K., Sommer, C., Reijerse, E., Birrell, J.A., Lubitz, W., Dyer, R.B., 2019a. Investigating the kinetic competency of CrHydA1 [FeFe] hydrogenase intermediate states via time-resolved infrared spectroscopy. J. Am. Chem. Soc. 141, 16064–16070. https://doi.org/10.1021/jacs.9b08348.
Sanchez, M.L.K., Wu, C.H., Adams, M.W.W., Dyer, R.B., 2019b. Optimizing electron transfer from CdSe QDs to hydrogenase for photocatalytic $H_2$ production. Chem. Commun. 55, 5579–5582. https://doi.org/10.1039/c9cc01150a.
Seadira, T.W.P., Sadanandam, G., Ntho, T., Masuku, C.M., Scurrell, M.S., 2018. Preparation and characterization of metals supported on nanostructured $TiO_2$ hollow spheres for production of hydrogen via photocatalytic reforming of glycerol. Appl. Catal. B Environ. 222, 133–145. https://doi.org/10.1016/j.apcatb.2017.09.072.
Shen, M., Jia, W., You, Y., Hu, Y., Li, F., Tian, S., Li, J., Jin, Y., Han, D., 2013. Luminescent properties of CdTe quantum dots synthesized using 3-mercaptopropionic acid reduction of tellurium dioxide directly. Nanoscale Res. Lett. 8, 1–6. https://doi.org/10.1186/1556-276x-8-253.
Song, X.W., Wen, H.M., Ma, C.B., Hu, M.Q., Chen, H., Cui, H.H., Chen, C.N., 2014. Photocatalytic hydrogen evolution by two comparable [FeFe]-hydrogenase mimics assembled to the surface of ZnS. Appl. Organomet. Chem. 28, 267–273. https://doi.org/10.1002/aoc.3119.
Stern, O., Volmer, M., 1919. Über die Abklingzeit der Fluoreszenz. Z. Phys. 20, 183–188.
Streich, D., Astuti, Y., Orlandi, M., Schwartz, L., Lomoth, R., Hammarström, L., Ott, S., 2010. High-turnover photochemical hydrogen production catalyzed by a model complex of the [FeFe]-hydrogenase active site. Chem. Eur J. 16, 60–63. https://doi.org/10.1002/chem.200902489.
Stripp, S.T., Happe, T., 2009. How algae produce hydrogen—news from the photosynthetic hydrogenase. Dalton Trans. 9960–9969. https://doi.org/10.1039/b916246a.
Supplis, C., Gros, F., Dahi, G., Dauchet, J., Roudet, M., Gloaguen, F., Cornet, J.F., 2018. Spectral radiative analysis of bio-inspired $H_2$ production in a benchmark photoreactor: a first investigation using spatial photonic balance. Int. J. Hydrogen Energy 43, 8221–8231. https://doi.org/10.1016/j.ijhydene.2018.03.097.
Trincado, M., Banerjee, D., Grützmacher, H., 2014. Molecular catalysts for hydrogen production from alcohols. Energy Environ. Sci. 7, 2464–2503. https://doi.org/10.1039/c4ee00389f.
Troppmann, S., König, B., 2016. Functionalized vesicles with Co-embedded CdSe quantum dots and [FeFe]-Hydrogenase mimic for light-driven hydrogen production. ChemistrySelect 1, 1405–1409. https://doi.org/10.1002/slct.201600032.
Tu, Y.J., Njus, D., Schlegel, H.B., 2017. A theoretical study of ascorbic acid oxidation and $HOO^{\bullet}/O_2^{\bullet-}$ Radical scavenging. Org. Biomol. Chem. 15, 4417–4431. https://doi.org/10.1039/c7ob00791d.
Wang, F., Liang, W.J., Jian, J.X., Li, C.B., Chen, B., Tung, C.H., Wu, L.Z., 2013. Exceptional poly(acrylic acid)-based artificial [FeFe]-hydrogenases for photocatalytic $H_2$ production in water. Angew. Chem. Int. Ed. 52, 8134–8138. https://doi.org/10.1002/anie.201303110.
Wang, F., Wang, W.G., Wang, H.Y., Si, G., Tung, C.H., Wu, L.Z., 2012. Artificial photosynthetic systems based on [FeFe]-hydrogenase mimics: the road to high efficiency for light-driven hydrogen evolution. ACS Catal. 2, 407–416. https://doi.org/10.1021/cs200458b.
Wang, F., Wang, W.G., Wang, X.J., Wang, H.Y., Tung, C.H., Wu, L.Z., 2011. A highly efficient photocatalytic system for hydrogen production by a robust hydrogenase mimic in an aqueous solution. Angew. Chem. Int. Ed. 50, 3193–3197. https://doi.org/10.1002/anie.201006352.
Wang, H.Y., Wang, W.G., Si, G., Wang, F., Tung, C.H., Wu, L.Z., 2010. Photocatalytic hydrogen evolution from rhenium(I) complexes to [FeFe] hydrogenase mimics in aqueous SDS micellar systems: a biomimetic pathway. Langmuir 26, 9766–9771. https://doi.org/10.1021/la101322s.
Wang, M., Han, K., Zhang, S., Sun, L., 2015a. Integration of organometallic complexes with semiconductors and other nanomaterials for photocatalytic $H_2$ production. Coord. Chem. Rev. https://doi.org/10.1016/j.ccr.2014.12.005.
Wang, P., Zhang, J., He, H., Xu, X., Jin, Y., 2015b. The important role of surface ligand on CdSe/CdS core/shell nanocrystals in affecting the efficiency of $H_2$ photogeneration from water. Nanoscale 7, 5767–5775. https://doi.org/10.1039/c4nr07343f.
Wang, W., Song, X.W., Hong, Z., Li, B., Si, Y., Ji, C., Su, K., Tan, Y., Ju, Z., Huang, Y., Chen, C.N., Yuan, D., 2019. Incorporation of iron hydrogenase active sites into a stable photosensitizing metal-organic framework for enhanced hydrogen production. Appl. Catal. B Environ. 258, 117979. https://doi.org/10.1016/j.apcatb.2019.117979.
Wen, M., Li, X.B., Jian, J.X., Wang, X.Z., Wu, H.L., Chen, B., Tung, C.H., Wu, L.Z., 2016. Secondary coordination sphere accelerates hole transfer for enhanced hydrogen photogeneration from [FeFe]-hydrogenase mimic and CdSe QDs in water. Sci. Rep. 6, 29851. https://doi.org/10.1038/srep29851.
Wen, M., Wu, H.L., Jian, J.X., Wang, X.Z., Li, X.B., Chen, B., Tung, C.-H., Wu, L.-Z., 2017. Integrating CdSe quantum dots with a [FeFe]-Hydrogenase mimic into a photocathode for hydrogen evolution at a low bias voltage. ChemPhotoChem 1, 260–264. https://doi.org/10.1002/cptc.201700041.
Wittkamp, F., Senger, M., Stripp, S.T., Apfel, U.P., 2018. [FeFe]-Hydrogenases: recent developments and future perspectives. Chem. Commun. 54, 5934–5942. https://doi.org/10.1039/c8cc01275j.
Wroblewska-Wolna, A.M., Harvie, A.J., Rowe, S.F., Critchley, K., Butt, J.N., Jeuken, L.J.C., 2020. Quantum dot interactions with and toxicity to Shewanella oneidensis MR-1. Nanotechnology 31, 134005. https://doi.org/10.1088/1361-6528/ab5f78.
Yang, J., Miao, H., Jing, J., Zhu, Y., Choi, W., 2021a. Photocatalytic activity enhancement of PDI supermolecular via π-π action and energy level adjusting with graphene quantum dots. Appl. Catal. B Environ. 281, 119547. https://doi.org/10.1016/j.apcatb.2020.119547.
Yang, Y., Zhou, C., Wang, W., Xiong, W., Zeng, G., Huang, D., Zhang, C., Song, B., Xue, W., Li, X., Wang, Z., He, D., Luo, H., Ouyang, Z., 2021b. Recent advances in application of transition metal phosphides for photocatalytic hydrogen production. Chem. Eng. J. 405, 126547. https://doi.org/10.1016/j.cej.2020.126547.
Yu, T., Zeng, Y., Chen, J., Li, Y.Y., Yang, G., Li, Y., 2013. Exceptional dendrimer-based mimics of diiron hydrogenase for the photochemical production of hydrogen. Angew. Chem. Int. Ed. 52, 5631–5635. https://doi.org/10.1002/anie.201301289.
Yu, W.W., Qu, L., Guo, W., Peng, X., 2003. Experimental determination of the extinction coefficient of CdTe, CdSe, and CdS nanocrystals. Chem. Mater. 15, 2854–2860. https://doi.org/10.1021/cm034081k.
Yue, D., Qian, X., Kan, M., Ren, M., Zhu, Y., Jiang, L., Zhao, Y., 2017. Sulfurated [NiFe]-based layered double hydroxides nanoparticles as efficient co-catalysts for photocatalytic hydrogen evolution using CdTe/CdS quantum dots. Appl. Catal. B Environ. 209, 155–160. https://doi.org/10.1016/j.apcatb.2017.02.075.
Zamkov, M., 2017. Solar hydrogen generation: exceeding 100% efficiency. Nat. Energy 2, 17072. https://doi.org/10.1038/nenergy.2017.72.

# 4. Conclusions and future perspectives

## 4.1. Conclusions

In this thesis different strategies have been adopted to overcome some challenges for the photocatalytic generation of hydrogen. The main objectives are: i) improving the performance of $TiO_2$ photocatalysts with noble metal-free materials; ii) fabricating photocatalytic membranes based on immobilized rGO/$TiO_2$ composites on Nafion membranes to facilitate separation and recovery of the photocatalyst from the treated solution after the photocatalytic process; iii) developing quantum dots (QDs) based photocatalytic systems with visible light activity.

In order to achieve the first objective, $TiO_2$ and graphene oxide (GO) composite materials were prepared with GO/$TiO_2$ ratios from 1% to 10%. The stability of the composites was studied in methanol photoreforming experiments.

Immobilization of rGO/$TiO_2$ composites on Nafion polymeric membranes was carried out following three different simple methods: solvent-casting (SC), dip-coating (DP) and photocatalyst spraying (SP). The performance of the resulting membranes performances was evaluated in the photocatalytic generation of hydrogen.

Finally, hybrid systems consisting of homogeneous biomimic [Fe-Fe]$H_2$-ase catalysts and chalcogenides QDs photosensitizers were studied in the generation of hydrogen under visible light. The comparison of CdSe and CdTe QDs photosensitizers was carried out. The stability of the photocatalytic system and the influence of the photosensitizer concentration were also studied. Specific conclusions drawn from the results of this thesis, are listed below.

### 4.1.1. Photocatalytic hydrogen production

First, a thorough literature review of photoreforming catalysts was carried out. This review revealed that although homogeneous and hybrid photocatalytic systems provided the highest hydrogen production rates, heterogenous systems are closer to the large-scale application due to the high stability of the semiconductor photocatalyst and the ability to be recovered from the treated solution. Nevertheless, the following challenges were identified:

i) Although the highest hydrogen production rates have been achieved with homogeneous systems, the system stability is usually compromised due to the decomposition of the catalyst, the photosensitizer, or both. Hybrid systems combine homogeneous catalysts with semiconductor photosensitizers. Therefore, they would be a great alternative to overcome the low stability of homogeneous photosensitizers combined with the high performance of homogeneous catalysts.

ii) Although noble metal catalysts and photosensitizers offer higher performances, avoiding the use of noble metals is currently preferred. In this way bio-inspired [FeFe]-hydrogenase mimics composed by noble metal-free material appear as promising catalysts because they achieve very high hydrogen production rates.

### 4.1.2. Heterogeneous systems

rGO/$TiO_2$ composites were synthetized to improve $TiO_2$ photoactivity. GO ratios from 1% to 10% in the rGO/$TiO_2$ composites were studied and

compared with bare $TiO_2$. Further composite immobilization on Nafion membranes was carried out by SC, DP and photocatalyst SP methods. The following conclusions were drawn:

i) The combination of $TiO_2$ with rGO improved the total amount of produced hydrogen. Among the studied GO ratios from 1% to 10%, 2% of GO in the rGO/$TiO_2$ composite showed the highest hydrogen production rates, however, the hydrogen production rate is similar to the rate achieved with $TiO_2$. The inhibitory effect of accumulated hydrogen in the photocatalytic reactor was avoided by removing it with argon.

ii) Photocatalytic membranes obtained by rGO/$TiO_2$ SP and DP on Nafion membranes provided higher hydrogen production rates than SC because of the higher mass transport resistance that the sacrificial agent needed to overcome to contact the active sites in the latter membrane. Moreover, SP method showed only 0.4% photocatalyst leaching after 80 h of operation, whereas DP leaching resulted in 4.8% for the same time. Therefore, SP seems to be the most effective method among the studied ones to immobilize the composite photocatalyst on Nafion membranes.

iii) The study of the process at longer times, 96 h, showed a decrease of approximately 20% in the hydrogen production rate with suspended rGO/$TiO_2$ catalyst. This could be attributed to further rGO reduction in the composite during the photocatalytic process. SP reused membrane also showed a decrease in the initial rate in comparison with a fresh membrane.

### 4.1.3. Hybrid systems

Hybrid systems were studied using biomimic [Fe-Fe]$H_2$-ase, [$Fe_2$(μ-1,2-benzenedithiolate)$(CO)_6$], as catalyst, CdSe or CdTe QDs as photosensitizers, and ascorbic acid as sacrificial agent under visible light irradiation.

i) By drawing a comparison between the two photosensitizer QDs, CdSe showed higher hydrogen production than CdTe leading to a TOF (Turnover Frequency, $mol_{H2} \cdot mol_{catalyst}^{-1} \cdot h^{-1}$) of 6.5 $h^{-1}$, 13-times higher than CdTe with a TOF of 0.5 $h^{-1}$.

ii) Emission quenching experiments revealed $1.55 \cdot 10^{12}$ and $4.02 \cdot 10^{11}$ $M^{-1} \cdot s^{-1}$ values of electron transfer rate from the photosensitizer to the catalyst ($k_{ET}$) for CdSe and CdTe, respectively. These experiments also revealed a value of $5.42 \cdot 10^{9}$ $M^{-1} \cdot s^{-1}$ of electron transfer rate from the sacrificial agent to the catalyst ($k_{asc}$) for the CdSe, 13-fold higher than for the CdTe with a $k_{asc}$ of $4.31 \cdot 10^{8}$ $M^{-1} \cdot s^{-1}$. The higher $k_{asc}$ was explained by the difference between the oxidation potential of ascorbic acid and the valence band energy of CdSe when compared to CdTe. $k_{ET}$ is of 2-3 orders of magnitude higher than $k_{asc}$ indicating that the electron transfer from ascorbic acid to the photosensitizer was the rate-limiting step. This conclusion could be supported because the 13-fold ratio $k_{asc,CdSe}/k_{asc,CdTe}$ coincided with the 13-fold higher hydrogen production rate with CdSe.

iii) The photocatalytic system led to 75% reduction in the hydrogen generation rate after 18 h of process. New catalyst was added after this time and the hydrogen generation rate was recovered. This fact

confirmed that the decrease in the hydrogen production rate was due to the catalyst deactivation.

### 4.1.4. Comparison between systems

Table 4.1 collects hydrogen production rates of the studied heterogeneous and hybrid systems expressed in the same units although they were evaluated in different experimental setups. It should be specially remarked that heterogeneous systems were evaluated under UVA light irradiation while hybrid systems were evaluated under visible light irradiation.

**Table 4.1**. Hydrogen production rates

| System | Light source | Rate (μmol $H_2$ $\cdot g_{catalyst}^{-1} \cdot h^{-1}$) | Apparent quantum yield (%) |
|---|---|---|---|
| Slurry heterogeneous system | UVA Fluorescent lamp (315 nm < λ <400 nm) 0.75 mW/cm$^2$ | 1.6 | 0.014 % |
| Immobilized heterogeneous system | UVA Fluorescent lamp (315 nm < λ <400 nm) 0.75 mW/cm$^2$ | 1.1 | 0.010 % |
| Hybrid system | Halogen lamp (400 nm < λ <800 nm) 31 mW/cm$^2$ | 15476.2 | 12.320 % |

i) Hybrid system clearly showed the highest hydrogen production rates and apparent quantum yield with values 4 orders of magnitude higher than with the heterogeneous systems.

ii) Hybrid systems allowed working with visible light irradiation due to the narrow band gap of CdSe QDs, while heterogeneous systems needed UVA light to promote electrons from the valence band to the conduction band.

iii) Heterogeneous systems exhibited longer stability showing a slight decrease in the production rate when using rGO/$TiO_2$ and no decrease with bare $TiO_2$ after almost one week of running time. The photocatalyst recovery after photoreforming would be easier than in homogeneous or hybrid systems, especially when the photocatalyst was immobilized on polymeric membranes.

## 4.2. Future perspectives

Hydrogen is a clean fuel and will be a game changer in global energy sectors. It is predicted that hydrogen will play a key role in shifting the global energy system towards a more sustainable one by 2050. Considering the future need and demand for hydrogen, it is important to find routes to produce it in a renewable way. Photocatalytic hydrogen production is among the routes to produce green hydrogen. This technology could be suitable for any location where the availability of an organic solution could act as sacrificial agent. However, several challenges need to be overcome before its large-scale application. In order to facilitate future research, the following guidelines have been drawn based on the knowledge accumulated during the development of this thesis:

i) Although homogeneous and hybrid systems show higher hydrogen production rates than heterogeneous ones, heterogeneous systems seem to be more promising for large scale photocatalytic hydrogen

production due to their high photocatalyst stability. Up to our knowledge, only heterogeneous systems have been deployed at pilot plant scale so far. An additional advantage is the easy recovery of the photocatalyst or its immobilization on photocatalytic membranes. According to the obtained results in this thesis, the immobilized rGO/$TiO_2$ showed 30% less hydrogen production rate than the suspended photocatalyst in the reforming of methanol but, the photocatalyst recovery and reuse was facilitated. Therefore, it should be evaluated what option is the most convenient. Future efforts should be done in developing effective noble metal-free photocatalyst semiconductors to improve hydrogen production rates in heterogeneous systems. Some promising strategies to achieve this objective could be coupling two semiconductors or doping a semiconductor photocatalyst with different elements.

ii) Hybrid systems provide high hydrogen production rates, photosensitizer semiconductors show great stability, and the photosensitizers could be recovered or immobilized. These systems could be promising candidates if the challenge of catalyst stability is met. Although the catalyst is solubilized, it could be immobilized. [FeFe]$H_2$-ase mimic molecules could be promising catalysts because they are composed of earth abundant elements and they offer competitive hydrogen production rates and apparent quantum yield values.

iii) Electron transfer from sacrificial agent to CdSe and CdTe QDs was determined as the rate limiting step. Therefore, future efforts should be focused on improving this electron transfer. Further

research in the interaction between the pairs of sacrificial agents and QDs ligands could help improving this electronic transfer rate.

iv) The activity loss of the [FeFe]$H_2$-ase mimic catalysts with operation time was demonstrated, thus, developing long-term stable [FeFe]$H_2$-ase mimics becomes a challenge for future process development.

.

# Conclusiones y perspectivas futuras

## Conclusiones

En esta tesis se han propuesto varias estrategias para solventar algunos de los desafíos que actualmente presenta la generación fotocatalítica de hidrógeno. Los objetivos principales son: i) mejorar el rendimiento del $TiO_2$ combinándolo con materiales que no contengan metales nobles; ii) fabricar membranas fotocatalíticas de Nafion con fotocatalizadores de $rGO/TiO_2$ para evitar la necesidad de una posterior recuperación del fotocatalizador de la disolución tratada después del proceso fotocatalítico; iii) desarrollar sistemas fotocatalíticos empleando puntos cuánticos (QDs) con actividad bajo luz visible.

Con el fin de superar el primer objetivo, se combinaron partículas de $TiO_2$ con óxido de grafeno (GO) empleando relaciones de $GO/TiO_2$ entre 1% y 10%. La estabilidad del $rGO/TiO_2$ durante el proceso de foto-reformado fue estudiada en disoluciones de metanol. La inmovilización del $rGO/TiO_2$ fue llevada a cabo a través de 3 sencillos métodos: solvent-casting (SC), dip-coating (DP) y spraying (SP). Se evaluó el rendimiento en la producción fotocatalítica de hidrógeno de las membranas fotocatalíticas sintetizadas.

Finalmente, se estudiaron sistemas híbridos compuestos por catalizadores homogéneos biomiméticos [Fe-Fe]-hidrogenasa y empleando como fotosensibilizadores QDs basados en calcogenuros para la generación de hidrógeno empleando luz visible. Se llevó a cabo la comparación de QDs de CdSe y CdTe en su desempeño como fotosensibilizadores. La estabilidad del sistema fotocatalítico y la influencia de la concentración de los QDs también fueron estudiadas. A continuación, se muestran conclusiones más específicas extraídas de los resultados de esta tesis.

**Producción de hidrógeno por fotocatálisis**

En primer lugar, se realizó una revisión bibliográfica sobre los catalizadores empleados para el foto-reformado. Esta revisión reveló que a pesar de que los catalizadores homogéneos e híbridos eran los que proporcionaban las mayores velocidades de producción de hidrógeno, los sistemas heterogéneos eran los que estaban más cerca de su aplicación a gran escala debido a la alta estabilidad de los semiconductores empleados como fotocatalizadores y su facilidad para ser recuperados de la disolución tratada. Se identificaron los siguientes desafíos:

i) Aunque las producciones más altas de hidrógeno han sido alcanzadas con sistemas homogéneos, la estabilidad de estos sistemas está comprometida generalmente por la descomposición del catalizador, del fotosensibilizador o ambos. Los sistemas híbridos combinan catalizadores homogéneos con fotosensibilizadores semiconductores. Por lo tanto, estos serían una buena alternativa para superar el problema de la baja estabilidad de los fotosensibilizadores homogéneos combinados con el alto rendimiento de producción de los catalizadores homogéneos.

ii) Actualmente se prefiere evitar el uso de los metales nobles a pesar del alto desempeño de los catalizadores y fotosensibilizadores que los contienen. En esta línea, las [Fe-Fe]-hidrogenasas biomiméticas compuestas por materiales que no contienen metales nobles aparecen como fotocatalizadores prometedores debido a las altas velocidades de producción de hidrógeno que alcanzan.

**Sistemas heterogéneos**

Se sintetizaron fotocatalizadores rGO/$TiO_2$ para mejorar la fotoactividad del $TiO_2$. Se estudiaron fotocatalizadores con relaciones rGO/$TiO_2$ entre el 1% y el 10%, y se compararon con el $TiO_2$. Posteriormente se inmovilizaron en membranas de Nafion mediante los métodos de SC, DP y SP. Se obtuvieron las siguientes conclusiones:

i) La combinación del $TiO_2$ con el rGO mejoró la cantidad total de hidrógeno producido. Entre los porcentajes estudiados de GO en el rGO/$TiO_2$, el 2% fue el que mostró una mayor producción de hidrógeno, sin embargo, la velocidad de producción de hidrógeno fue similar a la obtenida con el $TiO_2$. El efecto inhibidor sobre la reacción producido por el hidrógeno acumulado fue eludido evitando la acumulación de hidrógeno con argón.

ii) Las membranas fotocatalíticas fabricadas por SP y DP del rGO/$TiO_2$ en Nafion proporcionaron mayores producciones de hidrógeno que las fabricadas por SC debido a que en esta última la resistencia a la transferencia de materia que tenía que vencer el agente de sacrificio para alcanzar los centros activos es mayor. Además, el método SP mostró sólo un 0.4% de lixiviación del fotocatalizador después de 80 h de operación, mientras que el método DP mostró un 4.8% para el mismo tiempo. Por tanto, SP parece ser el método más efectivo entre los estudiados para inmovilizar el rGO/$TiO_2$ en membranas de Nafion.

iii) El estudio del proceso a tiempos largos de operación, 96 h, mostró una reducción aproximadamente del 20% de la

velocidad de hidrógeno con el rGO/$TiO_2$ en suspensión. Esto podría ser atribuido a una reducción adicional del rGO durante el proceso fotocatalítico. La membrana SP reutilizada también mostró una reducción de la velocidad de producción de hidrógeno respecto a la membrana sin utilizar.

**Sistemas híbridos**

Se estudiaron los sistemas híbridos irradiados por luz visible utilizando como catalizador [Fe-Fe]-hidrogenasas biomiméticas, [$Fe_2$(μ-1,2-bencenoditiolato)$(CO)_6$], QDs de CdSe o CdTe como fotosensibilizador y ácido ascórbico como agente de sacrificio.

i) Haciendo la comparación entre los dos QDs fotosensibilizadores, el CdSe mostró mayor producción de hidrógeno que el CdTe proporcionando un TOF ($mol_{H2} \cdot mol_{catalizador}^{-1} \cdot h^{-1}$) de 6,5 $h^{-1}$, 13 veces mayor que con el CdTe, con un TOF de 0,5 $h^{-1}$.

ii) Los experimentos de extinción de la emisión revelaron unos valores de velocidad de transferencia de electrones desde el fotosensibilizador al catalizador ($k_{ET}$) de $1{,}55 \cdot 10^{12}$ y $4{,}02 \cdot 10^{11}$ $M^{-1} \cdot s^{-1}$ para el CdSe y el CdTe, respectivamente. Estos experimentos también revelaron unas velocidades de transferencia electrónica del agente de sacrificio al catalizador ($k_{asc}$) de $5{,}42 \cdot 10^{9}$ $M^{-1} \cdot s^{-1}$ para el CdSe, 13 veces mayor que para el CdTe que mostró un valor de $4{,}31 \cdot 10^{8}$ $M^{-1} \cdot s^{-1}$. La mayor $k_{asc}$ se explicó por la mayor diferencia entre el potencial de oxidación del ácido ascórbico y banda de valencia con el CdSe que con el CdTe.

iii) El sistema fotocatalítico sufrió una reducción en la generación de hidrógeno del 75% después de 18 h de proceso. Después de ese tiempo se añadió catalizador nuevo y se recuperó la velocidad de producción inicial. Este hecho confirmó que la reducción de la velocidad de hidrógeno fue debido a la desactivación del catalizador.

**Comparación de sistemas**

La Tabla 1 recoge los valores de producción de hidrógeno en las mismas unidades de los sistemas heterogéneos e híbridos estudiados, a pesar de que fueron evaluados en diferentes sistemas experimentales. Cabe destacar que los sistemas heterogéneos fueron evaluados bajo radiación UVA mientras que los sistemas híbridos fueron evaluados bajo radiación visible.

**Tabla 1**. Velocidades de producción de hidrógeno

| **Sistema** | **Fuente de luz** | **Velocidad (μmol $H_2$ $\cdot g_{catalizador}^{-1} \cdot h^{-1}$)** | **Rendimiento cuántico aparente (%)** |
|---|---|---|---|
| Sistema heterogéneo en suspensión | Lámpara fluorescente UVA (315 nm< λ <400 nm) 0.75 mW/cm$^2$ | 1,6 | 0,014% |
| Sistema heterogéneo inmovilizado | Lámpara fluorescente UVA (315 nm< λ <400 nm) 0.75 mW/cm$^2$ | 1,1 | 0,010% |
| Sistema híbrido | Lámpara halógena (400 nm < λ <800 nm) 31 mW/cm$^2$ | 15476,2 | 12,320% |

i) El sistema híbrido mostró claramente la mayor producción de hidrógeno y rendimiento cuántico aparente con valores 4 órdenes de magnitud superiores a los sistemas heterogéneos.

ii) Los sistemas híbridos permitieron trabajar con luz visible debido al estrecho bang gap de los QDs de CdSe, mientras que los sistemas heterogéneos necesitaron luz UVA para promocionar los electrones desde la banda de valencia a la banda de conducción.

iii) Los sistemas heterogéneos mostraron estabilidades más largas, llegando después de una semana de operación a una leve reducción en la producción de hidrógeno empleando el rGO/$TiO_2$ y ninguna reducción al usar $TiO_2$. La recuperación del catalizador después del foto-reformado sería más fácil que en los sistemas homogéneos o híbridos, especialmente cuando el fotocatalizador se inmoviliza en membranas poliméricas.

## Perspectivas futuras

El hidrógeno es un combustible limpio y supondrá un cambio en el sector energético mundial. Para el año 2050 se predice que el hidrógeno jugará un papel clave hacia un sistema más sostenible. Teniendo en cuenta las necesidades y demandas futuras de hidrógeno es importante encontrar rutas para producirlo de forma renovable. La producción de hidrógeno por fotocatálisis es una de las rutas para producir hidrógeno verde. Esta tecnología podría emplearse en cualquier localización donde se encuentren disoluciones de compuestos orgánicos que puedan actuar como agente de sacrificio. Sin embargo, deben superarse varios desafíos antes de su

aplicación a gran escala. Las siguientes recomendaciones para investigaciones futuras han sido extraídas del conocimiento acumulado durante el desarrollo de esta tesis:

i) Aunque los sistemas homogéneos e híbridos muestren producciones de hidrógeno más altas que los heterogéneos, estos últimos parecen ser más prometedores para la producción a gran escala debido a la alta estabilidad de los fotocatalizadores. Hasta donde sabemos, solo los heterogéneos han sido llevados a planta piloto. Una ventaja adicional es la facilidad de recuperación del fotocatalizador o su inmovilización en membranas fotocatalíticas. Según los resultados obtenidos en esta tesis, el rGO/$TiO_2$ inmovilizado mostró una velocidad de producción de hidrógeno un 30% menor que el fotocatalizador suspendido en metanol, sin embargo, la etapa recuperación del fotocatalizador no sería necesaria y su reutilización es más sencilla. Por tanto, debería ser evaluada cual es la opción más conveniente. Los esfuerzos futuros deberían centrarse en desarrollar fotocatalizadores semiconductores que no contengan metales nobles para mejorar las velocidades de producción de hidrógeno en sistemas heterogéneos. Algunas estrategias prometedoras para alcanzar este objetivo podrían ser combinar dos semiconductores o dopar un fotocatalizador semiconductor con diferentes elementos.

ii) Los sistemas híbridos proporcionan altas velocidades de producción, los fotosensibilizadores semiconductores muestran buena estabilidad y pueden ser recuperados o inmovilizados. Estos sistemas podrían ser buenos candidatos

si se consigue superar el desafío de la estabilidad de los catalizadores. El catalizador podría inmovilizarse a pesar de ser soluble. Las moléculas de [Fe-Fe]-hidrogenasa podrían ser catalizadores prometedores porque están compuestos por elementos abundantes en la naturaleza y ofrecen velocidades de producción de hidrógeno y rendimientos cuánticos competitivos.

iii) La transferencia de electrones del agente de sacrificio hacia los QDs del CdSe y CdTe fue identificada como la etapa limitante. Por tanto, los esfuerzos futuros deberían centrarse en mejorar esta transferencia electrónica. Investigar en profundidad la interacción entre los pares de agentes de sacrificio y los ligandos de los QDs podría ayudar a mejorar esta velocidad de transferencia electrónica.

iv) Se demostró la pérdida de actividad con el tiempo del catalizador [Fe-Fe]-hidrogenasa biomimético. Por tanto, el desarrollo de moléculas de [Fe-Fe]-hidrogenasas biomiméticas es un desafío futuro para el desarrollo del proceso.

# Nomenclature

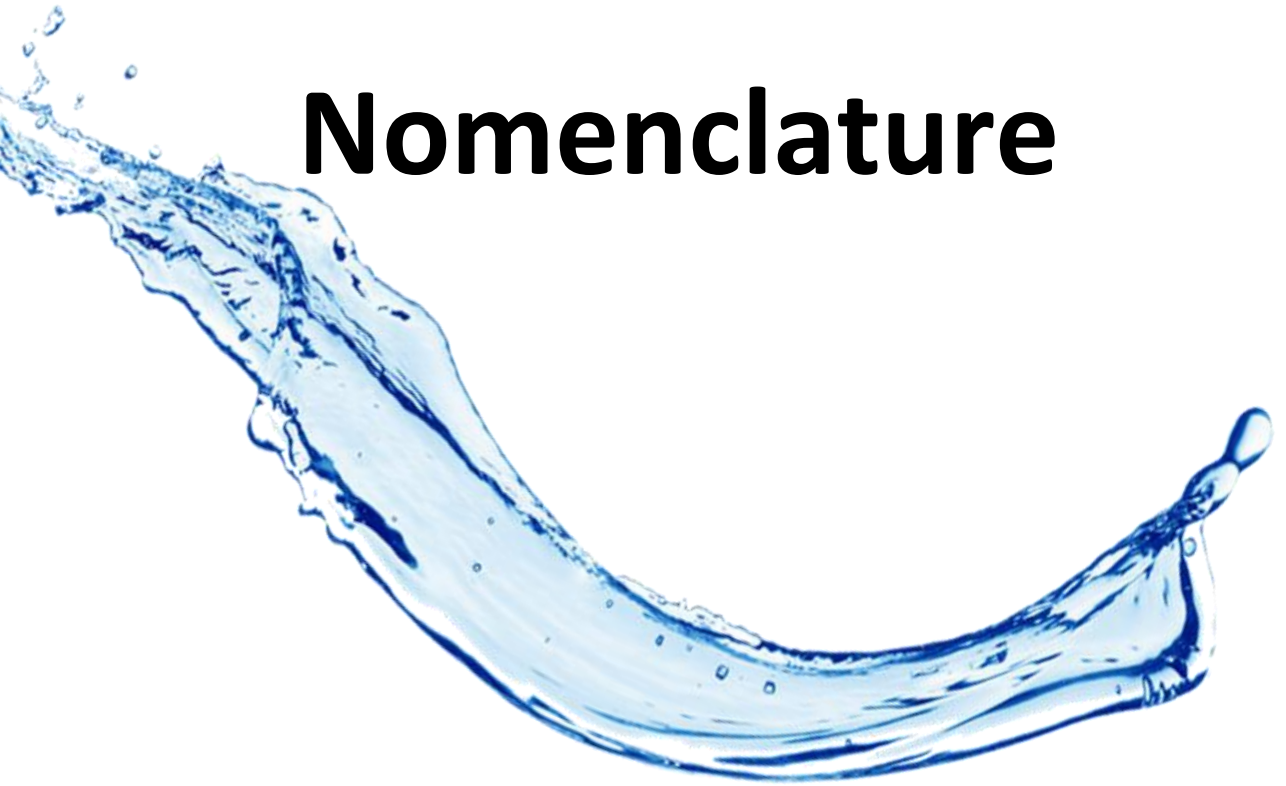

# *Nomenclature*

| | |
|---|---|
| BET | Brunauer-Emmett-Teller |
| CB | Conduction Band |
| DP | Dip-coating |
| $E_{CB}$ | Conduction band potential |
| $E_{VB}$ | Valence band potential |
| [FeFe]$H_2$-ase | Hydrogenase |
| FTIR | Fourier Transform Infrared |
| GC | Gas Chromatograph |
| GO | Graphene Oxide |
| H-NMR | Proton Nuclear Magnetic Resonance |
| $k_{asc}$ | Rate constant of electron transfer from the sacrificial agent (ascorbic acid) to the photosensitizer (QD) |
| $k_{ET}$ | Rate constant of electron transfer from the photosensitizer (QD) to the catalyst ([FeFe]$H_2$-ase mimic) |
| QD | Quantum Dot |
| rGO | Reduced Graphene Oxide |
| SC | Solvent-Casting |
| SEM | Scanning Electron Microscopy |
| SP | Spraying |

| | |
|---|---|
| TGA | Thermogravimetric analysis |
| TOF | Turnover Frequency |
| TON | Turnover Number |
| VB | Valence Band |

# Appendix

## A.1. Contributions to scientific congresses

Presenting author underlined.

1. Juan Corredor, Paula Ribao, Maria J. Rivero, Inmaculada Ortiz. New developments on Photocatalytic Process Intensification. 10th World Congress of Chemical Engineering. Barcelona, Spain, 1-5 octubre, 2017. *Poster presentation.*

2. Paula Ribao, Juan Corredor, Maria J. Rivero, Inmaculada Ortiz. Selecting an optimal concentration of benzoquinone for a sustainable use as superoxide radical scavenger. 3rd Iberoamerican Conference on Advanced Oxidation Technologies (III CIPOA). Guatape, Colombia, 14-17 noviembre, 2017. *Poster presentation.*

3. Juan Corredor, Maria J. Rivero, Inmaculada Ortiz. $TiO_2$/rGO composites for photocatalytic hydrogen production from methanol. 10th European meeting on Solar Chemistry and Photocatalysis: Environmental Applications (SPEA10). Almería, Spain, 4-8 junio, 2018. *Poster presentation.*

4. Maria J. Rivero, Juan Corredor, Inmaculada Ortiz. Waste Upgrading with Photocatalytic Hydrogen Recovery. Stability of $TiO_2$-Based Materials. World Hydrogen Technologies Convention 2019 (WHTC19). Tokio, Japan, 2-7 junio 2019. *Poster presentation.*

5. Juan Corredor, Maria J. Rivero, Inmaculada Ortiz. Composite Nafion membranes with supported reduced graphene oxide

rGO/$TiO_2$ photocatalysts. ANQUE-ICCE-CIBIQ 2019. Santander, Spain, 19-21 junio 2019. *Poster presentation.*

6. Juan Corredor, Maria J. Rivero, Inmaculada Ortiz. Photocatalytic Membranes Based on the Use of Graphene Oxide/$TiO_2$ Composite for Hydrogen Production. ICCMR 2019. Eindhoven, The Netherlands 8-11 julio 2019. *Poster presentation.*

## A.2 Supplementary material of Publication 4

Supplementary Material:

# Influence of QD photosensitizers in the photocatalytic production of hydrogen with biomimetic [FeFe]-hydrogenase. Comparative performance of CdSe and CdTe

Juan Corredor [a], Dulanjan Harankahage [b], Frederic Gloaguen [c], Maria J. Rivero [a], Mikhail Zamkov [b], Inmaculada Ortiz [a*]

[a] Department of Chemical and Biomolecular Engineering, ETSIIT, University of Cantabria, Avda. de los Castros s/n, 39005, Santander, Spain

[b] Department of Physics and Center for Photochemical Sciences, Bowling Green State University, Bowling Green, Ohio 43043, USA

[c] UMR 6521, CNRS, Université de Bretagne Occidentale, CS 93837, 29238 Brest, France

* Corresponding author. E-mail address: inmaculada.ortiz@unican.es (I. Ortiz)

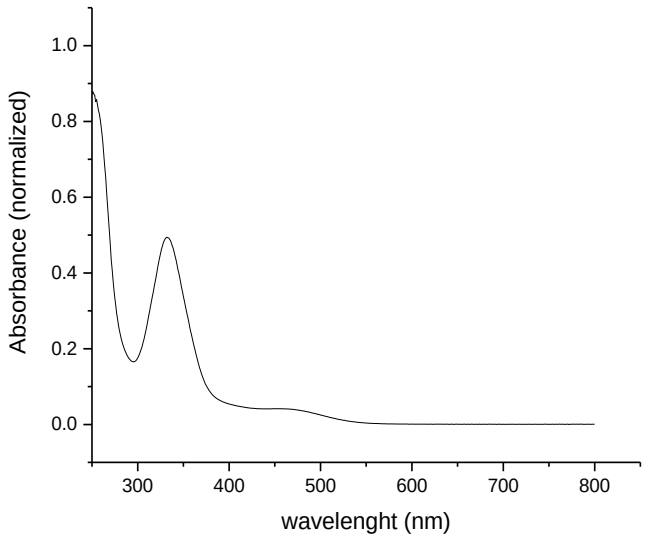


***Fig. SM-1**. [Fe-Fe]$H_2$-ase mimic UV-Vis absorption spectrum.*

## Plot of Peng's correlations for CdSe and CdTe

The size of the CdTe particles synthetized in this study was 2.95 nm. However, Peng's correlation for CdTe was validated for particle diameter from 3.5 nm to 8.5 nm. Nevertheless, Navarrete et al. (Navarrete S. et al., 2019) compared diameter values obtained from TEM measurements of CdTe particles from 1.5 nm with the predicted values by these correlations and the deviation was as low as 10%.

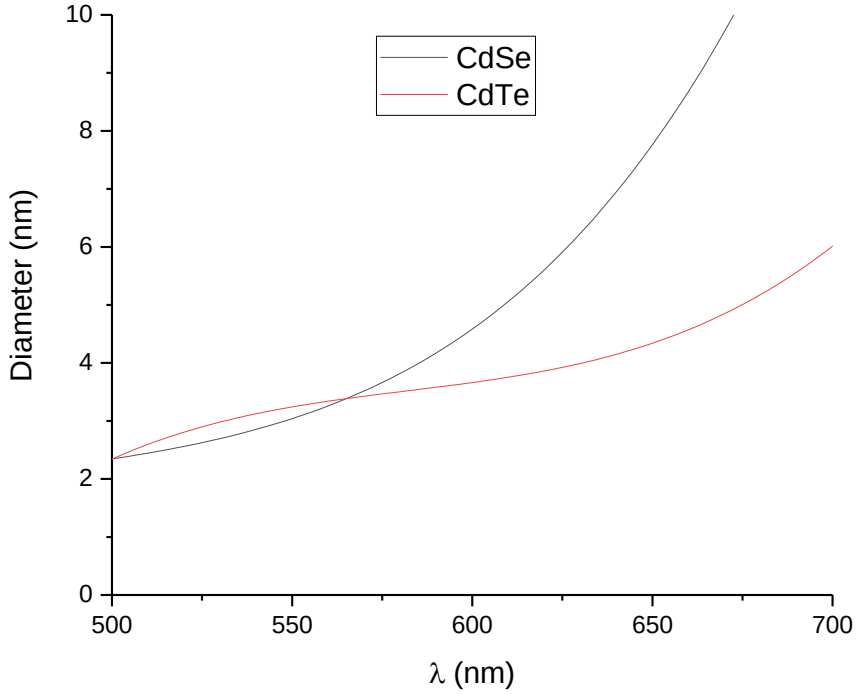


***Fig. SM-2**. QDs diameter calculated according to Peng's correlations for CdSe and CdTe.*

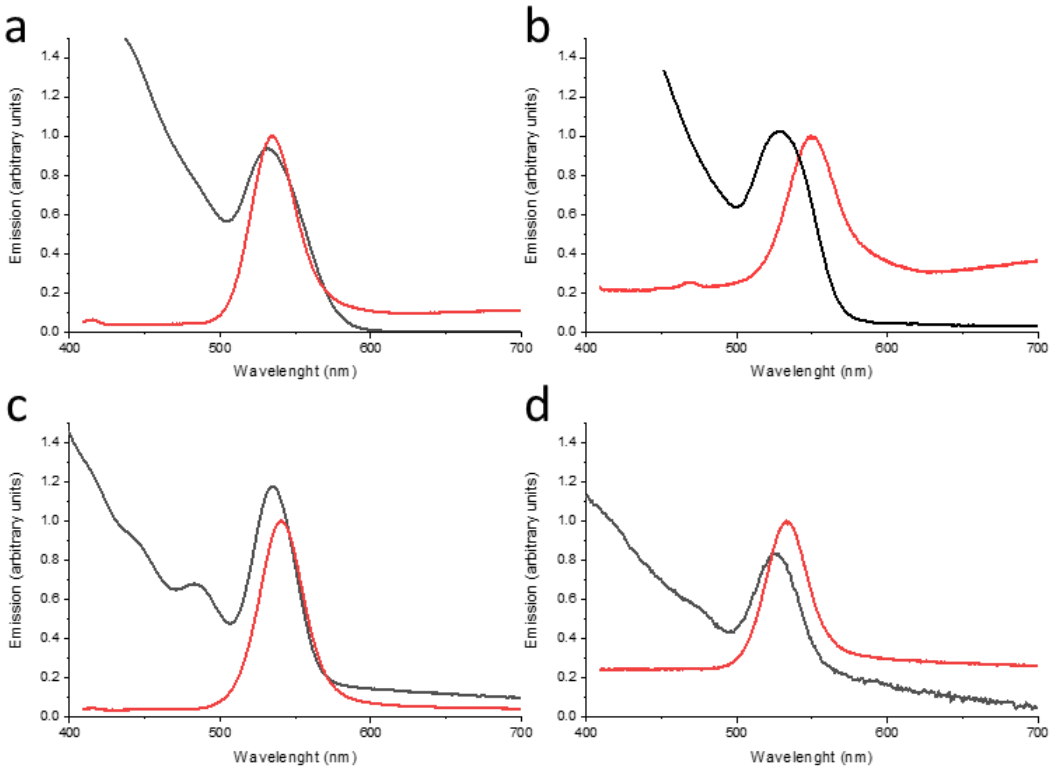


***Fig. SM-3.*** *CdSe and CdTe absorption (black) and emission (red) spectra of: (a) CdSe-OA; (b) CdSe-MPA; (c) CdTe-ODPA; (d) CdTe-MPA.*

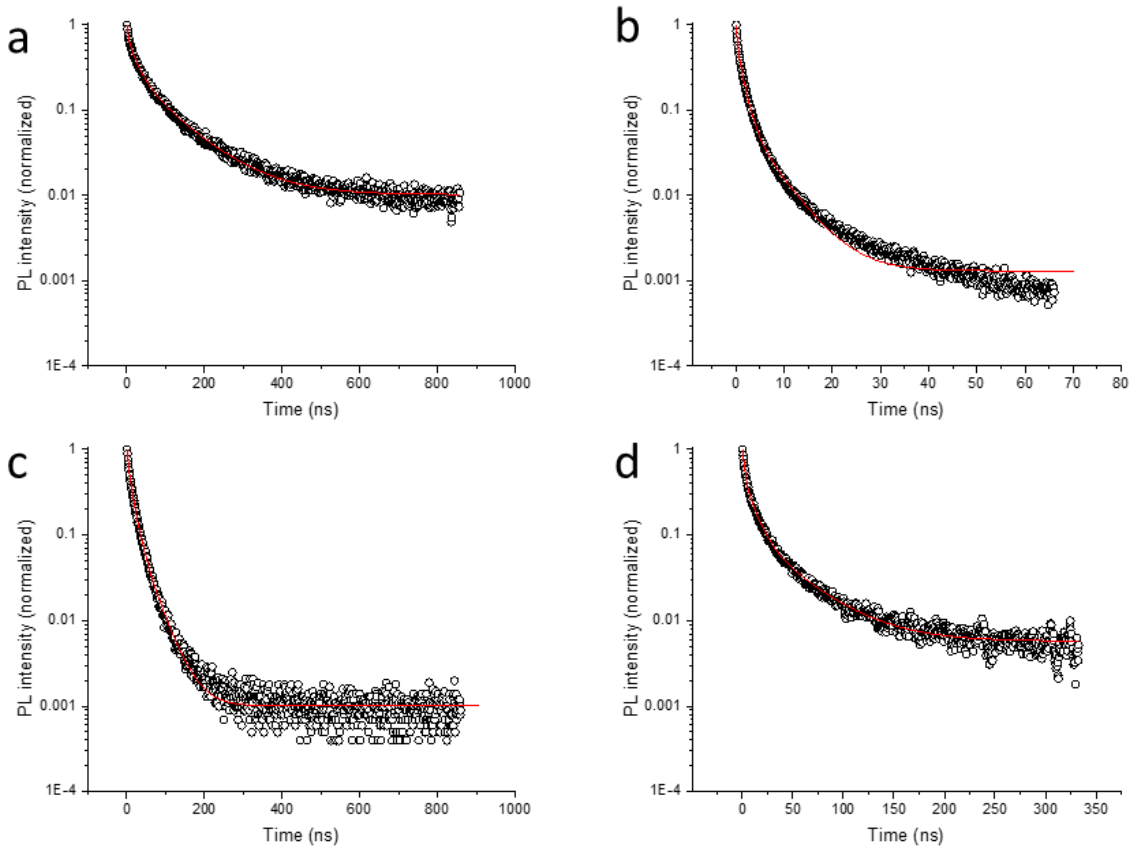


***Fig. SM-4.*** *Time-resolved photoluminescence decay spectra for (a) CdSe-OA, (b) CdSe-MPA, (c) CdTe-ODPA and (d) CdTe-MPA.*

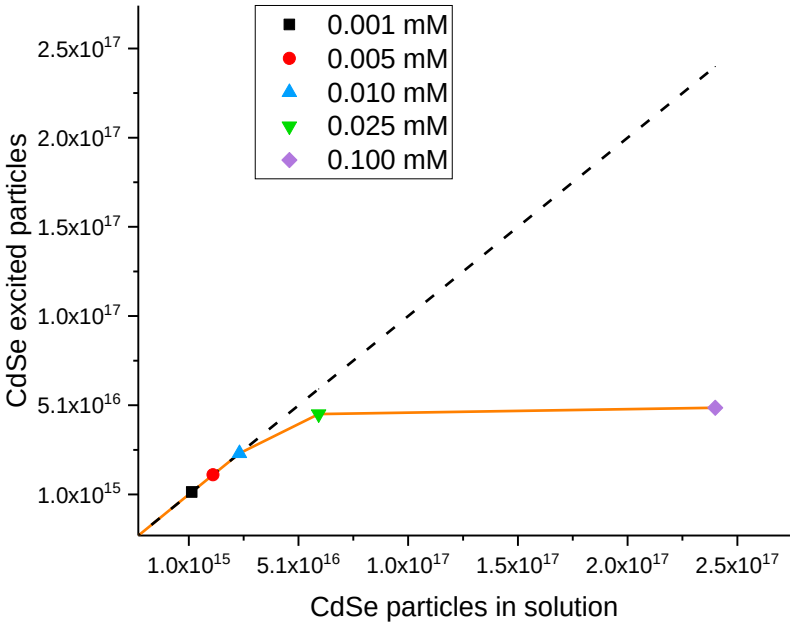


***Fig. SM-5**. Number of excited CdSe particles versus the total number of CdSe particles in the solution.*

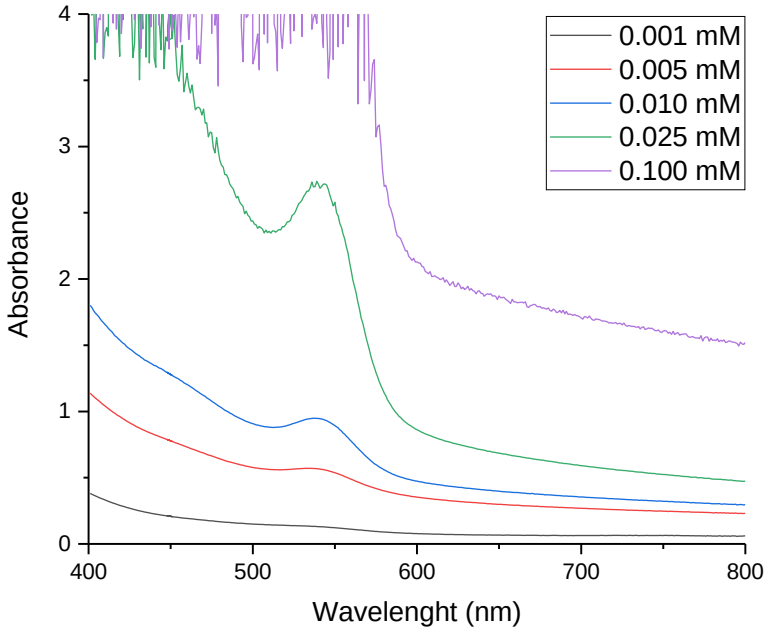


***Fig. SM-6**. Absorbance spectra for several CdSe concentrations*

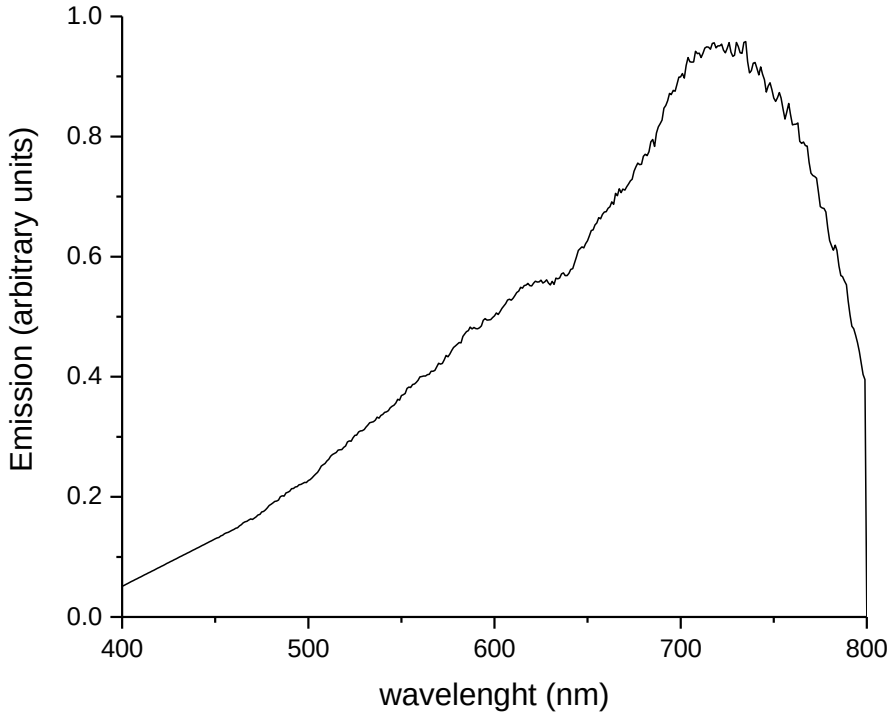


***Fig. SM-7**. Lamp emission spectrum.*

**Calculation of CdSe excited particles in the solution**

The number of photons which reach the solution could be obtained with eq. SM-3:

$$P_{Wall}=A_{wall}\cdot P_A \qquad \text{(equation SM-1)}$$

$$P_{solution}=P_{Wall}\cdot T_{glass} \qquad \text{(equation SM-2)}$$

$$Nº\text{total photons}_{solution}=\frac{P_{solution}}{E_{photon}}=\frac{P_{solution}}{\frac{c}{\lambda_p}\cdot h} \qquad \text{(equation SM-3)}$$

$P_A$: Irradiance measured with a photoradiometer ($mW\cdot cm^{-2}$)

$P_{Wall}$: irradiance that reached the reactor wall (mW)

$A_{wall}$: irradiated surface of the reactor wall ($cm^2$)

$P_{solution}$: irradiance that reached the solution (mW)

$T_{glass}$:glass transmittance (dimensionless)

$E_{photon}$: Energy of a photon ($J\cdot photon^{-1}$)

c: speed of light in vacuum ($m\cdot s^{-1}$)

h: Planck's constant ($m^2\cdot kg\cdot s^{-1}$)

$\lambda_p$: λ of measurement of the photoradiometer

$Nº\text{total photons}_{solution}$:number of total photons that reach the solution ($photons\cdot s^{-1}$)

The coefficient that allows calculation of the number of photons emitted by the lamp for each λ (K) can be calculated from $Nº\text{total photons}_{solution}$ and lamp emission profile (Fig. SM-7).

$$Nº\text{ total photons}_{solution}=K\cdot\int_{\lambda=400\text{ nm}}^{\lambda=800\text{ nm}} Em\,(\lambda)\cdot d\lambda \qquad \text{(equation SM-4)}$$

K: coefficient

Em (λ):lamp emission profile measured with the detector

K·[Em (λ)]: represents the number of photons for each λ that reach the solution

The absorbance for each CdSe concentration was corrected subtracting the absorbance at 600 nm because it was considered that the absorption at higher λ is due to the reflectance of the reaction medium.
From the absorbance data:

$$P(\lambda)=1-10^{-A(\lambda)} \qquad \text{(equation SM-5)}$$

P(λ):absorbance probability at certain λ
A(λ):Absorbance at certain λ (retrieved from Fig. SM-6)

The number of excited CdSe particles was calculated from K·Em(λ) and P(λ) with equation SM-6:

$$\text{Nº excited CdSe particles}=\int_{\lambda=400\ nm}^{\lambda=800\ nm} P(\lambda)\cdot K\cdot Em\ (\lambda)\cdot d\lambda \qquad \text{(equation SM-6)}$$

***Table SM-****¡Error! No hay texto con el estilo especificado en el documento.**1.** Produced hydrogen after 3 h, hydrogen production rates and $K_{asc}$ with CdSe and CdTe. [Photosensitizer]: 0.01 mM [Ascorbic acid]: 200 mM and [$Fe_2$(μ-1,2-benzenedithiolate)$(CO)_6$]: 0.1 mM, pH 4.5.*

| **Photosensitizer** | **TON after 3 h** | **Total $H_2$ after 3 h (μmol)** | **TOF ($h^{-1}$)** | **$H_2$ production rate (μmol·$h^{-1}$)** | **$k_{asc}$ ($M^{-1}\cdot s^{-1}$)** |
|---|---|---|---|---|---|
| CdSe | 18.3 | 7.3 | 6.5 | 2.6 | $5.42\cdot10^{9}$ |
| CdTe | 1.2 | 0.5 | 0.5 | 0.2 | $4.31\cdot10^{8}$ |

***Table SM-2.*** *TOF reported values in literature for aqueous systems with ascorbic acid as sacrificial agent, MPA-capped CdSe or CdTe QDs as photosensitizers and natural or biomimetic [Fe-Fe]H2-ase as catalyst.*

| Catalyst | Light source | PS | TOF ($h^{-1}$) | Stability (h) | Ref. |
|---|---|---|---|---|---|
| [FeFe]$H_2$-ase (1 µM) | LED (λ 450 nm) | CdSe-MPA | 12456 | 10 | (Jian et al., 2016) |
| [FeFe]$H_2$-ase-poly(acrilic acid) (1.46 µM) | LED 3 W (450 nm) | CdSe-MPA | 7000 | 5 | (Wen et al., 2016) |
| [FeFe]$H_2$-ase-Polyethylenimine (0.7 µM) | LED 3 W (λ 410 nm) | CdSe-MPA | 400 | 40 | (Liang et al., 2015) |
| [FeFe]$H_2$-ase-poly(acrilic acid) (1 µM) | LED (λ 450 nm) | CdSe-MPA | 9720 | 10 | (Wang et al., 2013) |
| [FeFe]$H_2$-ase (0.073 µM) | LED 750 mW (λ 405 nm) | CdTe-MPA | 9000 | n.r. | (Brown et al., 2014) |
| Chitosan-confined [FeFe]$H_2$-ase (0.01 mM) | LED (410 nm) | CdTe-MPA | 5040 | 60 | (Jian et al., 2013) |
| [FeFe]$H_2$-ase (156 µM) | Hg lamp 500 W (λ > 400 nm) | CdTe-MPA | 50 | 10 | (Wang et al., 2011) |
| [FeFe]$H_2$-ase (0.25 µM) | Halogen lamp 150 W (400 nm < λ <800 nm) | CdTe-MPA | 90000 | 1 | (Brown et al., 2010) |
| [FeFe]$H_2$-ase (100 µM) | Halogen lamp (400 nm < λ <800 nm) 31 mW/$cm^2$ | CdSe-MPA | 6.5 | 20 | Present study |
| | | CdTe-MPA | 0.5 | n.r. | |

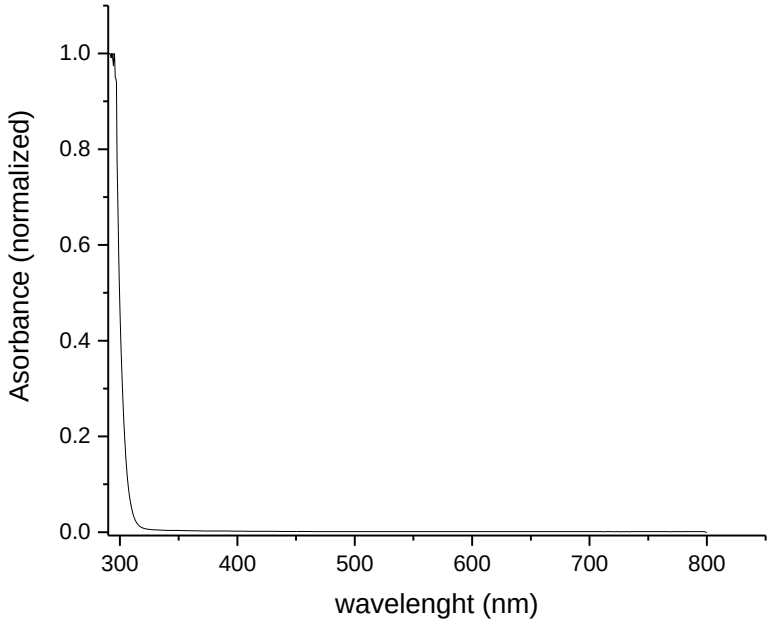


***Fig. SM-8****. UV-Vis absorbance spectra of 200 mM ascorbic acid solution.*

**Stern-Volmer equation plots**

The quenching rate constant, when catalyst or ascorbic acid were added, was calculated with the Stern-Volmer equation:

$$\frac{I_0}{I} = 1 + K_{sv} \cdot [Q] \qquad \text{(equation SM-7)}$$

$$\frac{I_0}{I} - 1 = k_q \cdot \tau_0 \cdot [Q] \qquad \text{(equation SM-8)}$$

$I_0$: Fluorescence intensity without quencher

I: Fluorescence intensity for a certain concentration of quencher

$K_{sv}$: Stern-Volmer constant

$k_q$: quenching rate constant

$\tau_0$: excitation decay lifetime

[Q]: quencher concentration

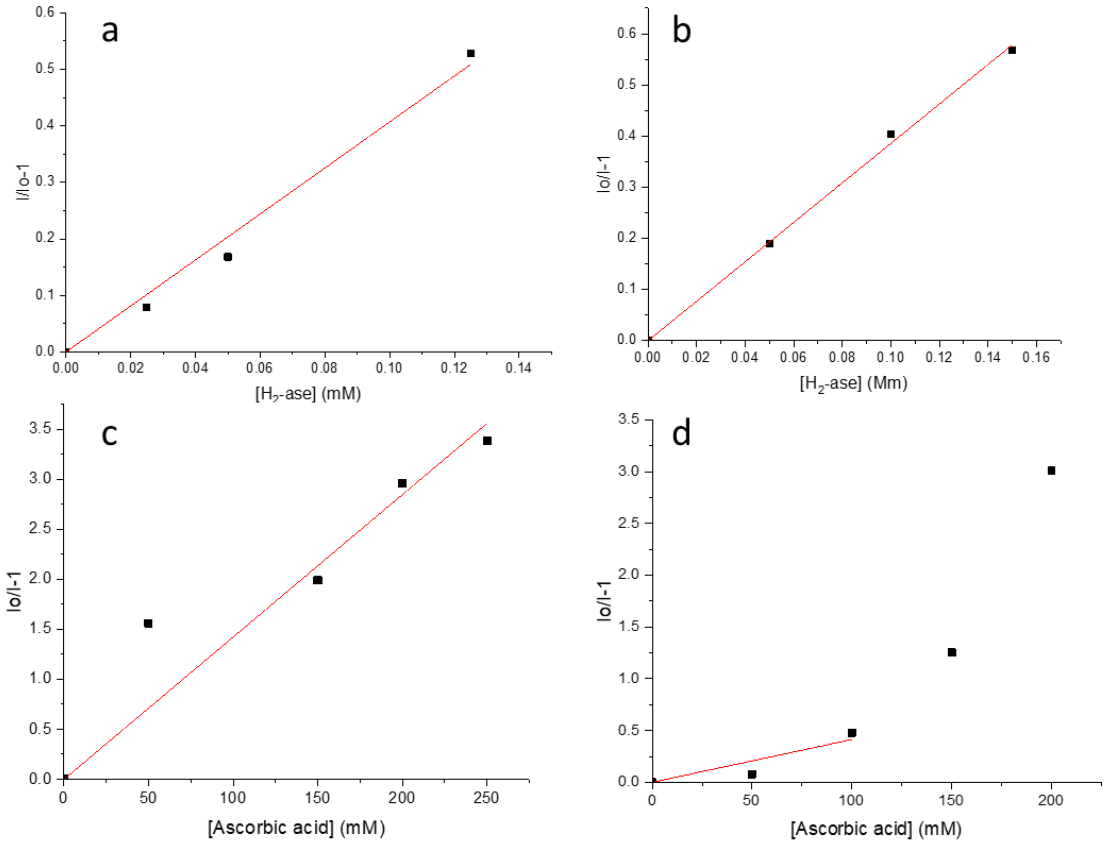


***Fig. SM-9**. Stern-Volmer plots for different quencher concentrations. (a) Catalyst addition to CdSe-MPA solution; (b) Catalyst addition to CdTe-MPA solution; (c) Ascorbic acid addition to CdSe-MPA solution; (d) Ascorbic acid addition to CdTe-MPA solution.*

***Table SM-3.** Fitting parameters to Stern-Volmer equation*

| Graph | $K_{SV}$ ($mM^{-1}$) | $R^2$ |
|---|---|---|
| **A** | 4.07 | 0.99 |
| **B** | 3.86 | 0.99 |
| **C** | $1.42 \cdot 10^{-2}$ | 0.97 |
| **D** | $4.14 \cdot 10^{-3}$ | 0.91 |

## References

Brown, K.A., Dayal, S., Ai, X., Rumbles, G., King, P.W., 2010. Controlled assembly of hydrogenase-CdTe nanocrystal hybrids for solar hydrogen production. J. Am. Chem. Soc. 132, 9672–9680. https://doi.org/10.1021/ja101031r

Brown, K.A., Song, Q., Mulder, D.W., King, P.W., 2014. Diameter dependent electron transfer kinetics in semiconductor-enzyme complexes. ACS Nano 8, 10790–10798. https://doi.org/10.1021/nn504561v

Jian, J.X., Liu, Q., Li, Z.J., Wang, F., Li, X.B., Li, C.B., Liu, B., Meng, Q.Y., Chen, B., Feng, K., Tung, C.H., Wu, L.Z., 2013. Chitosan confinement enhances hydrogen photogeneration from a mimic of the diiron subsite of [FeFe]-hydrogenase. Nat. Commun. 4, 2695. https://doi.org/10.1038/ncomms3695

Jian, J.X., Ye, C., Wang, X.-Z., Wen, M., Li, Z.-J., Li, X.-B., Chen, B., Tung, C.-H., Wu, L.-Z., 2016. Comparison of $H_2$ photogeneration by [FeFe]-hydrogenase mimics with CdSe QDs and $Ru(bpy)_3$ $Cl_2$ in aqueous solution. Energy Environ. Sci. 9, 2083–2089. https://doi.org/10.1039/C6EE00629A

Liang, W.J., Wang, F., Wen, M., Jian, J.X., Wang, X.Z., Chen, B., Tung, C.H., Wu, L.Z., 2015. Branched polyethylenimine improves hydrogen photoproduction from a CdSe quantum dot/[FeFe]-hydrogenase mimic system in neutral aqueous solutions. Chem. Eur. J. 21, 3187–3192. https://doi.org/10.1002/chem.201406361

Navarrete S., E., Román S., J., Rojas C., V., Henríquez N., R., Schrebler G., R., Córdova O., R., Bravo M., M., Muñoz C., E., 2019. Chemometric approach to study the influence of synthesis parameters on the size of CdTe quantum dots obtained from aqueous solutions. Arab. J. Chem. 12, 5103–5110. https://doi.org/10.1016/j.arabjc.2016.10.011

Wang, F., Liang, W.J., Jian, J.X., Li, C.B., Chen, B., Tung, C.H., Wu, L.Z., 2013. Exceptional poly(acrylic acid)-based artificial [FeFe]-hydrogenases for photocatalytic $H_2$ production in water. Angew. Chemie Int. Ed. 52, 8134–8138. https://doi.org/10.1002/anie.201303110

Wang, F., Wang, W.G., Wang, X.J., Wang, H.Y., Tung, C.H., Wu, L.Z., 2011. A highly efficient photocatalytic system for hydrogen production by a robust hydrogenase mimic in an aqueous solution. Angew. Chemie Int. Ed. 50, 3193–3197. https://doi.org/10.1002/anie.201006352

Wen, M., Li, X.B., Jian, J.X., Wang, X.Z., Wu, H.L., Chen, B., Tung, C.H., Wu, L.Z., 2016. Secondary coordination sphere accelerates hole transfer for enhanced hydrogen photogeneration from [FeFe]-hydrogenase mimic and CdSe QDs in water. Sci. Rep. 6, 29851. https://doi.org/10.1038/srep29851

**NOTES**